



Jerzy Haber
INSTITUTE OF CATALYSIS AND SURFACE CHEMISTRY
POLISH ACADEMY OF SCIENCES

Agnieszka Czakaj

**Liquid foams
stabilised
by cellulose nanocrystals**

PhD Thesis

Supervisor

Prof. dr hab. inż. Piotr Warszyński

Co-supervisor

Dr Marcel Krzan

KRAKÓW 2023

Funding

This PhD thesis has been completed in the framework of the Program POWER, project No. POWR.03.02.00-00-I004/16, co-financed by the European Union.



European Union
European Social Fund



**European
Funds**
Knowledge Education Development

Research presented in the PhD dissertation was also funded by:

- National Science Centre of Poland (grant number 2016/21/B/ST8/02107).



NATIONAL SCIENCE CENTRE
POLAND

- European Union's Horizon 2020 research and innovation programme under grant agreement No 731019 (European Union Soft Matter Infrastructure).



And partly by statutory subsidy for Jerzy Haber Institute of Catalysis and Surface Chemistry PAS.



**Jerzy Haber Institute of Catalysis
and Surface Chemistry**
Polish Academy of Sciences

ACKNOWLEDGEMENTS

I would like to express my sincere gratitude to
my supervisor Professor Piotr Warszyński - for his valuable scientific advice and mentoring.

In his team I finally learned how not to “worry in advance.”

my co-supervisor Dr. Marcel Krzan – for the opportunity to participate in the research project
and for the cooperation with excellent researchers.

I also want to thank my family for the love and patience. After this time you are grown-up and can say
that Anastazja wants to be a *researcher* and Dominik wants to *focus only on mathematics and music*.

You will achieve much more than that in the ocean of possibilities.



I also want to express my gratitude to the following persons for their cooperation and contribution to the research presented in the PhD thesis:

Professor Gerald G. Fuller, Department of Chemical Engineering, Stanford University
(Stanford, United States)

Dr. Aadithya Kannan, Department of Chemical Engineering, Stanford University
(Stanford, United States)

Dr. Vineeth Chandran Suja, Department of Chemical Engineering, Stanford University
(Stanford, United States), presently at Harvard University (Cambridge, MA, United States)

Professor Jan Vermant, Department of Materials, ETH Zürich (Zürich, Switzerland)

Dr. Emmanouil Chatzigiannakis, Department of Materials, ETH Zürich (Zürich, Switzerland),
presently at Department of Mechanical Engineering, Eindhoven University of Technology
(Eindhoven, The Netherlands)

Professor Francesca Ravera, National Research Council – CNR, Institute of Condensed Matter
Chemistry and Technologies for Energy (Genova, Italy)

Dr. Eva Santini, National Research Council – CNR, Institute of Condensed Matter Chemistry and
Technologies for Energy (Genova, Italy)

Professor Szczepan Zapotoczny, Department of Chemistry, Jagiellonian University (Kraków, Poland)

Professor Robert Holyst, Institute of Physical Chemistry Polish Academy of Sciences
(Warszawa, Poland)

Professor Theo van de Ven, Department of Chemistry, McGill University (Montreal, Canada)

~

I also want to acknowledge

- Jerzy Haber Institute of Catalysis and Surface Chemistry PAS cooperating with the Leading National Research Center (KNOW) supported by the Ministry of Science and Higher Education
- The PROM Programme International – Scholarship exchange of Ph.D. candidates and academic staff

TABLE OF CONTENTS

ABSTRACT	7
STRESZCZENIE	11
PUBLICATIONS	15
LIST OF SYMBOLS AND ABBREVIATIONS	16
1. Introduction	19
1.1 Motivation	19
1.2 Adsorption of surfactants basic information	21
1.3 Interfacial tension and rheology	23
1.4 Thin films	31
1.5 Foam formation and stability	32
1.6 Experimental methods for studying thin films dynamics	34
1.7 Objectives	38
2. Research methodology	39
2.1 Cellulose nanocrystals dispersion preparation	39
2.2 Cryo-TEM microscopy	39
2.3 Ethyl lauroyl arginate – cellulose nanocrystals dispersion preparation	40
2.4 Experimental conditions	40
3. Experimental and instrumental methods	41

	3.1 Pendant drop experiments	41
	3.2 Zeta potential	41
	3.3 Dynamic light scattering	42
	3.4 Dynamic viscosity	43
	3.5 Interfacial shear rheology	43
	3.6 Thin film balance	43
	3.7 Dynamic fluid film interferometry	44
	3.8 Double syringe foaming experiments	45
4.	Review of articles constituting the PhD Thesis	46
	4.1 Article 1	46
	4.2 Article 2	50
	4.3 Article 3	53
	4.4 Article 4	56
5.	Discussion and conclusions	59
6.	References	62
ORIGINAL PUBLICATIONS		68
SCIENTIFIC ACHIEVEMENTS		133
AUTHORSHIP DECLARATIONS	supplement	

ABSTRACT

Doctoral thesis “Liquid foams stabilised by cellulose nanocrystals” consists of the cycle of 4 articles strictly linked thematically with the analysis of surface activity or foamability and foam stability mechanisms of mixtures of a relatively novel amino acid-based surfactant, ethyl lauroyl arginate (LAE), and cellulose nanocrystals (CNC) with sulfate (sCNC) or carboxyl (cCNC) hydrophilic groups. The surface activity of ethyl lauroyl arginate was described and compared with existing literature data with the explanation of the source of differences in results from various researchers. Native CNC are not surface active, thus, in this work, the idea of synergistic interactions between the surfactant and hydrophilic particles was used to modify the surface activity of nanoparticles and achieve industrially relevant foaming enhancement with limited surfactant use. The most important scientific goal of this work concerns the determination of the mechanism of foam stability.

The commercially available surfactant Mirenat of 85% purity was mainly used for foaming experiments, and the analytical standard of 99% purity for the determination of adsorption isotherm and the explanation of the effect of surfactant hydrolysis on its adsorption properties supported by molecular modelling. The publications contain surface activity data for both Mirenat and the analytical standard. The conclusions obtained for analytical standard might serve as the reference for commercial surfactants of lower purity.

In the experiments, commercially available cellulose nanocrystals were used. The use of cellulose nanocrystals of well-defined surface chemistry allowed for experiments concerning its effect on surface activity and mutual interactions between nanoparticles, surfactant and nanoparticles and nanoparticle-nanoparticle aggregation.

The papers are presented here in a different order than they were published. For example, Article 2 describing the foamability of LAE (Mirenat) was published before Article 1 referring to LAE analytical standard. In the course of the first experiments with the commercially available surfactant, many questions and ideas appeared concerning further experiments and peculiarities of the surface activity, that required our focus on a better-defined system.

In Article 1 „Ethyl lauroyl arginate, an inherently multicomponent system”, the review of the literature data on LAE surface activity indicated on many discrepancies between results obtained by different researchers. The surface activity of pure ethyl lauroyl arginate (99% purity), the role of residual synthesis products like dodecanoic acid and N α -lauroyl-L-arginine and the influence of hydrolysis products were determined and described in my work for the first time as referred to existing literature. The dependence of surface tension of LAE concentration was determined by analysing of the shape of the pendant drop using the Young-Laplace equation. LAE surface activity was compared with the

surface activity of surfactants with the same hydrophobic tail, concluding that LAE properties were between non-ionic and ionic surfactants. The surface tension of LAE at critical micelle concentration was much lower than for typical cationic surfactants, thus LAE showed properties similar to di-chain or Gemini surfactants. It was explained that LAE undergoes hydrolysis that can proceed along two paths. Quantum mechanical calculations were applied to determine the preferred hydrolysis path. Details of computations are given in Supplement to Article 1. It was determined that the preferred path was the base hydrolysis. The DFT computation was used to prove the possibility of the formation of dimeric structures of LAE and its hydrolysis products, LAE-dodecanoate anion and LAE-N α -lauroyl-L-arginine. Molecular dynamics calculations were applied to determine the probability of occurrence and stability of those dimeric structures at the interface. The LAE adsorption isotherm was modelled with STDE model considering the effect of surfactant hydrolysis. Details of the model were given in Supplement to Article 1. A good agreement of model prediction with experimentally determined surface tension were obtained.

Oscillations of the pendant drop were applied to determine the surface viscoelastic properties of LAE. The Lucassen-van den Tempel model based on the diffusion of soluble surfactant to the interface was applied for the interpretation of experimental data. The characteristic oscillation frequency was calculated from the model. It was shown that the model could be applied only for LAE concentrations not exceeding 0.5 mM. A non-linearity of surface tension oscillations was observed for higher concentrations with significant values of the second harmonic amplitude, which was attributed to micellization.

The research presented in Article 2, „Viscoelastic interfaces comprising of cellulose nanocrystals and lauroyl ethyl arginate for enhanced foam stability”, concentrated on thin foam film stability and its correlation with foamability. The main experimental method used was dynamic fluid film interferometry (DFI) based on the thin film formed at the bubble put into motion and colliding with air/liquid interface. The DFI technique is used only by several research groups in the world. Experimental results consisted of coalescence times of bubbles made in the solution with different LAE-CNC ratios, as well as recorded interferometric images of the thin liquid film showing its thickness. The moving bubble colliding with the interface can be considered as partially representing the foam film formation. When the bubble reached the interface the film formed was subjected to water drainage. For the film thickness approximately below 100 nm, its stability was governed by intermolecular interactions described by the DLVO theory. If the film is unstable, it breaks after a certain coalescence time. It was shown that coalescence time significantly increased with the presence of CNC in the solution. For 0.006% of LAE, maximum coalescence time was observed, whereas, for higher LAE concentrations, the break of the thin liquid film was induced by cellulose nanocrystals aggregation. Such observation was in agreement with CNC hydrodynamic diameter measurements by dynamic light scattering and foam stability experiments that showed foam lifetime decrease for LAE concentrations larger than 0.006% wt. In addition, the maximum of surface dilatational elastic modulus measured by oscillating

pendant drop and the maximum of the shear interfacial elastic modulus, coincided with the same LAE concentration of 0.006% wt. in the mixture with CNC.

In Article 3, „The Effect of Electrolytes and Urea on the Ethyl Lauroyl Arginate and Cellulose Nanocrystals Foam Stability”, foamability and foam stability of LAE – CNC were presented with the use of cellulose nanocrystals having similar colloidal properties but differing in hydrophilic groups. Cellulose nanocrystals with carboxyl groups (cCNC), manufactured by Anomera, were described in this work in detail with reference to the state of the art. Nanocrystals with sulfate half ester groups (sCNC) were described in Article 2. Dispersions of both types of nanoparticles were characterized for surface tension, hydrodynamic diameter and zeta potential. For the size and zeta potential no significant differences were seen, except for lower polydispersity of cCNC. Surface activity of LAE and CNC differed in sulfate- or carboxyl-modified CNC depending on surfactant concentrations but differences were very small. Despite their similarity, the cCNC showed twofold increase of foamability in a mixture with LAE compared to sCNC.

The foam breaking factor was the key point in a series of experiments with electrolytes or urea that were added to LAE-cCNC mixtures. A minor effect of electrolytes on foamability was observed for concentrations used, except for sodium salicylate that adsorbed at interface in a competitive way to LAE. It was shown that electrolyte addition at concentration of 5 mM has an insignificant effect on foam stability, including the case of the surface active NaSal or NaCl, which doubled the size of CNC due to their aggregation. The most significant differences were seen for urea added to the LAE-CNC mixture at a concentration of 6 mol/L. Foamability measured in the same time scale as for other mixtures decreased several times however, the transient foam was observed. Notably, foam stability was ultimately reduced. It was experimentally verified that urea addition at high concentrations decreased the polydispersity of CNC due to efficient elimination of large CNC aggregates. Large CNC aggregates reduce liquid drainage from liquid films, so with their absence in concentrated urea solution and LAE-CNC foams drainage is very fast. In addition, urea can to some extent influence the viscoelasticity of surface monolayers. Literature reports show that urea at high concentrations orients at the interface in the presence of ionic surfactant, disturbing the interfacial water structure. Water reorientation can play a role in foam stability, but this effect could not be studied in this work. Further experiments with LAE and CNC verifying this hypothesis would be an interesting continuation of this research topic.

In Article 4, “The influence of the Surface Chemistry of Cellulose Nanocrystals on Ethyl Lauroyl Arginate Foam Stability”, *thin film balance* experiments were used to elucidate the differences in thin film and foam stability in the suspension of cCNC and sCNC with LAE. Thin film balance in the bike-wheel configuration, the improvement of the Sheludko-Exerowa cell, enables precise control of the thin film pressure with uniform drainage from the thin liquid film. In the same time film thickness is controlled interferometrically with nanometric resolution. Presented in the paper, measurements in the dynamic conditions enabled drainage dynamics observation and determination of coalescence time. Obtained coalescence times corresponded with coalescence time from DFI experiments for the single

bubble described in the Article 2. The type of cellulose nanocrystal surface hydrophilic group significantly influenced interfacial film morphology and its viscoelastic properties. The interfacial film showed a different response to pressure change depending on surfactant-nanoparticle stoichiometry. Films containing sulfated cellulose nanocrystals showed smaller interfacial aggregates and were less resistant to pressure changes. Cellulose nanocrystals with carboxyl groups modified thin liquid film character to a greater extent. These films contained much bigger interfacial aggregates, they showed higher coalescence times and complex response to pressure changes and film reforming after rupture: wrinkling and folding of interfacial layer with nanoparticles for moderate LAE concentration and possibly competitive surfactant adsorption for high LAE concentration with the disintegration of the interfacial layer containing cellulose nanocrystals.

The main conclusion stemming from the experimental results presented in the series of articles is that the cellulose nanocrystals interfacial properties can be effectively, precisely tuned by interactions with ionic surfactant, LAE. The presented results of various experiments for LAE-CNC dispersions, including foaming, interfacial rheology, and thin film stability are consistent. Unfortunately none of the method could solely characterize this system for its complexity. Very small change of the dispersion composition resulted in dramatic change of interfacial layer structure and dynamic response. The knowledge of these properties can help to design functional interfaces for various food, cosmetic or medical products.

STRESZCZENIE

Praca doktorska Piany ciekłe stabilizowane przez nanokryształy celulozy składa się z cyklu 4 publikacji ściśle powiązanych ze sobą tematycznie poprzez analizę aktywności powierzchniowej lub pianotwórczości i stabilności pian relatywnie nowego surfaktantu arginianu laurylowo-etylowego (LAE), będącego pochodną aminokwasu, oraz nanokryształów celulozy (CNC) z siarczanowymi (sCNC) lub karboksylowymi (sCNC) grupami hydrofilowymi. Aktywność powierzchniowa arginianu laurylowo-etylowego została opisana i porównana z istniejącymi danymi literaturowymi. Nanokryształy celulozy w czystej postaci nie są aktywne powierzchniowo, stąd w pracy wykorzystano koncepcję badań efektów synergistycznych surfaktant-hydrofilowa nanocząstka dla zmiany aktywności powierzchniowej nanocząstek i osiągnięcia użytecznego w przemyśle efektu pianotwórczości przy zmniejszeniu zużycia surfaktantu. Najważniejszą częścią pracy było dowiedzenie mechanizmu stabilności piany.

Do badań użyto komercyjnie dostępnego surfaktantu Mirenat: o czystości ok. 85%, głównie w przypadku badań pianotwórczości oraz standardu analitycznego o czystości 99% - do wyznaczenia izotermy adsorpcji i wyjaśnienia efektów hydrolizy surfaktantu na jego właściwości powierzchniowe, z uzupełnieniem o modelowanie molekularne. Prace zawierają dane na temat aktywności powierzchniowej zarówno surfaktantu Mirenat jak i standardu analitycznego, a wnioski uzyskane dla standardu analitycznego mogą służyć jako odniesienie do komercyjnego surfaktantu o niższej czystości.

W eksperymentach użyto komercyjnie dostępnych nanokryształów celulozy. Użycie nanokryształów celulozy o dobrze zdefiniowanej strukturze chemicznej powierzchni pozwoliło na eksperymenty badające wpływ tej powierzchni na aktywność powierzchniową i wzajemne oddziaływania pomiędzy nanocząstkami, pomiędzy nanocząstkami i surfaktantem oraz na agregację nanocząstek.

Prace naukowe zostały zaprezentowane w niniejszej pracy doktorskiej w innej kolejności niż były publikowane, np. Publikacja 2 opisująca pianotwórczość LAE (Mirenat) została opublikowana przed Publikacją 1 odnoszącą się do standardu analitycznego. W trakcie pierwszych badań nad komercyjnie dostępnym surfaktantem pojawiło się wiele pytań i idei na temat dalszych eksperymentów oraz szczególnej aktywności powierzchniowej LAE, co wymagało lepiej zdefiniowanego przedmiotu badań.

W Artykule 1 „Ethyl lauroyl arginate, an inherently multicomponent system” podano przegląd literaturowy dotyczący badań nad aktywnością powierzchniową LAE, który wykazał duże rozbieżności wyników otrzymanych przez różnych badaczy. Aktywność powierzchniowa czystego arginianu laurylowo-etylowego (czystość bliska 99%), rola reszkowych produktów syntezy takich jak kwas dodekanowy i $N\alpha$ -lauroyl-L-arginine oraz wpływ produktów hydrolizy LAE zostały zmierzone i opisane po raz pierwszy w mojej pracy w odniesieniu do całej światowej literatury.

Zależność napięcia powierzchniowego od stężenia LAE została wyznaczona metodą analizy kształtu wiszącej kropli z zastosowaniem równania Younga-Laplace'a. Aktywność powierzchniowa LAE została porównana z aktywnością powierzchniową surfaktantów o tym samym łańcuchu hydrofobowym, wykazując, że właściwości LAE są pośrednie między surfaktantami niejonowymi, a jonowymi. Napięcie powierzchniowe LAE dla krytycznego stężenia micelizacji było znacznie niższe niż napięcie powierzchniowe typowych surfaktantów kationowych, przez co LAE wykazał zbliżone właściwości powierzchniowe do surfaktantów dwułańcuchowych lub Gemini. Wykazano, że LAE podlega hydrolizie, która może przebiegać dwoma ścieżkami. Obliczenia kwantowo-mechaniczne pozwoliły określić preferowaną ścieżkę hydrolizy. Szczegóły obliczeń podano dodatkowo w materiałach Suplementu do Artykułu 1. Określono, że preferowaną ścieżką hydrolizy jest hydroliza zasadowa i przy pomocy DFT zoptymalizowano struktury tworzących się produktów hydrolizy w postaci dimerów, LAE-anion dodekanowy oraz LAE-N α -lauroyl-L-arginine. Obliczenia dynamiki molekularnej posłużyły następnie do określenia występowania i stabilności tych dimerów na granicy faz. Izoterma LAE została opisana przy pomocy modelu adsorpcji mieszaniny surfaktantów STDE. Szczegóły modelu opisano w Suplemencie do Artykułu 1. Uzyskano dobrą zgodność modelowego napięcia powierzchniowego z otrzymanymi wynikami. Oscylacje wiszącej kropli pozwoliły na wyznaczenie właściwości wiskoelastycznych LAE. Model Lucassen i van den Tempel opierający się na dyfuzji rozpuszczalnego surfaktantu do granicy faz posłużył do interpretacji danych eksperymentalnych. Z modelu wyliczono częstotliwość charakterystyczną oscylacji. Wykazano, że model może odnosić się tylko do stężeń LAE nieprzekraczających 0.5 mM. Dla wyższych stężeń zaobserwowano nieliniowość oscylacji napięcia powierzchniowego i znaczący udział amplitudy drugiej harmonicznej, co zostało przypisane do micelizacji.

Badania opisane w artykule „Viscoelastic interfaces comprising of cellulose nanocrystals and lauroyl ethyl arginate for enhanced foam stability” koncentrowały się na stabilności cienkich filmów piany w korelacji z pianotwórczością. Główną metodą eksperymentalną były interferometryczne badania ciekłego filmu w warunkach dynamicznych (ang. DFI), oparte na badaniach cienkiego filmu wytworzonego w pęcherzyku będącym w ruchu i zderzającym się z granicą fazy ciekłej i gazowej. Technikę DFI stosuje tylko kilka grup badawczych na świecie. Wynikami eksperymentu były zarówno czasy koalescencji pęcherzyka wytworzonego z roztworów o różnej stechiometrii LAE-CNC, jak i zarejestrowane interferometryczne obrazy ciekłego filmu obrazujące jego grubość. Poruszający się pęcherzyk zderzający się z granicą faz może być częściową reprezentacją tworzenia się filmu pianowego. Gdy pęcherzyk osiągnął granicę faz wytworzony cienki film ulegał wyciekaniu cieczy. Dla grubości filmu poniżej 100 nm jego stabilność zależy od oddziaływań międzycząsteczkowych opisanych przez teorię DLVO. Jeżeli film jest nietrwały, pęka po określonym czasie koalescencji. Wykazano znaczny wzrost czasu koalescencji przy obecności nanocząstek celulozy w roztworze surfaktantu. Dla stężenia 0.006% LAE czas koalescencji był maksymalny, przy czym dla wyższych stężeń przyczyną pęknięcia ciekłego filmu była agregacja nanocząstek celulozy. Ta obserwacja zgadzała

się ze średnicą hydrodynamiczną CNC mierzoną przy pomocy dynamicznego rozpraszania światła oraz badaniami pianotwórczości, które wykazały spadek czasu życia piany dla stężeń wyższych niż 0.006%. Dodatkowo, maksymalny powierzchniowy moduł elastyczności mierzony techniką oscylującej kropli, a także maksymalny moduł powierzchniowy elastyczności mierzony w warunkach międzyfazowego ścinania przypadła także dla tego samego stężenia LAE, 0.006% w mieszaninie z CNC.

W Artykule 3 „The Effect of Electrolytes and Urea on the Ethyl Lauroyl Arginate and Cellulose Nanocrystals Foam Stability” przedstawiono wyniki pianotwórczości i stabilności pian LAE z nanocząstkami celulozy o bardzo zbliżonych właściwościach koloidalnych, ale różniących się grupami hydrofilowymi. Nanocząstki z grupami siarczanowymi (sCNC) zostały opisane w Artykule 2. Mieszanki obu rodzajów cząstek scharakteryzowano w zakresie napięcia powierzchniowego, średnicy hydrodynamicznej i potencjału zeta. Nie wykazano istotnych różnic między dyspersjami, poza mniejszą poldispersyjnością nanocząstek z grupami karboksylowymi. Aktywność powierzchniowa LAE i CNC różniła się między CNC z grupami siarczanowymi w stosunku do karboksylowych w zależności od stężenia surfaktantu, ale różnice były niewielkie. Mimo podobnych właściwości, pianotwórczość cCNC była dwa razy wyższa w porównaniu do mieszanin LAE z sCNC.

W serii eksperymentów z elektrolitami lub mocznikiem dodawanymi do mieszanin LAE-cCNC kluczowym było znalezienie czynnika eliminującego pianotwórczość. Wykazano niewielki wpływ elektrolitów na pianotwórczość. Wyjątkiem był salicylan sodu (NaSal), który konkurencyjnie do LAE adsorbuje się na granicy faz. Wykazano, że dodatek elektrolitów o stężeniu 5 mM ma znikomy wpływ na stabilność pian, w tym dodatek aktywnego powierzchniowo NaSal lub chlorku sodu, NaCl podwajającego średni rozmiar CNC ze względu na agregację nanocząstek.

Najistotniejsze różnice zaobserwowano dla mocznika obecnego w mieszaninie LAE-CNC w stężeniu 6 mol/L. Z dodanym mocznikiem pianotwórczość mierzona w tej samej skali czasowej jak dla pozostałych mieszanin zmniejszyła się kilkukrotnie, przy czym zaobserwowano bardzo niestabilną pianę. W szczególności czas życia pianu został znacząco zredukowany. Zweryfikowano eksperymentalnie, że dodatek mocznika w dużym stężeniu zmniejsza poldispersyjność nanokryształów celulozy, poprzez skuteczną eliminację większych agregatów celulozowych. Duże agregaty celulozowe zmniejszają wyciek cieczy z filmów pianowych, więc w mieszaninach ze stężonym mocznikiem wyciek cieczy z pian LAE-CNC jest bardzo szybki. Dodatkowo, mocznik może w pewnym zakresie modyfikować właściwości wiskoelastyczne warstw powierzchniowych. Doniesienia literaturowe podają, że mocznik przy dużych stężeniach i obecności surfaktantów jonowych może orientować się na granicy faz zgodnie z ładunkiem surfaktantu przez co zaburza międzyfazową strukturę wody. Reorientacja wody może mieć kluczowe znaczenie dla stabilności pian, ale ten efekt nie mógł zostać zbadany w niniejszej pracy. Dalsze eksperymenty z LAE oraz CNC weryfikujące tę hipotezę byłyby interesującą kontynuacją tego tematu badawczego.

W Artykule 4, „The influence of the Surface Chemistry of Cellulose Nanocrystals on Ethyl Lauroyl Arginate Foam Stability”, zamieszczono wyniki eksperymentów wykonanych z zastosowaniem *thin film balance*, aby uwypuklić różnice w stabilności cienkich filmów i pian w dyspersjach cCNC i sCNC z LAE. Thin film balance w konfiguracji „bike-wheel”, ulepszenie celki Sheludko-Exerowa pozwala na precyzyjną kontrolę ciśnienia w cienkim filmie z jednorodnym wyciekaniem cieczy z cienkiego ciekłego filmu. W tym samym czasie grubość filmu jest kontrolowana interferometrycznie z precyzją nanometrową. Jak zaprezentowano w artykule, pomiar w warunkach dynamicznych umożliwił zbadanie dynamiki wyciekania cienkiego filmu oraz określenie czasu koalescencji. Uzyskane wyniki czasu koalescencji dobrze korespondowały z czasem koalescencji mierzonym w metodzie DFI dla pojedynczego pęcherzyka jak opisano w Publikacji 2. Rodzaj grup hydrofilowych nanokryształów celulozy znacząco wpływał na morfologię filmów powierzchniowych oraz ich właściwości wiskoelastyczne. W zależności od stechiometrii surfaktant-nanocząstka film powierzchniowy dawał różną odpowiedź na zmianę ciśnienia. Filmy zawierające nanocząstki z grupami siarczanowymi wykazywały mniejsze agregaty powierzchniowe oraz były mniej odporne na zmiany ciśnienia. Nanocząstki z grupami karboksylowymi znacznie modyfikowały charakter cienkich filmów ciekłych. Filmy te zawierały dużo większe agregaty powierzchniowe, wykazywały większe czasy koalescencji oraz złożoną odpowiedź na zmiany ciśnienia i odtwarzanie ciekłego filmu: marszczenie i zwijanie powierzchniowej warstwy nanocząstek dla średnich stężeń LAE oraz mogły powodować konkurencyjną adsorpcję surfaktantu dla dużych stężeń LAE wraz z dezintegracją warstwy powierzchniowej nanocząstek. Dalsze precyzyjne badania zmian ciśnienia dla cienkich filmów złożonych z LAE i CNC mogłyby pomóc w dokładnym opisie tych fascynujących zjawisk.

PUBLICATIONS

The main findings of the PhD dissertation are published in the following articles:

Article 1. Ethyl lauroyl arginate, an inherently multicomponent surfactant system, Agnieszka Czakaj, Ewelina Jarek, Marcel Krzan, Piotr Warszyński *Molecules* **2021**, *26(19)*, 5894; DOI 10.3390/molecules26195894, IF=4.926

Article 2. Viscoelastic interfaces comprising of cellulose nanocrystals and lauroyl ethyl arginate for enhanced foam stability. Agnieszka Czakaj, Aadithya Kannan, Agnieszka Wiśniewska, Gabriela Grześ, Marcel Krzan, Piotr Warszyński, Gerald G. Fuller. *Soft Matter* **2020**, *16*, 3981-3990. DOI: 10.1039/C9SM02392E, IF=4.046

Article 3. The effect of electrolytes and urea on the ethyl lauroyl arginate and cellulose nanocrystals foam stability. Agnieszka Czakaj, Marcel Krzan, Piotr Warszyński, *Applied Sciences* **2022**, *12(6)*,2797; DOI 10.3390/app12062797, IF=2.838

Article 4. The influence of the Surface Chemistry of Cellulose Nanocrystals on Ethyl Lauroyl Arginate Foam Stability. Agnieszka Czakaj, Emmanouil Chatzigiannakis, Jan Vermant, Marcel Krzan, Piotr Warszyński. *Polymers* **2022**, *14(24)*,5402; DOI: 10.3390/polym14245402, IF=4.967.

List of symbols and abbreviations

LAE – ethyl lauroyl arginate

CNC – cellulose nanocrystals

sCNC – sulfated cellulose nanocrystals

cCNC – carboxylated cellulose nanocrystals

CMC – critical micelle concentration

DFT – density functional theory

DLVO theory – Derjaguin Landau Vervey Overbeek theory

F – free energy

s – surface area

T – temperature

V – volume

σ – surface tension

Γ_i – excess surface concentration of a species i

C_i – bulk concentration of a species i

R – gas constant

EDL – electric double layer

STDE – surface quasi-two-dimensional electrolyte

$a_s, a_{h,i}$ – activity coefficient of surface active species

$\alpha_s, \alpha_{h,i}$ – standard free energy of adsorption of surfactant ion or hydrolysis product after separating the contribution of the electric component

$\phi_s, \phi_{h,i}$ – correction for the activity of the two dimensional electrolyte in the surface layer accounting for the lateral interaction between ions

$\theta_s, \theta_{a,i}, \theta_{h,i}$ – relative surfactant surface concentration

Γ_s – surfactant excess concentration

$\Gamma_{s,\infty}$ – limiting surfactant surface concentration at the maximal coverage

H_s – surface interaction parameter defining the attractive lateral interactions among the adsorbed surfactant hydrophobic tails

$z_{h,i}$ – charge parameter

$g_s, g_{h,i}$ – the ratio of the size of surfactant cations
 Ψ_i – the electric potential in the Stern layer
 σ – surface charge density - *Equation 7*
 e – elementary charge
 ϵ_0 – vacuum dielectric permittivity
 ϵ – dielectric constant of a solution
 δ – thickness of the Stern layer
 k – Boltzmann constant
 κ – Debye - Hückel reciprocal length
 R_1, R_2 – radii of surface curvature
 Δp – pressure change
 σ_s – surface stress tensor
 τ – surface stress
 A – surface area
 I_s – surface unit tensor
 τ_v – extra surface stress
 tr - trace
 η_s – surface (interfacial) shear viscosity
 κ_s – surface dilatational (interfacial) viscosity
 U_s – infinitesimal strain tensor
 ∇_s – surface gradient operator
 v_s – surface velocity vector on the interface
 D_s – surface deformation tensor
 σ_e^B – stress tensor for the liquid-like interface
 σ_e^S – stress tensor for the solid-like interface
 K_s – interfacial dilatational modulus
 G_s – interfacial shear elastic modulus
 \mathcal{E}_r – real part of the dilatational elasticity modulus
 \mathcal{E}_i – imaginary part of the dilatational elasticity modulus
 A_0 – average area of the drop
 $\Delta A_1, \Delta \sigma_1$ – principal Fourier components of the area and surface tension variations
 ξ – dimensionless parameter of Lucassen and van den Tempel model

D – diffusion coefficient
 ω – oscillation frequency
 Π – disjoining pressure
 Π_{vdW} – disjoining pressure, van der Waals interactions component
 Π_{el} – disjoining pressure, electric component
 g – gravity constant
 ρ – density
 θ – tangential angle
 γ – shear strain
 σ_{sh} – shear stress
 B_0 – Boussinesq number
 η_s – interfacial shear viscosity
 η – bulk shear viscosity
 L – length
TFB – thin film balance
 P_c – capillary pressure
 R_{bw} – radius of the bike-wheel cell hole
 R_f – radius of the film
TEM – transmission electron microscope
 U_E – electrophoretic mobility
 ζ – zeta potential
 r_h – hydrodynamic diameter
 ϕ_c – liquid fraction

1. Introduction

1.1 Motivation

Foams are important for many technologies, including froth flotation, food technology, health care and cosmetic product development, detergency, or wastewater treatment. Liquid foams, dispersions of gas bubbles in a liquid, are unstable systems. They undergo liquid drainage by gravity and capillary suction from the regions of Plateau borders in which bubbles interconnect. Foams are also destructed by coarsening, in which gas diffuses from smaller to larger bubbles. Finally, when the liquid films are very thin, foams collapse (bubbles coalesce), which is influenced by molecular interactions.

The history of scientific research on foam films dates back to the XVII century. At that time, foam films were generally called soap films. They introduced many researchers to the world of surface science. Foams fascinated such great scientists as Boyle, Hook and Newton, who studied in detail the colour and thickness of films. Much later, Plateau and Gibbs discovered the fundamentals of our present knowledge in this field¹. After Plateau and Gibbs, Perrin extensively studied thin liquid film thickness by interferometry, describing transitions between the thinnest parts of the films. That work was continued by other researchers. Finally, Lyklema, Scholten and Mysels classified thin liquid films according to their drainage behaviour².

The concept of disjoining pressure as the derivative of the free energy with respect to film thickness was introduced by Derjaguin in the 1930s. In 1959 Sheludko and Exerowa introduced the methodology of microscopic film measurements. In the 1960s Mysels, Cox and Skewis and independently van den Tempel studied thin film elasticity as the change of the surface tension with the surface area³.

Experimentally surface forces between liquid films were first studied with the thin film balance technique by Sheludko⁴ and Mysels.^{5,6} Sheludko developed a special cell, holding liquid film connected to a liquid reservoir, with controlled hydrostatic pressure and optical reflectivity set up to measure film thickness (Sheludko cell). Mysels invented the porous plate technique that was extensively used by Exerowa⁷ and improved by Bergeron and Radke.⁸ Sheludko cell was primarily used to measure disjoining pressure in surfactant thin films. In dynamic mode, it was used to follow the dynamics of drainage with the assessment of the elasticity of the interface.

Foaming properties are desirable in food and cosmetic applications. Foams usually contain low molecular weight surfactants with some additives. These molecules are not indifferent to living organisms. They might be irritant to the body or cause allergies. From an ecological and economic perspective, they should be used in the lowest possible quantity. Common synthetic surfactants are often

replaced nowadays by green surfactants. On the other hand, the limiting of surfactant use can be achieved by synergistic foam stability enhancement by the addition of nano- or microparticles. In such systems, the mechanism of foam stability depends on both particle and surfactant properties. That includes surfactant adsorption, elasticity, dissociation, particle size, charge and wettability. The effect of particles' properties on foam stability depends closely on their interaction with the interface and their mutual interactions. For example, hydrophilic particles, like cellulose nanocrystals used in this work, are non-surface active despite having hydrophobic crystal planes, and they do not adsorb at the air-water interface. In the presence of surfactants, hydrophilic particles or particles with intermediate wettability, like cellulose nanocrystals, may adsorb to the interface either as a monolayer or as multilayer. They may be present in foam films as separate particles, aggregates or aggregates in the thin film gel state. Additionally, the aggregates can be present in the liquid and get stuck in the Plateau borders.⁹

Nanocellulose is a natural, charged polymeric component, which addition can tune various chemical properties of the mixtures, including their interfacial properties. That allows their technological applications. For example, biodegradable cellulose nanofibers were mixed with various surfactants to stabilise foams as a fracturing fluid in petroleum extraction¹⁰. Nanocellulose can be chemically hydrolyzed into purely crystalline cellulose nanocrystals form. Hexylamine-modified cellulose nanocrystals were reported to be very efficient for froth flotation of quartz¹¹. Super-stable foams made from a high content of cellulose nanofibers and hydrophobized fumed silica¹² were successfully transformed into a solid foam.

Despite numerous works on liquid foam stabilisation by cellulose micro- or nanofibers (also as solid foam precursors)¹³ or by cellulose derivatives,¹⁴ the effect of cellulose nanocrystals on foam properties is still largely unexplored research area. Dispersions with low content of water-dispersible hydrophilic cellulose nanocrystals (<1% wt.), particles having a nanometric size and low polydispersity, and very low surfactant concentrations - much below critical micelle concentration and without additional additives, have been rarely studied. In such systems, mutual surfactant and nanoparticle interactions in the thin liquid film phase are of primary importance. There, interfacial rheological properties and thin film coalescence might be effectively studied due to the negligible effect from the bulk liquid phase. Applicability of similar, diluted CNC-surfactant dispersions also has new emerging applications, like the generation of supercritical CO₂ emulsions and foams that can be used for potential underground carbon storage to mitigate global warming¹⁵. Surfactant presence in dispersions also has a huge impact on the production of spray-dried nanocellulose granules, which gain new morphologies with the surfactant presence in spray-drying dispersions¹⁶. Those properties can be important for multiple applications like the design of drug delivery systems¹⁷.

Ethyl lauroyl arginate (LAE) is an amino acid-based surfactant. It is considered as green, biocompatible, and safe for food processing and cosmetic applications¹⁸. It is synthesized from L-arginine, lauric acid and ethanol.¹⁹ In neutral pH it is cationic due to charged guanidine group. LAE has strong antimicrobial activity against molds, yeasts and bacteria as it can penetrate the cytoplasmic

membrane^{20,21,22} but it also has low toxicity as it can be hydrolysed by chemical and metabolic pathways into components that are further easily metabolised.^{23,24} LAE reveals strong binding to negatively charged biopolymers and nanoparticles so it can be used to modify their surface properties for particular applications including improvement of stability of emulsions²⁵ and foams.²⁶ The surface activity of LAE, despite its wide use in the food industry as a food preservative and antimicrobial agent and in the cosmetic industry as a green, biodegradable surfactant, was not thoroughly characterized before. There are also no detailed data on its adsorption isotherm, and the reported surface activity of commercially used surfactants varied to a large extent, which can lead to wrong conclusions. Due to chemical instability, the surface activity of surfactant, even with the highest purity, might differ after prolonged storage so detailed data are of the highest demand.

Ethyl lauroyl arginate can form biodegradable foam and stabilize liquid interfaces in various consumer products with addition of cellulose nanocrystals. LAE-CNC interactions are governed by electrostatic attraction at lower surfactant concentrations and hydrophobic interaction and polymer-induced micellization at higher ones.²⁷

The mixture of LAE with cellulose nanocrystals with different properties, considering the stability of liquid/air interface and foaming, is an interesting research topic with practical significance. Mixtures of cellulose nanocrystals and surfactants form complexes of various sizes, surface properties and surface charge. As cellulose nanocrystals have mainly hydrophilic character, the explanation of LAE-CNC suspension thin liquid film stability, the determination of coalescence time in relation to its surface activity, interfacial rheology, nanoparticles surface charge and aggregation is relevant, complex and interesting research aim.

Foam column stability is a fundamental and technologically relevant observation in macro-scale experiments. Foam column stability has a multi-parameter character: it depends on the thermodynamic properties of the interface as well as on the drainage dynamics and coalescence of thin films, in which molecular forces are at play. At the same time, the air diffuses from smaller to larger bubbles. That changes the size and the area of the air/liquid interface, with the different adsorbed species and response to interfacial forces. A wide variety of interfacial rheology responses can be seen at this point²⁸. That response can be visualised and assessed by a single bubble and film interferometry. Furthermore, it can be studied by various rheological techniques, including pendant drop oscillations to study mainly surfactant transport or by interfacial shear rheology to assess viscoelastic properties in two dimensions. Single bubble experiments are relevant to foaming behaviour in macroscale systems and can model coalescence in macroscopic systems. Knowledge of these properties can help design functional interfaces in various food and cosmetic products.

1.2 Adsorption of surfactants – basic information

Surfactants are a special class of molecules with amphiphilic properties showing a tendency for adsorption at interfaces and aggregation in water. The word “amphiphilic” originates from ancient Greek. It translates as amphi – both, philic – love. Amphiphilic properties are related to the preference of the molecules to occur in both phases, at their boundaries. In the case of the aqueous liquid phase, we define components as hydrophilic (“water-preferring”) or hydrophobic (“water-repelling”).

Surfactants have both properties: they are partially hydrophilic and partially hydrophobic. The hydrophobic part usually contains a hydrocarbon chain of various lengths. Simple surfactant classification relates to their hydrophilic group charge, which may be cationic, anionic, non-ionic or zwitterionic (dual opposite charge). The typical industrial classification relates to their functionality. A separate group of surfactants consists of so-called green surfactants, either derived from natural products or biodegradable with the special class of amino acid-based surfactants.

The most important property of surfactants is their tendency to accumulate at the interface. The interface separates two distinct phases solid and liquid, solid and gaseous or liquid and gaseous. All the molecules in the liquid are attracted by their neighbours and the system tends to minimize its free energy. Therefore, the extension of the interface area in constant temperature T without the volume change ($V=\text{const}$) needs the amount of free energy, defined in thermodynamics as surface tension σ .

$$\left(\frac{\partial F}{\partial s}\right)_{T,V} = \sigma \text{ [J m}^{-2}\text{]}$$

Equation 1

where, F denotes the free energy, s surface area.

Variation of the surface tension upon adsorption at the interface with bulk concentration is a fundamental feature that characterizes surfactants. The accumulation of surfactants at the interface by adsorption and their rearrangement changes the free energy of the surface.

Amphiphilic molecules with sufficiently long hydrocarbon chain aggregate into structures called micelles to minimise contact of the hydrophobic part of the molecules with water. In such a configuration, they minimise the free energy of the mixture. Initially, amphiphilic molecules are present in the solution as monomers. Aggregation starts after reaching a certain concentration, which is called critical micelle concentration (abbreviation: CMC). Micelles can form spheres with hydrophobic tails pointing inwards, cylinders, spherical or flat lipid bilayers or reversed micelles, depending on the structure and size of a surfactant molecule. At critical micelle concentration, some solution properties like surface tension, electrical conductivity, osmotic pressure and turbidity discontinuously change. At CMC, surface tension reaches a plateau, surfactants no longer adsorb at the interface but aggregate into micelles.

Out of equilibrium surfactant adsorption may induce spatial gradients of the surface tension, which are associated with the mass (liquid) transfer along an interface from the regions of low surface tension to the regions of high surface tension. That is called the Marangoni effect.

1.3 Interfacial tension and rheology

Ethyl lauroyl arginate is a positively charged surfactant of pKa at about 10-11 and the isoelectric point above 12. Its molecular weight is 421 g/mol. In an aqueous solution at 25°C it is stable for more than one year at pH 4 but only 57 days at pH 7 and 34 hours at pH 9,²⁹ which is indication of base-catalysed decomposition. Therefore, for the description of the LAE adsorption at the water/air interface an adequate theoretical model needs to be used. Adsorption isotherm is defined as the dependence between the change of chemical potentials of substances present at the interface and the surface tension at constant temperature and pressure. The interface separates two homogenous phases and according to Gibbs is volume-less³⁰. As surfactants tend to accumulate at the interface sum of the amount of all species in the two neighbouring phases considered as homogeneously distributed differs from the total amount and the difference per surface area is the excess surface concentration Γ_i .

The equation describing surfactant adsorption was mathematically derived by J.W. Gibbs. For surfactant monolayers the surface excess concentration of a species, Γ_i , is related directly to its activity, a_i , and at equilibrium is described by the following Gibbs formula:

$$\Gamma_i = -\frac{1}{RT} \left(\frac{\partial \sigma}{\partial \ln a_i} \right)_{T,V}$$

Equation 2

in which σ is surface tension, T is temperature, V is volume and R is gas constant.

At low concentrations of surfactant, in particular for non-ionic ones, the activity can be replaced by bulk concentration, c_i ,

The adsorption isotherm is defined as the relation between bulk surfactant concentration and surfactant adsorption Γ at equilibrium. As an example, the Langmuir adsorption isotherm originally derived for molecules in the gas phase adsorbing at the surface:

$$\Gamma = \frac{b}{RT} \frac{ac}{1 + ac}$$

Equation 3

In the Langmuir model molecules adsorb at the surface as a monolayer, and there is a dynamic equilibrium between adsorption and desorption, while adsorption is proportional to the surface area unoccupied by molecules and desorption is proportional to the surface area occupied by molecules.

The Langmuir isotherm can be put into the Gibbs formula to recover the dependence first derived by Szyszkowski for empirical relation between the surface tension of fatty acid solutions and their bulk concentrations.

$$\sigma_0 - \sigma = b \ln(1 + ac)$$

Equation 4

The adsorption of surfactants at the liquid/gas or liquid/liquid interfaces can be modelled by Langmuir or more complex models such as Frumkin or Helfand, Frish, and Lebovitz (HFL) isotherms. They describe well the adsorption of single nonionic surfactants with a limited number of adjustable parameters.

Thermodynamic description of ionic surfactant adsorption at the interface of liquid and gas phase is complex as the system is multicomponent. In the simplest case it contains surfactant ions, counterions and electrolyte ions. The description in terms of the integration of the Gibbs adsorption equation at equilibrium cannot give information about the structure of the adsorption layer and distribution of the surfactant ions and other salt ions at the interface. In such cases, other models should be used³¹. They are based on the assumption of the condition of equilibrium for all components in bulk and in the adsorbed layer, which can be expressed as the requirement of equal electrochemical potentials³². The electrochemical potential of each component at the interface depends on the surface concentration, but it also considers the chemical interactions with all other species present at the interface. These interactions are accounted for by the activity coefficient, which depends on their surface concentrations and takes into account electrostatic interactions between ions in the surface layer, the excluded volume effects or lateral interactions of hydrophobic chains. An adsorption of ionic surfactant is always accompanied by the electric double layer (EDL) formation at the interface. The electric potential of the EDL hinders further adsorption of the ionic surfactant, facilitates the adsorption of counterions and ions with an opposite sign than surfactant ions and presumably does not influence the nonionic surfactant adsorption. An electric double layer model for ionic surfactant adsorption was used by several research groups. Davis and Rideal used Gouy-Chapman theory to describe the electric double layer and considered the adsorption of surfactant ions based on the Langmuir isotherm.³³ Diamant and Andelman³⁴ presented a model of the kinetics of surfactant adsorption at the liquid interfaces based on free energy formulation. The model described diffusive transport from the bulk to the interface and kinetics at the interface for nonionic and ionic surfactants in the presence and absence of added salt. The model was extended by Borwankar and Wasan,³⁵ who used Frumkin adsorption isotherm to describe the adsorption of surface active ions. In these models, there is an assumption that surfactant ions adsorb at the interface in the Stern layer and the counter ions remain in the diffuse part of the double layer and

the surface potential depends on the charge of adsorbed surfactant ions and the ionic strength of the solution. Kalinin and Radke extended the model, including Graham's triple-layer electrostatic structure of the interface: a surface layer of adsorbed surfactant, a plane of bound counterions (inner Helmholtz plane), and a diffuse double layer commencing at the plane of the hydrated co-ions and counterions (outer Helmholtz plane).³⁶ Kralchevsky and Danov modified that model taking into account that counterions of a certain size could bind to the ionic headgroups.³⁷ In the model of Warszyński and co-workers^{38,39} penetration of counterions into the interfacial Stern layer was postulated. The assumption of this model is the formation of the “surface quasi-two-dimensional electrolyte” (STDE), in which the electroneutrality condition at the interface is not fulfilled due to interfacial surface charge originating from the difference in surfactant ion and counterion surface concentrations. The surface potential is determined by the adsorption of ionic surfactant, counterions and ionic strength of the solution.

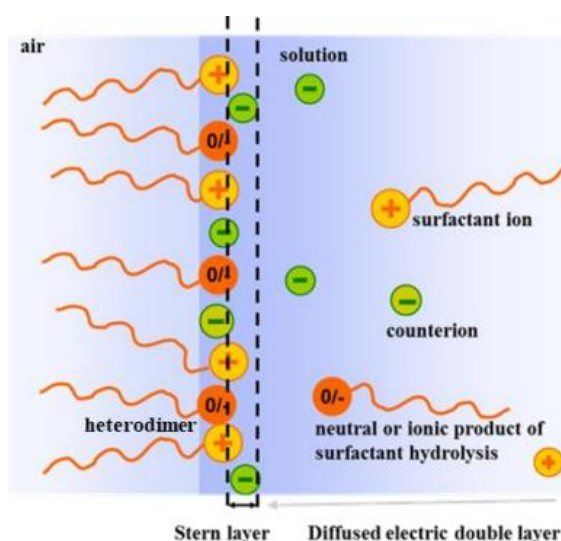


Figure 1. Schematic description of the double layer structure in STDE model.

The STDE model of ionic surfactant adsorption was first used to describe surface tension and surface potential isotherms of SDS in the presence of NaCl.⁴⁰ Warszyński, Lunkenheimer and Czichocki modified this model by taking into account the lateral interactions in the Stern layer.⁴¹ The STDE model was applied for the adsorption of cationic surfactants with different anions⁴² and ionic – nonionic surfactant mixtures adsorption at air/solution interfaces.⁴³ Therefore, it can be used for the description of LAE solutions, which, also contain surface active products of surfactant decomposition.

The mathematical formulation of the model is based on the equilibrium condition for adsorption of surfactant ions, surfactant-counterion associates (dimers), hydrolysis products and other ions present in the solution from the solution to the Stern layer and assuming that the excluded volume effects and the lateral interactions between the hydrophobic parts can be accounted for by the Frumkin model. The equation for cationic surfactant has the form:

$$\frac{a_s}{\alpha_s} \exp\left(-\frac{e\psi_s}{kT}\right) \left(1 - \theta_s - \sum_i \theta_{h,i} - \sum_i \theta_{a,i}\right) = \theta_s \exp\left[-2H_s \left(\theta_s + \sum_i \theta_{h,i}\right)\right] \exp\left(\frac{\phi_s}{kT}\right)$$

Equation 4

The equation for neutral or charged hydrolysis products can be written as

$$\begin{aligned} \frac{a_{h,i}}{\alpha_{h,i}} \exp\left(-\frac{z_{h,i}e\psi_s}{kT}\right) \left(1 - \theta_s - \sum_i \theta_{h,i} - \sum_i \theta_{a,i}\right)^{g_{h,i}} \\ = \theta_{h,i} \exp\left[-2H_s \left(\theta_s + \sum_i \theta_{h,i}\right)\right] \exp\left(\frac{z_{h,i}\phi_{h,i}}{kT}\right) \end{aligned}$$

Equation 5

a_s is the activity coefficient of surface active species that can be calculated from the extended Debye – Hückel theory of strong electrolyte solutions;

α_s is a measure of the standard free energy of adsorption of surfactant ion after separating the contribution of the electric component

$a_{h,i}, \alpha_{h,i}$ refers to neutral or ionic hydrolysis products

ψ_s is the electric potential in the Stern layer

$\phi_s, \phi_{h,i}$ is the correction for the activity of the two dimensional electrolyte in the surface layer accounting for the lateral interaction between ions

$$\theta_s = \frac{\Gamma_s}{\Gamma_\infty}$$

is the relative surfactant surface concentration, where Γ_s is surfactant excess concentration and $\Gamma_{s\infty}$ is the limiting surfactant surface concentration at the maximal coverage

$\theta_{a,i}$ and $\theta_{h,i}$ are the same quantities for dimers and electrolyte anions

H_s is the surface interaction parameter defining the attractive lateral interactions among the adsorbed surfactant hydrophobic tails

$z_{h,i}$ is the charge parameter, $z_{h,i} = 0$ for neutral dimer, -1 for anionic dimer

$g_s, g_{h,i}$ are the ratios of the size of surfactant cations, dimers relatively to the size of the adsorption site; for surfactant g_s is taken as 1

A separate equation is defined for adsorption of ions in the Stern layer³².

The electric potential in the Stern layer ψ_s is determined from the equation:

$$\psi_s = \psi_d + \frac{\sigma \delta}{\varepsilon_0 \varepsilon_s}$$

Equation 6

in which σ is the surface charge density derived from all the ions adsorbed in the Stern layer,

$$\sigma = F \left(\Gamma_s - \sum_i \Gamma_{h,i} - \sum_i \Gamma_{a,i} \right)$$

Equation 7

F is Faraday constant ψ_d is the electric potential at the boundary of the Stern layer and the diffuse part of electric double layer, δ is the thickness of the Stern layer and ε_0 the dielectric permittivity of the vacuum.

The diffuse layer potential at the boundary between the Stern layer and the diffuse part of electric double layer can be determined from the formula:

$$\left(\psi_d = \frac{2kT}{e} \sinh^{-1} \left(\frac{\sigma e}{2\varepsilon_0 \varepsilon_s k T \kappa} \right) \right)$$

Equation 8

where: e is the elementary charge, k is the Boltzmann constant, ε_0 is the vacuum dielectric permittivity, ε is the dielectric constant of the solution, κ is the Debye - Hückel reciprocal length.

By the numerical solution of the set of equations 4-5 the surface concentration of all components in the Stern layer can be determined directly. Total surface excess concentration of all components Γ_j^T has to include the adsorption of all electrolyte and surfactant ions in the diffuse part of the electric double layer, where the distribution of ions has to be found using the solution of the Poisson-Boltzmann equation. Finally the surface tension of the solution is calculated by integration of the Gibbs equation for the mixture of all components:

$$d\gamma = -RT \left(\sum_j \Gamma_j^T d \ln a_j \right)$$

Equation 9

The surface tension can then be compared with experimental data to calculate values of parameters of STDE model. The data quantitatively characterize the adsorption layer, including the kind of species which are preferentially adsorbed.

Surfactants and their mixtures with interfacially active species that stabilize bubbles can form complex interfaces. The properties of such interfaces can be measured by various techniques described in the next paragraphs. The experimental methods should be selected with special attention considering fundamental knowledge and basic methodology as given below.

If we consider a curved fluid – fluid interface, the increment in pressure Δp is caused by tangential surfaces stress.

$$\Delta p = \tau \left(\frac{1}{R_1} + \frac{1}{R_2} \right)$$

Equation 10

Where R_1, R_2 refer to radii of surface curvature and τ – surface stress function.

Surface stress function τ in Equation 10, first proposed by Gibbs, is often substituted by surface tension σ , and the equation is known as the Young-Laplace equation. In that form it can be applied only for simple interfaces, including interfaces with soluble surfactants.⁴⁴ For compressible liquid interfaces, it is possible to calculate the response of the interface to small changes of surface area A , known as Gibbs elasticity modulus⁴⁵.

$$E = \frac{d\sigma}{d \ln A}$$

Equation 11

For insoluble monolayers, systematic variation of the surface area and the resulting surface pressure (the difference between surface tension with and without the film) are usually measured by Langmuir trough. Since molecules do not diffuse into the bulk phase, the surface pressure increases as the layers are compressed. Equation 11 might be used to obtain the surface stress as a function of the deformation of the interface, which is a true 2D material function of a deformed microstructure⁴⁶. Care should be taken, however, as monolayers can exhibit rich phase behaviour.

For soluble monolayers, additional interfacial transport processes of surfactant to and from the interface are involved: after expansion of the area of the film, diffusion of surfactant to the depleted film surfaces will decrease the excess surface tension, and the measured modulus E is only the estimate of a true material function.

A general expression for the surface stress for a rheologically complex interface is expressed as a tensor:⁴⁷

$$\sigma_s = \sigma(\Gamma, T)I_s + \tau_v$$

Equation 12

Where $\sigma(\Gamma, T)$ is interfacial or surface tension, a state variable that depends only on excess concentration and temperature, I_s is the surface unit tensor and τ_v is the extra surface stress.

The elasticity of surfactant monolayers can be studied experimentally by dilatational experiments by imposing sinusoidal area changes to the interface and measuring the surface tension of the deformed interface. In oscillating bubble or oscillating drop methods, surface tension is calculated by analyzing the profile of the bubble or the drop. In the bubble pressure tensiometry the pressure in the interior of the bubble is measured⁴⁸. The applicability of the Young – Laplace equation for oscillating drop experiment is possible when several conditions are fulfilled⁴⁹:

- in-plane inertial stresses are negligible,
- stresses resulting from gradients in surface tension are negligible,
- contributions from in-plane viscous stresses may be ignored,
- inertial and viscous stresses exerted on the interface by the adjoining bulk phases may be neglected,
- the applied deformation is uniform.

Taking the above into consideration and linking Equation 10 and Equation 12, the pressure difference over the interface is given by the formula:

$$\Delta p = 2\sigma \left(\frac{1}{R_1} + \frac{1}{R_2} \right) + 2 \left(\frac{1}{R_1} + \frac{1}{R_2} \right) tr(\sigma_s)$$

Equation 13

In which $tr(\sigma_s)$ is the trace of the surface extra stress tensor.

When the response of the interface is surface tension dominated, the deformation of the interface changes the surface concentrations. In such a case, the magnitude of the dilatational rheological properties is determined by the rate of exchange of the surface active components between the interface and the adjoining bulk phases⁵⁰. Thermodynamic and rheological properties, especially the contribution for purely elastic interfaces, can be decoupled by choice of experimental conditions and scaling⁵⁰.

For a liquid-like, viscous interface, the stress tensor σ_e^B can be described by the Boussinesq-Scriven model.⁵¹

$$\sigma_e^B = [(\kappa_s - \eta_s)\nabla_s * \mathbf{v}_s] \mathbf{I}_s + 2\eta_s D_s$$

Equation 14

In which κ_s is surface dilatational (interfacial) viscosity, η_s is the surface (interfacial) shear viscosity, ∇_s is the surface gradient operator, \mathbf{v}_s is the surface velocity vector on the interface and D_s is the surface deformation tensor. The stress tensor σ_e^S for a solid-like elastic interface is described by a linear elastic model,⁵² which is valid for infinitely small deformations.

$$\sigma_e^S = [(K_s - G_s)\nabla_s * \mathbf{u}_s] \mathbf{I}_s + 2G_s U_s$$

Equation 15

In which K_s is the interfacial dilatational modulus equal to the inverse of the isothermal compressibility of the interface and represents the resistance of the interface against in-plane all-sided compression⁵³, G_s is the interfacial shear modulus, u_s is the surface displacement vector, and U_s is the infinitesimal strain tensor.

For soluble surfactants, the value of dilatational modulus as defined by Equation 11 can be approximated by measurement of the surface tension when periodically changing the area of the bubble or drop. In such measurements the diffusion is not limited by the thickness of the liquid film but by the time scale of periodic area variations and the modulus can be described by the Lucassen-van den Tempel model.⁵⁴ In this model, the harmonic response of surface tension to surface area changes in pendant drop experiments⁵⁵ is expressed by surface dilatational modulus, a complex number⁵⁶ given by the formula:

$$\varepsilon = \varepsilon_r + i \varepsilon_i = A_0 \frac{\Delta\sigma_1}{\Delta A_1}$$

Equation 16

ε_r , ε_i , are the real and imaginary parts of the dilatational elasticity modulus, A_0 is the average area of the drop, ΔA_1 and $\Delta\sigma_1$ are the principal Fourier components of the area and surface tension variations that correspond to the frequency of drop oscillations. Dilatational modulus is a complex number obtained in certain experimental conditions, so it can not replace the modulus K_s as presented in Equation 15 for a purely elastic interface.

At sufficiently high frequencies, molecules cannot diffuse due to the rapidly expanding interface, and elasticity is equal to the limiting value of an insoluble surfactant monolayer.

$$\varepsilon_0 = \left(\frac{d\sigma}{d\ln A} \right)_N = \frac{-d\gamma}{d\ln\Gamma} = \frac{d\Pi}{d\ln\Gamma}$$

Equation 17

The definition of the modulus as given in Equation 17 is similar in this form to the definition of Gibbs but in reality ε_0 has a different meaning. The limiting elasticity ε_0 can be calculated for high-frequency limit from Lucassen-van den Tempel equations, whereas, for soluble surfactants the measured elasticity is always lower than that limiting value.

$$\varepsilon = \varepsilon_0 \frac{1 + \xi + i\xi}{1 + 2\xi + 2\xi^2}$$

Equation 18

$$\xi = \frac{dc}{d\Gamma} \sqrt{\frac{D}{2\omega}}$$

Equation 19

ξ is dimensionless parameter in the model, D is the diffusion coefficient and ω is the oscillation frequency.

The limiting elasticity ε_0 must be lower than the limiting value for an insoluble monolayer as shown in Equation 17. The limiting elasticity is thus not formally the Gibbs elasticity, but it depends exclusively on the surface equation of state⁵⁷.

1.4 Thin films

The fundamental explanation of foam stability is based on the molecular theory of surface forces in dispersed systems (foams and emulsions) that stabilize thin liquid films of thickness less than 100 nm. The theory of dispersion stability based on electrostatic and van der Waals interactions was formulated by Derjaguin, Landau⁵⁸, Verwey and Overbeek⁵⁹ (DLVO theory). The surface force of molecular origin (usually referred to as the disjoining pressure for thin liquid films, i.e. force per unit area of the film) is the sum of electrostatic and van der Waals interactions components:

$$\Pi = \Pi_{vdw} + \Pi_{el}$$

Equation 20

The van der Waals forces Π_{vdw} represent an averaged dipole-dipole interaction, a superposition of three contributions: orientation interaction between two permanent dipoles, induction interaction between one permanent dipole and one induced dipole, and dispersion interaction between two induced dipoles. The electrostatic - double layer interactions Π_{el} originate from the overlap of the double electric layers formed at two charged interfaces. Special oscillatory structural forces are present in thin films containing small colloidal particles: surfactant micelles, polymer coils, protein macromolecules, or charged particles.⁶⁰

Short-living bubbles can be created even in pure air/water or water/oil interfaces. There is evidence of a very weak interfacial charge of these pure interfaces.⁶¹ Such a weak charge, however, does not stabilize liquid films efficiently by the electrostatic repulsion of film interfaces. Thus, without surfactants, the interactions in foam films are mainly attractive van der Waals interactions and short-range hydrophobic forces. Adsorption of ionic surfactants introduces charge at the interface, and the surface potential grows. Strong electrostatic repulsion at the interface counterbalances van der Waals attraction, which leads to thin film stabilization.

Thin liquid film forms and evolves at the fluid interfaces upon the simultaneous action of disjoining pressure and hydrodynamic forces with the appearance of the dimple (instability) at the interface approach when hydrodynamic pressure exceeds capillary pressure. Then film evolution is

followed by growth and outflow of the dimple, formation of the plane-parallel film, metastable primary thin film (common black film) stabilised by long-range repulsive forces, and eventually, if the film did not break before, thin and stable Newton black film is created, which is stabilised by short-range repulsive forces. Thus, the dynamics of film draining is controlled by the complex interplay of capillary and intermolecular forces as well as hydrodynamic and interfacial stresses. Small differences in the balance of forces can result in thin film lifetimes spanning over six orders of magnitude.⁶²

Dimple dynamics and thin film stability depend on the rheological properties of the interface. If the monolayer has a large interfacial elastic modulus, the dimple remains centrosymmetric, and the interface is immobile. In case of the mobile interface, instability can occur in which the dimple loses its circular shape and is washed out rapidly into the film border.⁶³ During this process, the film often ruptures. The threshold for dimple wash-out is predicted to depend upon the interfacial shear viscosity.

1.5 Foam formation and stability

Foams are dispersions of gas bubbles in a liquid. Gas bubbles have various shapes and interconnect by Plateau borders. The amount of liquid trapped in the foam divided by the total foam volume defines the liquid fraction ϕ_c . The maximum value of the liquid fraction, or critical liquid fraction ϕ_C , is thus $\phi_C \approx 0.36$, as obtained theoretically for random packings of (monodisperse) hard spheres. Foams with a liquid fraction higher than about 0.15 are referred to as wet foams. Foams with ϕ less than about 0.05 are called dry and their bubbles are nearly polyhedral in shape.⁶⁴

All foaming techniques require generating bubbles within a liquid. That implies the creation of gas/liquid interfaces of interfacial tension γ and an energy input of at least $U = 4\pi\gamma r^2$ per bubble of the radius r . For typical interfacial tensions and bubble sizes, this is many orders of magnitude larger than thermal energies (kT), which means that bubble formation is not a spontaneous process and much energy is required to create a foam. Foams can be prepared by physical methods with various techniques, including bubbling, sparging, wave breaking, shaking, mixing, blending or the double syringe technique⁶⁵. Among them, the double syringe method is a well-established technique which facilitates fixing the initial liquid fraction in foams. Two identical syringes are connected by a narrow tube and the air is injected by back and-forth pushing of the pistons of the syringes. The method is precise, mainly when performed automatically. It was applied to study bubble size evolution in foams prepared with different surfactants and gases⁶⁶. The double syringe method became well known in medicine for foam sclerotherapy in the treatment of varicose veins. The efficacy of sclerosing foam compared with sclerosing liquid in the therapy of the greater saphenous vein was reported as superior⁶⁷. Foam sclerotherapy is a well-known method of treatment with rare serious adverse effects⁶⁸. The optimisation of the double syringe foam preparation method for varicose vein sclerotherapy with the drug sodium morrhuate was described with a very experimental approach in Nature Scientific Reports.⁶⁹ Foam

sclerotherapy is a very interesting example showing how important tuning the foam stability is in the macroscopic system under many medical constraints⁷⁰.

Three main processes are responsible for foam stability: coarsening – diffusion of gas from bubbles, drainage – an outflow of the liquid from thin films and coalescence – merging of two interfaces. Foamability can be directly correlated with surfactant adsorption rate at the interface and its competition with drainage. Experiments for both non-ionic and ionic surfactants showed that obtained foam volume is directly correlated with the Gibbs elasticity.⁷¹

Unlike surfactant molecules, the adsorption of nanoparticles at the air-liquid interface is usually irreversible. Nanoparticle-covered interfaces show high surface elasticity⁷² and prevent foam coarsening.⁷³ Adsorbed nanoparticles reduce the rate of film thinning.^{74,75} Binks et al. demonstrated that, when combined, nanoparticles and surfactants produced very stable foams at a suitable surfactant concentration.⁷⁶ The stabilisation mechanism in surfactant-nanoparticle systems depends on various interactions: between surfactant molecules, between surfactant and nanoparticles and between nanoparticles.⁷⁷ For soluble surfactants, surfactant-nanoparticle interactions might be of primary importance.⁷⁸ As an example, hydrophobic, polymeric microrod particles without any additives stabilised foams for over 3 weeks due to the formation of rigid hairy shells and microrod entanglement,⁷⁹ but with the addition of sodium dodecyl sulfate, the foam broke in 30 minutes. It was hypothesized that surfactant addition made particles more hydrophilic. On the contrary, it was demonstrated in many studies that the addition of surfactant to partially hydrophilic particles made them more surface active and enhanced the interfacial elasticity. Ravera et al. showed that cetyltrimethylammonium bromide increased the surface activity of silica nanoparticles and applied Lucassen-van den Tempel model to describe the elasticity of the CTAB-silica monolayer at water/hexane interface.⁸⁰ For a relatively small amount of silica nanoparticles (1% wt.), diffusional transport at the interface dominated, but it changed to kinetic-controlled after the ageing of the interfacial layer. That was accompanied by wrinkling of the interfacial layer around the droplet.

Foams containing nanoparticles might be very stable when surfactant and nanoparticle concentrations are high or the liquid suspension phase gels,⁸¹ but for some systems it is achieved even without gelation. For example, multilamellar tubes, having the advantages of solid particles and the low-molecular weight amphiphiles, formed stable foam when mixing 12-hydroxystearic acid with oppositely charged ethanolamine or hexanolamine.⁸²

Cellulose nanocrystals are an excellent candidate for liquid foam stabilisation due to their availability, dispersivity in water and low toxicity.⁸³ Crystalline cellulose particles are released from polymeric cellulose material by acid hydrolysis. Depending on the process, they possess different hydrophilic groups by replacing hydroxyl (-OH) surface groups. What is also essential they can show different surface charge and dispersivity.⁸⁴ Wood-derived cellulose nanocrystals with sulfate ester groups are commercially available as a spray-dried powder that needs to be redispersed in water without

aggregation. Since they are highly hydrophilic and do not exhibit any surface activity, hydrophobic modification or the addition of surface active components is needed to use them as foam stabilisers.^{85,86} Carboxylated cellulose nanocrystals (cCNC) are produced by dilute oxidation with hydrogen peroxide.⁸⁷ The cCNC has a lower surface charge density than sulfated cellulose nanocrystals (sCNC). They are also less crystalline.

Cellulose is chiral in many length scales, from molecules up to mesophases.⁸⁸ Nanocellulose crystals and fibres are twisted, which affects the exposure of their more hydrophobic planes at the air/water interface. CNC may form liquid crystals in water.⁸⁹ The liquid crystalline behaviour of CNC is solvent-dependent. At lower dielectric screening, they are more hydrogen-bonded and form needle-like elongated micro-aggregates.⁹⁰

The addition of cellulose nanocrystals might stabilise foams by the formation of a gel phase upon the addition of methylcellulose.⁹¹ In other reports, significantly large cellulose nanofibers were used for foam preparation, while the addition of amines was essential for cellulose hydrophobicity.⁸⁵ There are fewer reports on CNC foam stabilisation in which cellulose nanocrystals concentration does not exceed 1% and without adding polymers. Interesting observations were made for CNC emulsion stabilisation, pointing to the aspect ratio of nanocellulose as a key parameter for the stability of Pickering emulsion.⁹² Emulsion stability was inversely proportional to the surface charge density of cellulose nanocrystals since less charged CNC were more amphiphilic.⁹³ Importantly, screening of CNC surface charge with the addition of salt can impact their surface properties.⁹⁴ Cellulose nanocrystals might form more hydrophobic aggregates with electrolyte addition. A similar effect can be achieved with charge screening by surfactant. Specifically, the droplets of sunflower emulsion were stabilized by the complexes of LAE and CNC containing partially neutralized CNC at low LAE addition or by surfactant admicelles at higher LAE concentration.²⁵

1.6 Experimental methods for studying thin films dynamics

The drop and bubble profile analysis tensiometry is well-established method for measuring the dynamic surface and interfacial tensions of liquid interfaces. The method is suitable both for liquid/air and liquid-liquid interfaces with the time scale of experiments from 1 second to days. Precisely controlled liquid amount and temperature enable experiments involving long adsorption processes. The set-up integrates a dosing system and a thin capillary at the tip of which the drop or bubble is formed. With a video camera an image of the drop is taken, digitized and transferred to a PC. The light source is required to get a sharp image of the drop profile⁴⁸. The software determines the coordinates of the drop profile by image analysis. Then, the Young-Laplace equation is fitted to the drop profile. The target function describing the sum of the squares of the distances between the experimental points and the calculated curve needs to be minimized. The input parameters except drop coordinates are density difference across the interface, the gravitational constant, and the distance between the base of the drop and the horizontal

coordinate axis. The output parameters are interfacial tension, the drop surface area, the drop volume and local radius of curvature, which are determined from the set of equations:

$$\frac{dx}{ds} = \cos\theta$$

Equation 21

$$\frac{dz}{ds} = \sin\theta$$

Equation 22

$$\frac{d\theta}{ds} = \frac{1}{R_1} \pm cz - \frac{\sin\theta}{x}$$

Equation 23

s is the arc length as shown in Figure 2, x,z are coordinates of the drop profile, R_1 is the radius of curvature at (x,z), $c = \frac{\Delta\rho g}{\sigma}$ is the capillary constant of the system, θ is the tangential angle.

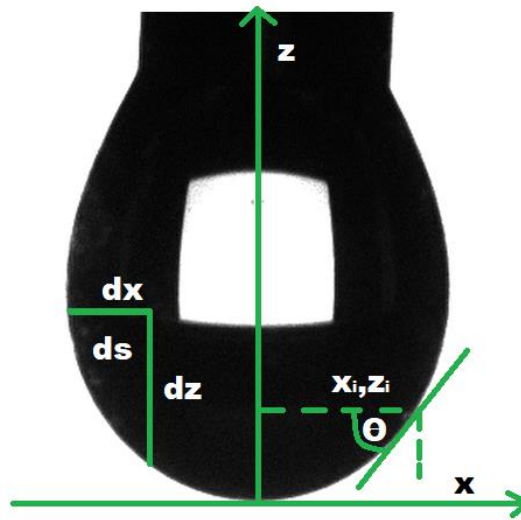


Figure 2. The image of the shape of a pendant drop with coordinates indicated.

The set of the above equations can be solved by numerical integration according to the Runge-Kutta-Verner integration algorithm.⁹⁵

Precise control of the drop volume in the drop tensiometer enables the accurate change of the surface area by imposing periodic drop volume changes. Sinusoidal perturbations are most advantageous and therefore, most often used in interfacial rheological or relaxation studies⁴⁸⁸. The volume $V(t)$ of the drop or bubble is changed in a harmonic way with a dosing system. As the drops or bubbles have a quasi-equilibrium shape at any moment during slow oscillation, the interfacial tension and surface area

are determined with drop shape analysis as previously described. The phase shift between surface tension and the surface area must be determined accurately by Fourier analysis.

Pendant drop dilatational experiments can reveal the complexity of surfactant-covered interfaces when the response to dilation is non-linear.⁹⁶ In such cases, there is a strong interaction between molecules and the surface stress of the interface needs to be expressed as a tensor with respect to the strain. The knowledge of extra stresses at the interface can be obtained from interfacial shear rheometry with in-plane interface deformation conducted at constant surface area and applying shear force F . The general definition of the shear force (in between two plates) is shown in Figure 3.

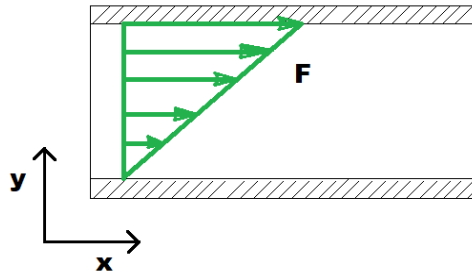


Figure 3. The illustration of the shear force.

By displacement of the top plate with the shear strain $\gamma = \frac{dx_x}{dy}$ the shear stress σ_{sh} is generated in area A .

$$\sigma_{sh} = \frac{F}{A}$$

Equation 24

The ratio of the shear stress to the shear strain is defined as the shear modulus, which is a material property.

$$G = \frac{\sigma_{sh}}{\gamma}$$

Equation 25

In interfacial shear rheometry, interfacial flows are created either by moving solid boundaries within the interface or by applying gradients in surface pressure. Special care should be taken to decouple the surface and bulk fluid stresses, which practically means the analysis in the limit of a high Boussinesq number,⁴⁴ and using the rheometer that minimizes the measurement probe and maximizes the contact perimeter between the surface probe and the interface and the contact area with the surrounding subphases. Boussinesq number B_0 is defined as the equation

$$B_0 = \frac{\eta_s}{\eta L}$$

Equation 26

where η_s is the interfacial shear viscosity, η is the bulk shear viscosity and L is a length scale defined by the geometry of a given problem.

Those conditions are fulfilled by applying the double wall ring (DWR),⁹⁷ which is mounted onto a sensitive rotational stress rheometer.

Experimentally the evolution of liquid films are usually studied by the thin film balance (TFB). In the experimental cell the film drains due to the capillary pressure of the cell's hole, which is approximated by the formula:

$$P_c = \frac{2\sigma R_{bw}}{R_{bw}^2 - R_f^2}$$

Equation 27

where R_{bw} is the radius of the hole, and R_f - the radius of the film.

In a modified version of the Sheludko cell, the thin film balance with so-called bike wheel cell, the thin film hole is connected radially to the external annulus by 24 channels.⁹⁸ In such a configuration, larger disjoining pressure can be measured, and drainage is radial and uniform. The flow rate or the driving pressure can be controlled using either a syringe pump or a more sensitive piezoelectric pressure system with active feedback control⁹⁹. Thin film balance can visualize Marangoni flows, micelles or particles structuring in the thin film, the existence of aggregates, nucleation of lipids and black film formation.¹⁰⁰

In the dynamic method of thin film balance, the pressure is applied to the initially pre-equilibrated thin film, which induces drainage. The film might break after the pressure step of a certain magnitude. Film break after the pressure change is equivalent to contact of two fluid interfaces and models the coalescence – merging of two interfaces⁹⁹.

Thin film balance is an excellent tool for the investigation of the complexity of interfacial properties in mixtures containing nanoparticles, surfactants or proteins. For example, the interfacial aggregation and its role in thin film stabilisation after pressure steps were studied in TFB experiments for β -lactoglobulin protein.¹⁰¹ Proteins do not have the same mobility as surfactants at the interface but adsorb irreversibly. They can form well-defined self-assembled aggregates and unfold at the interface exposing their hydrophobic part towards the air.

Investigations into thin film stability can also be performed with single drop or bubble experiments. The details are given in the review of Chandran Suja et al.¹⁰² In a particular configuration, the bubble attached to the capillary interacts with a flat air-liquid interface. Fluctuations in the size of the bubble are detected by pressure changes inside the bubble. After bubble size stabilization, the bubble

moves at a fixed velocity towards the air-liquid interface from its initial to its predetermined final position. The camera records the spatiotemporal evolution of the liquid film between the bubble and the air-liquid interface. When the thickness of the draining film becomes comparable to the wavelength of light, interference patterns are seen by the top camera. The experiment ends when the film ruptures and the bubble coalesces at a critical film thickness. The coalescence time is accurately identified with the pressure transducer. Coalescence time, measured as single bubble/drop coalescence times is inherently stochastic with some distribution depending on the properties of interfaces.¹⁰³

The coalescence time of single bubbles is correlated with the stability of foams and enables the prediction of foam stability,¹⁰⁴ as well as following the interplay of interfacial phenomena governing the stability. Frostad et al.¹⁰⁵ have revealed the role of Marangoni stresses in controlling foam density for different types of surfactants. The amount of liquid entrapped in the thin film was not solely dependent on the surface tension. Surfactants generating larger Marangoni stresses formed thicker liquid films. Experiments also revealed significant differences in the rate of thin film drainage. Kannan et al.¹⁰⁶ examined the role of interfacial shear elasticity in the entrained liquid volume by measuring the dimple size and mobility in single bubble experiments with monoclonal antibodies and pharmaceutical surfactant additives. Viscoelasticity-induced dimple immobility correlated with the formation of insoluble aggregates due to monoclonal antibodies interactions.

1.7 Objectives

Foam stability is a complex phenomenon because in thin liquid films, surfactant thermodynamics, bubble pressure, interfacial rheology, and disjoining pressure forces simultaneously play a role. The situation is even more complicated when considering foam columns: bursting thin films influence drainage and induce pressure shocks. The addition of nanoparticles to surfactants induces additional complexity: nanoparticles can reveal surface activity, dependent on surfactant to particle ratio, and the interfacial rheology is more complex. Nanoparticles can carry the charge of complex distribution, and last but not least, they can block flow in Plateau borders that separate bubbles.

The main objectives of the PhD thesis are:

- description of adsorption isotherm of amino acid-based green surfactant ethyl lauroyl arginate, as the necessary constituent to produce and stabilize foam,
- characterization of synergistic properties of ethyl lauroyl arginate in the mixtures with non-surface active cellulose nanocrystals concerning foaming and foam stability,
- comparison of the different surface groups at cellulose nanocrystals in relation to foam properties prepared from the mixtures with ethyl lauroyl arginate,
- determination of the correlation of foam column stability with the stability of single thin films made from ethyl lauroyl arginate – cellulose nanocrystals dispersions.

As a result, I expected to show that fine-tuning of ethyl lauroyl arginate and cellulose nanocrystals interactions by their relative concentrations affects surface tension, surface rheology and nanoparticles interfacial aggregation. The optimization of CNC-LAE suspension regarding its film-forming properties enables the formation of thin films containing green, biodegradable components that can be useful in the preparation of liquid/air interfaces in a variety of products with antibacterial properties, in which foaming properties are relevant like in food and cosmetic products.

2. Research methodology

2.1 Cellulose nanocrystals dispersion preparation

Spray-dried cellulose nanocrystals (CNC) used in my research had two different hydrophilic groups and originated from two manufacturers. Sulfate-CNC (sCNC) were purchased from CelluForce (Canada) and carboxyl-CNC (cCNC) were purchased from Anomera (Canada). Large quantities of commercially available, well-characterized cellulose nanocrystals helped to investigate CNC-surfactant interactions, foaming and foam stability, including coalescence of bubbles and thin films. Water CNC dispersions were prepared using a magnetic stirrer with mild stirring and manual addition of very small portions of CNC (about 10 mg each) to the dispersions in such a way as to avoid aggregation. After each portion, the dispersion was sonicated for 10 minutes and the final dispersion was controlled with dynamic light scattering measurements. Both dispersions had slightly acidic pH, between 6 and 7.

2.2 Cryo-TEM microscopy of CNC

Freshly prepared CNC dispersions with 300 ppm of 10 nm colloidal gold as TEM markers were sampled with Vitrobot at temperature 4°C (relative humidity 100%, blotting time 2s) onto *Quantifoil* 2-1µm Cu TEM grids. The excess liquid was removed with blotting paper. Samples were vitrified by plunge freezing in liquid ethane and in liquid nitrogen. Samples were imaged with Titan Krios G3i cryo-transmission electron microscope (Thermo Fisher Scientific) with field emission gun and K3 Gatan detector at Solaris National Synchrotron Radiation Centre in Kraków. Electrons were accelerated with the voltage 300 kV, 100 electrons reached Å² of the sample.



Figure 4. Cryo-TEM image of thin film sample of cCNC vitrified from 0.3% wt. water dispersion, showing single rod-like cellulose nanocrystals (LAE is present in the sample at concentration 0.075 mM). Scale bar 30 nm is indicated.

2.3 Ethyl lauroyl arginate – cellulose nanocrystals dispersion preparation

Cellulose nanocrystals – surfactant mixtures were prepared by the addition of cellulose nanocrystals to surfactant solution drop by drop using magnetic stirring. For all experiments, 0.3% wt. of cellulose nanocrystals were used in final dispersions. Dispersions were prepared from the CNC stock dispersion 0.6% wt. Three representative ethyl lauroyl arginate concentrations were chosen to study foaming and interfacial properties of LAE-CNC dispersions: low 0.075 mM, middle 0.15 mM and high 0.35 mM. At such quantities, surfactant had a minor effect on dispersion pH.

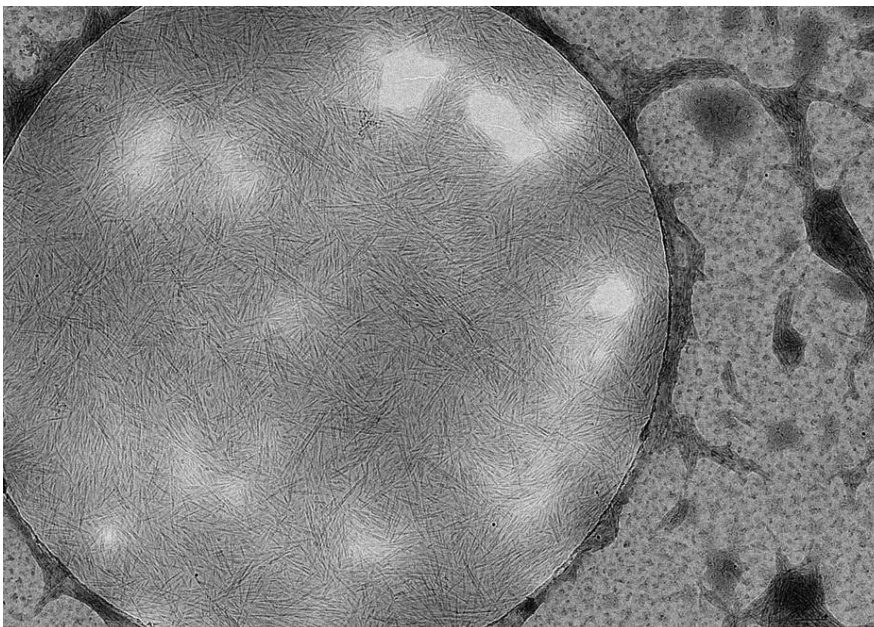


Figure 5. Cryo-TEM image of vitrified thin film sample of dispersion of LAE 0.15 mM with cCNC at concentration 0.3% wt. CNC rods are randomly distributed and form densely-packed structure in thin liquid film after adding ethyl lauroyl arginate.

2.4 Experimental conditions

All dispersions were standardised to provide as low polydispersity of dispersions as can be achieved with available time and equipment. Surfactant concentrations chosen for experiments were only a fraction of CMC. Concentrations were chosen after preliminary experiments in which significant aggregation and viscosity increase were observed for ethyl lauroyl arginate concentrations higher than 0.35 mM in 0.3% wt. of cellulose nanocrystals dispersions. The range of concentrations was very narrow but sufficient to show complex phenomena at the dispersion/air interface.

Dispersions of CNC with ethyl lauroyl arginate were characterized by zeta potential, hydrodynamic diameter and partially by dynamic viscosity measurements. All LAE-CNC dispersions were nano-sized with some fraction of micro-aggregates increasing the polydispersity index. The dynamic viscosity of CNC dispersion without surfactant was the same as the viscosities of LAE-CNC mixtures for low and middle LAE concentrations. A small viscosity increase was only observed in dispersions with the highest LAE concentration. With such experimental conditions, variability between samples was minimised for the purpose of studying interfacial phenomena.

Pendant drop oscillations experiments were carried out to investigate surfactant transport and calculate dilatational modulus according to Lucassen van den Tempel model (*Equation 17*). Foaming experiments were carried out with a double syringe technique, described in the details below. Electrolytes and urea were added separately to LAE-CNC dispersion to assess their influence on the dispersion parameters and foam stability. In parallel, single bubble coalescence experiments, thin film balance coalescence experiments, and interfacial shear rheology measurements were performed to explain complex interactions between ethyl lauroyl arginate and cellulose nanocrystals and the influence of interfacial rheology on the thin film and foam stability.

3. Experimental and instrumental methods

3.1 Pendant drop experiments

Adsorption properties of ethyl lauroyl arginate were determined by studying surface tension for an extended concentration range in order to construct the adsorption isotherm. Then theoretical models to describe the isotherm were applied for LAE and for mixtures with LAE hydrolysis products. Adsorption properties of ethyl lauroyl arginate with mixtures of cellulose nanocrystals were investigated in the same experimental conditions. Surface tension was measured using the pendant drop technique with a Sinterface PAT-1M tensiometer (Germany). A drop of solution (11 μ l) was created from a 2 mm diameter capillary and kept in the thermostated chamber for up to 2000 seconds. The drop profile was

monitored and fitted with the Young-Laplace equation to calculate the surface tension until it did not change during the consecutive measurements. Then the value of the equilibrium surface tension was recorded.

3.2 Zeta potential

Dispersed, charged particles are surrounded by adsorbed and closely packed counterions which form a layer of the thickness of the order of the ion size called the Helmholtz-Stern layer. The ions in the Stern layer are considered to be immobile and this region is considered as a capacitor in which electrostatic potential changes linearly with the distance to the particle. The outer limit of this region is the plane of shear, beyond which the liquid around a moving particle is no longer trapped to move with the particle. The potential at this point is called the zeta potential (ζ) and is determined by electrophoretic mobility measurements¹⁰⁷.

When the electric field is applied, charged particles are attracted to the oppositely charged electrode and move. Viscous forces in the liquid oppose this movement and when the equilibrium is reached, particles move with the constant velocity called electrophoretic mobility.

Relation between electrophoretic mobility U_E and the zeta potential ξ is given by Henry equation.

$$U_E = \frac{2\varepsilon\xi f(\kappa a)}{3\eta}$$

Equation 28

where η is the viscosity of the solvent, ε is the dielectric constant and $f(\kappa a)$ is the Henry function

For aqueous media and moderate electrolyte concentration $f(\kappa a)$ is equal 1.5 and is referred as Smoluchowski approximation. I used that approximation considering the fact that particles with sizes 70-500 nm are present in CNC dispersions and cellulose nanocrystals used in experiments has an ionic strength of about 230-270 mmol/kg. The electrophoretic mobility is measured by laser Doppler velocimetry. In this technique, the light scattered from the particle is combined with the light from the reference beam to determine the Doppler shift of the scattered light. The Doppler shift depends on the speed of particles and the angle of measurement. Potential ξ was measured in electrophoretic mobility experiments with commercial equipment Zetasizer Nano ZS instrument (Malvern-Panalytical, Malvern, UK).

3.3 Dynamic light scattering

Particles in dispersed systems and colloids are in chaotic Brownian motion due to collisions with molecules of dispersing medium. Smaller particles move (diffuse) faster in the medium than larger ones. A laser beam is diffracted by particles in suspension. The movements of particles cause rapid fluctuations in the scattering intensity of the laser around a mean value at a certain angle. The correlation

time and the calculated correlation function depends on a diffusion coefficient D , for a given temperature T and viscosity of the medium η . The diffusion coefficient can be converted into the hydrodynamic particle size, r_h , using the Einstein-Smoluchowski equation:

$$D = \frac{kT}{6\pi\eta r_h}$$

Equation 29

Measurements of nanoparticles size and the polydispersity of the suspension, made with the Zetasizer Nano ZS instrument (Malvern-Panalytical, Malvern, UK), were based on photon correlation spectroscopy for the light scattered at the angle 90° .

3.4 Dynamic viscosity

Shear viscosity measurements were performed with Malvern Kinexus Pro rotational rheometer with cone-plate geometry with a diameter of 50 mm, angle of 1° , and 0.3 mm of a gap. The experiments were conducted in controlled shear stress mode with a constant temperature of 298K. All concentrations were prepared twice, sonicated for a time of 10 min and measured. The range of shear stress was 0.01 to 1.25 Pa. Assuming the proportional relation between shear stress and shear rate for Newtonian fluid, the dynamic viscosity was calculated by extrapolation to zero shear rate. In the experiment, the sample was placed between the cone and the bottom plate. The cone rotated and created the shear stress. For a small cone angle, the assumption was that $\tan\beta = \beta$ and the shear rate was uniform in the entire sample area.

3.5 Interfacial shear rheology

Interfacial shear elastic modulus was measured with a DHR rheometer 5333-0310 (TA Instruments) using a “double wall DuNoüy ring” geometry (R/r 57.447) at the solution/air interface that enables measurement of small stresses in two dimensions. Before each measurement, the ring was cleaned with ethanol and deionised water, and then it was flame-dried. The instrument was calibrated after each ring installation. In the strain sweep experiments, a small oscillation mode was used with an amplitude of 0.5% of ring rotation and a frequency of 0.05 Hz. All the samples were sonicated 10 min before each measurement.

3.6 Thin film balance

Experiments were performed using the device made in ETH Zürich (Department of Materials, Jan Vermant Group), scheme shown in Figure 6. Initially, the thick fluid film (micron-size thickness) was created in the orifice of the bike-wheel cell. By adjusting the pressure in steps of every 1 Pa at the equilibrium pressure, P_{ceq} , was determined, and the film was visible when first interference fringes appeared at the thickness of a few μm . After that, the pressure inside the film was increased with the applied pressure step of 100 Pa. The film started to drain. Build up of hydrodynamic pressure caused the expansion of the film. The images of all film samples were collected to assess the dynamics of drainage. Interferometric images of the films were recorded by the camera and the time between the film expansion and rupture was registered.

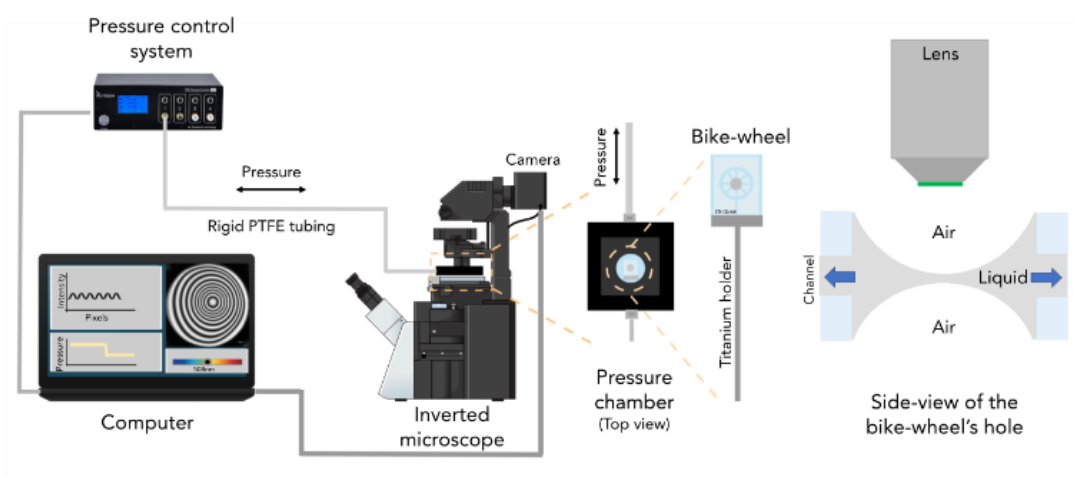


Figure 6. (The original figure from Article 4). Scheme of the thin-film balance setup used in the thin film imaging experiments.

3.7 Dynamic fluid film interferometry

Dynamic fluid film interferometry visualises film drainage and coalescence after the bubble formed in the solution stops moving while approaching liquid/air interface. I used an experimental set-up at Department of Chemistry, Stanford University (Gerald G. Fuller Group).

The volume change of the thin film formed at the apex of the bubble is the function of the average film thickness h at a fixed film radius. In the experiment, after approaching the interface, the thin film radius had a value of $350 \mu\text{m}$ and did not change with drainage time. If a bubble rose in the liquid, the hydrostatic pressure monotonically decreased until the bubble surface started to deform at the interface. Bubble deformation and formation of a liquid film were accompanied by the sudden increase

of the internal pressure and the film started to drain. At the endpoint, when the bubble broke, the internal pressure abruptly dropped. For determining film thickness, a numerical procedure on the Fresnel law of optics was used, assuming an aqueous phase (with a refractive index of 1.33), in between two air phases. The reservoir with the surfactant solutions was cleaned with ethanol and water and filled with filtered (0.45 mm PES NALGENEs) LAE or an LAE–CNC mixture. A bubble with a volume of approximately 1.5 μL was formed at the end of the needle submerged in the surfactant solution. The bubble was positioned such that the distance between the apex of the bubble and the air–solution interface was equal to the bubble radius. The reservoir with the surfactant solution was lowered at a constant velocity of 150 mm/s by a distance of 1.5 times the bubble radius. The pressure was monitored at the beginning of each experiment to determine if the bubble was stable and controlled throughout the experiment. A dome light source was used to induce a reflection interference pattern of the fluid film. Two orthogonally positioned cameras captured the image of the top view of the bubble and its side view image. The time was monitored.

3.8 Double syringe foaming experiments

Foams were generated with a double-syringe method by manually pushing 20 mL or 15 mL ethyl lauroyl arginate and cellulose nanocrystals dispersion with 40 mL or 30 mL (different experimental round) of air, correspondingly from one medical grade syringe to the other syringe (both of 60 mL total volume) that were connected through a narrow tube. After ten cycles the syringes were left in the vertical position. Initial foam volume was ascribed as the volume after 1 minute from the foam formation. Experimental error was introduced by different pushing speeds due to the manual operation of pistons. As that was demonstrated in the literature⁶⁹ the speed differences between 10 cm/s - 40 cm/s resulted in foam half-life differences of the order of 100 s.

4. Review of articles constituting the PhD Thesis

4.1 Article 1. *Ethyl lauroyl arginate, an inherently multicomponent surfactant system.*

Agnieszka Czajak, Ewelina Jarek, Marcel Krzan, Piotr Warszyński *Molecules* **2021**, *26(19)*, 5894.

Ethyl lauroyl arginate is commercially available as Mirenat in various forms: Mirenat-G, Mirenat P, Mirenat-CF, containing different amounts of ethyl lauroyl arginate together with additives. Adsorption of LAE at the air/water interface was studied mainly using LAE mixtures with other, usually unidentified components, with only a few reports of surface tension isotherms.^{108,109,110,111,112,113,114} In these reports, synthesized ethyl lauroyl arginate or supplied as a product of 10-95% LAE content showed the critical micelle concentration (CMC) spanning from 0.9 mM to 6.2 mM.¹¹⁵ Surface tension at CMC also varied significantly: 25.5 mN/m to 31.8 mN/m. These discrepancies between the results may originate from differences in LAE solution composition. The presence of surface active residuals from surfactant synthesis and/or surfactant hydrolysis products such as N-lauroyl-L- arginine (LAS) and dodecanoic acid (DDA) significantly modifies the observed adsorption properties, surface tension isotherm and CMC value. N α -lauroyl-L-arginine (LAS) that, in neutral and mildly acidic conditions (above pH 5), is the amphoteric surfactant with a much lower solubility in aqueous media (<0.1 mM) than cationic LAE and dodecanoic (lauric) acid, which is anionic at pH > 4.5. To explain and quantify the observed discrepancies in the surface activity results of LAE, the investigations of the surface activity of LAE with the analytical standard purity were performed. Such results have never been presented in the literature before.

The measured surface tension isotherms of ethyl lauroyl arginate (LAE) are presented in Figure 7. They were compared with isotherms for some model cationic and non-ionic surfactants.

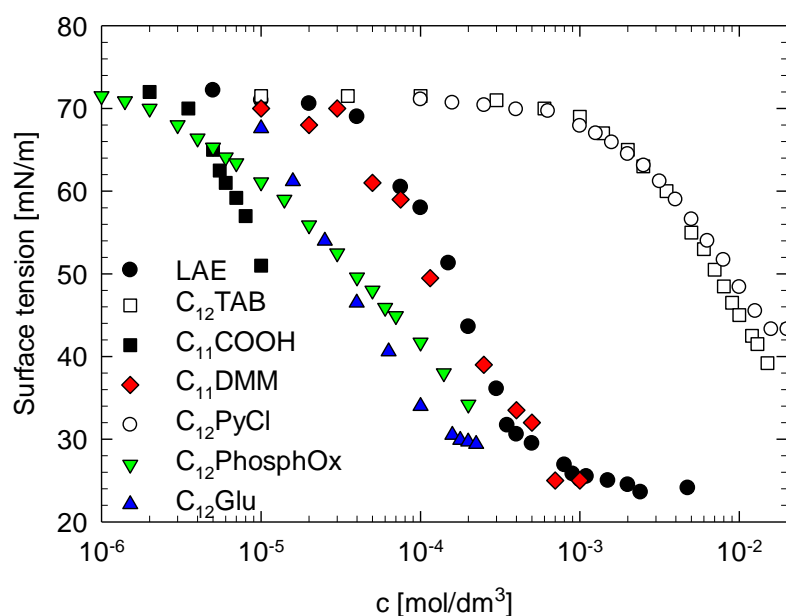


Figure 7. (Original figure from Article 1). The comparison of the surface tension isotherm of LAE with ones obtained for some model cationic and non-ionic surfactants: dodecyl trimethylammonium bromide (C₁₂TAB), dodecyl pyridinium chloride (C₁₂PyCl), (C₁₁COOH), n-dodecyl-β-D-glucoside (C₁₂Glu), n-dodecyl dimethyl phosphine oxide (C₁₂PhosphOx) and N,N,N-trimethyl-2-(dodecanoyloxy)ethane ammonium bromide (C₁₁DMM).

The onset of surface activity of LAE at 10^{-4} mol/dm³ was one order of magnitude lower than cationic surfactants with the same hydrocarbon chain length, dodecyltrimethylammoniumbromide (C₁₂TAB)³⁸ and dodecyl pyridinium chloride (C₁₂PyCl).¹¹⁶ The onset was also at least one order of magnitude higher than of non-ionic surfactants: nondissociated dodecanoic acid (C₁₁COOH),¹¹⁷ n-dodecyl-β-D-glucoside (C₁₂Glu)⁴³ and n-dodecyl dimethyl phosphine oxide (C₁₂PhosphOx).¹¹⁸ The surface activity of LAE resembled the surface activity of the solution of N,N,N-trimethyl-2-(dodecanoyloxy)ethane ammonium bromide (C₁₁DMM).³⁹ Importantly, for C₁₁DMM it was demonstrated that the surface activity is the result of synergistic adsorption of cationic surfactant – C₁₁DMM and surface active anion-dodecanoate, the product of surfactant hydrolysis that forms electrostatically bound heterodimer with the cation. The CMC of LAE was 1.0-1.1 mmol/dm³, in agreement with,¹¹⁵ and lower than in other reports. The surface tension value at CMC 25 mN/m is much lower than for typical cationic surfactants, closer to values for non-ionic surfactants and characteristic for di-chain or Gemini surfactants.^{119,120} Such a low value of surface tension at CMC suggests the formation of surface active dimers containing dodecanoate anion, the residual product of LAE synthesis and hydrolysis.

LAE can undergo hydrolysis via two paths, as illustrated in Supplementary Materials to Article 1. First path describes hydrolysis of the amide bond between the hydrophobic chain and hydrophilic headgroup resulting in L-arginine ethyl ester, which is not surface active and surface-active dodecanoic (lauric) acid that above its pK_a assumes the form of dodecanoate anion. and ethanol, in second ester bond linking side ethyl group hydrolyses, producing surface active Nα-lauroyl-L-arginine and ethanol.

Density functional theory computations used to evaluate the energetics of acid and base catalysis along these paths indicated that base-catalysed hydrolysis is irreversible. Free energy of hydrolysis was equal to 15.6 kcal/mol for the first path and 24.2 kcal/mol for the second one, indicated a much higher entropic barrier, associated with nucleophilic addition step producing dodecanoate anion than for the second, resulting in LAS formation. Acid-catalysed hydrolysis seemed to be non-favourable in standard conditions (298 K, 1 atm). The base-catalysed hydrolysis is expected to have a measurable rate due to the cationic charge of surfactant and the local concentration of hydroxyl anions at the interface. LAE-dodecanoate anion was expected to form electrostatically bound dimers while LAE-LAS – hydrogen bounded heterodimers. Density functional theory was used to evaluate the energetics of given heterodimers, indicating the preference for LAE-LAS heterodimers, despite missing electrostatic attraction. The LAE-LAS heterodimers can evolve into larger aggregates as hydrolysis progressed with the appearance of cloudy phase observed in the experiments.

The stability of heterodimers at the interface was assessed by molecular dynamics simulations with YASARA Structure simulation package.¹²¹ The results were presented in Fig. S3 (Supplementary Material) of Article 1. Despite the competition of surrounding water in the interfacial layer for hydrogen bonding, the intermolecular hydrogen bonds contributed to the formation of persistent dimers. For LAE-LAS the average number of hydrogen bonds 1.96 was higher than for LAE-dodecanoate, 1.71. The additional stabilisation of dimers might originate from the interaction of guanidinium groups which might pair in solution and are not considered in the applied molecular dynamics force field¹²². Molecular dynamics simulations snapshots illustrating heterodimers at air/water interface are shown in Figure 4, Article 1.

The "quasi two-dimensional electrolyte model" of ionic surfactant adsorption was used to model the LAE surface tension isotherm. Considering the outcome of QM and MD simulations, 0.2% molar content of dodecanoic acid was assumed in fresh LAE solution and 18% molar of LAS, resulting in LAE hydrolysis during storage. Less than 0.5% molar content of dodecanoic acid was considered as the LAE synthesis impurity. The fitting results are shown in Fig. 2a and 2b in Article 1. Best fit parameters are collected in Article 1, Table S1, Supplementary Material.

Oscillating drop-shape tensiometry at frequencies between 0.01 and 0.2 Hz was used to determine the dynamic interfacial properties and the surface dilatational viscoelasticity of LAE solutions. Figure 5 in Article 1 presents the oscillations of the drop area (dashed line) and the corresponding changes of the surface tension at concentrations as indicated. The oscillation of the surface tension at low frequencies was sinusoidal. The significant noisy signal appeared at higher frequencies, which can be explained as the relaxation of the interfacial layer composed of a surfactant mixture. For the concentration above 0.8 mM sinusoidal oscillations became distorted and a large phase shift was observed between the variations of drop area and surface tension. Surprisingly, at the end of the compression of the drop area, the surface tension started to increase, which can be explained by surfactant desorption. Figure 6 in Article 1 presents the real and imaginary parts of the dilatational

modulus for all studied LAE concentrations. The real part of the modulus increased with drop area oscillation frequency and can be fitted by Lucassen-van den Tempel diffusional adsorption model, which is valid for surfactant concentration below CMC. Parameters of the fitting are presented in Table 4, in Article 1. The imaginary part can be described by the Lucassen-van den Tempel model only for concentrations below 0.5 mM. Hence the conclusion that the elasticity of LAE solutions needs to be described by more complex model than single surfactant adsorption model. Moreover, for concentrations above CMC and higher frequencies, the imaginary part increased and was higher than the real one. This effect can be explained by the shear effect and nonlinear response for drop oscillation.¹²³ Loglio attributed the increase of the phase shift with the drop oscillation frequency to the presence of a surfactant mixture.¹²⁴ The effect of distortion of the surface tension oscillations from sinusoidal shape was presented as the ratio of the second to the first harmonic in the Fourier spectrum. The nonlinear response, which appeared around 0.5 mM and increased up to CMC (1mM) was attributed to the micellization of surfactant upon compression of oversaturated surfactant layer. Modulus dependence on concentration was presented in Fig S5 of Supporting Material.

In conclusion, in the article the theoretical models of ionic surfactant adsorption, based on the molecular properties of LAE and the tendency to its hydrolysis were applied for proper description of ethyl lauroyl experimental surface tension measurements. The surface dilational elasticity and its transport to the interface could be described by the simple diffusion model only for low surfactant concentrations.

4.2 Article 2. *Viscoelastic interfaces comprising of cellulose nanocrystals and lauroyl ethyl arginate for enhanced foam stability.* Agnieszka Czajak, Aadithya Kannan, Agnieszka Wiśniewska, Gabriela Grześ, Marcel Krzan, Piotr Warszyński, Gerald G. Fuller. *Soft Matter* 2020,16,3981-3990.

The article focuses on the foaming properties of sulfated cellulose nanocrystals (sCNC) dispersions with Mirenat-P, commercial grade ethyl lauroyl arginate surfactant (about 85% purity). Double syringe foaming experiments were compared with dynamic fluid film interferometry, interfacial shear rheology and dilatational rheology experiments measured by pendant drop oscillations. Starting from the observation that pure surfactant, as well as pure nanocrystals, do not form foam at all at such small concentrations ($c_{LAE} \ll \text{CMC}$) and experimental conditions (double syringe foaming, 40 mL of air), a series of experiments was presented for their mixtures – dispersions containing CNC 0.3% wt. and 3 different LAE concentrations. In the mixtures, huge synergistic effect was observed for foam amount obtained and for the stability of the foam column, reaching 4 hours. Experiments were designed to explain this synergistic foam stability effect in cellulose nanocrystals, having mostly hydrophilic character, when mixed with ionic surfactant. For that purpose dispersion characteristics was presented: dynamic viscosity, zeta potential and hydrodynamic diameter of cellulose nanocrystals which did not reveal significant differences between cellulose nanocrystals dispersion and dispersions containing surfactants (Supporting information, Table S1, Table S2). These might indicate that experimental samples were uniform concerning their bulk properties and that other important factors can be studied in the explanation of foam stability.

Surface tension was measured for single surfactant as well as for LAE-CNC mixtures with the same LAE concentration as in pure surfactant solution. Surface tension in the mixtures was significantly lower than for surfactant, which indicated cellulose nanocrystals presence at the interface, probably in the complexes with LAE. Surface tension kinetics was presented in *Correction: Viscoelastic interfaces comprising of cellulose nanocrystals and lauroyl ethyl arginate for enhanced foam stability.* Agnieszka Czajak, Aadithya Kannan, Agnieszka Wiśniewska, Gabriela Grześ, Marcel Krzan, Piotr Warszyński, Gerald G. Fuller. *Soft Matter* 2020,16, 5094-5094. The presence of CNC at the interface is supported by larger values of interfacial dilatational modulus in ethyl lauroyl arginate - cellulose nanocrystals mixtures compared to single surfactant.

In the article, single bubble coalescence experiments approximated the response of a foam column to pressure changes induced by bubble collision with an air/liquid interface. The experiments started when the bubble attached to the capillary stopped moving, the bubble surface was deformed, and the thin film of a radius of 350 μm started to drain. Ethyl lauroyl arginate solutions drained very quickly with the observable moving dimple. Thin films at all LAE concentrations were unstable. Thin films for bubbles made in LAE-CNC mixtures formed the dimple that was not moving at the time of drainage. Some micro-aggregates of surfactant and cellulose nanocrystals were seen, despite dispersion filtration.

Aggregates induced pre-mature thin film rupture in many trials. For moderately stable films, bubble coalescence time was calculated by averaging times measured in separate experiments.

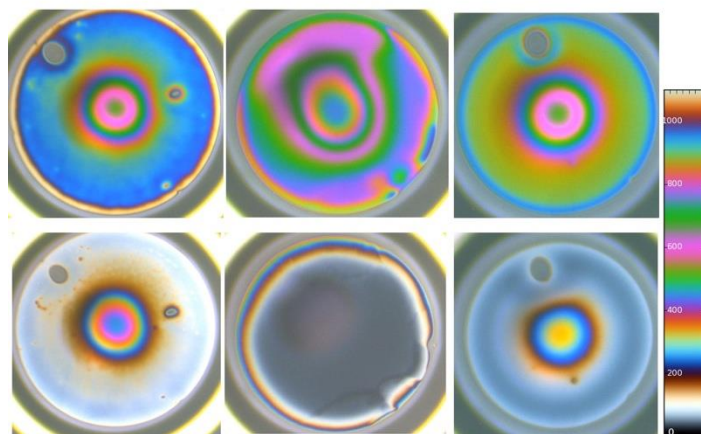


Figure 8. (Original figure from Article 2). Images presenting the top view of LAE-CNC dispersion liquid film formed during dynamic film interferometry experiment for various LAE concentrations. Left: 0.004% wt., Middle: 0.006% wt., Right: 0.015% wt. Upper row: Initial film, Lower row: Film just prior coalescence. A colour scale (in nm) corresponding to the film thickness is placed at the right hand side.

Further results revealed a strong dependence of the film thinning and coalescence time on the LAE concentration in the LAE-CNC mixtures in three representative LAE concentrations (0.004% wt., 0.006% wt., 0.015% wt.). The film coalescence time for the dispersion of pure cellulose nanocrystals never exceeded 20 seconds and drained rapidly, showing stratification. In the presence of LAE in the dispersion, the film thickness was in the range from 320 nm for an LAE concentration of 0.004% up to 600 nm for 0.006% wt. and then decreased to 350 nm for concentrations above 0.01% wt. In the initial draining period, the thinning rate was similar for all concentrations, with thinning to half of the initial film thickness in 10s and the formation of the dimple. The dimple dynamics indicated an immobile type interface. At LAE 0.006%, the dimple disappeared and the film achieved thickness below 100 nm with a much slower thinning rate, as illustrated in Figure 8 (bottom row in the middle). Figure 8 describes the spatially averaged film thickness. At other LAE concentrations in the mixtures presented here, the coalescence of dimpled films occurred directly after the thinning stage.

Coalescence time showed a maximum for LAE concentration of 0.006% (about 0.15 mM). As compared to other concentrations, the maximum of coalescence time can be associated with thicker film, hence longer drainage.

Interfacial shear rheology experiments confirmed findings of the dynamic fluid film interferometry and pendant drop oscillations experiments. At LAE concentration of 0.006% wt. the interfacial layer showed maximum shear elasticity and its growth over time was the most pronounced. It was hypothesized that at this optimal concentration, cellulose nanocrystals with ethyl lauroyl arginate formed a densely packed structure at the interface. The interfacial shear modulus value was relatively high (2-15 mN/m) as for nanoparticles with a 70 nm hydrodynamic diameter, much higher than for

surfactant–polyelectrolyte complexes or globular proteins,¹²⁵ higher than colloiddally aggregated polystyrene microparticles¹²⁶ but comparable to colloiddally aggregated CNC⁹⁴ or commercially available methylcellulose.¹²⁷ Finally, the modulae values were consistent with the measurements of shear properties of octylamine-modified cellulose nanocrystals and cellulose nanofibers⁸⁵ (nanofibers had microscale length). Such similarity might be explained by cellulose nanocrystals evolution into longer microstructures at the interface in the presence of surfactant. What is more, interfacial shear elastic modulus directly correlated with prolonged foam stability.

Foaming experiments were carried out complimentary to single bubble experiments with LAE-CNC dispersions. Pure surfactant solutions, as well as pure nanocrystals suspensions, did not form foam at all at low concentrations ($c_{LAE} \ll CMC$) and experimental conditions (double syringe foaming, 40 mL of air). Consequently, a series of experiments was presented for their mixtures – dispersions containing CNC 0.3% wt. and three different LAE concentrations. In the mixtures, a huge synergistic effect was observed for the foam amount obtained, and the stability of the foam column reached 4 hours. The initial foam volume was proportional to surfactant concentration in all concentrations in the range from 0.002% to 0.015 % wt. of LAE. (Figure 4, Article 2). On the contrary, foam stability showed a clear maximum at 0.006% wt. of LAE, which was consistent with the results from the dynamic fluid film interferometry experiments as well as with the outcome from the shear rheology experiments showing a maximum coalescence time or maximum interfacial shear elastic modulus, respectively.

In conclusion, the article integrates single bubble coalescence measurements with interfacial rheology experiments and, in further, with experiments on foam stability. All these methods show that sulfated cellulose nanocrystals have a hydrophobic character through electrostatic interactions with ethyl lauroyl arginate. LAE-CNC mixtures form complex rheological interface, which can not be characterized by a single method like pendant drop oscillations. LAE-CNC presence at the interface slows down the drainage and prevents bubble coalescence depending on surfactant concentration. For low and high concentrations of LAE, microaggregates with CNC can show an anti-foam effect. Such effect was the lowest for middle LAE concentration with the highest film coalescence time. For that concentration, micro-aggregates were immobile at the interface and did not act as anti-foam species with the same efficiency as low and high LAE concentrations.

4.3 Article 3. *The effect of electrolytes and urea on the ethyl lauroyl arginate and cellulose nanocrystals foam stability.* Agnieszka Czakaj, Marcel Krzan, Piotr Warszyński, *Applied Sciences* **2022**, 12(6),2797.

The article focused on the foaming properties of LAE and CNC mixtures under different conditions. Its goal was to have further insight on foam stability mechanism on the macroscopic scale. Different cellulose nanocrystals were used, carboxylated CNC (cCNC) as a comparison to sulfated ones (sCNC). The same method of foam fabrication, the double syringe method, was applied, as well as the same surfactant grade, its concentrations and sample preparation protocol. These results were compared with the previous data obtained for sCNC described in Article 2.

Both types of cellulose nanocrystals dispersions, LAE-sCNC and LAE-cCNC were characterized by dynamic light scattering and by zeta potential measurements with Malvern Nano ZS Instrument. sCNC characterization was described in Article 2 Supporting Information (Table S2). The hydrodynamic diameter of cCNC data were collected in Table 2, Article 3, while the zeta potentials in Table 3, Article 3. sCNC hydrodynamic diameter was lower than 100 nm and with polydispersity about 0.50 was kept after surfactant addition up to LAE concentration of 0.008%. Zeta potential with standard measurement error ± 5 mV did not change significantly at the level of -44 mV up to added LAE concentration of 0.015%. At 0.015% significant changes occurred in DLS measurements. LAE hydrodynamic diameter increased to 182 nm and the polydispersity index increased to 0.82. That was a clear indication of surfactant-induced aggregation. For cCNC polydispersity index was always smaller than for sCNC and at LAE 0.015%, hydrodynamic size had the value of 112 nm (PDI 0.44), which means that carboxylated CNC were less vulnerable to aggregation.

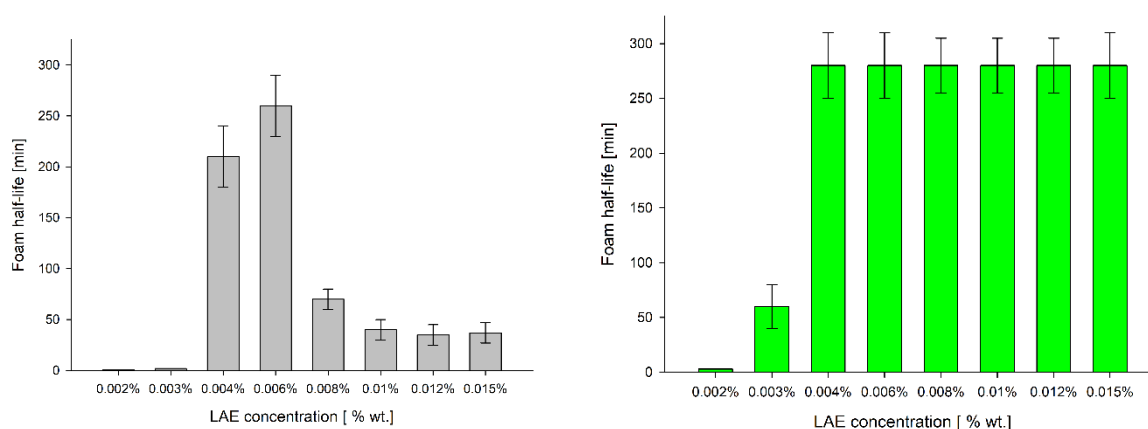


Figure 9. (Original figure from Article 3). Foam half-life of dispersion of the 0.3% wt. sulfated cellulose nanocrystals (picture in the left) with various LAE concentrations and of dispersion of the 0.3% wt. carboxylated cellulose nanocrystals (picture in the right) with various LAE concentrations. Error bars are given.

Contrary to sCNC, cCNC did not show the maximum of foam half-life in a comparable time for all experiments (Figure 9). Above 0.004% wt. of LAE with 0.3% wt. carboxylated CNC, the foam half-life was always longer than 250 minutes. Surprisingly foamability in dispersions with cCNC was two times higher than with sCNC (Table 1, Article 3).

Large sCNC aggregates had anti-foaming effect as seen in the Figure 5 in Article 2, where the increase in polydispersity and hydrodynamic diameter was correlated with a shorter foam lifetime. No such effect was observed for cCNC.

Various additives, electrolytes and urea were added to dispersions to examine their effect on LAE foaming with cCNC. Primarily, the aggregation effect was verified by using electrolytes: guanidine hydrochloride, sodium chloride and sodium salicylate, at a concentration of 5mM. All electrolytes reduced the initial foam volume: guanidine hydrochloride and sodium chloride about 10% of the total volume, while sodium salicylate reduced the foam volume almost 4 times, which is presented in Figure 2 in Article 3.

The foam half-life for LAE-cCNC dispersion with added electrolytes was reduced to about 200 minutes, almost the same for all electrolytes, including sodium salicylate, for which foamability was much lower. Results are collected in Figure 3, Article 3. Results for different electrolytes indicate that the foam drainage rate was independent of the type of salt. The most significant difference in foam stability was noted in the dispersion containing 6 mol/L urea. The foam half-life was reduced to less than 1 min, coinciding with the fast draining period in the foam.

The addition of sodium chloride or sodium salicylate at a concentration of 5 mM/L had a negligible effect on the zeta potential of LAE-cCNC dispersion. Guanidine hydrochloride (5 mM/L) and 6 mol/L urea increased zeta potential by about 10 mV. The addition of sodium chloride and guanidine hydrochloride doubled the hydrodynamic diameter, which indicated salt-induced aggregation. Almost no changes were seen after the addition of sodium salicylate to dispersion. For 6 mol/L urea, the dispersion turbidity almost disappeared, as seen by the naked eye and a hydrodynamic diameter of 100 nm was measured with a much lower polydispersity (0.28). The explanation of the urea effect could be that despite the average size (by intensity) of the dispersion grew, the larger cellulose nanocrystals aggregates were destroyed due to the urea effect on cellulose solubility.¹²⁸ The effect of electrolytes at concentration 5 mM/L on the surface tension of LAE-cCNC dispersion was typical for screening of electrostatic interactions in ionic surfactants as seen in Figure 4, Article 3. Surface tension increase might be the result of cellulose nanocrystals aggregation. Frequency dependence of dilatational elasticity of LAE-cCNC measured by oscillating drop technique revealed that LAE-cCNC elasticity was similar to the one for pure surfactant (Mirenat, as measured in Article 2) and also three times lower than for sCNC as seen in Figure 6, Article 3. This effect can be explained by the higher charge and bigger size of sCNC. The addition of 5 mM NaCl resulted in the highest dilatational elasticity which can be attributed to decrease of electrostatic repulsion between charged cellulose nanocrystals that can pack more closely at the interface. For GuaHCl the same effect was observed but the interfacial layer became

more viscous. (Figure 7, Article 3). The origin of that effect is unclear, but it is proof that both counterions and co-ions affect the dilatation moduli of ionic surfactants at liquid interfaces.¹²⁹ Ion effects having impact on foaming were already reported in the literature.¹³⁰ In my research NaCl and GuaHCl showed an almost equal effect on foaming properties of LAE-cCNC at electrolyte concentration of 5 mmol/L, despite different viscoelastic properties. The addition of 5 mmol/L NaSal or 6 mol/L urea to the LAE-cCNC dispersions caused a slight decrease of the elastic modulus as compared to LAE-cCNC. Different behaviour was observed for the imaginary part of the dilatational modulus. With the addition of GuaHCl, NaSal or urea, its values were increased compared to the ones for LAE-cCNC, while 5 mM NaCl decreased the modulus. The explanation might be that simple salt like NaCl induced closer packing of cellulose nanocrystals. The presence of hydrotropic NaSal or urea might introduce some dissipative structures at the interface. For NaSal, foaming was significantly reduced with relatively stable foam, while foamability was much lower, and no foam stability was observed for urea. Minor changes in the equilibrium and dynamic surface tension upon the addition of urea cannot explicate that decrease of foam stability. The main conclusion is that urea destroys large lamellar cCNC aggregates that reduce foam drainage, but other effects can be important, like waterstructure modification due to the preferential orientation of urea in the presence of ionic surfactant, which may have a large impact on foaming properties¹³¹.

4.4 Article 4. *The influence of the Surface Chemistry of Cellulose Nanocrystals on Ethyl Lauroyl Arginate Foam Stability.* Agnieszka Czakaj, Emmanouil Chatzigiannakis, Jan Vermant, Marcel Krzan, Piotr Warszyński. *Polymers* **2022**, 14(24),5402.

The article partly supplements former articles by the selection of LAE and CNC concentrations for further detailed experiments with thin film balance. That broadens the experimental perspective to accurately study coalescence under controlled conditions compared to the dynamic fluid film interferometry.

Experiments were performed in order to reveal foam stability differences between sulfate-(sCNC) or carboxyl-modified CNC (cCNC). As shown in previous experiments (Article 3) foamability of cCNC was two times higher at 0.006% wt. LAE (Mirenat). Thin film balance experiments were performed at an equivalent concentration, 0.15 mM of LAE in the dispersion with cCNC and sCNC. Additionally, two other surfactant concentrations were studied: 0.075 mM and 0.35 mM. Ethyl lauroyl arginate analytical standard (United States Pharmacopeia - declared purity 99%) was used in thin film balance experiments and in dispersion characterization..

The surface tension of dispersions was measured by pendant drop tensiometry with PAT-1 Sinterface instrument the same way as in Article 1, Article 2 and Article 3. Except for the lowest LAE concentration LAE – cCNC dispersions were more surface active than LAE-sCNC. At concentrations lower than 0.35 mM, all CNC dispersions showed better surface activity than pure surfactant. Zeta potential measurements showed that cCNC had a lower surface charge and became less charged after surfactant addition than sCNC. Hydrodynamic diameter of cCNC and polydispersity were significantly smaller than sCNC.

The interfacial behaviour of dispersions was studied by the dynamic thin film balance technique. The films of the pure LAE surfactant at a concentration of 0.075 M drained fast down to an equilibrium thickness of approximately 15 nm. Drainage occurred in 5-10 seconds, depending on surfactant concentration and proceeded symmetrically. The short drainage times are expected for surfactant films^{132,133} and are indicative of the relatively small magnitude of Marangoni stresses opposing the bulk outflow of the liquid. Drainage stopped when the equilibrium thickness was reached. This thickness is a result of the repulsive electrostatic interactions counteracting the sum of the applied pressure and the attractive van der Waals forces.

The film with 0.075 mM LAE was unstable at 100 Pa pressure change, while the ones with 0.15 mM LAE and 0.35 mM LAE were stable. An additional pressure jump for the assessment of the critical pressure for rupture revealed that film with 0.15 mM LAE broke at the applied pressure of 200 Pa, whereas with 0.35 mM LAE broke at 1250 Pa.

All investigated LAE-sCNC films at the end of drainage, after the pressure step of 100 Pa, were stable and rather uniform with some nanoparticle aggregates (Figure 10). After 15 min of stability of the film with sCNC-LAE 0.35 mM, an additional 50 Pa pressure jump was applied and that resulted in the film break.

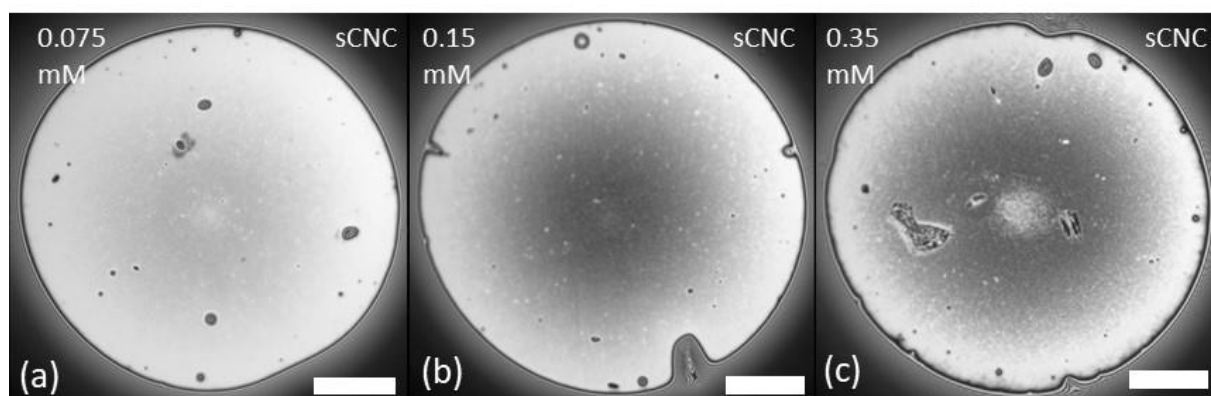


Figure 10. (The Original figure from Article 4). Morphology of LAE-sCNC- films at the end of drainage after the pressure step of 100 Pa. From left to right. CNC - LAE 0.075 mM, CNC - LAE 0.15 mM, CNC - LAE 0.35 mM.

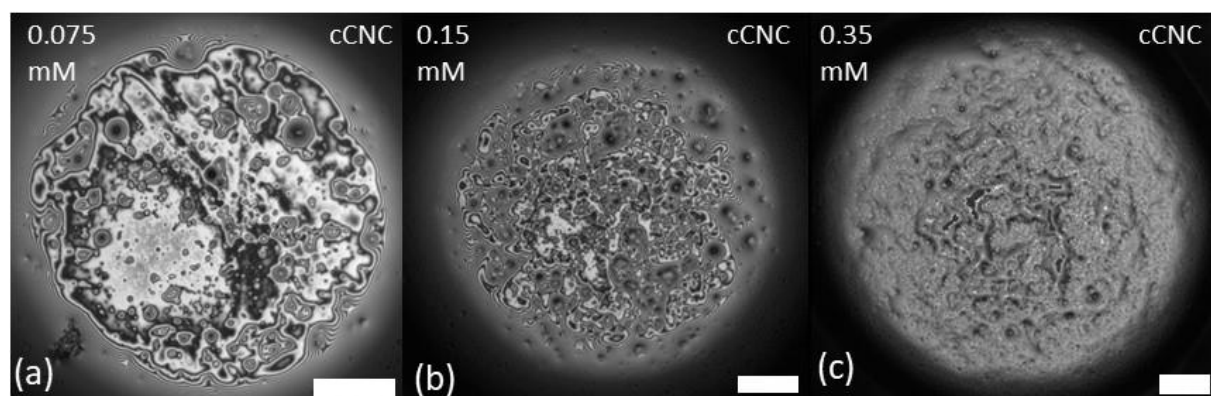


Figure 11. (The Original figure from Article 4). Morphology of LAE-cCNC films after the pressure step of 100 Pa at the end of the drainage. From left to right: CNC - LAE 0.075 mM, CNC - LAE 0.15 mM, CNC - LAE 0.35 mM. Cellulose nanocrystals concentration 0.3% wt. Scale bar is 100 μm

Figure 11 from the Article 4 (original Figure 4) illustrates that LAE-cCNC films were populated by larger cCNC aggregates for all surfactant concentrations. They seemed to have the tendency to occupy the interface, and the coverage increased with surfactant concentration. For the middle concentration, the aggregate interfacial structure seems well-ordered. Film drainage occurred at regions where no aggregates were present, and its rupture was preceded by the formation of a Newton Black film (regions with a thickness of approximately 10 nm), with the thin regions displacing the adsorbed particles. Such an effect hints that excess surfactant might compete for the surface, destabilising the CNC network. Film lifetime increased systematically with surfactant concentration for both particle types and was

corresponding to previous results with the bubble approaching liquid/air interface. However, in thin film balance experiments, sCNC-LAE 0.35 mM film was very stable to single pressure jump up to high pressure. Carboxylated CNC films were not so stable at the highest concentration, but overall they show a general tendency for higher coalescence time in the whole concentration range. Film lifetimes for all surfactant and surfactant–nanoparticle films are presented in Figure 6 in Article 4. The article includes foaming experiments for corresponding LAE-CNC mixtures with analytical standard ethyl lauroyl arginate used for thin film balance experiments. In the dispersion of cellulose nanocrystals with ethyl lauroyl arginate, the foamability was directly correlated to surfactant concentration. Assuming that the same volume of air was injected into the solution, foamability differences could be explained by the higher hydrophobicity of cCNC. In particle-stabilised foams, foamability depends on the number of particles, the size of aggregates and their hydrophobicity. Interestingly, the polydispersity of cCNC solution was lower than sCNC, but their interfacial aggregation was much higher, as demonstrated by thin-film balance experiments. The half-life of foams formed in the CNC-LAE suspensions with the double-syringe method was illustrated in Figure 10 in Article 4. The optimal concentration of LAE (0.15 mM) seemed to exist for both types of cellulose nanocrystals as the highest foam stability was observed. That differed from thin film balance experiments where the film lifetime was increased with LAE concentration. This may result from the antifoaming action of larger aggregates that induce premature film rupture.

5. Discussion and conclusions

As determined by oscillating drop surface tension measurements, the surface activity of ethyl lauroyl arginate is in between cationic and non-ionic surfactants that possess the same kind of hydrophobic tail. Even the analytical standard of LAE solution contains lauric acid as the residue of synthesis. LAE undergoes base-catalysed hydrolysis during storage with $N\alpha$ -lauroyl-L-arginine (LAS), the preferred surface active zwitterionic hydrolysis product. Therefore, LAE should be considered as a multicomponent system. The model of surfactant mixtures was successfully applied to describe LAE adsorption isotherm with the assumption that the solution contains 0.2% dodecanoic acid in fresh LAE solution and 18% LAS after LAE solution prolonged storage. The preferred hydrolysis path was determined using DFT computations indicating the formation of highly surface active heterodimers, LAE-dodecanoate anion and LAE- $N\alpha$ -lauroyl-L-arginine(LAS). Molecular dynamics simulations were used to determine the stability of those dimers linked by electrostatic interactions and hydrogen bonds in the case of LAE-dodecanoate anion or hydrogen bonds and stacking of guanidinium groups in the case of LAE-LAS.

The surface dilatational modulus determined by the oscillating drop method showed surface elasticity modulae values between ones for ionic and non-ionic surfactants. Close to and above CMC surface tension revealed a nonlinear response which can be explained by the presence of micelles and reorganisation of the interfacial surfactant layer.

The presence of cellulose nanocrystals in low concentration (0.3% wt.), the very diluted and mildly aggregated colloidal solution significantly enhances foamability in low concentration of LAE solution (up to 0.35 mM). Although, for surfactant concentration up to 0.35 mM, foams surviving more than a minute are not formed when using the double-syringe foaming technique, in the presence of cellulose nanocrystals, foam half-life reaches several hours. Cellulose nanocrystals reduce drainage of the liquid phase from the foam and increase the coalescence time of the bubbles made in the LAE-CNC solution. In the case of sulfated cellulose nanocrystals, coalescence time shows a maximum with respect to LAE concentration at about 0.006% wt. of LAE. For larger concentrations, bubble coalescence and thin film brake might be the result of the presence of large cellulose nanocrystal aggregates in the thin film and at the interface, which can act as anti-foamers.

LAE-CNC mixtures show high interfacial shear elastic modulus as considering their size. The modulus evolves with time, and it is expected to be influenced by the elongated shape of nanoparticles, capillary interactions and interfacial CNC aggregation into larger structures.

Carboxylated cellulose nanocrystals show superior foaming properties than sulfated cellulose nanocrystals. They also show better foam stability. It can be explained by higher hydrophobicity and lower polydispersity of carboxylated cellulose nanocrystals and a lower tendency to form such large cellulose aggregates that act as antifoamers.

Large aggregates should have a preferential effect on foam stability when CNC are added. Firstly, large CNC aggregates might block water flow through Plateau borders; secondly, they are interfacially active and contribute to the increase of dilatational and shear elasticity. The role of large aggregates is justified by the results of the foaming experiment with concentrated urea (6 mol/L). Urea's presence caused the break of the foam column in a time of seconds. In the LAE-CNC-urea suspension, surface tension is not altered significantly as compared to LAE-CNC. The same refers to the zeta potential of the nanoparticles. Hydrodynamic diameter, as measured by dynamic light scattering, slightly increased, but the most important observation was a decrease of polydispersity of LAE-CNC in urea presence by a factor of 2. Such a decrease in polydispersity can be the result of the elimination of large aggregates, as urea contributes to cellulose solubility. Hence the conclusion is that large CNC aggregates maintain to a great extent LAE-CNC foam stability.

Foam drains and breaks rapidly in the presence of urea, which dissolves larger CNC structures. Conversely, the role of mild aggregation with the addition of electrolytes resulting in CNC size increase up to 200 nm is minor, as shown in Article 3. Faster drainage that leads to faster coalescence can only be a partial explanation for the foam break. Urea at concentrations as large as 6 mol/L in the presence of ionic surfactant can orient itself and significantly influence the structure of water at the interface, as presented by Moll et al.¹³¹ Interfacial water structure is an important factor for foam stability. Urea effect in the presence of cellulose nanocrystals on both drainage and coalescence is a very promising research perspective.

Ethyl lauroyl arginate and cellulose nanocrystals show a synergistic effect for achieving foam stability. Pure LAE solutions do not form foams surviving longer than a minute. In the presence of surfactant CNC become more hydrophobic. The presence of cellulose nanocrystals reduces water outflow from thin liquid films and prevents the coalescence of bubbles. Moreover, the degree of aggregation and polydispersity of cellulose nanocrystals in bulk is not equivalent to those at the interface. While carboxylated CNC were less polydisperse in water dispersions, they more readily aggregated at the interface and formed larger structures. Thin film balance experiments showed that thin liquid film stability made from LAE-CNC is highly vulnerable to nanoparticle-surfactant ratio, nanoparticle polydispersity and surface properties of aggregates. Overall, cCNC thin films are more resistant to coalescence. They show longer coalescence times compared to sCNC, up to the LAE concentration of 0.15 mM.

Thin film balance experiments provided new information about interfacial properties in ethyl lauroyl arginate cellulose nanocrystals mixtures, inaccessible to surface tension measurements with drop oscillations. They showed that nanoparticle/surfactant ratio influences interfacial properties of mixtures and interfacial response to applied stress might be very complex.

Although single thin film and single bubble experiments can only give an estimation of the foam column stability, a quantitative agreement can be achieved if the experiments are conducted at similar

capillary pressures.¹³⁴ Despite that constraint, the obtained results are very consistent, considering the complexity of the nature of dispersions under investigation.

The results presented in the thesis may significantly contribute to broadening the knowledge of interfacial rheology of dispersions of predominantly hydrophilic cellulose nanocrystals when they are mixed with ionic surfactants. In those mixtures, nanocrystals gain new properties after synergistic interactions with ethyl lauroyl arginate. Results show that interfacial aggregation of cellulose nanocrystals is different than in bulk, and it depends on small surfactant concentration changes. The LAE-CNC nano-dispersions were studied in the regime of negligible viscosity changes among dispersions and for low surfactant concentrations. Such experimental arrangements are rare in the literature concerning studies of foam column drainage and long-term foam stability. Thus, it provides a solid base for further experiments in the field of interfacial rheology and foam technology.

6. References

- ¹ Gochev G., Platikanov D., Miller R. *Adv. Colloid Interface Sci.* 2016, 233, 115-125.
- ² Lyklema J., Scholten P.C., Mysels K.J. *J Phys Chem* 1965,69,116.
- ³ Mysels K.J., Cox M.C., Skewis J.D. *J Phys Chem* 1961, 65,1107.
- ⁴ Sheludko A. *Adv Colloid Interface Sci* 1967,1(4),391–464.
- ⁵ Mysels K., Shinoda K., Frankel S. *Soap films*. Pergamon press, 1959.
- ⁶ Mysels K.J., Jones M.N. *Discuss Faraday Soc* 1966,42,42–50.
- ⁷ Exerowa D., Kashchiev D., Platikanov D. *Adv Colloid Interface Sci* 1992,40,201–56.
- ⁸ Bergeron V., Radke C.J. *Langmuir* 1992,8(12),3020–6.
- ⁹ Fameau A.-L., Salonen A., C.R. *Physique* 2014, 15, 748-760.
- ¹⁰ Ishii M, Murata S., Ishitsuka K.,Lin W. *Journal of Petroleum Science and Engineering* 2022, 208, 109512.
- ¹¹ Hartmann R., Rinne T., Serna-Guerrero R., *Langmuir* 2021, 37, 7, 2322–2333.
- ¹² Beaumont M., Tardy B.L., Mattos B.D., Rojas O.J. *ACS Nano* 2021, 15, 19712–19721.
- ¹³ Johansson E., Cervin N.T., Wagberg L.E., Cnf cellular solid material with anionic surfactants, US Patent US20170313838A1
- ¹⁴ Wege H.A., Kim S., Paunov V.N., Zhong Q., Velev O.D., *Langmuir* 2008, 24, 17, 9245–9253.
- ¹⁵ Parajuli S., Prater L.A., Heath T., Green K.A., Moyer W., Hutton-Prager B., Ureña-Benavides E.E., *ACS Appl. Nano Mater.* 2020, 3, 12, 12198–12208.
- ¹⁶ Esparza Y., Ngo T.-D., Fraschini C., Boluk Y., *Ind. Eng. Chem. Res.* 2019, 58, 19926–19936.
- ¹⁷ Wu J., Andrews M.P., *Microbeads from Crystalline Nanocellulose: Regulating Physical Properties by Chemical Modification and Hybridization*, PhD Thesis, McGill University (Canada).
- ¹⁸ EFSA FAF Panel (EFSA Panel on Food Additives and Flavourings), Younes, M, Aquilina, G, Engel, K-H, Fowler, P, Frutos Fernandez, MJ, Fürst, P, Gürtler, R, Gundert-Remy, U, Husøy, T, Mennes, W, Moldeus, P, Oskarsson, A, Shah, R, Waalkens-Berendsen, I, Wölfle, D, Gott, D, Leblanc, J-C, Smeraldi, C, Tard, A and Castle, L, *EFSA Journal* 2019,17(3):5621
- ¹⁹ Tripathy, D.B.; Mishra, A., Clark, J., Farmer, T. *Comptes Rendus Chim.* 2018, 21, 112–130.
- ²⁰ Lozano, N., Pérez, L., Pons, R., Luque-Ortega, J.R., Fernández-Reyes, M., Rivas, L., Pinazo, A. *Colloids Surfaces A Physicochem. Eng. Asp.* 2008, 319, 196–203.
- ²¹ Rodríguez, E., Seguer, J., Rocabayera, X., Manresa, A. *J. Appl. Microbiol.* 2004, 96, 903–912.
- ²² Haghghi, H., Leugoue, S.K., Pfeifer, F., Siesler, H.W., Licciardello, F., Fava, P., Pulvirenti, A. *Food Hydrocoll.* 2020, 100, 105419.
- ²³ Nerin, C., Becerril, R., Manso, S., Silva, F. *Ethyl Lauroyl Arginate (LAE): Antimicrobial Activity and Applications in Food Systems*. In *Antimicrobial Food Packaging*; Elsevier Inc., 2016, 305–312
- ²⁴ Ruckman, S.A.; Rocabayera, X.; Borzelleca, J.F.; Sandusky, C.B. *Food Chem. Toxicol.* 2004, 42, 245–259.

-
- ²⁵ Bai, L., Xiang, W., Huan, S., Rojas, O.J. *Biomacromolecules* 2018, 19, 1674–1685.
- ²⁶ Czakaj, A., Kannan, A., Wisniewska, A., Grzes, G., Krzan, M., Warszynski, P., Fuller, G.G. *Soft Matter* 2020, 16, 3981–3990.
- ²⁷ Chi, K., Catchmark, J.M. *Carbohydr. Polym.* 2017, 175, 320–329.
- ²⁸ Langevin D. *Annual Review of Condensed Matter Physics*, 2023,14,21-33.
- ²⁹ Younes M., Aquilina G., Engel K.H., Fowler P., Frutos Fernandez F., Fürst M.J., Gürtler P., Gundert-Remy R., Husøy U., Mennes T., W. *EFSA J.* 2019, 17, 5621.
- ³⁰ Gibbs WJ. On the equilibrium of heterogeneous substances. 1878 *Trans. Conn. Acad.* III:108–248, 343– 524.
- ³¹ Danov K., Kralchevsky P., Ivanov I., Equilibrium and dynamics of surfactant adsorption monolayers and thin liquid films, M. Dekker (Ed.), 1055 *Handbook of Detergents, Part A: Properties*, G. Broce, CRC, 1999.
- ³² Warszynski P., Szyk-Warszynska L., Wilk K.A., Lamch Ł., *Current Opinion in Colloid & Interface Science* 2022, 59:101577.
- ³³ Davies J.T., Rideal E.K. *Adsorption at liquid interfaces. Interfacial phenom.* New York, London: Academic Press; 1963, 154–216.
- ³⁴ Diamant H, Andelman D., *J Phys Chem* 1996, 100,13732–13742.
- ³⁵ Borwankar R.P., Wasan D.T. *Chem Eng Sci* 1986,1,199.
- ³⁶ Kalinin V.V., Radke C.J. *Colloids Surf A Physicochem Eng Asp* 1996,114,337.
- ³⁷ Kralchevsky P.A., Danov K.D., Broze G., Mehreteab A. *Langmuir* 1999,15,2351.
- ³⁸ Para G., Jarek E., Warszynski P. *Adv. Colloid Interface Sci.* 2006, 122, 39–55.
- ³⁹ Para G., Łuczyński, Palus, J., Jarek E., Wilk K.A.,Warszyński P. *J. Colloid Interface Sci.* 2016, 465, 174–182.
- ⁴⁰ Warszyński P., Barzyk W., Lunkenheimer K., Fruhner H. *J Phys Chem B* 1998;102:10948.
- ⁴¹ Warszynski P., Lunkenheimer K., Czichocki G. *Langmuir* 2002,18,2506.
- ⁴² Para G., Jarek E., Warszyński P., Adamczyk Z. *Colloids Surf A Physicochem Eng Asp* 2003,222,213.
- ⁴³ Jarek E., Wydro P., Warszyński P. Paluch M.J. *Colloids Interface Sci.* 2006,293:194.
- ⁴⁴ Fuller G.G., Vermant J., *Annu. Rev. Chem. Biomol. Eng.* 2012. 3:519–43.
- ⁴⁵ Langevin D., *ChemPhysChem* 2008,9,510-522.
- ⁴⁶ Pepicelli M., [Verwijlen](#) T., [Tervoort](#) T.A., Vermant J., *Soft Matter*, 2017,13, 5977-5990.
- ⁴⁷ Jaensson N., Vermant J. *Current Opinion in Colloid and Interface Science* 2018,37, 136-150.
- ⁴⁸ Javadi A., Mucic N.,Karbaschi M., Won J.Y., Lotfi M., Dan A., Ulaganathan V., Gochev G., Makievski A.V., Kovalchuk V.I., Kovalchuk N.M., J. Krägel, Miller R., *Eur. Phys. J. Special Topics*, 2013, 222, 7–29.
- ⁴⁹ Sagis L.M.C, *Eur. Phys. J. Special Topics*, 2013, 222, 31–38.
- ⁵⁰ Sagis L.M.C, *Eur. Phys. J. Special Topics*, 2013, 222, 39–46.
- ⁵¹ Scriven L. *Chemical Engineering Science* 1960, 12.2,98–108.

-
- ⁵² Verwijlen T., Imperiali L., Vermant J. *Advances in Colloid and Interface Science* 2014,206, 428–436.
- ⁵³ Sagis L., *Rev. Mod. Phys.*, 2011, 83(4), 1367-1403.
- ⁵⁴ Lucassen, J., Van Den Tempel, M. *Chem. Eng. Sci.* 1972, 27, 1283–1291.
- ⁵⁵ Loglio G., Pandolfini P., Miller R, Makievski A.V., Ravera F., Ferrari M., Liggieri L. in: D. Mobius, R. Miller (Eds.), *Novel Methods to Study Interfacial Layers*, 11, Elsevier, Amsterdam, 2001, pp. 439–483.
- ⁵⁶ Ravera, F., Ferrari, M., Santini, E., Liggieri, L. *Proceedings of the Advances in Colloid and Interface Science*; 2005; Vol. 117, pp. 75–100.
- ⁵⁷ Lucassen-Reynders E.H., Cagna A. , Lucassen J., *Colloids and Surfaces A: Physicochemical and Engineering Aspects*,2001, 186, 63–72.
- ⁵⁸ Derjaguin B.V., Landau L.D. *Acta Physicochim. USSR*, 1941,14,633.
- ⁵⁹ Verwey E. J. W., Overbeek J. Th. G., *The Theory of Stability of Liophobic Colloids*, Elsevier, Amsterdam, 1948.
- ⁶⁰ Danov K.D., Kralchevsky P.A., Ivanov I.B., *Equilibrium and dynamics of surfactant adsorption monolayers and thin liquid films. Handbook of Detergents, Part A: Properties*, G. Broze, Ed.; M. Dekker, 1999,303-418.
- ⁶¹ Karakashev S.I., Grozev N.A. *Coatings* 2020, 10, 1003.
- ⁶² Chatzigiannakis E., Jaensson N., Vermant J. *Current Opinion in Colloid and Interface Science*,2021,53,101441.
- ⁶³ Langevin D., Marquez-Beltran C., Delacotte J. *Advances in Colloid and Interface Science* 2011,168,124-134.
- ⁶⁴ Drenckhan W., Hutzler S., *Advances in Colloid and Interface Science* 2015, 224, 1-16.
- ⁶⁵ Drenckhan W., Saint-Jalm A., *Advances in Colloid and Interface Science* 2015, 222, 228-259.
- ⁶⁶ Briceño-Ahumada Z., Langevin D., *Advances in Colloid and Interface Science* 2017,244,124-131.
- ⁶⁷ Hamel-Desnos C., Desnos P., Wollmann J. C., Ouvry P., Mako S., Allaert F. A., Duffy, D. M. *Dermatologic Surgery* 2003, 29(12), 1170–1175.
- ⁶⁸ Jia, X., Mowatt, G., Burr, J. M., Cassar, K., Cook, J., & Fraser, C. *British Journal of Surgery* 2007.
- ⁶⁹ Bai T., Jiang W., Chen Y., Yan F., Xu Z., Fan Y., *Scientific Reports* 2018,8,15683.
- ⁷⁰ Star P., Connor D.E., Parsi K., *Phlebology* 2018, 33(3), 150–162.
- ⁷¹ Petkova B., Tcholakova S.,Chenkova M., Golemanov K., Denkov N., Thorley D., Stoyanov S. *Adv Colloid Interface Sci* 2020,276,102084.
- ⁷² Stocco A., Drenckhan W., Rio E., Langevin D., Binks B.P. *Soft Matter* 2009, 5, 2215–2222.
- ⁷³ Meinders M. B. J. , Vliet T. V. *Adv. Colloid Interface Sci.* 2004, 108, 119–126.
- ⁷⁴ Kam S.I., Rossen W.R., *J. Colloid Interface Sci.* 1999, 213, 329–339.
- ⁷⁵ Du Z.P., Bilbao-Montoya M. P., Binks B. P., Dickinson E., Ettelaie R., Murray B.S. *Langmuir* 2003, 19, 3106–3108.
- ⁷⁶ Binks B.P., Kirkland M., Rodrigues J.A. *Soft Matter* 2008, 4, 2373–2382.

-
- ⁷⁷ Liggieri L., Santini E., Guzmán E., Maestro A., Ravera F., *Soft Matter* 2011,7,7699–7709.
- ⁷⁸ Hunter T. N., Pugh R. J., Franks G. V., Jameson G. J., *Adv. Colloid Interface Sci.* 2008, 137, 57–81.
- ⁷⁹ Alargova R.G., Warhadpande D.S., Paunov V.N., Veleev O.D. *Langmuir* 2004,20,10371–4.
- ⁸⁰ Ravera F., Ferrari M., Liggieri L., Loglio G., Santini E., Zanolini A., *Colloids and Surfaces A: Physicochem. Eng. Aspects* 2008, 323, 99–108.
- ⁸¹ Rio E., Drenckhan W., Salonen A., Langevin D. *Advances in Colloid and Interface Science* 2014,205,74-86.
- ⁸² Fameau A-L., Saint-Jalmes A., Cousin F., Houinsou Houssou B.H., Novales B., Navailles L., Nallet F., Gaillard V., Bou F., Douliez J.-P., *Angew. Chem. Int. Ed.* 2011, 50, 8264 –8269.
- ⁸³ Hamad W. Y., *Cellulose Nanocrystals, Properties, Production and Applications*, Wiley, 2017.
- ⁸⁴ Abitbol T., Kam D., Levi-Kalisman Y., Gray D. G., Shoseyov O. *Langmuir* 2018, 34(13), 3925–3933.
- ⁸⁵ Cervin N.T., Johansson E., Benjamins J.-W., Wågberg L., *Biomacromolecules* 2015, 6(3), 822–831.
- ⁸⁶ Wege H. A., Kim S., Paunov V. N., Zhong Q., Veleev O. D. *Langmuir* 2008, 24, 9245–9253.
- ⁸⁷ Andrews, M.P.; Morse, T. Method for Producing Functionalized Nanocrystalline Cellulose and Functionalized Nanocrystalline Cellulose Thereby Produced. U.S. Patent 20,170,260,298 A1, 14 September 2017.
- ⁸⁸ Usov, I.; Nyström, G.; Adamcik, J.; Handschin, S.; Schütz, C.; Fall, A.; Bergström, L.; Mezzenga, R., *Nat. Commun.* 2015, 6, 7564.
- ⁸⁹ Kádár R., Spirk S., Nypelö T., *ACS Nano* 2021, 15, 5, 7931–7945.
- ⁹⁰ Kang, K.; Eremin, A., *Phys. Rev. E* 2021, 103, 032606.
- ⁹¹ Hu, Z.; Xu, R.; Cranston, E.D.; Pelton, R.H., *Biomacromolecules* 2016, 17, 12, 4095–4099.
- ⁹² Kalashnikova, I., Bizot, H., Bertoncini, P., Cathalaa, B., Capron, I. *Soft Matter* 2013, 9, 952–959.
- ⁹³ Kalashnikova, I.; Bizot, H.; Cathala, B.; Capron, I. *Biomacromolecules* 2012, 13, 267–275.
- ⁹⁴ Bertsch, P.; Diener, M.; Adamcik, J.; Scheuble, N.; Geue, T.; Mezzenga, R.; Fischer, P. *Langmuir* 2018, 34, 50, 15195–15202.
- ⁹⁵ C. Maze, G. Burnet, *Surface Sci.*, 1969,13, 451.
- ⁹⁶ Giménez-Ribes G., Habibi M., Sagis L.M.C *Journal of Colloid and Interface Science*,563,2020,281-290.
- ⁹⁷ Vandebril S, Franck A, Fuller G.G., Moldenaers P, Vermant J. *Rheol. Acta* 2010, 49,131–44.
- ⁹⁸ Cascao Pereira L.G., Johansson C., Blanch H.W., Radke C.J. *Colloids and Surfaces A: Physicochemical and Engineering Aspects* 2001,186, 103–111.
- ⁹⁹ Chatzigiannakis E., Veenstra P., Bosch D., Vermant J. *Soft Matter*,2020,16, 9410-9422.
- ¹⁰⁰ Beltramo P.J., Rob Van Hooghten R., Vermant J. *Soft Matter* 2016,12, 4324-4331.
- ¹⁰¹ Rullier B., Axelos M.A.V., Langevin D., Novales B. *Journal of Colloid and Interface Science* 2010, 343,330–337.
- ¹⁰² Chandran Suja V., Rodríguez-Hakim M., Tajuelo J., Fuller G.G. *Advances in Colloid and Interface Science* 2020,286, 102295.

-
- ¹⁰³ Chandran Suja V., Kar A., Cates W., Remmert S., Savage P., Fuller G. Proceedings of the National Academy of Sciences 2018,115(31),7919–7924.
- ¹⁰⁴ Chandran Suja V., Kar A., Cates W., Remmert S., Fuller G.G. Journal of Colloid and Interface Science 2020,567,1–9.
- ¹⁰⁵ Frostad J.M., Tammaro D., Santollani L., de Araujo S.B., Fuller G.G. Soft matter 2016, 12(46), 9266–9279.
- ¹⁰⁶ Kannan A., Shieh I.C., Fuller G.G. Journal of colloid and interface science. 2019,550,128–138.
- ¹⁰⁷ Mewis J., Wagner N.J., Colloidal suspension rheology, Cambridge University Press, 2012.
- ¹⁰⁸ Asker, D., Weiss, J., McClements, D.J. Langmuir 2009, 25, 116–122.
- ¹⁰⁹ Bonnaud, M., Weiss, J., McClements, D.J. J. Agric. Food Chem. 2010, 58, 9770–9777.
- ¹¹⁰ Infante, R., Domingues, J.G., Erra, P., Julia, R., Prats, M. Int. J. Cosmet. Sci. 1984,6,275–282.
- ¹¹¹ Kawamura, Y., Whitehouse, B. Ethyl Lauroyl Arginate. Chemical and Technical Assessment; FAO: Rome, Italy,2008.
- ¹¹² Singare, P., D. Mhatre, J. Am. J. Chem. 2012, 2,186–190.
- ¹¹³ Yoshida, R., Baba, K., Saito, T., Yoshimura, I. J. Japan Oil Chem. Soc. 1976, 25, 404–408.
- ¹¹⁴ Takehara, M. Colloids and Surfaces 1989, 38, 149–167.
- ¹¹⁵ Czakaj A., Jarek E., Krzan M., Warszyński P. Molecules 2021, 26, 5894.
- ¹¹⁶ Góralczyk, D.; Hąc, K.; Wydro, P.S. Colloids Surfaces A Physicochem. Eng. Asp. 2003, 220, 55–60.
- ¹¹⁷ Lunkenheimer, K.; Barzyk, W.; Hirte, R.; Rudert, R. Langmuir 2003, 19, 6140–6150.
- ¹¹⁸ Lunkenheimer, K., Haage, K., Miller, R. Colloids and Surfaces 1987, 22, 207–214.
- ¹¹⁹ Para, G.; Hamerska-Dudra, A.; Wilk, K.A.; Warszyński, P. Colloids Surfaces A Physicochem. Eng. Asp. 2010, 365, 215–221.
- ¹²⁰ Para, G.; Hamerska-Dudra, A.; Wilk, K.A.; Warszyński, P. Colloids Surfaces A Physicochem. Eng. Asp. 2011, 383, 67–72.
- ¹²¹ Krieger, E.; Vriend, G. J. Comput. Chem. 2015, 36, 996–1007
- ¹²² Vazdar M., Heyda, J., Mason P.E., Tesi G., Allolio, C. Lund, M., Jungwirth, P. Acc. Chem. Res. 2018, 51, 1455–1464.
- ¹²³ Zamora, J.M.; Marquez, R.; Forgiarini, A.M.; Langevin, D.; Salager, J.L. J. Colloid Interface Sci. 2018, 519, 27–37.
- ¹²⁴ Loglio G., Kovalchuk, V.I., Bykov, A.G., Ferrari, M., Krägel, J., Liggieri, L., Miller, R., Noskov, B.A.; Pandolfini, P., Ravera, F. et al. Colloids and Interfaces 2018, 2, 53.
- ¹²⁵ Monteux C., Fuller G.G., Bergeron V. J. Phys. Chem. B 2004, 108, 16473-16482.
- ¹²⁶ Reynaert S., Moldenaers P., Vermant J. Phys. Chem. Chem. Phys., 2007, 9, 6463–6475.
- ¹²⁷ Bertsch P., Fischer P. Advances in Colloid and Interface Science, 220, 276,102089.
- ¹²⁸ Xiong, B., Zhao, P., Hu, K., Zhang L., Cheng G., Cellulose, 2014, 21, 1183–1192.

¹²⁹ Firouzi M., Kovalchuk V.I., Loglio G., Miller R., *Current Opinion in Colloid & Interface Science*, 2021, 101538.

¹³⁰ Amani P., Karakashev S.I., Grozev N.A., Simeonova S.S., Miller R., Rudolph V., Firouzi M., *Advances in Colloid and Interface Science*, 2021, 295, 102490.

¹³¹ Moll, C.J.; Versluis, J.; Bakker, H.B. *J. Phys. Chem. Lett.* 2021, 12, 10823–10828.

¹³² Traykov, T. T., Manev, E. D., & Ivanov, I. B. *International Journal of Multiphase Flow*, 1977, 3(5), 485-494.

¹³³ Bhamla, M. S., Chai, C., Alvarez-Valenzuela, M. A., Tajuelo, J., & Fuller, G. G. *PloS one* 2017, 12(5), e0175753.

¹³⁴ Mikhailovskaya, A., Chatzigiannakis, E., Renggli, D., Vermant, J., Monteux, C. *Langmuir* 2022, 38, 10768–10780.

Article

Ethyl Lauroyl Arginate, an Inherently Multicomponent Surfactant System

Agnieszka Czakaj ^{*}, Ewelina Jarek , Marcel Krzan  and Piotr Warszyński ^{*} 

Jerzy Haber Institute of Catalysis and Surface Chemistry, Polish Academy of Sciences, 30-239 Krakow, Poland; ewelina.jarek@ikifp.edu.pl (E.J.); marcel.krzan@ikifp.edu.pl (M.K.)

^{*} Correspondence: ncczakaj@cyf-kr.edu.pl (A.C.); piotr.warszynski@ikifp.edu.pl (P.W.)

Abstract: Ethyl lauroyl arginate (LAE) is an amino acid-based cationic surfactant with low toxicity and antimicrobial activity. It is widely used as a food preservative and component for food packaging. When stored, LAE decomposes by hydrolysis into surface-active components N α -lauroyl-L-arginine (LAS) or dodecanoic (lauric) acid. There are only a limited number of reports considering the mechanism of surface activity of LAE. Thus, we analysed the surface tension isotherm of LAE with analytical standard purity in relation to LAE after prolonged storage. We used quantum mechanical density functional theory (DFT) computations to determine the preferred hydrolysis path and discuss the possibility of forming highly surface-active heterodimers, LAE-dodecanoate anion, or LAE-LAS. Applying molecular dynamics simulations, we determined the stability of those dimers linked by electrostatic interactions and hydrogen bonds. We used the adsorption model of surfactant mixtures to successfully describe the experimental surface tension isotherms. The real part surface dilational modulus determined by the oscillation drop method follows a diffusional transport mechanism. However, the nonlinear response of the surface tension could be observed for LAE concentration close to and above Critical Micelle Concentration (CMC). Nonlinearity originates from the presence of micelles and the reorganisation of the interfacial layer.

Keywords: ethyl lauroyl arginate (LAE); surface tension; surface activity; surface dilational elasticity; hydrolysis; dimerisation



Citation: Czakaj, A.; Jarek, E.; Krzan, M.; Warszyński, P. Ethyl Lauroyl Arginate, an Inherently Multicomponent Surfactant System. *Molecules* **2021**, *26*, 5894. <https://doi.org/10.3390/molecules26195894>

Academic Editor: Katarzyna Szymczyk

Received: 9 August 2021

Accepted: 25 September 2021

Published: 29 September 2021

Publisher's Note: MDPI stays neutral with regard to jurisdictional claims in published maps and institutional affiliations.



Copyright: © 2021 by the authors. Licensee MDPI, Basel, Switzerland. This article is an open access article distributed under the terms and conditions of the Creative Commons Attribution (CC BY) license (<https://creativecommons.org/licenses/by/4.0/>).

1. Introduction

Ethyl lauroyl arginate (LAE) is an amino acid-based cationic surfactant synthesised from L-arginine, lauric acid and ethanol [1]. It has been approved and generally recognised as safe (GRAS) for some food and biomedical applications by the USA Food and Drug Administration (FDA) and the European Food Safety Agency (EFSA) [2,3]. Toxicological studies have demonstrated LAE's low toxicity as it can be hydrolysed by chemical and metabolic pathways into components that are easily further metabolised [3,4]. Ethyl lauroyl arginate has strong antimicrobial activity against various microorganisms, including moulds, yeasts, Gram-positive, and Gram-negative bacteria. As a cationic surfactant, it can penetrate the bacterial cytoplasmic membrane that causes its deformation and the loss of cell viability [5–7]. There are numerous reports on the application of LAE as a food preservative and component for food packaging [2,8]. The interactions of ethyl lauroyl arginate with biopolymers were investigated using various physicochemical methods [2,9]. The results indicated strong electrostatic binding between LAE and anionic biopolymers leading to complex formation that can have implications for the formulation of delivery systems [10] or other industrial applications [11]. Strong binding of LAE to the surface of negatively charged nanoparticles can be used to modify their surface properties for particular applications. For example, ethyl lauroyl arginate was used to modify the cellulose nanocrystals (CNC) for the improvement of foamability and foam stability [12] or stability of emulsions [13]. Three types of LAE-CNC interactions were recognised: the electrostatic

attraction at low surfactant concentrations, followed by the hydrophobic interaction, and polymer-induced micellisation [14].

LAE molecular weight is 421 g/mol. It is a positively charged surfactant with pKa at about 10–11 and the isoelectric point above pH 12. It is stable for more than two years at room temperature in a closed container. In an aqueous solution at 25 °C, its half-life decreases from more than one year at pH 4, to 57 days at pH 7, and 34 h at pH 9 [15], indicating its decomposition by base-catalysed hydrolysis. Thus, the combined effect of temperature with pH conditions markedly influences the hydrolysis of LAE to N α -lauroyl-L-arginine (LAS) or arginine and lauric acid [15]. The commercially available food-grade LAE consists of not less than 85%, and not more than 95%, ethyl-N- α -lauroyl-L-arginate·HCl with the limits for contaminants from the synthesis set for: LAS (<3%); lauric acid (<5%); ethyl laurate (<3%); L-arginine·HCl (<1%) and ethyl arginate·2HCl (<1%) [3].

Adsorption properties of LAE at the water/air interface, its surface tension and critical micellisation concentration (CMC) have been investigated by many authors, but there are only a few reports where the surface tension isotherms can be found. Chi and Catchmark measured the surface tension isotherm of food-grade ($\geq 98\%$ purity) LAE and determined the CMC at 4.5 mM with the surface tension at CMC, $\sigma_{\text{CMC}} = 26.4$ mN/m [14]. Bai et al. used Mirenat-G containing 10.5% LAE in glycerol, measured the surface tension isotherm and established the CMC value at 0.1%wt (2.4 mM), and the σ_{CMC} around 26 mN/m [13]. In our recent work, we determined the surface tension isotherm of LAE surfactant (commercial name Mirenat-P/100) with about 90% surfactant content and obtained similar results [12]. Other authors presented CMC and σ_{CMC} values without reporting the isotherms. Their results are collected in Table 1.

Table 1. The results of characterization of CMC of LAE solution by various authors.

Scheme	LAE Content	CMC (mM)	σ_{CMC} (mN/m)	Method	Reference
Mirenat-CF	10.5% in propylene glycol	4.9	-	Isothermal titration calorimetry	[2]
Mirenat-CF	10.5% in propylene glycol	4.5	-	Isothermal titration calorimetry	[9]
LAE Synthesized	-	6.0	31.8	Ring tensiometer	[16]
LAE (LAMIRSA)	85–95%	2.4	25.4	Ring tensiometer	[17]
LAE.HCl (local supplier)	-	0.9	25.5	Conductivity, ring tensiometer	[18]
LAE synthesized	>95%	6.2	30.2	Ring tensiometer	[19,20]

The discrepancies between the results reported above can be attributed to the differences in LAE solution composition. They can contain surface-active residuals from LAE synthesis that are also the surfactant hydrolysis products. Namely, N α -lauroyl-L-arginine (LAS), that in neutral and mildly acidic conditions (above pH 5), is the amphoteric surfactant with a much lower solubility in aqueous media (<0.1 mM) than cationic LAE. Its minimal surface tension at the solubility limit is 43.8 mN/m [16]. Dodecanoic (Lauric) acid (DDA) has pK_a = 4.95. It is neutral at acidic pH and anionic at pH > 4.5. Consequently, each LAE solution is a mixed surfactant system, and the presence of additional surface-active components affects surface tension and CMC values.

The arguments presented above indicate that the thorough analysis of the surface activity of the well-defined LAE solutions still needs to be performed and the effect of surface-active contaminants evaluated. Moreover, the analysis of the dynamic surface tension and surface elasticity of LAE has never been conducted before. Our paper aimed to fill that void and to measure the surface tension isotherm of LAE of high purity (USP Reference Standard), determine the importance of different hydrolysis pathways by making quantum mechanical DFT calculations, and estimate the effect of the formation of LAE-DDA and LAE-LAS dimers that should exhibit very high surface activity. Considering the

possibility of broad applications of LAE in biomedical, cosmetic and food processing areas, it is crucial to determine the mechanisms of its surface activity and aggregation properties.

2. Results and Discussion

We measured the surface tension of the freshly prepared LAE solution and determined its dependence on the surfactant concentration. The results are illustrated in Figure 1. The surface tension isotherm of LAE was compared with ones obtained for some model cationic and nonionic surfactants.

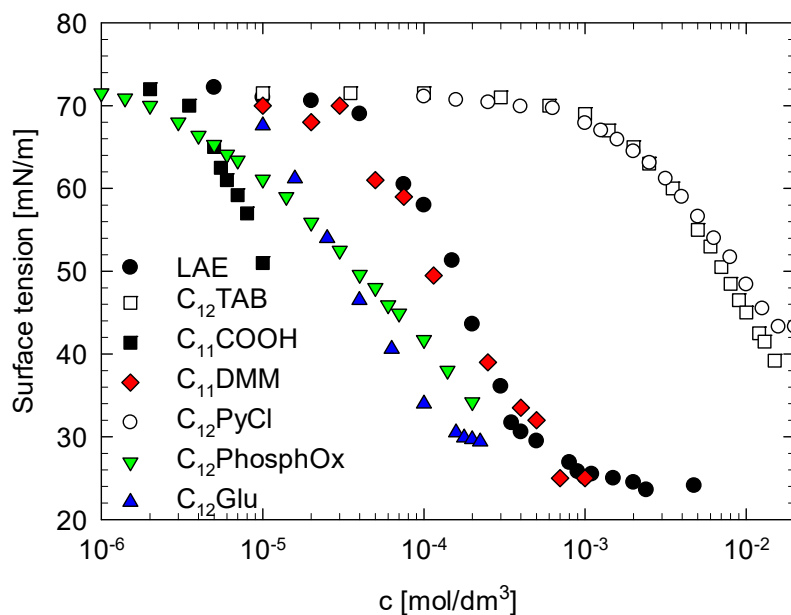


Figure 1. The comparison of the surface tension isotherm of LAE with ones obtained for some model cationic and nonionic surfactants: dodecyl trimethylammonium bromide ($C_{12}TAB$), dodecyl pyridinium chloride ($C_{12}PyCl$), ($C_{11}COOH$), *n*-dodecyl- β -D-glucoside ($C_{12}Glu$), *n*-dodecyl dimethyl phosphine oxide ($C_{12}PhospOx$) and *N,N,N*-trimethyl-2-(dodecanoyloxy)ethane ammonium bromide ($C_{11}DMM$).

The onset of the surface activity of LAE was at the concentration 10^{-4} mol/dm³ and so at c.a. one order of magnitude lower concentration than of typical cationic surfactants with the same hydrocarbon chain length, dodecyl trimethylammonium bromide ($C_{12}TAB$) [21] and dodecyl pyridinium chloride ($C_{12}PyCl$) [22]. Simultaneously, that onset was at the concentration at least one order of magnitude higher than of nonionic surfactants such as nondissociated dodecanoic acid ($C_{11}COOH$) [23], *n*-dodecyl- β -D-glucoside ($C_{12}Glu$) [24] or *n*-dodecyl dimethyl phosphine oxide ($C_{12}PhospOx$) [25]. The surface activity of LAE was the most similar to that observed for the solution of *N,N,N*-trimethyl-2-(dodecanoyloxy)ethane ammonium bromide ($C_{11}DMM$) [26]. It was demonstrated that the surface activity of that surfactant resulted from the synergistic effect of adsorption of cationic surfactant— $C_{11}DMM$ and surface-active anion—dodecanoate that was the product of surfactant hydrolysis. $C_{11}DMM$ and dodecanoate can form electrostatically bound heterodimers with very high surface activity [26]. The CMC value of LAE was at the concentration 1.0–1.1 mmol/dm³, in agreement with the value reported in [18], lower than in other reports (see Table 1). The surface tension value at CMC (σ_{CMC}) was 25 mN/m, much lower than for typical cationic surfactants, closer to σ_{CMC} for nonionic surfactants and characteristic for di-chain or Gemini surfactants [27,28]. Thus, such a low value of σ_{CMC} may support the idea of the formation of surface-active dimers, dodecanoate anion, that can be present in the solution at pH > 4.5 as the residual product of LAE synthesis or its hydrolysis. There are reproducible peculiarities of the isotherm shape at the concentration above 0.5 mM. The surface tension decreases but with a much lower slope to CMC.

Upon addition of salt, LAE behaves as a typical ionic surfactant, i.e., its surface tension drops due to the screening of electrostatic interaction between adsorbing surfactant molecules that contributes to the increase in surface activity, as illustrated in Figure 2a. After prolonged storage of the stock solution (over two weeks in 4 °C, pH 4.5), a significant change of the isotherm shape was observed, as shown in Figure 2b. It had a less steep slope, and the surface tension values were lower than for freshly prepared LAE solution for concentrations below 0.2 mM, and higher above that value. We hypothesised that the observed variation of the surface tension values resulted from changes in the surfactant solution composition due to LAE hydrolysis.

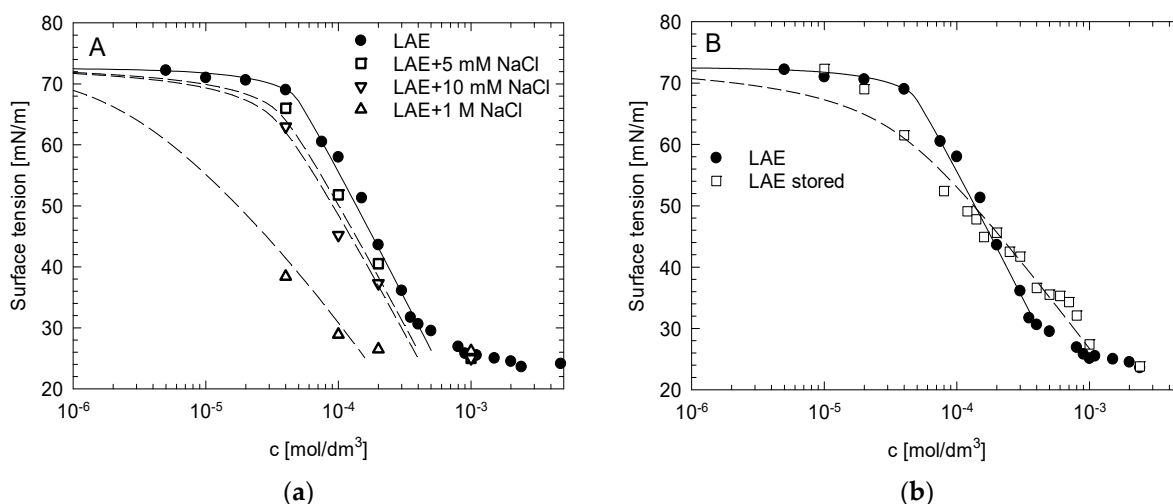


Figure 2. (a) The change of the dependence of surface tension on the concentration of LAE solution upon addition of salt (NaCl); (b) the comparison of LAE surface tension isotherms for freshly prepared and “stored” solution. Lines represent fits to the model of LAE adsorption accounting for the formation of LAE-dodecanoate or LAE-LAS heterodimers.

LAE can undergo hydrolysis via two paths. In the first path, the amide bond between the hydrophobic hydrocarbon chain and the hydrophilic headgroup can be hydrolysed, resulting in the L-arginine ethyl ester that is not a surface-active component, and surface-active dodecanoic (lauric) acid (see Figure 1) that above its pKa assumes the form of dodecanoate anion. In the second path, the ester bond linking side ethyl group hydrolyses, giving the surface-active N $_{\alpha}$ -lauroyl-L-arginine and ethanol. We used the quantum chemical DFT computations to evaluate the energetics of base and acid-catalysed hydrolysis proceeding along these pathways. The schemes of reactions are depicted in the Supplementary Materials (Figures S1 and S2) and the results of computations are given in Table 2.

Table 2. Energies, enthalpies and free energies of LAE hydrolysis reactions ΔE_h and their transition states ΔE_t .

Hydrolysis Path	Data	Base Catalysed		Acid Catalysed	
		ΔE_t [kcal/mol]	ΔE_h [kcal/mol]	ΔE_t [kcal/mol]	ΔE_h [kcal/mol]
LAE \rightarrow L-arginine ethyl ester + dodecanoate/dodecanoic acid	energy	7.0	−10.3	20.7	11.2
	enthalpy	6.4	−10.3	20.1	11.2
	free energy	17.5	−15.6	31.3	9.0
LAE \rightarrow LAS + ethanol	energy	−4.3	−21.6	12.8	5.7
	enthalpy	−4.3	−21.6	12.2	5.7
	free energy	4.9	−24.2	23.8	4.4

Considering the DFT computation results given in Table 2, we concluded that base-catalysed hydrolysis is irreversible; free energy of hydrolysis is equal to 15.6 kcal/mol for the first path and 24.2 kcal/mol for the second path. The entropic barrier, associated with

the nucleophilic addition step, was much higher for the first path producing dodecanoate anion, than for the second, resulting in LAS formation. On the other hand, the acid-catalysed hydrolysis seemed to be not favourable at standard conditions (298 K, 1 atm). Although fresh LAE solution is mildly acidic, pH 5.15 at 4×10^{-5} M and pH 5 at 0.1 mM concentration (possibly because of the presence of lauric acid residues), due to the cationic charge of the surfactant, the base-catalysed hydrolysis can occur with a measurable rate. This occurs, in particular, at the water/air interface or at interfaces of surfactant micelles that are highly positively charged, whereby a local concentration of hydroxyl anions is increased. LAS was identified as the main product of LAE hydrolysis in simulated gastrointestinal conditions [29], and the LAS involving hydrolysis path was recognised as the first stage of the metabolic pathway for ethyl lauroyl arginate [30].

Hydrolysis products of both paths, bearing the hydrocarbon tail, dodecanoate anion or dodecanoic acid and LAS, are surface-active. Moreover, they can interact with LAE molecule forming heterodimers. In the solution, besides the hydrophobic effect of two hydrophobic tails, the LAE-dodecanoate heterodimer is bound by the electrostatic interaction of oppositely charged molecules. Moreover, due to three hydrogen bond donors of LAE, that heterodimer can be stabilised by hydrogen bonds. LAS is a zwitterionic molecule (at pH around 5); thus, its electrostatic interaction with LAE is weaker. On the other hand, due to 4 hydrogen bond donors and 6 acceptors, they can form hydrogen bounded heterodimers. Moreover, it was reported that guanidinium groups, despite their positive charge, could pair in salts solutions that may additionally contribute to the heterodimers' stabilisation [31,32].

We used the DFT computations to evaluate the energetics of formation of the heterodimers LAE-dodecanoate anion and LAE-LAS. The optimised structures of those dimers are illustrated in Figure 3, and the results of computations are given in Table 3. They indicate the favourable formation of heterodimers with a stronger tendency to form LAE-LAS aggregates despite missing electrostatic attraction between molecules. The creation of LAE-LAS heterodimers can be followed by the formation of larger aggregates as the hydrolysis progresses. We observed that after a week of storage of 1 mM LAE solution, a white cloudy phase appeared with precipitated needle-like crystals, and the surface tension of the supernatant phase systematically increased. After 14 days, it reached 30 mN/m, about 5 mN/m higher than for fresh LAE solution, while pH of the solution decreased to 4.5.

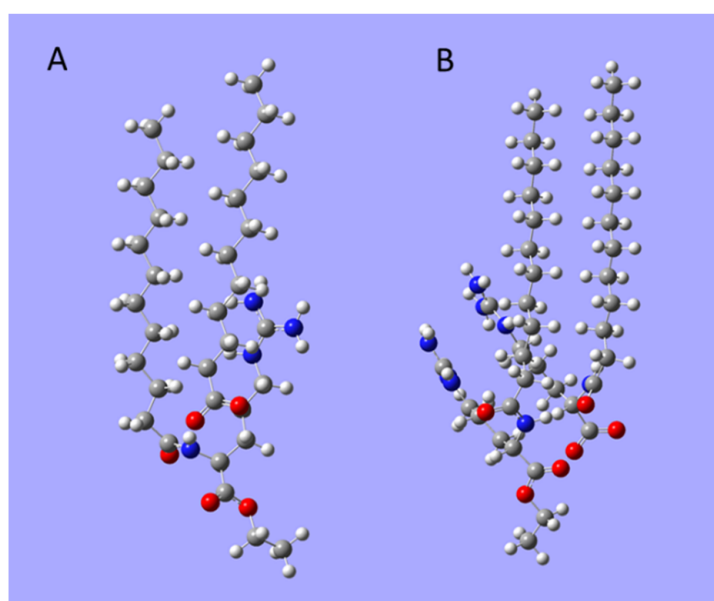


Figure 3. The optimised structures of (A) LAE-dodecanoate, (B) LAE-LAS heterodimers. Grey, carbon; white, hydrogen; red, oxygen; blue, nitrogen.

Table 3. Energies, enthalpies and free energies of formation of LAE heterodimers.

Dimerization	Energy [kcal/mol]	Enthalpy [kcal/mol]	Free Energy [kcal/mol]
LAE-dodecanoate	−20.2	−21.0	−1.6
LAE-LAS	−29.4	−29.9	−6.5

We examined the existence and stability of the heterodimers at the air/water interface by molecular dynamics simulations. Figure 4 presents the representative snapshots illustrating the conformation of dimers at the interface.

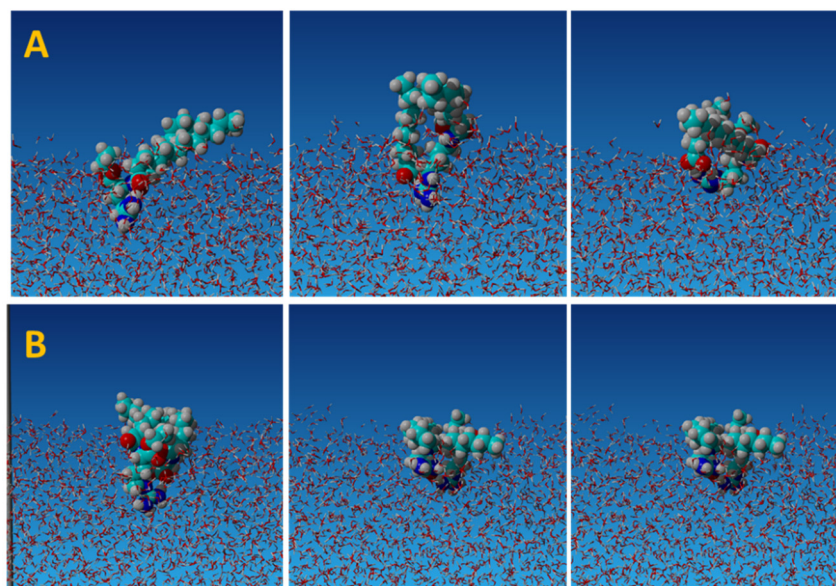


Figure 4. The examples of snapshots of molecular dynamics simulations of heterodimers at air/water interface. (A) LAE–dodecanoate; (B) LAE-LAS. Light blue, carbon; white, hydrogen; red, oxygen; blue, nitrogen.

Using the algorithm implemented in the YASARA Structure simulation package [33], we determined the distance between molecules forming heterodimers during the simulation run (300 ns) after the molecules appeared at the interface, and counted the number of hydrogen bonds. The results are illustrated in Figure S3. Despite the competition of surrounding water in the interfacial layer for hydrogen bonding, the intermolecular hydrogen bonds contributed to the formation of persistent dimers. The LAE-dodecanoate formed the heterodimer during 35% of the simulation run with the average number of bonds 1.71, while the average number of hydrogen bonds of both molecules with water was 9.8. Additionally, the heterodimer was stabilised by electrostatic interactions between cationic LAE and the dodecanoate anion. The LAE-LAS formed the heterodimer during 50% of the simulation run with the average number of intermolecular hydrogen bonds 1.96, while the average number of hydrogen bonds of both molecules with water was 14.6. The heterodimer can be additionally stabilised by the interactions of guanidinium groups not accounted for in the applied molecular dynamics force field [32]. The presence of the intermolecular hydrogen bonds between *n*-dodecyl- β -D-maltoside molecules at the air/water interface was recently demonstrated by molecular dynamics simulations and grazing-incidence X-ray (GIX) scattering and diffraction [34]. The molecular dynamics simulations result was in agreement with QM computations and indicated that LAE forms more stable heterodimers with LAS. It means that with the progress of hydrolysis, the amount of those dimers increases, which should be reflected in the change of the surface activity of the resulting surfactant mixture.

We attempted to model the LAE surface tension isotherms utilising the description of adsorption of mixtures of surface-active compounds based on the quasi-two dimensional

electrolyte model of ionic surfactants adsorption [21,26]. Details of the model are given in the Supplementary Materials. Considering the outcome of QM and MD simulations, we assumed that for the fresh solution, LAE was not hydrolysed but contained less than 0.5% molar of decanoic acid as a residual component from the synthesis. For the surfactant stored for more than two weeks, we assumed that the solution comprised a mixture of LAE and LAS. Since the formation of heterodimers was energetically favourable, we assumed that in both cases, the mixture contained monomeric LAE and LAE-dodecanoate anion or LAE-LAS dimers, respectively. As illustrated in Figure 2a, we obtained a satisfactory description of the experimental surface tension isotherms for the fresh LAE solution assuming 0.2% molar of dodecanoate anions, without and with the addition of NaCl. For the stored solution, a satisfactory description could be received assuming 18% molar of LAS resulting from the hydrolysis of the LAE stock solution during storage (cf. Figure 2b). The values of the best-fit parameters are collected in Table S1 in the Supplementary Materials. Since, with ageing, the composition of the mixture changes, fraction of LAS increases and pH decreases, the LAE-DDA neutral heterodimers are replaced with positive heterodimers LAE-LAS that result in the apparent CMC increase. Simultaneously, when pH decreases, fraction of LAS becomes protonated, cationic, and thus less surface-active with a lower tendency to form heterodimers with LAE.

We used the oscillating drop shape tensiometry to determine the dynamic interfacial properties and the surface dilational viscoelasticity of LAE solutions. The applied frequency of the drop oscillation was in the range of 0.01 and 0.2 Hz. Figure 5 presents the oscillations of the drop area (dashed line) and the corresponding changes of the surface tension for LAE concentration: A, 0.2 mM; B, 0.5 mM; C, 0.8 mM; D, 1 mM; and E, 1.5 mM, for the oscillation frequency 0.01 Hz and 0.1 Hz. For low surfactant concentration, the oscillation of the surface tension had a sinusoidal shape. At higher frequencies, the signal was noisy, presumably due to the slow relaxation of the interfacial layer composed of surfactant mixture. For the concentration 0.8 mM, the sinusoidal oscillations of the surface tension became distorted at the compression, with a large phase shift between the variations of drop area and surface tension. Even though the drop area continued to be compressed, the surface tension started to increase due to surfactant desorption. The distortion of the surface tension was more pronounced at higher frequencies and increased for the LAE concentration close to (1 mM) and above (1.5 mM) CMC.

Figure 6 illustrates the frequency dependence of the real and imaginary part of the dilational elasticity modulus determined for various concentrations of LAE solutions. The real part of the modulus increases with drop area oscillation frequency (ν) and can be successfully described by fitting the Lucassen-van den Tempel diffusional adsorption model valid for the surfactant concentration below CMC [35,36]:

$$\varepsilon = \varepsilon_0 \frac{1 + \xi + i\xi}{1 + 2\xi + 2\xi^2}, \quad \xi = \sqrt{\frac{\nu_D}{2\nu}} \quad (1)$$

where: ε_0 is the Gibbs elasticity, ν_D is the characteristic frequency of the diffusion transport mechanism. Best fit parameters are collected in Table 4. On the other hand, the imaginary part of the dilational elasticity modulus can be described by that model only for low frequencies and the concentrations below 0.5 mM, which indicates that the surface elasticity of LAE solutions needs to be described by more complex models than diffusional adsorption of single surfactant [37]. The maximum of the real and imaginary part of surface dilational elasticity moduli was observed at 0.3 mM and they decreased with increasing surfactant concentration (cf. Figure S5 in the Supplementary Materials). Above the CMC at higher frequencies, the surfactant layer seemed to be more viscous as the imaginary part of the modulus increased and exceeded the real one. This can be a consequence of shear effects and a nonlinear response for drop oscillation [36]; however, Loglio et al. attributed the increase in the phase shift, i.e., the imaginary part of the modulus, with the drop oscillation frequency, to the presence of surfactant mixture [38]. After storage for 14 days, as the

surface tension at CMC (1 mM) increased by c.a. 5 mN/m, both modulus components also increased and surfactant layers seemed more elastic.

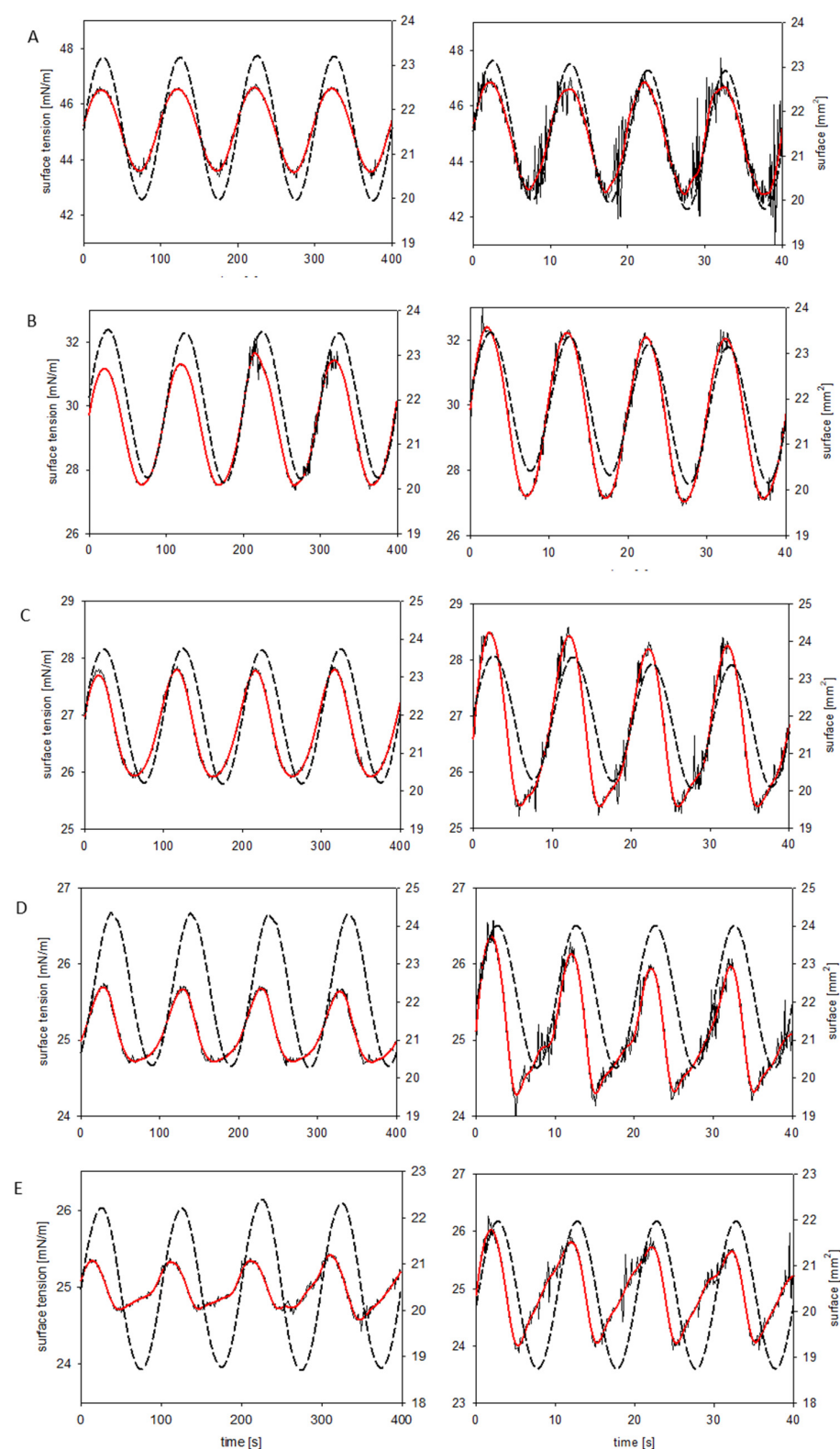


Figure 5. Oscillations of the drop area (dashed line) and the corresponding changes of the surface tension. Red line: the surface tension after Loess smoothing. LAE concentration: (A) 0.2 mM; (B) 0.5 mM; (C) 0.8 mM; (D) 1 mM; (E) 1.5 mM. Frequency: left, 0.01 Hz; right, 0.1 Hz.

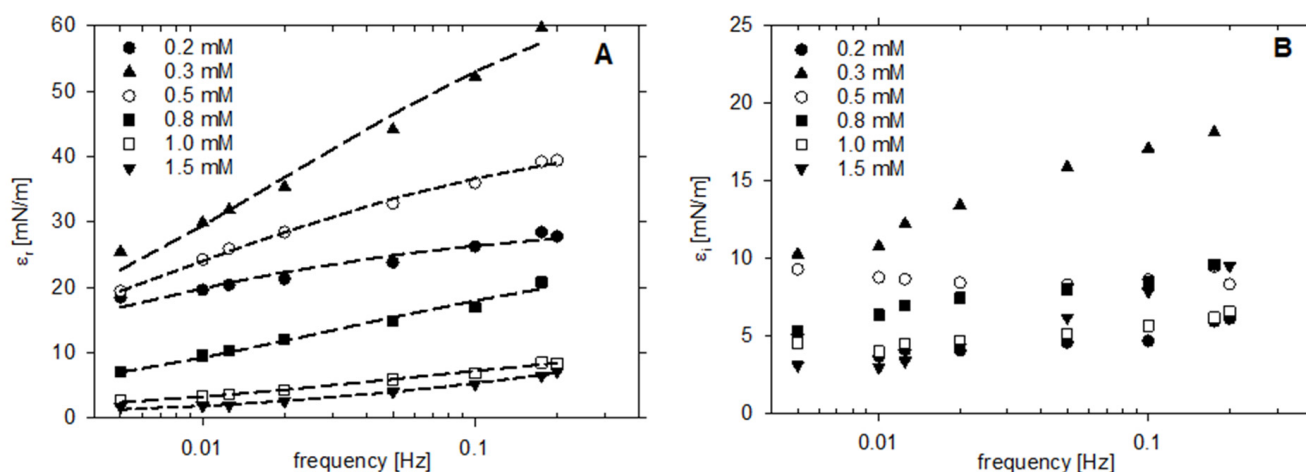


Figure 6. The dependence of (A) real, and (B) imaginary, parts of the dilational elasticity modulus on the drop surface oscillation frequency for various concentrations of LAE solutions. Dashed lines: fits of the Lucassen-van den Tempel diffusional adsorption model.

Table 4. Best fit parameters of the Lucassen-van der Tempel model to the real part of surface dilational elasticity modulus of LAE solutions.

Concentration [mM]	ε_0 [mN/m]	ν_D [Hz]
0.2	30.1	0.0032
0.3	73.9	0.02
0.5	45.3	0.0081
0.8	26.9	0.03
1.0	12.6	0.06

To evaluate the effect of the distortion of the surface tension oscillations from a sinusoidal shape, we calculated the dependence of the ratio of amplitudes of second to first harmonics in the Fourier spectrum $\frac{F(\Delta\sigma)_2}{F(\Delta\sigma)_1}$ on LAE concentration. The results are illustrated in Figure 7. The onset of the nonlinear response of the LAE surface layer was around 0.5 mM; it increased up to CMC (1 mM) and levelled off. Therefore, low values of the elasticity modulus and the nonlinear response can be attributed to micellisation. Let us consider a single cycle of drop surface compression and decompression at the surfactant concentration at CMC. At the particular level of compression, the surface becomes oversaturated with the surfactant, desorption starts, and the desorbed surfactant is integrated into micelles; thus, the desorption rate is not attenuated by the local increase in monomeric surfactant concentration. Consequently, higher surface tension is observed with respect to sinusoidal dependence. Additionally, the heterodimers with higher area demand could be the first to be desorbed. Upon surface decompression, the desorption continues as long as the surface is oversaturated, then surfactant adsorption starts. Micelles play the role of the reservoir speeding up the adsorption, and the surface tension starts to decrease before the onset of drop surface compression. Consequently, the upper half of the surface tension oscillation cycle has a more regular shape. On the other hand, the irregular shape of the surface tension oscillations at LAE concentration 0.8 mM could also be attributed to the rearrangement of the surfactant layer due to the presence of heterodimers.

For low surfactant concentrations, the values of surface dilational modulus of LAE solutions were similar to those for DTAB [39]. However, for concentrations closer to CMC, they were much smaller, probably due to the neutralisation of the interfacial layer due to the presence of LAE-dodecanoate dimers. A similar dependence of the elasticity modulus on the surfactant concentration was observed for nonionic surfactant dodecyl dimethyl phosphine oxide [40]. The maximum was observed at a concentration about 10 times lower than CMC, a sharp drop at the CMC, and the constant value above. We found the increase

in the phase shift of the surface tension variations with the drop oscillation frequency as suggested by Loglio et al. for surfactant mixtures [38]. The above observation is consistent with our claim that LAE solution should be considered as the mixed surfactant system consisting of monomeric LAE molecules and its heterodimers with dodecanoate anions or LAS.

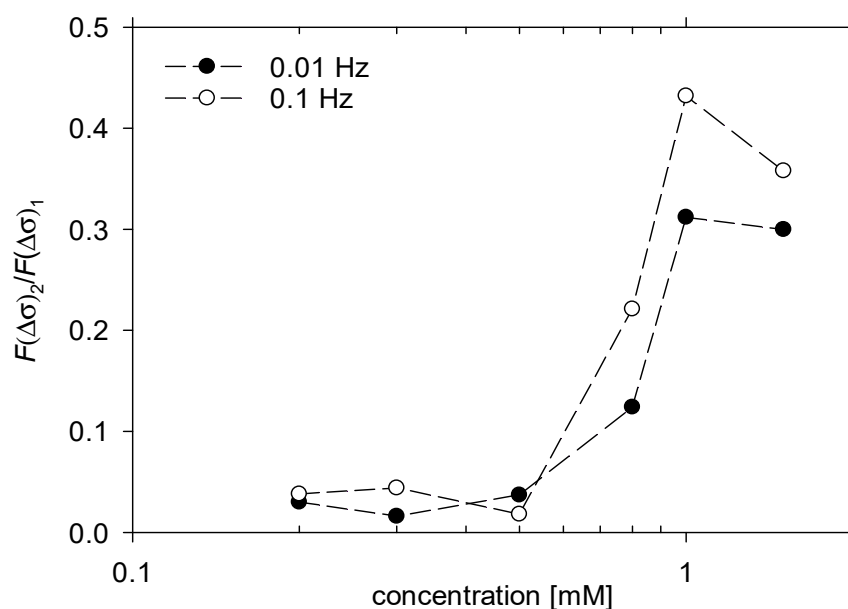


Figure 7. The dependence of the ratio of second to first harmonics in the Fourier spectrum of surface tension oscillations on LAE concentration for frequency of 0.01 Hz and 0.1 Hz. Lines were drawn to guide the eye.

To substantiate our hypothesis concerning the progressing hydrolysis of LAE during its storage as an aqueous solution, we compared the infrared absorption spectra of the freshly prepared solution of LAE, and after storing the stock solution of 0.2 wt% concentration for three weeks at room temperature. Additionally, we measured spectra of the freshly prepared 1.3×10^{-3} M solution of lauroyl arginine (LAS). To assign the frequencies of the vibration bands, we determined the theoretical spectra of LAE, LAS and LAE-LAS heterodimer in the IR region by the DFT computations. The results are illustrated in Figure S6 in the Supplementary Materials.

After storing LAE solution, we observed precipitate in the form of needle-like crystals as shown in the microscopic image in Figure 8. Figure 9 illustrates the comparison of the IR spectra of freshly prepared LAE and LAS solution in the range $1800\text{--}900\text{ cm}^{-1}$ with ones obtained for the “stored” LAE solution taken from the precipitate and supernatant. Comparing the spectra illustrated in Figure 9 and Figure S6, we concluded that precipitate contained both LAE and LAS, and the formation of heterodimers was followed by the growth of needle-like crystallites. On the other hand, the supernatant phase consisted of a mixture of LAE and LAS in the protonated (as pH of the solution decreased with time to 4.5) form with a higher ratio of the latter. In both cases, we observed a decrease in the intensity and shift of the band associated with carbonyl of the ester group to lower wavenumbers and the appearance of the bands characteristic for the carboxylic group in the ionic (1400 cm^{-1}) and nonionic (1200 cm^{-1}).

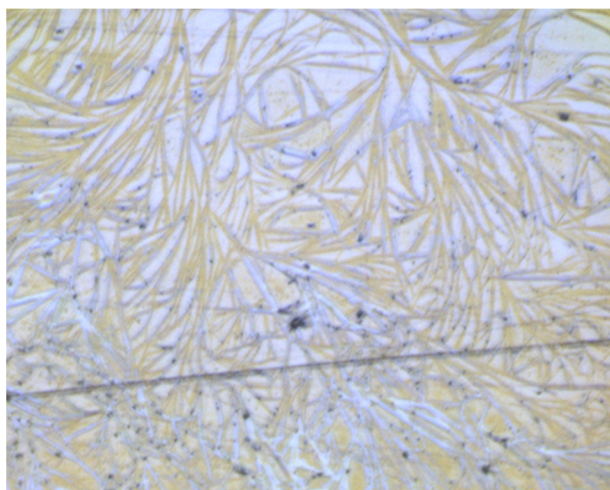


Figure 8. Microscopic image of a precipitate from “stored” LAE solution. Image size 500 × 400 μm.

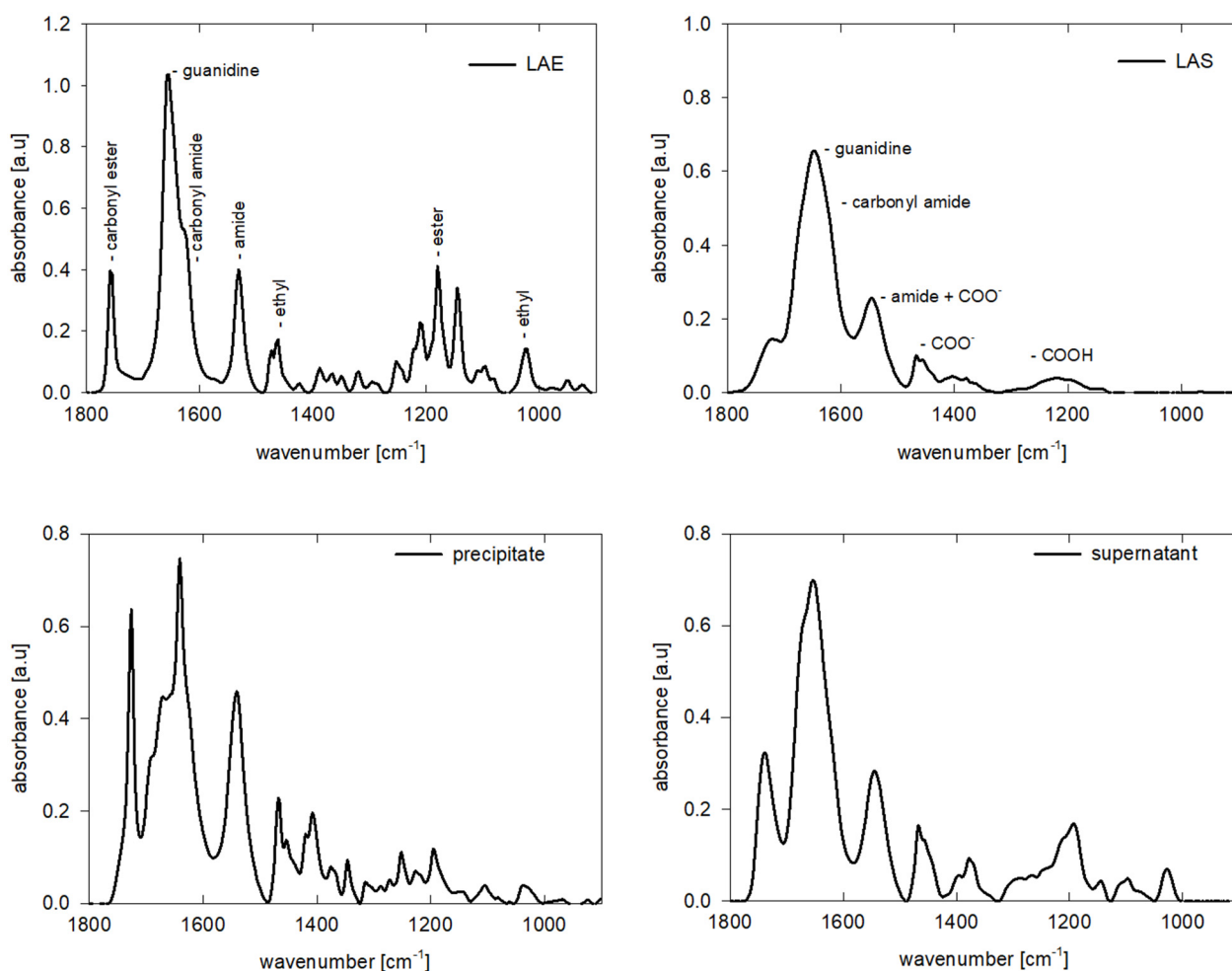


Figure 9. IR spectra of fresh LAE and LAS solutions and of “stored” LAE, precipitate and supernatant phase.

3. Materials and Methods

3.1. Materials

Ethyl lauroyl arginate, United States Pharmacopeia analytical standard (declared purity 99%) and lauroyl arginine hydrochloride (LAS), (United States Pharmacopeia reference standards) were purchased from Merck, Warsaw, Poland). Sodium chloride (99%) was

acquired from Sigma-Aldrich, Poznan, Poland and calcinated in 650 °C for eight hours before use. Laboratory glassware was cleaned with Helmanex solution, sulfuric acid, and deionised water. LAE was stored at 4 °C and protected from light. Before measurements, the stock solution was prepared in deionised cold water (4 °C, 20 MΩ) and then diluted to the appropriate concentration. Stock solution and dilutions were used within one day if not described otherwise.

3.2. Surface Tension and Elasticity

Surface tension and elasticity were measured by the pendant drop technique with the Sinterface PAT-1M (Sinterface, Berlin, Germany) tensiometer. Steel capillary of 2 mm diameter was cleaned carefully before each measurement. A drop of solution (11 µL) was created and kept in a thermostated chamber (22 °C) until reaching equilibrium surface tension. If not described otherwise, the surface tension and elasticity measurements were performed within one day after solutions' preparation. For the dynamic surface tension measurements, the drop profile coordinates were recorded every second and fitted with the Young-Laplace equation to calculate the surface tension. The precision of measurements was 0.1 mN/m.

Surface elasticity modulus was determined after reaching surface tension equilibrium by imposing drop oscillations of less than 10 percent of its volume. Raw data of the surface tension variations in response to periodic drop surface area changes were smoothed applying Loess smoother. Then Fourier transform was calculated and the surface dilatational modulus was determined as the complex number [37]:

$$\varepsilon = \varepsilon_r + i\varepsilon_i = A_0 \frac{\Delta\sigma_1}{\Delta A_1} \quad (2)$$

where: ε_r , ε_i are the real and imaginary part of the dilational elasticity modulus, A_0 is the average area of the drop, ΔA_1 and $\Delta\sigma_1$ are the principal Fourier components of the area and surface tension variations that correspond to the frequency of drop oscillations. All calculations were performed with the Mathcad (Parametric Technology Corporation, Needham, MA, USA) script.

3.3. Quantum Chemical DFT Computations

The quantum mechanics computations were performed using density functional theory (DFT) with wb97XD functional, which includes corrections for dispersion and long-range interactions, using a 6-31G+(d,p) basis set [41]. Solvation effects (water) were accounted for applying the SMD variation of the Polarizable Continuum Model [42]. To evaluate the relative rates of hydrolysis, the molecular structures of LAE, all its hydrolysis products and transition states were minimised, and energy, enthalpy, and free energy of a particular structure were determined. Then the respective energies, enthalpies and free energies of hydrolysis and the height of energetic barriers were calculated for basic and acidic hydrolysis in standard conditions (298 K, 1 atm).

The energy of dimerisation of LAE with surface-active hydrolysis products, dodecanoate anion and LAS was determined as follows. We placed two molecules with optimised geometries with parallel oriented hydrophobic chains and random position and orientation of the headgroup. The optimising procedure was run until the convergence was achieved, and the energy, enthalpy and free energy of the heterodimer were obtained. The procedure was repeated three times for different initial positions of headgroups and the conformation with the lowest energy was selected. The energy, enthalpy, and free energy of dimerisation were calculated according to: $\Delta E_{dimerization} = E_{dimer} - E_{LAE} - E_{LAS/dodecanoate}$. All DFT calculations were carried out using the Gaussian 09 program [43].

3.4. Molecular Dynamics Calculations

The optimised structures of heterodimers obtained in the DFT computations were imported to the YASARA Structure Molecular Dynamics Software [33], placed in the sim-

ulation box with the size of $5 \times 5 \times 5$ nm filled with water molecules (TIP3P, density 1 g/dm^3). The simulation was run for 20 ns using AMBER 14 force field [44] to equilibrate the system. Then it was continued for 300 ns and the positions of the investigated molecules were monitored. For the simulation of molecules at interface, after equilibration, the simulation box was extended in z coordinate to 15 nm to obtain a water slab with two interfaces. While the simulation was running, the transfer of molecules to one of the interfaces was observed. Then the simulation was continued for 300 ns with the recording of molecules' positions. The distance between LAE and LAS or dodecanoate anion was monitored and the number of hydrogen bonds between heterodimer forming molecules and the number of hydrogen bonds between these molecules and water was determined every 0.1 ns using the algorithm implemented in the YASARA Structure Software [33] and AMBER force field parameters.

3.5. Infrared Spectroscopy

The infrared spectra were collected using IR microscope Nicolet iN10 (Thermo Scientific™ part of Thermo Fisher Scientific, Madison, WI, USA) with high sensitivity, LN-cooled MCT detector by the reflection mode measurements within the spectral range from 4000 cm^{-1} to 675 cm^{-1} . After recording the background, aqueous solutions of investigated compounds were drop-casted on a gold layer sputtered on glass plates. Spectra (128 scans during 45 s with high resolution 4 cm^{-1}) were recorded after water evaporation. The fully automated adjustable aperture for measuring field extraction was $150 \mu\text{m} \times 150 \mu\text{m}$. After measurements, the automatic correction, namely, atmospheric, baseline subtraction and scale normalisation, was applied, and the averaged spectra were created from at least three spectra collected from different places of a sample.

4. Conclusions

Considering ethyl lauroyl arginate (LAE) applications in biomedical, cosmetic and food processing areas, it is crucial to define the mechanisms of its surface activity and aggregation properties. We determined the surface tension isotherm and surface dilational viscoelastic moduli of LAE solutions with analytical standard purity ($>99\%$). We established that the surface activity was in-between one for cationic and nonionic surfactants with the same length of the hydrophobic tail. LAE solution can contain the residues from the synthesis that are surface-active, namely lauric acid. Moreover, during storage, LAE undergoes base-catalysed hydrolysis that is enhanced at a positively charged interface or surface of micelles of LAE cationic surfactant. The preferred hydrolysis pathway of that process leads to $N\alpha$ -lauroyl-L-arginine (LAS), a zwitterionic surface-active component, that was supported by the IR spectroscopy analysis. Therefore, every LAE solution is a multicomponent system.

We used quantum mechanical DFT computations to determine the energetics of the hydrolysis paths and evaluated the possibility of the formation of highly surface-active heterodimers, LAE-dodecanoate anion or LAE-LAS. We used molecular dynamics simulations to determine the stability of those dimers linked by electrostatic interactions and hydrogen bonds (LAE-dodecanoate anion) or hydrogen bonds and stacking of guanidinium groups (LAE-LAS). We applied the model of surfactant mixtures adsorption to successfully describe the experimental surface tension isotherms assuming the presence of 0.2% of dodecanoic acid in fresh LAE solution and 18% of LAS after its hydrolysis during prolonged storage. The surface dilational modulus measurements by the oscillation drop method revealed values of surface elasticity moduli between ones for ionic and nonionic surfactants. The nonlinear response of the surface tension for the drop oscillations that could be observed for LAE concentration close to, and above, CMC was attributed to the presence of micelles and the reorganisation of the interfacial surfactant layer.

Supplementary Materials: The following are available online, Figure S1: Scheme of base catalysed hydrolysis of LAE; Figure S2: Scheme of acid catalysed hydrolysis of LAE; Figure S3: The variation of the number of intradimer hydrogen bonds during the simulation of the heterodimer at water/air

interface, A—LAE-dodecanoate, B—LAE-LAS; Figure S4: Schematic illustration of the main concept of the model of the adsorption of LAE and its heterodimers with hydrolysis products; Figure S5: The dependence of the real (right) and imaginary (left) part of the dilational elastic modulus on LAE solution concentration; Table S1: Best fit parameters of STDE adsorption model; Figure S6: Infrared spectra of A—LAE, B—LAS, C—LAE-LAS heterodimer. Left—spectra resulting from the DFT computations (for LAS non-protonated and protonated), right experimental spectra of LAE and LAS. [45].

Author Contributions: Conceptualisation, P.W. and A.C.; methodology, P.W., A.C., M.K., E.J.; validation, A.C., E.J., P.W., M.K.; formal analysis, P.W.; investigation, A.C., P.W., E.J.; resources, M.K.; data curation, A.C., E.J., P.W.; writing—original draft preparation, P.W.; writing—review and editing, A.C., M.K.; visualisation, A.C., E.J., P.W.; software, P.W.; supervision, P.W.; project administration, M.K.; funding acquisition, M.K., P.W. All authors have read and agreed to the published version of the manuscript.

Funding: This research was funded by the National Science Centre of Poland (grant number 2016/21/B/ST8/02107) and statutory subsidy for Jerzy Haber Institute of Catalysis and Surface Chemistry PAS. AC has been partly supported by EU Project POWR.03.02.00-00-I004/16. The IR microscopy experiments were supported by the National Science Centre of Poland (grant number 2017/25/B/ST4/02450).

Institutional Review Board Statement: Not applicable.

Informed Consent Statement: Not applicable.

Data Availability Statement: The data presented in this study are openly available from the authors upon reasonable request.

Conflicts of Interest: The authors declare no conflict of interest. The funders had no role in the design of the study; in the collection, analyses, or interpretation of data; in the writing of the manuscript, or in the decision to publish the results.

Sample Availability: Not available.

References

1. Tripathy, D.B.; Mishra, A.; Clark, J.; Farmer, T. Synthesis, chemistry, physicochemical properties and industrial applications of amino acid surfactants: A review. *C. R. Chim.* **2018**, *21*, 112–130. [[CrossRef](#)]
2. Asker, D.; Weiss, J.; McClements, D.J. Analysis of the interactions of a cationic surfactant (Lauric arginate) with an anionic biopolymer (Pectin): Isothermal titration calorimetry, light scattering, and microelectrophoresis. *Langmuir* **2009**, *25*, 116–122. [[CrossRef](#)]
3. Nerin, C.; Becerril, R.; Manso, S.; Silva, F. Ethyl Lauroyl Arginate (LAE): Antimicrobial Activity and Applications in Food Systems. In *Antimicrobial Food Packaging*; Elsevier Inc.: Amsterdam, The Netherlands, 2016; pp. 305–312. ISBN 9780128007235.
4. Ruckman, S.A.; Rocabayera, X.; Borzelleca, J.F.; Sandusky, C.B. Toxicological and metabolic investigations of the safety of N- α -Lauroyl-L-arginine ethyl ester monohydrochloride (LAE). *Food Chem. Toxicol.* **2004**, *42*, 245–259. [[CrossRef](#)] [[PubMed](#)]
5. Lozano, N.; Pérez, L.; Pons, R.; Luque-Ortega, J.R.; Fernández-Reyes, M.; Rivas, L.; Pinazo, A. Interaction studies of diacyl glycerol arginine-based surfactants with DPPC and DMPC monolayers, relation with antimicrobial activity. *Colloids Surf. A Physicochem. Eng. Asp.* **2008**, *319*, 196–203. [[CrossRef](#)]
6. Rodríguez, E.; Seguer, J.; Rocabayera, X.; Manresa, A. Cellular effects of monohydrochloride of L-arginine, N α -lauroyl ethylester (LAE) on exposure to Salmonella typhimurium and Staphylococcus aureus. *J. Appl. Microbiol.* **2004**, *96*, 903–912. [[CrossRef](#)] [[PubMed](#)]
7. Haghghi, H.; Leugoue, S.K.; Pfeifer, F.; Siesler, H.W.; Licciardello, F.; Fava, P.; Pulvirenti, A. Development of antimicrobial films based on chitosan-polyvinyl alcohol blend enriched with ethyl lauroyl arginate (LAE) for food packaging applications. *Food Hydrocoll.* **2020**, *100*, 105419. [[CrossRef](#)]
8. Ma, Q.; Davidson, P.M.; Zhong, Q. Properties and potential food applications of lauric arginate as a cationic antimicrobial. *Int. J. Food Microbiol.* **2020**, *315*, 108417. [[CrossRef](#)] [[PubMed](#)]
9. Bonnaud, M.; Weiss, J.; McClements, D.J. Interaction of a food-grade cationic surfactant (Lauric Arginate) with food-grade biopolymers (pectin, carrageenan, xanthan, alginate, dextran, and chitosan). *J. Agric. Food Chem.* **2010**, *58*, 9770–9777. [[CrossRef](#)]
10. Asker, D.; Weiss, J.; McClements, D.J. Formation and stabilisation of antimicrobial delivery systems based on electrostatic complexes of cationic-non-ionic mixed micelles and anionic polysaccharides. *J. Agric. Food Chem.* **2011**, *59*, 1041–1049. [[CrossRef](#)]
11. Loeffler, M.; McClements, D.J.; Mclandsborough, L.; Terjung, N.; Chang, Y.; Weiss, J. Electrostatic interactions of cationic lauric arginate with anionic polysaccharides affect antimicrobial activity against spoilage yeasts. *J. Appl. Microbiol.* **2014**, *117*, 28–39. [[CrossRef](#)]

12. Czakaj, A.; Kannan, A.; Wisniewska, A.; Grzes, G.; Krzan, M.; Warszynski, P.; Fuller, G.G. Viscoelastic interfaces comprising of cellulose nanocrystals and lauroyl ethyl arginate for enhanced foam stability. *Soft Matter* **2020**, *16*, 3981–3990. [CrossRef]
13. Bai, L.; Xiang, W.; Huan, S.; Rojas, O.J. Formulation and Stabilization of Concentrated Edible Oil-in-Water Emulsions Based on Electrostatic Complexes of a Food-Grade Cationic Surfactant (Ethyl Lauroyl Arginate) and Cellulose Nanocrystals. *Biomacromolecules* **2018**, *19*, 1674–1685. [CrossRef]
14. Chi, K.; Catchmark, J.M. Crystalline nanocellulose/lauric arginate complexes. *Carbohydr. Polym.* **2017**, *175*, 320–329. [CrossRef]
15. Younes, M.; Aquilina, G.; Engel, K.H.; Fowler, P.; Frutos Fernandez, M.J.; Fürst, P.; Gürtler, R.; Gundert-Remy, U.; Husøy, T.; Mennes, W.; et al. Safety of ethyl lauroyl arginate (E 243) as a food additive in the light of the new information provided and the proposed extension of use. *EFSA J.* **2019**, *17*, 5621.
16. Infante, R.; Domínguez, J.G.; Erra, P.; Julia, R.; Prats, M. Surface active molecules: Preparation and properties of long chain α -acyl-L- α -amino- ω -guanidine alkyl acid derivatives. *Int. J. Cosmet. Sci.* **1984**, *6*, 275–282. [CrossRef] [PubMed]
17. Kawamura, Y.; Whitehouse, B. *Ethyl Lauroyl Arginate. Chemical and Technical Assessment*; FAO: Rome, Italy, 2008.
18. Singare, P.U.; Mhatre, J.D. Cationic Surfactants from Arginine: Synthesis and Physicochemical Properties. *Am. J. Chem.* **2012**, *2*, 186–190. [CrossRef]
19. Yoshida, R.; Baba, K.; Saito, T.; Yoshimura, I. Surfactants Derived from Amino Acids. III. *Jpn. Oil Chem. Soc.* **1976**, *25*, 404–408. [CrossRef]
20. Takehara, M. Properties and applications of amino acid based surfactants. *Colloids Surf.* **1989**, *38*, 149–167. [CrossRef]
21. Para, G.; Jarek, E.; Warszynski, P. The Hofmeister series effect in adsorption of cationic surfactants—Theoretical description and experimental results. *Adv. Colloid Interface Sci.* **2006**, *122*, 39–55. [CrossRef] [PubMed]
22. Góralczyk, D.; Hąc, K.; Wydro, P.S. Surface properties of the binary mixed systems of alkylpyridinium halides and sodium alkylsulfonates. *Colloids Surf. A Physicochem. Eng. Asp.* **2003**, *220*, 55–60. [CrossRef]
23. Lunkenheimer, K.; Barzyk, W.; Hirte, R.; Rudert, R. Adsorption properties of soluble, surface-chemically pure n-alkanoic acids at the air/water interface and the relationship to insoluble monolayer and crystal structure properties. *Langmuir* **2003**, *19*, 6140–6150. [CrossRef]
24. Jarek, E.; Wydro, P.; Warszyński, P.; Paluch, M. Surface properties of mixtures of surface-active sugar derivatives with ionic surfactants: Theoretical and experimental investigations. *J. Colloid Interface Sci.* **2006**, *293*, 194–202. [CrossRef]
25. Lunkenheimer, K.; Haage, K.; Miller, R. On the adsorption properties of surface-chemically pure aqueous solutions of n-alkyl-dimethyl and n-alkyl-diethyl phosphine oxides. *Colloids Surf.* **1987**, *22*, 207–214. [CrossRef]
26. Para, G.; Łuczyński, J.; Palus, J.; Jarek, E.; Wilk, K.A.K.A.; Warszyński, P. Hydrolysis driven surface activity of esterquat surfactants. *J. Colloid Interface Sci.* **2016**, *465*, 174–182. [CrossRef]
27. Para, G.; Hamerska-Dudra, A.; Wilk, K.A.; Warszyński, P. Surface activity of cationic surfactants, influence of molecular structure. *Colloids Surf. A Physicochem. Eng. Asp.* **2010**, *365*, 215–221. [CrossRef]
28. Para, G.; Hamerska-Dudra, A.; Wilk, K.A.; Warszyński, P. Mechanism of cationic surfactant adsorption—Effect of molecular structure and multiple charge. *Colloids Surf. A Physicochem. Eng. Asp.* **2011**, *383*, 67–72. [CrossRef]
29. Aznar, M.; Gómez-Estaca, J.; Vélez, D.; Devesa, V.; Nerín, C. Migrants determination and bioaccessibility study of ethyl lauroyl arginate (LAE) from a LAE based antimicrobial food packaging material. *Food Chem. Toxicol.* **2013**, *56*, 363–370. [CrossRef] [PubMed]
30. Application A1015 Ethyl Lauroyl Arginate as a Food Additive Approval Report. Available online: <https://www.foodstandards.gov.au/code/applications/documents/A1015%20Lauric%20Arginate%20AppR%20FINAL1.pdf> (accessed on 25 September 2021).
31. Vondrášek, J.; Mason, P.E.; Heyda, J.; Collins, K.D.; Jungwirth, P. The molecular origin of like-charge arginine—Arginine pairing in water. *J. Phys. Chem. B* **2009**, *113*, 9041–9045. [CrossRef]
32. Vazdar, M.; Heyda, J.; Mason, P.E.; Tesei, G.; Allolio, C.; Lund, M.; Jungwirth, P. Arginine “magic”: Guanidinium Like-Charge Ion Pairing from Aqueous Salts to Cell Penetrating Peptides. *Acc. Chem. Res.* **2018**, *51*, 1455–1464. [CrossRef] [PubMed]
33. Krieger, E.; Vriend, G. New ways to boost molecular dynamics simulations. *J. Comput. Chem.* **2015**, *36*, 996–1007. [CrossRef] [PubMed]
34. Kanduč, M.; Schneck, E.; Stubenrauch, C. Intersurfactant H-bonds between head groups of n-dodecyl- β -D-maltoside at the air-water interface. *J. Colloid Interface Sci.* **2021**, *586*, 588–595. [CrossRef] [PubMed]
35. Lucassen, J.; Van Den Tempel, M. Dynamic measurements of dilational properties of a liquid interface. *Chem. Eng. Sci.* **1972**, *27*, 1283–1291. [CrossRef]
36. Zamora, J.M.; Marquez, R.; Forgiarini, A.M.; Langevin, D.; Salager, J.L. Interfacial rheology of low interfacial tension systems using a new oscillating spinning drop method. *J. Colloid Interface Sci.* **2018**, *519*, 27–37. [CrossRef] [PubMed]
37. Ravera, F.; Ferrari, M.; Santini, E.; Liggieri, L. Influence of surface processes on the dilational visco-elasticity of surfactant solutions. *Adv. Colloid Interface Sci.* **2005**, *117*, 75–100. [CrossRef]
38. Loglio, G.; Kovalchuk, V.I.; Bykov, A.G.; Ferrari, M.; Krägel, J.; Liggieri, L.; Miller, R.; Noskov, B.A.; Pandolfini, P.; Ravera, F.; et al. Dynamic properties of mixed cationic/nonionic adsorbed layers at the n-hexane/water interface: Capillary pressure experiments under low gravity conditions. *Colloids Interfaces* **2018**, *2*, 53. [CrossRef]

39. Lai, L.; Mei, P.; Wu, X.M.; Cheng, L.; Ren, Z.H.; Liu, Y. Interfacial Dynamic Properties and Dilational Rheology of Sulfonate Gemini Surfactant and its Mixtures with Quaternary Ammonium Bromides at the Air–Water Interface. *J. Surfactants Deterg.* **2017**, *20*, 565–576. [[CrossRef](#)]
40. Noskov, B.A.; Alexandrov, D.A.; Miller, R. Dynamic surface elasticity of micellar and nonmicellar solutions of dodecyldimethyl phosphine oxide. Longitudinal wave study. *J. Colloid Interface Sci.* **1999**, *219*, 250–259. [[CrossRef](#)]
41. Chai, J.D.; Head-Gordon, M. Long-range corrected hybrid density functionals with damped atom-atom dispersion corrections. *Phys. Chem. Chem. Phys.* **2008**, *10*, 6615–6620. [[CrossRef](#)]
42. Marenich, A.V.; Cramer, C.J.; Truhlar, D.G. Universal solvation model based on solute electron density and on a continuum model of the solvent defined by the bulk dielectric constant and atomic surface tensions. *J. Phys. Chem. B* **2009**, *113*, 6378–6396. [[CrossRef](#)]
43. Frisch, M.J.; Trucks, G.W.; Schlegel, H.B.; Scuseria, G.E.; Robb, M.A.; Cheeseman, J.R.; Scalmani, G.; Barone, V.; Petersson, G.A.; Nakatsuji, H.; et al. *GAUSSIAN 09*; Gaussian Inc.: Wallingford, CT, USA, 2010.
44. Case, D.A.; Babin, V.; Berryman, J.T.; Betz, R.M.; Cai, Q.; Cerutti, D.S.; Cheatham, T.E.; Darden, T.A.; Duke, R.E.; Gohlke, H.; et al. *AMBER 14*; University of California: San Francisco, CA, USA, 2014.
45. Jarek, E.; Jasiński, T.; Barzyk, W.; Warszyński, P. The pH regulated surface activity of alkanolic acids. *Colloids Surf. A Physicochem. Eng. Asp.* **2010**, *354*, 188–196. [[CrossRef](#)]

Ethyl lauroyl arginate (LAE), an inherently multicomponent surfactant system

Agnieszka Czajak, Ewelina Jarek, Marcel Krzan, Piotr Warszyński

Jerzy Haber Institute of Catalysis and Surface Chemistry Polish Academy of Sciences

Supporting Information

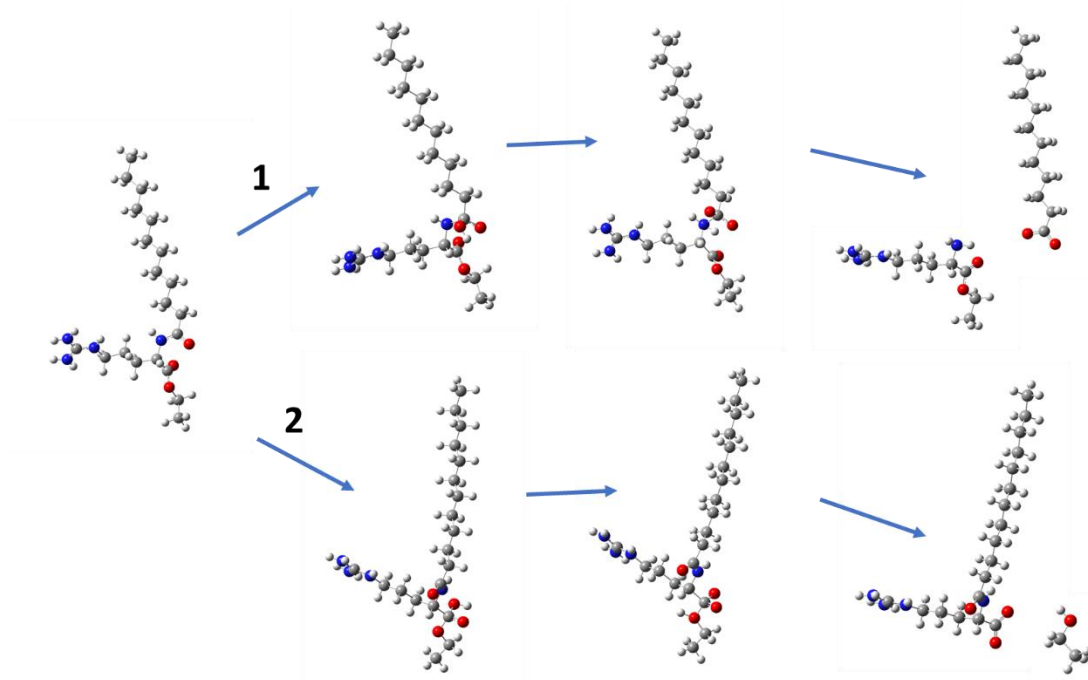


Figure S1. Scheme of base catalyzed hydrolysis of LAE. Path $\text{LAE}^+ + \text{OH}^- \leftrightarrow \text{C}_{11}\text{COO}^- + \text{EthylARG}^+$;
 1 - Path $\text{LAE}^+ + \text{OH}^- \leftrightarrow \text{LAS} + \text{EtOH}$

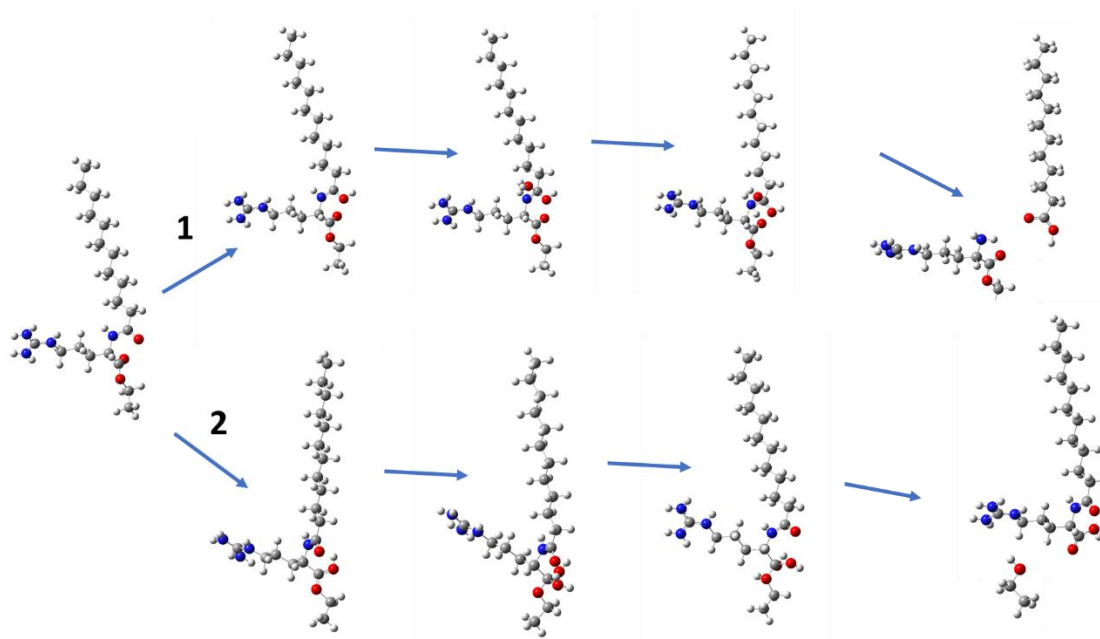


Figure S2. Scheme of acid catalyzed hydrolysis of LAE. Path 1 - $\text{LAE}^+ + \text{H}_3\text{O}^+ \leftrightarrow \text{C}_{11}\text{COOH} + \text{EthylARG}^+ + \text{H}_3\text{O}^+$; Path 2 - $\text{LAE}^+ + \text{H}_3\text{O}^+ \leftrightarrow \text{LAS}^+ + \text{EtOH} + \text{H}_3\text{O}^+$

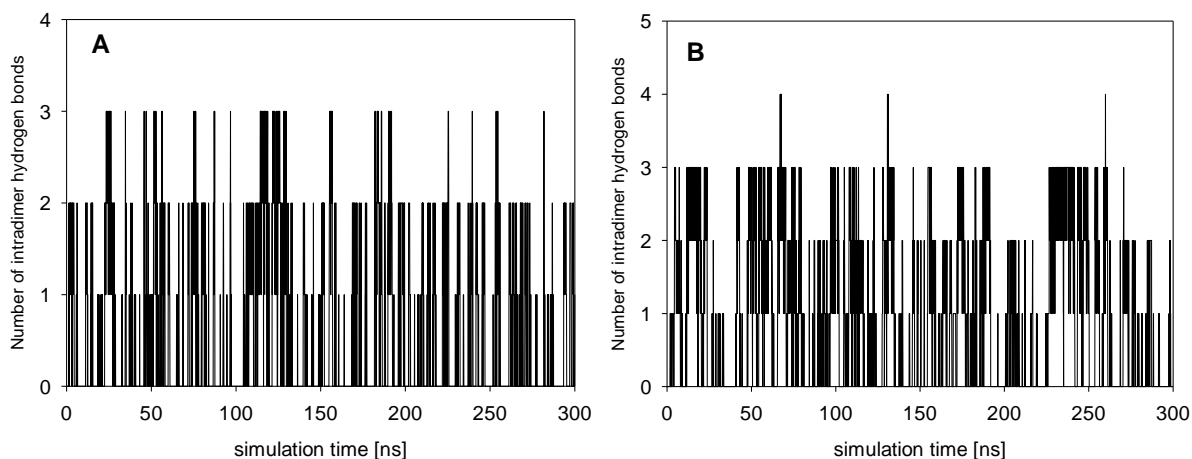


Figure S3. The variation of the number of intradimer hydrogen bonds during the simulation of the heterodimer at water/air interface. A – LAE-dodecanoate; B – LAE-LAS

Model of adsorption of surfactants and surface active hydrolysis products.

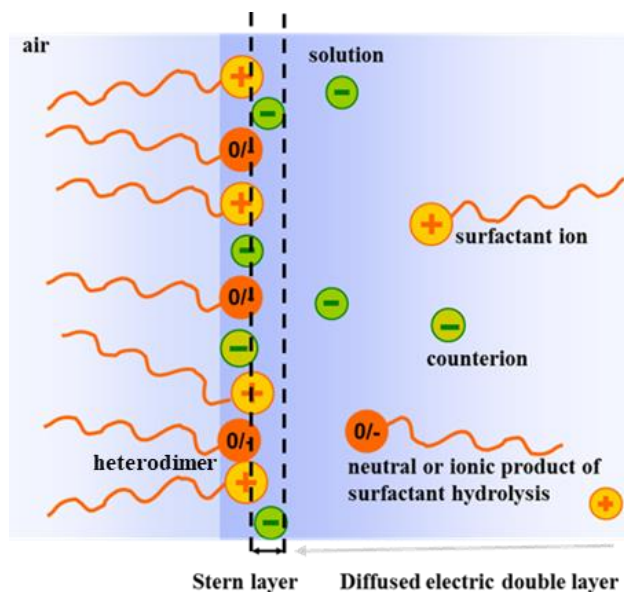


Figure S4. Schematic illustration of the main concept of the model of the adsorption of LAE and its heterodimers with hydrolysis products.

The main concept of the model is illustrated in Scheme 1. The hydrolysis of surfactants containing ester or amide bonds results in the formation of surface active products, either neutral (LAS) or negatively charged (dodecanoate anion) (see Scheme S1, where the hydrolysis products are denoted by 0/-), thus, the model of adsorption for the surfactant mixture needs to be used to describe the experimental results for the surface

tension. For that purpose we applied the extended model of adsorption of ionic/non-ionic surfactant mixtures [24,26,45] that is the extension of the surface two dimensional electrolyte (STDE) model proposed earlier by Warszyński et al. [21] to describe adsorption of ionic surfactants. We consider the system containing cationic surfactant (LAE) and anionic or neutral heterodimer with its hydrolysis product, dodecanoate anion and LAS, respectively. The system of adsorption equation derived from the equilibrium condition for the transfer from the solution to the Stern layer at the solution surface can be formulated as:

$$\frac{a_s}{\alpha_s} \exp\left(-\frac{e\psi_s}{kT}\right) \left(1 - \theta_s - \sum_i \theta_{h,i} - \sum_i \theta_{a,i}\right) = \theta_s \exp\left[-2H_s \left(\theta_s + \sum_i \theta_{h,i}\right)\right] \exp\left(\frac{\phi_s}{kT}\right) \quad (1)$$

for the cationic surfactant,

$$\frac{a_{h,i}}{\alpha_{h,i}} \exp\left(-\frac{z_{h,i}e\psi_s}{kT}\right) \left(1 - \theta_s - \sum_i \theta_{h,i} - \sum_i \theta_{a,i}\right)^{g_{h,i}} = \theta_{h,i} \exp\left[-2H_s \left(\theta_s + \sum_i \theta_{h,i}\right)\right] \exp\left(\frac{z_{h,i}\phi_{h,i}}{kT}\right) \quad (2)$$

for the hydrolysis products ($z_{h,i} = 0$ for neutral, -1 for anionic),

$$\frac{a_{a,i}}{\alpha_{a,i}} \exp\left(\frac{e\psi_s}{kT}\right) \left(1 - \theta_s - \sum_i \theta_{h,i} - \sum_i \theta_{a,i}\right)^{g_{a,i}} = \theta_{a,i} \exp\left(\frac{\phi_{a,i}}{kT}\right) \quad (3)$$

for the non-surface active anions of the electrolyte (Cl^- and OH^-).

The symbols in the above equations denote: $a_s, a_{h,i}, a_{a,i}$ - the activities of the respective components that can be calculated from the extended Debye – Hückel theory of strong electrolyte solutions - for the neutral species equal to their concentrations, $\theta_s = \Gamma_s/\Gamma_{s\infty}$ is the relative surfactant surface concentration, where Γ_s is its surface (excess) concentration and $\Gamma_{s\infty}$ is the limiting surfactant surface concentration at the maximal coverage, $\theta_{h,i} = \Gamma_{h,i}/\Gamma_{h\infty,i}$, $\theta_{a,i} = \Gamma_{a,i}/\Gamma_{a\infty,i}$, $\theta_n = \Gamma_n/\Gamma_{n\infty}$, $\Gamma_{h,i}, \Gamma_{a,i}, \Gamma_{H\infty}, \Gamma_{C\infty}$ and $\Gamma_{n\infty}$ are the same quantities for dimers and electrolyte anions; $g_s, g_{h,i}$, and $g_{a,i}$ are the ratios of the size of surfactant cations, dimers and electrolyte anions relatively to the size of the adsorption site ($g_s = 1$ for the sake of simplicity), H_s is the surface interaction parameter accounting mainly for the attractive lateral interactions among the adsorbed surfactant hydrophobic tails, α_s is the "surface activity" of surfactant ion, being a measure of the standard free energy of adsorption after separating the contribution of the electric component, $\alpha_{h,i}$ is the same parameter for the respective heterodimers and $\alpha_{a,i}$ are the "surface activities" electrolyte anions that are a measure of their affinity to the surface layer, $\phi_s, \phi_{h,i}, \phi_{a,i}$, are the corrections for the activity of the two dimensional electrolyte in the surface layer accounting for the lateral interaction between ions. In the derivation of equations 1-3 we assumed that non-surface active cations resulting from the hydrolysis (see Scheme 1) and H_3O^+ (HCl) or Na^+ (NaOH) added to adjust pH, do not penetrate Stern layer due to

electrostatic repulsion of the positively charged interface. The electric potential of the Stern layer, ψ_s , can be found from:

$$\psi_s = \psi_d + \frac{\sigma \delta}{\varepsilon_0 \varepsilon_s} \quad (4)$$

while the diffuse layer potential at the boundary between the Stern layer and the diffuse part of electric double layer can be determined from the formula:

$$\psi_d = \frac{2kT}{e} \sinh^{-1} \left(\frac{\sigma e}{2\varepsilon_0 \varepsilon_s kT \kappa} \right) \quad (5)$$

where: e is the elementary charge, k is the Boltzmann constant, ε_0 is the vacuum dielectric permittivity, ε is the dielectric constant of the solution, κ is the Debye - Hückel reciprocal length

$$\sigma = F \left(\Gamma_s - \sum_i \Gamma_{h,i} - \sum_i \Gamma_{a,i} \right) \quad (6)$$

is the surface charge density, F is the Faraday constant, δ is the thickness of the Stern layer and ε_s is the dielectric constant in the Stern layer. We assumed that adsorption of non-ionic surface active molecules does not influence the electric properties of the Stern layer.

The procedure of solving the system of Eqs. 1-6 and the detailed interpretation of parameters are described elsewhere [21,26]. By the numerical solution of this system of equations, the surface concentration of all components in the Stern layer can be determined directly. Total surface excess concentration Γ_j^T of all components has to include adsorption of all electrolyte and surfactant ions in the diffuse part of the electric double layer, where the distribution of ions has to be found using the solution of Poisson-Boltzmann equation. The surface tension of the solution can be predicted by integration of the Gibbs equation for the mixture of ionic–nonionic surfactant:

$$d\gamma = -RT \left(\sum_j \Gamma_j^T d \ln a_j \right) \quad (7)$$

From the fit of the calculated isotherm to the experimental data the parameters of the model for investigated system can be obtained.

Table S1

Best fit parameters of STDE adsorption model

Surfactant/Model parameter	LAE	LAE-dodecanoate anion	LAE-LAS
$\Gamma_{s\infty}[\text{mol}/\text{cm}^2]$	5.4×10^{-10}	7.2×10^{-10}	4.5×10^{-10}
$\alpha_s[\text{mol}/\text{dm}^3]$	5.0×10^{-6}	7.0×10^{-7}	5.0×10^{-7}
H_s	4.5	4.5	4.5

Other model parameters [21]

g_a	0.64
$\alpha_{Cl^-}[\text{mol}/\text{dm}^3]$	10000
a_{Cl^-} or $a_{OH^-}[\text{nm}]$	0.35
$\delta[\text{nm}]$	0.35
ε_s	24

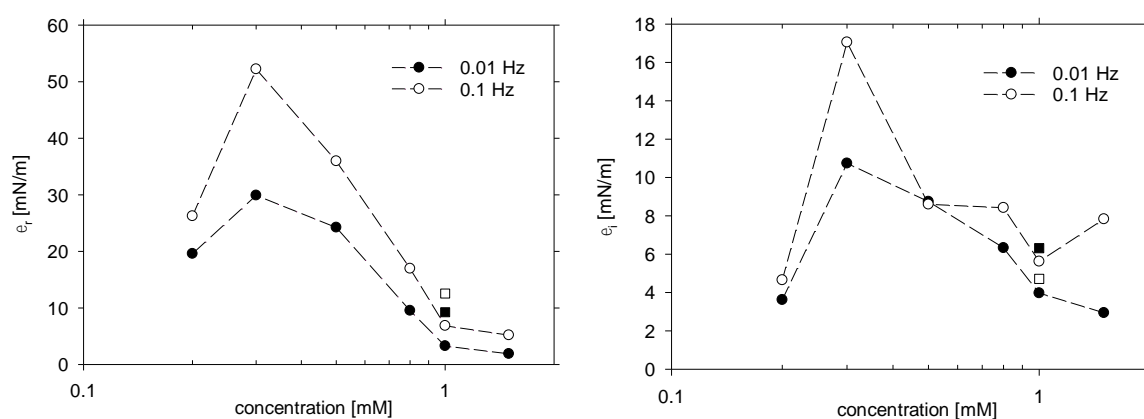


Figure S5. The dependence of the real (right) and imaginary (left) part of the dilational elastic modulus on LAE solution concentration for the drop oscillation frequency 0.01 Hz and 0.1 Hz. Squares the values for 1 mM LAE solution stored for two weeks.

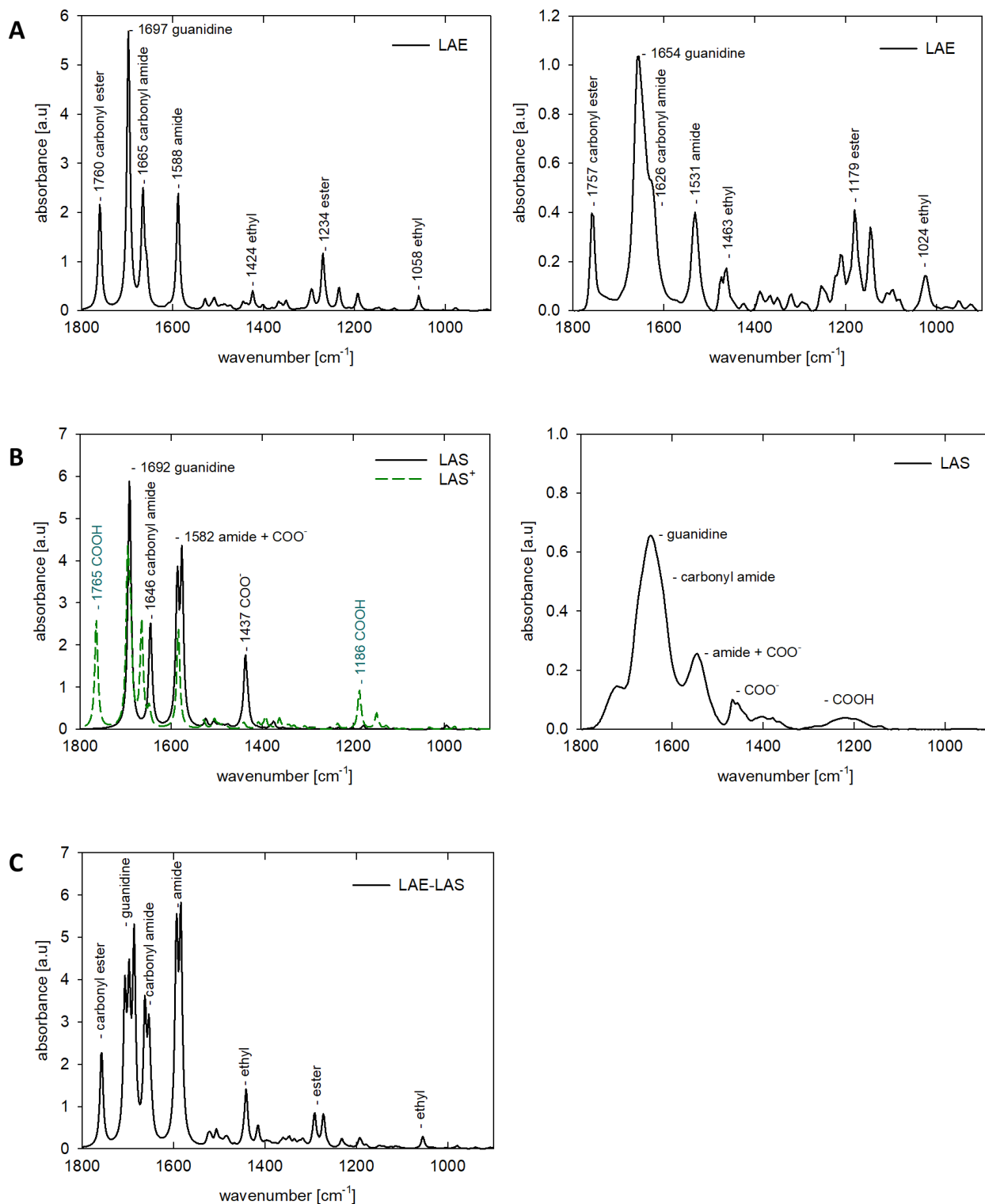


Figure S6. Infrared spectra of A – LAE, B – LAS, C – LAE-LAS heterodimer. Left – spectra resulting from the DFT computations (for LAS non-protonated and protonated), right – experimental spectra for LAE and LAS


 Cite this: *Soft Matter*, 2020, 16, 3981

Viscoelastic interfaces comprising of cellulose nanocrystals and lauroyl ethyl arginate for enhanced foam stability†

 Agnieszka Czakaj,^a Aadithya Kannan,^b Agnieszka Wiśniewska,^c Gabriela Grześ,^d Marcel Krzan,^a Piotr Warszyński^a and Gerald G. Fuller^b

Stable aqueous foams composed of oppositely charged nanoparticles and surfactants have recently gained attention. We studied the draining of thin liquid films and the foam stability of aqueous mixtures of food grade cellulose nanocrystals (CNCs) and an oppositely charged surfactant – lauroyl ethyl arginate (LAE). Dynamic fluid film interferometry experiments with the bubble approaching the air/solution interface revealed a two-fold increase of the initial bubble film thickness and a maximum in drainage time at the optimal stoichiometry of LAE and CNC. The temporal evolution of the fluid film shape indicated a large contribution of structural forces to the film stability. The results of single liquid film drainage time and coalescence time experiments were partially correlated with bulk foam stability. With a further increase of LAE concentration, aggregation-induced foam destruction was observed. In the presence of a cationic surfactant, anisotropic and initially hydrophilic cellulose nanocrystals became partially hydrophobized and self-assembled at the interface. Cellulose nanocrystal shape anisotropy and wetting behaviour which have their origins in OH-exposed and buried crystalline planes are the sources of capillary interactions that promote CNC aggregation at planar and curved liquid/air interfaces. Dilatational and shear interfacial rheology experiments confirmed the formation of a highly elastic surfactant–nanoparticle interfacial layer. To the best of our knowledge, this is the first report on foaming properties for this system with fast adsorption kinetics influenced by CNC.

 Received 4th December 2019,
Accepted 11th March 2020

DOI: 10.1039/c9sm02392e

rsc.li/soft-matter-journal

Introduction

Foams with highly extended liquid/gas interfaces are thermodynamically unstable systems. Research on foam stability is of great importance for flotation science, the oil and gas industry, and many consumer product applications, including food and cosmetics. The main characteristic parameters of foam are the average bubble size, polydispersity and liquid content. They are dependent on the foam formation method and do not usually attain their equilibrium values. Three interrelated mechanisms are responsible for foam destruction: coarsening (Ostwald ripening), drainage and coalescence.¹ Coarsening occurs due to gas diffusion through the foam lamella that results in the growth of larger bubbles at the expense of smaller ones due to

differences in capillary pressure. Drainage is the effect of liquid flow in lamella borders due to gravity and capillary forces at curved interfaces. Higher fluid bulk viscosity usually reduces the drainage rate and results in larger liquid content in the foam. The drainage is directly linked with coalescence, the next mechanism of foam destruction, in which a liquid film reaches a critical thickness with molecular forces determining its stability. Foams significantly differ when prepared with different methods: by laminar air bubbling or turbulent mixing.² Turbulent mixing produces polydisperse small-size bubbles with the initial radii up to hundreds of micrometres.³ Coarsening of bubbles of such small size is the primary effect seen in foam destruction, and it is associated with bubble reorganisation processes (T1 process), in which new bubble lamellae are created.⁴

Coalescence of single soap bubbles at the air/water interface is a stochastic process,⁵ but it has been shown that in the foam column the coalescence process is deterministic.⁴ The single bubble coalescence characteristic can also be significantly altered at complex, viscoelastic interfaces. A theory describing coalescence of a single bubble has been developed⁶ and the coalescence time is related to the bubble radius and surface viscoelasticity. However, Marangoni stresses driven by surface

^a Jerzy Haber Institute of Catalysis and Surface Chemistry PAS, Krakow, Poland.
E-mail: ncczakaj@cyf-kr.edu.pl

^b Department of Chemical Engineering, Stanford University, Stanford, USA

^c Institute of Physical Chemistry, Polish Academy of Sciences, Warsaw, Poland

^d Department of Chemistry, Jagiellonian University, Krakow, Poland

† Electronic supplementary information (ESI) available: Viscosities of solutions, CNC particle size and zeta potential, AFM and SEM imaging, foaming set up. See DOI: 10.1039/c9sm02392e

tension gradients and dimpling of the thin films,⁷ which play a role when dealing with viscoelastic systems with partial surface mobility, have to be accounted for.⁸ For the consideration of films with a thickness below 100 nm, the additional partial molar free energy (disjoining pressure) resulting from the balance of electrostatic and dispersive interactions needs to be considered.⁹ Besides, in polymer or nanoparticle solutions, the steric component of the disjoining pressure might have the greatest contribution to thin film stability.¹⁰ Single bubble coalescence can only be regarded as an approximation of the processes occurring in a bulk foam, as neighbouring bubbles deform each other and breaking bubbles modify the liquid lamella shape, pressure gradients and flow. Each coalescence event also lowers the surface to volume ratio,¹¹ which increases the surface concentration of the surface active species and such changes may limit further coalescence. Thus, as it was pointed out in the review of Małysa and Lunkenheimer,¹² there are many factors to be taken into account for foam stability: disjoining pressure forces, diffusion kinetics, surface tension gradients induced by deformations of local foam film and/or by rising bubbles, non-equilibrium adsorption coverage, mutual interactions of bubbles in a growing foam, local deformations of bubbles and foam films, and pressure shocks caused by the bursting film.

Unlike surfactant molecules, the adsorption of nanoparticles at the air–liquid interface is usually irreversible. Moreover, when the amount of adsorbed nanoparticles is high, the elasticity of the interface increases accordingly.¹³ The enhanced dilatational elasticity leads to the inhibition of bubble coarsening.¹⁴ Besides, the adsorbed nanoparticles also hinder the water flow at bubble surfaces and thus slow down film thinning.^{15,16} Binks *et al.* clearly demonstrated that, when combined, nanoparticles and surfactant molecules can produce stable foams at a suitable surfactant concentration.¹⁷ The mechanism of stabilisation in such systems is complicated due to the presence of various interactions: between surfactant molecules, surfactant and nanoparticles, and, last but not least, interactions between nanoparticles.¹⁸ Surfactant–nanoparticle interactions in a foaming process are of primary importance for understanding foam stability and nanoparticle behaviour at the liquid/gas interface.^{19,20}

Cellulose nanocrystals (CNCs) are convenient to use for foam stabilisation due to their availability, dispersivity in water, high surface charge and low toxicity.²¹ Cellulose nanofibers vary according to their size, geometry and surface chemistry. It has become common to use the name ‘cellulose nanocrystals’ for rod-like particles no longer than 300 nm, while for longer ones the term – ‘cellulose nanofibers’ – is applied. Considering the source of the origin, they are classified as wood, tunicate, cotton, or bacteria-derived.²² The physicochemical properties depend on processing chemistry. Both hydrochloric acid and sulphuric acid hydrolysis release the crystalline part from the amorphous region of cellulose fibres but sulphuric acid-derived CNCs show higher surface charge, thus, stronger electrostatic interactions in an aqueous environment and higher dispersivity.²³ Cellulose nanocrystals have many intriguing properties such as intrinsic chirality on various length scales. On a nanometric scale, a

longitudinal (unidirectional) twist geometry along the fibrillar axes is found and this can be altered upon drying.²⁴

Cellulose nanoparticles, specifically with sulphate surface groups, show long-range repulsion in water determined by their surface charge. This electrostatic interaction can be screened without imposing aggregation by the addition of an electrolyte of up to 30 mM NaCl. Above this salt concentration, the aggregates are formed with random associations of CNC particles.²⁵ It was observed that upon screening the electrostatic interactions, CNCs start to exhibit interfacial behaviour and saturated the interface at concentrations of 0.5 wt%.²⁶ They also showed interfacial shear elastic modulus of the order of 10^{-3} Pa m, that is however not sufficient enough either for foam creation or its stabilisation. Wood-derived cellulose nanocrystals with sulphate ester groups are commercially available as a spray-dried powder that needs to be re-dispersed in water for avoiding aggregation. Since they do not exhibit any surface activity, a direct hydrophobic modification of cellulose or the addition of some surface active component is necessary to use them as foam stabilisers.^{27,28} Therefore, in this work, we focused on the interactions of cellulose nanocrystals with a cationic surfactant, lauroyl ethyl arginate (LAE), to investigate their effect on the surface properties of the surfactant/nanoparticle mixture, foamability and foam stability.

Lauroyl ethyl arginate, LAE (pK_a 9–10), is a positively charged surfactant synthesized from L-arginine, lauric acid and ethanol (molecular structure presented in ESI,† Fig. S1). Its molecular weight, M_w , is 421 g mol⁻¹ and its pK_a is about 9–10. LAE is a green, biodegradable component used as a food additive with antimicrobial properties. It interacts electrostatically with cellulose nanocrystals, and their mutual interactions in water are dependent on solution pH, influencing the surfactant protonation state. As determined using atomic force microscopy, at submillimolar concentrations of LAE, cellulose nanocrystals aggregate laterally or longitudinally and form elongated fibres.²⁹ Their binding interactions resemble the complexation process of oppositely charged polymer–surfactant systems.³⁰ At low surfactant concentrations, the binding of LAE to the CNC surface is exothermic, governed by the long-range electrostatic attractions between CNC sulfate groups and surfactant cationic guanidinium headgroups.²⁹ Above the critical micellization concentration (c.m.c. \sim 4 mM) of LAE, in the presence of CNC, the micelles of LAE may adsorb at the surface of nanocrystals or dissociate to monomers that electrostatically bind to the anionic CNC surface or adsorb at the air/water interface. The binding enthalpy gradually decreases with NaCl addition and finally equals the one for pure LAE titration curve at 100 mM NaCl, which is evidence of the screening of electrostatic LAE–CNC interactions.²⁹ These interactions are also weakened at a pH value of 9 when the guanidinium group is partially deprotonated. LAE–CNC interactions were also studied using a commercial surfactant (89.5% purity). The aggregates showed the point of zero charge at a 4.5 mM concentration of LAE and 0.27 wt% of 174 nm long CNC containing 0.19 mmol g⁻¹ sulphate groups.³¹ Pickering emulsions of sunflower oil and water with tunable droplet diameters and stability against

coalescence for long-term storage were prepared with high LAE concentrations.³¹

Nanoparticle solutions, which do not have surface activity and do not foam, may exhibit stratification upon film thinning. In a mixture with surfactant they become surface active, and therefore they can exhibit a variety of viscoelastic responses depending on the surfactant concentration. This can be related to the changes of nanoparticle/surfactant surface charge upon adsorption of surfactant at various LAE–CNC stoichiometries, or the appearance of some surfactant–nanoparticle structures.²⁹ Other phenomena such as capillary forces need to be considered. It was demonstrated that non-spherical particles with a high aspect ratio very efficiently stabilise foams³² and emulsions.³³ Adsorbed particles deform the interface depending on their size and density. For large particles, the deformation is induced by gravity. When particles are small and the contact line radius does not exceed 5 μm , the gravity-induced interaction energy is smaller than the thermal energy kT . Still, another type of interaction might occur. Irregular particle shape and presence of surface roughness or chemical inhomogeneity can cause displacement of the interface around a capillary quadrupole. In such a case, the three phase contact line is no longer planar and even nanosized contact line undulation amplitudes are characterized by the interaction energy of orders of magnitude larger than kT .^{34,35} Contact line undulations at a nanocellulose surface have their origin in the CNC shape with a high aspect ratio and also non-uniform wetting of the cellulose crystal in which the hydroxyl groups are exposed or buried, depending on the plane.³⁶ Molecular dynamics simulations for a perfect crystal demonstrated a contact line undulation amplitude in the order of 0.5 nm for the (010) plane.³⁷ Cellulose nanocrystals with a length of 100 nm interact with the surfactant and self-assemble, so differences in wettability might be much larger. Strong attractive interparticle forces induce particle assembly into various structures depending on the particle shape or interface curvature. In particular, for cylindrical particles, planar interface distortion results in a tip-to-tip particle assembly while at a curved geometry cylindrical particles assemble side-to-side and may migrate towards regions of higher curvature.³⁸ Such migration might induce particle ordering in the meniscus region. Particles tend to self-organize at a film thickness corresponding to an integral number of the effective particle diameter and the structural energy in the thin film can dominate the van der Waals and electrostatic contribution.³⁹

The primary goal of our paper is to demonstrate the effect of LAE–CNC interactions at the liquid/gas interface on the kinetics of liquid film drainage and its stability in relation to foamability and foam stability. For these purposes, we carried out dynamic fluid film interferometry measurements with a single bubble colliding with the liquid/gas interface to determine fluid flow behaviour during film thinning and thin film coalescence time. We then compared the stability of films formed by a single bubble with the properties of bulk foams made in the process of turbulent liquid–air mixing. Detailed interfacial characteristics of sustainable foam components of LAE and CNC are presented as an example of adsorption layer behaviour under dynamic conditions. The high aspect ratio of

cellulose nanoparticles enhances interfacial viscoelasticity, although the interface response is purely reversible in compression and expansion. Our system is unique concerning the kinetics of adsorption of lauroyl ethyl arginate at the liquid/air interface in the presence of cellulose nanoparticles as well as excellent foaming properties at very low surfactant concentrations, relative to its c.m.c. The presented results should motivate the research community to further investigate non-spherical nanoparticle–surfactant interactions and their effect on the properties of a dynamic adsorption layer, interfacial rheology and foam stability.

Experimental

Materials

Sulphuric acid-hydrolysed cellulose nanocrystals (CNC) were purchased from CelluForce (Canada). According to the manufacturer specification, the average size of CNC was 100 nm length, 5 nm diameter and the average content of sulfate groups was 0.25 mmol g^{-1} . The nanocrystals were carefully dispersed in deionised water with magnetic stirring and ultrasonication. Lauroyl ethyl arginate (LAE) under the commercial name Mirenat-P/100 (about 90% LAE surfactant content) was generously provided by Vedesqua (Spain). LAE–CNC dispersions were prepared by adding 0.6 wt% of CNC solution to an appropriate surfactant concentration (50 : 50 v/v) with magnetic stirring. All chemicals were used without further purification. Experiments were performed at a room temperature of 22 ± 0.1 °C.

Dynamic fluid film interferometry

Dynamic fluid film interferometry is the technique used to study the dynamic evolution of the film formed by a single bubble being pressed against a planar air–liquid interface.⁴⁰ It can be considered as representative of foam systems when taking into account convection effects due to rising the bubble in the liquid. It enables simultaneous measurement of the inner bubble pressure changes upon approaching the interface as well as spatially resolved fluid film thickness with the curvature related error of less than 5%. The bubble approach velocity, bubble size, and internal bubble pressure can be controlled. The DFI technique is suitable to follow complex tangential-stress boundary conditions at bubble interfaces directly related to the drainage rate. Complex viscoelastic systems like polymers, proteins and surfactant–nanoparticle systems can be studied to evaluate the mobility of the interfaces. For example, the DFI setup was used to correlate bulk foam density with the thickness of a single bubble fluid film in various surfactant solutions with negligible surface viscosity: Triton, HTAB, and SDS.⁴⁰ Single bubble coalescence time was successfully measured by the DFI for viscoelastic interfaces of monoclonal antibody solutions and air.⁴¹ Competitive adsorption of polyethylene glycol (PEG) added to these proteins increased the interface mobility, lowered the relaxation moduli and decreased the coalescence time.

In the DFI experiment, when a bubble approached the interface, a change in its volume, V , with time t , can be described by the equation⁴²

$$\frac{dV}{dt} = \pi a^2 \frac{dh}{dt} + 2\pi a h \frac{da}{dt}$$

where h is the spatial average of the film thickness and a is the film radius. When the bubble stops moving, the second term is zero and the volume change is the function of the average film thickness h at a fixed film radius. In our experiment, after the interface approach, the thin film radius had a value of 350 μm and it did not change with drainage time. Drainage of the fluid film of the bubble approaching the interface is considered for the conditions of small Reynolds number $\text{Re} \ll 1$ and no slip boundary condition. If a bubble rises in the liquid, the hydrostatic pressure monotonically decreases until the moment when it starts to deform at the interface. Bubble deformation and formation of a liquid film are accompanied by the sudden increase of the internal pressure. Thus, the moment a minimum in the bubble pressure is reached can be considered as the starting time of film drainage. At the endpoint, when the bubble breaks, the internal pressure suddenly drops. For the determination of film thickness, a numerical procedure based on the Fresnel law of optics was used, assuming an aqueous phase (with a refractive index of 1.33), between two air phases. The details concerning the thickness determination by digital image processing can be found elsewhere.^{43–45}

The dynamic fluid film interferometry measurements for LAE–CNC systems were performed using the arrangement described in detail by Frostad *et al.*⁴⁰ The reservoir with the surfactant solutions was cleaned with ethanol and water and filled with filtered (0.45 μm PES NALGENE[®]) LAE or an LAE–CNC mixture. A bubble with a volume of approximately 1.5 μL was formed at the end of the needle submerged in the surfactant solution. The bubble was positioned such that the distance between the apex of the bubble and the air–solution interface was equal to the bubble radius. The reservoir with the surfactant solution was lowered at a constant velocity of 150 $\mu\text{m s}^{-1}$ by a distance of 1.5 times the bubble radius. The pressure was monitored at the beginning of each experiment to determine if the bubble was stable and controlled throughout the experiment. A dome light source was used to induce a reflection interference pattern of the fluid film. Two orthogonally positioned cameras captured the image of the top view of the bubble and its side view image.

Foaming and foam stability

Bulk foaming experiments were performed using a home-made double syringe setup consisting of two identical syringes connected by a narrow tube.⁴ At first, one single syringe of 60 mL volume was filled with 20 mL of solution and 40 mL of air. Then a series of ten back-and-forth cycles were performed by moving the pistons manually and emptying one syringe into the other. Immediately after the formation of foam, the syringes were positioned vertically and the foam and liquid volume were monitored by video-recording for 5 hours.

Surface tension and rheology

Surface tension was measured by the pendant drop technique with a Sinterface PAT-1M tensiometer immediately after fresh solutions were prepared. Samples were equilibrated for 15 minutes under stirring and then sonicated. A drop of solution (11 μL) was created from a 2 mm diameter capillary and kept in a thermostated chamber for 2000 seconds. The drop profile was monitored and fitted with the Young–Laplace equation to calculate the surface tension. The critical micellisation concentration was calculated from the intercept of the surface tension curve with its plateau. The variation of measurements was $\pm 2 \text{ mN m}^{-1}$ maximum.

A surface viscoelastic response can be measured in shear, at a constant area, in order to track the extra stresses at the interface⁴⁶ or as the apparent viscoelasticity upon surface area changes described mainly by the Lucassen–van den Tempel model⁴⁷ and related to the diffusional transport to and from the interface. Interfacial dilatational moduli were measured in the linear viscoelastic regime by small drop oscillation at a maximum of 10 percent of the drop volume. Periodic surface tension variations are followed and the dilatational modulus is calculated as the Fourier transform of temporal surface tension changes. The Sinterface PAT-1M tensiometer was utilized to determine surface dilatational elasticity.

Interfacial shear elastic modulus was measured with a DSA hybrid rheometer 5333-0310 (TA Instruments) using a “double-wall DuNoüy ring” geometry (R/r 57.447) at the solution/air interface.⁴⁸ Before each measurement, the ring was cleaned with ethanol and deionised water and then flame-dried. The instrument was calibrated after each ring installation. In the strain sweep experiments, a small oscillation mode was used with the amplitude of 0.5% of ring rotation and a frequency of 0.05 Hz. All the samples were sonicated 10 min before each measurement.

Results and discussion

The dynamic film interferometry experiments were performed with the concentration of CNC fixed at 0.3 wt% and increasing LAE content in the range well below c.m.c. The results showed a strong dependence of the film thinning and coalescence time on the LAE concentration in the LAE–CNC mixtures as illustrated for three representative LAE concentrations (0.004, 0.006 and 0.015 wt%) in the top view images in Fig. 1.

The film coalescence time for the dispersion of pure cellulose nanocrystals never exceeded 20 seconds and the film drained rapidly showing stratification. In the presence of LAE, the initial film thickness ranged from 320 nm for a LAE concentration of 0.004 wt% up to about 600 nm for 0.006 wt% and then decreased to 350 nm for concentrations above 0.01 wt%. In the initial drainage period, the thinning rate was similar for all studied LAE concentrations; films were drained to half of their initial thickness in *ca.* 10 s and a dimple in the centre of the film was formed. However, later on, the thinning pattern was drastically different. At 0.006 wt%, the LAE dimple disappeared and the film achieved a quasi-equilibrated

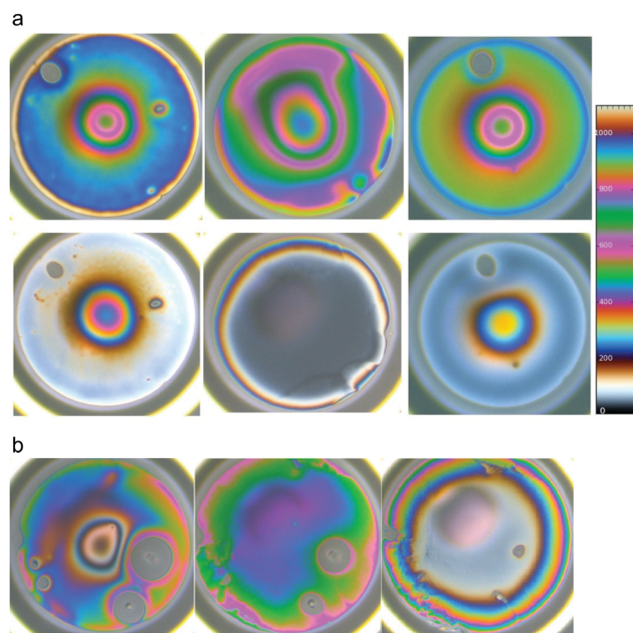


Fig. 1 (a) Images presenting the top view of the LAE–CNC dispersion liquid film taken during a dynamic film interferometry experiment for various LAE concentrations. Left: 0.004 wt%, middle: 0.006 wt%, right: 0.015 wt%, upper row: initial film, lower row: film just prior to coalescence. A color scale (in nm) corresponding to the film thickness is placed at the right hand side. (b) LAE–CNC unfiltered dispersion at a 0.006% LAE concentration. Left: Initial film shape when the bubble stopped moving. Middle: Film shape after about 1 minute of film thinning. Right: Quasi-stable film lasting up to 300 seconds.

thickness below 100 nm with a much slower thinning rate up to coalescence as illustrated in Fig. 2. The rim of the quasi-equilibrated film was much thicker than the centre (*cf.* Fig. 1) and the symmetry of the rim appeared to be essential for a long coalescence time. The calculated height difference between adjacent inner layers in the rim of $70 \text{ nm} \pm 10 \text{ nm}$ was comparable to the measured hydrodynamic diameter of cellulose nanocrystals that can be an indication of layered structures. At other LAE concentrations, the coalescence of dimpled films occurred directly after the thinning stage. Gray spots visible on film images came from particle aggregates and it appeared that they did not influence the thinning rates but they might affect the coalescence time when the film thickness was comparable to the aggregate size. In particular, the aggregates influenced the coalescence time for the highest LAE concentration (0.015%) for which the film always broke in less than 20 s. To verify the effect of large aggregates on the film drainage kinetics, we repeated the experiments with unfiltered mixtures of CNC. For the unfiltered 0.006% LAE–0.3% CNC dispersion, the film thinned much below 100 nm in the centre, while keeping the rim thick and was stable against coalescence for *ca.* 300 seconds (Fig. 1b), which is almost a 3-fold increase in the coalescence time. For unfiltered mixtures of 0.004% LAE, the film drainage time was extended by only 10 seconds compared to the filtered mixture, while for 0.015% LAE no single bubble stability was observed in the unfiltered mixture. The overall dependence of the average coalescence time on the composition of a filtered CNC–LAE mixture is illustrated in Fig. 3 showing the maximum in

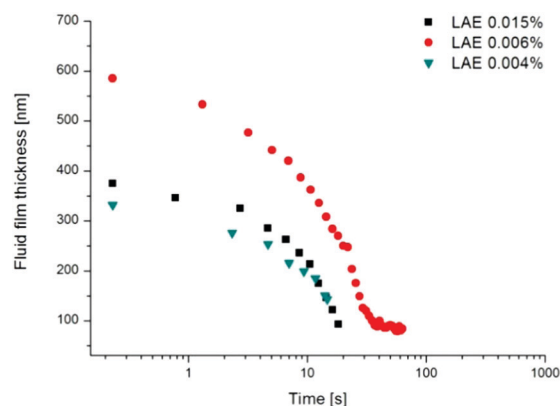


Fig. 2 Evolution of liquid film thickness observed by dynamic film interferometry. Different concentrations of LAE in CNC 0.3 wt% mixtures are indicated. The last measurement point corresponds to the moment of coalescence.

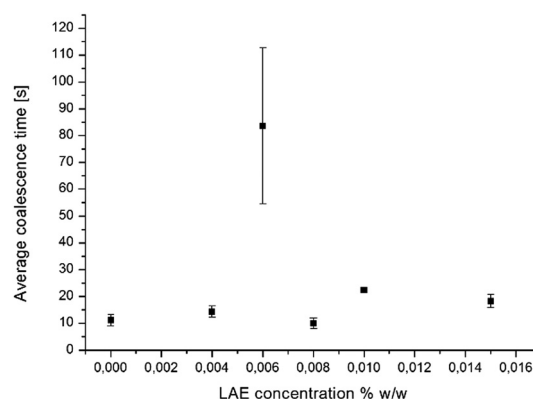


Fig. 3 The dependence of the average coalescence time on the composition of the LAE–CNC mixture.

the bubble coalescence time at around 0.006 wt% of LAE in the LAE–CNC mixture.

To elucidate the effect of adsorption kinetics on the initial film thickness, a separate set of experiments were performed. Before the DFI experiment, the bubbles were aged in the solutions for a particular aging time. The results showed that the initial film thickness for a freshly formed bubble in 0.015 wt% LAE solution was the same, without and with nanoparticles. For the aged bubble in the LAE solution, an increase of the initial film thickness was observed due to surfactant adsorption, whereas for the LAE–CNC mixtures no such increase was noted even after 110 minutes of adsorption time. In contrast, when the bubble surface was freshly formed in a pure LAE solution with a concentration of 0.006%, the film thickness was measured to be half of the thickness that was found in the mixture with cellulose nanoparticles.

To correlate the findings of the dynamic film interferometry experiments with the foamability of the LAE–CNC dispersion, a series of measurements were performed with the double syringe setup. The results indicated a linear increase of foam height with LAE concentrations of up to 0.01 wt% with leveling off *ca.* 40 mL foam volume for higher concentrations. On the

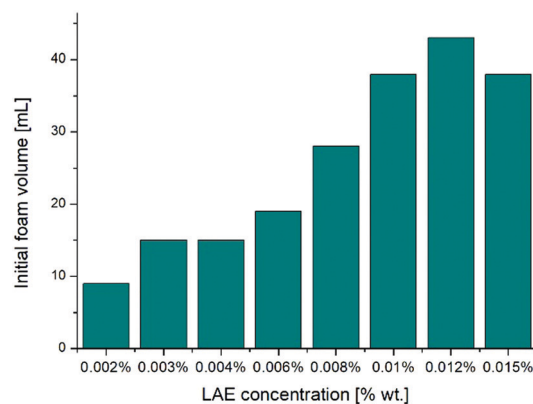


Fig. 4 Initial foam volume dependent on LAE concentration in 0.3 wt% CNC. Error bar ± 2 mL.

other hand, the foam stability followed a different dependence on the LAE concentration. In the absence of a surfactant, foams could not be formed with the dispersion of CNC, whereas in the LAE solutions, in the studied concentration range without the presence of nanoparticles, only unstable foams could be created (life-time below 5 s). In the LAE–CNC mixture with a surfactant concentration of 0.004 wt%, the initial foam volume was 15 mL and its half-life time was 210 minutes. At 0.006 wt%, the initial volume increased to 19 mL and the half-life time increased to 260 min. Significant foam column stability for 0.004 wt% LAE is unexpected from the point of view of a single film coalescence time but it should be considered that the coalescence events in the bulk foam increase the surfactant concentration locally due to the decrease of surface to volume ratio as well as the foam column is supplied from the top with new cellulose nanocrystal portions which again might self-structure at the interface. At the highest LAE concentration of 0.015 wt%, although the initial volume grew to 38 mL, its half-life time drastically decreased to 30 minutes (Fig. 4 and 5).

Foam height is correlated with the liquid content – breaking foams redistribute and also release the liquid into the bulk solution. Liquid content in the foam was measured with the accuracy of 0.5 mL (Fig. 6).

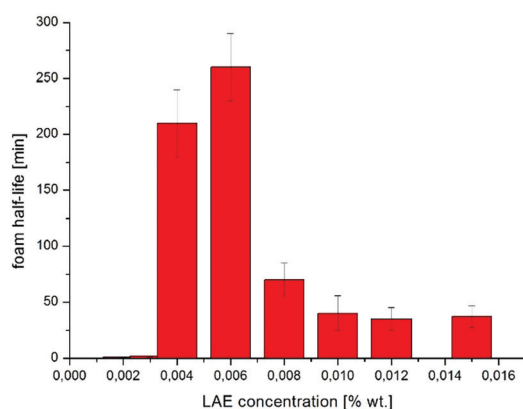


Fig. 5 Foam half-life time as a function of LAE concentration in LAE–CNC (0.3 wt%) mixtures.

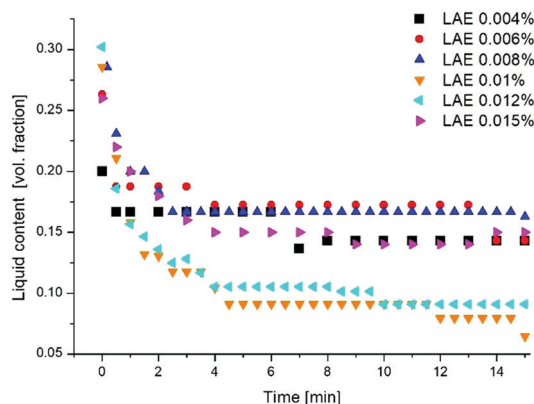


Fig. 6 Evolution of the liquid content in the LAE–CNC foam with the time of drainage.

The initial liquid content in the foam formed with the LAE–CNC mixtures at 0.006 and 0.015 wt% was almost identical, indicating similar foam structures. On the other hand, with the 0.004 wt% LAE, drier foams were initially produced. At lower LAE concentrations, foam drainage seemed to proceed in a two-step process. In the first step, rapid drainage occurred. In the second step of drainage associated with bubble reorganization and coalescence, the relative liquid content was changed less rapidly. In the foam containing 0.015 wt% LAE, a more gradual initial reduction of liquid content was observed during the first stage of draining. A much larger initial foam volume can explain the initial slower drainage. The second stage can be attributed to the aggregation-induced antifoaming effect resulting in bubble breaking in the early stages of foam life and continuous release of liquid.

The observed differences in film thinning rate and foam stability cannot be explained by changes in the viscosity of the surfactant–nanoparticle mixtures. Differences between bulk shear viscosity of LAE–CNC mixtures with increasing surfactant concentration up to 0.015 wt% are negligible, and all mixtures show Newtonian behaviour. The methodology and results of viscosity measurement are reported in Table S1 in the ESI.†

Surface tension measurements of the LAE solution indicated the critical micellization concentration (c.m.c.) value at *ca.* 0.03 wt%, which was in agreement with the literature data for a commercial lauryl ethyl arginate surfactant.³¹ Presence of 0.3 wt% CNC in the surfactant solution below the c.m.c. tends to decrease the equilibrium surface tension as shown in Fig. 7. In particular, the surface tension reaches 45 mN m^{-1} for a LAE concentration about 0.006 wt%, while for a pure surfactant solution its surface tension was 49 mN m^{-1} . At that particular concentration, significant differences in dynamic surface tension, *i.e.*, in the kinetics of adsorption could be observed in the absence and presence of CNC nanoparticles as illustrated in Fig. 8. This might suggest a correspondence with the critical aggregation concentration observed in ionic surfactant–polyelectrolyte mixtures. The observed synergistic effect in the surface tension decreases and the difference in kinetics originates from the co-adsorption of the LAE surfactant and

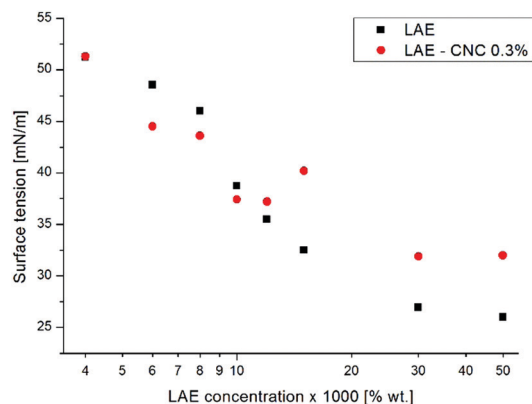


Fig. 7 The dependence of surface tension values on LAE concentration after 2000 s of adsorption without and with CNC (0.3 wt%).

partly hydrophobized nanoparticles as described in ref. 29. For higher LAE concentrations, the tendency was reversed and the surface tension of mixtures with CNC had higher values as compared to pure surfactant solutions. That is, the consequence of aggregation of cellulose nanoparticles due to their extended hydrophobization by surfactant adsorption decreases the concentration of free LAE monomers.²⁹ On the other hand, the aggregates can serve as a reservoir of surfactant molecules, enhancing the rate of transport to the interface. Differences in surfactant kinetics depending on nanoparticle concentration might be further explained by an enhanced mass transport in nanofluids, already reported for Al_2O_3 .⁴⁹ Thus, it can be inferred from Fig. 7 that the onset of the bulk aggregation in LAE–CNC mixtures is around 0.01 wt% of LAE concentration. This corresponds to the surfactant concentration at which foam destruction becomes more rapid, presumably due to the defoaming effect of CNC aggregates.

The dependence of interfacial properties on surfactant concentration in the LAE–CNC mixtures is also reflected in the surface rheological behavior. As shown in Fig. 9, surface dilatational elasticity modulus is systematically higher by *ca.* 50 mN m^{-1} for these mixtures compared with a pure surfactant solution.

The maximum of the dilatational elasticity modulus is observed for the mixture with an LAE concentration of 0.006 wt%

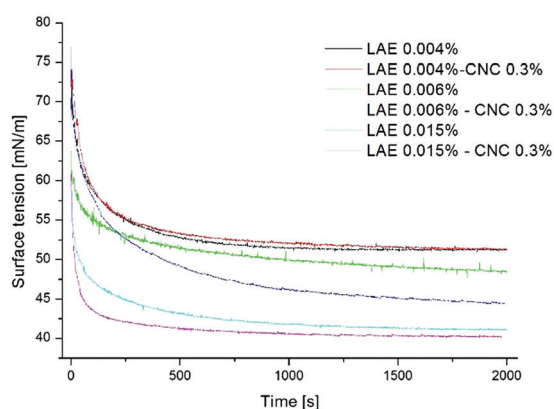


Fig. 8 Time evolution of the dynamic surface tension as a function of LAE concentration without and with the presence of 0.3 wt% CNC.

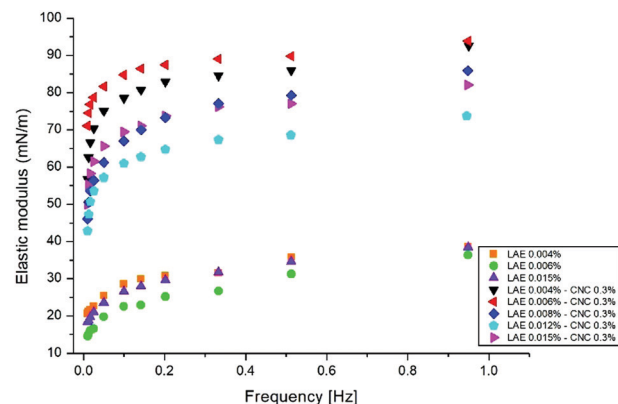


Fig. 9 Frequency dependence of the interfacial dilatational modulus of a LAE solution without and with CNC.

that corresponds to the maximum in thin film thickness and foam life-time. Foam stability is correlated primarily with the value of surface dilatational elasticity.⁵⁰ We obtained a similar maximum in the measurements of the interfacial shear elastic modulus of LAE–CNC mixtures as illustrated in Fig. 10. It attained the highest value of 0.014 N m^{-1} for the same concentration that was well correlated with the maximum of interfacial dilatational modulus. Interfacial shear elastic modulus was constantly developing in the time of 1800 seconds due to the adsorption and self-organization processes in the interfacial layer. We verified in separate experiments that the solution with the highest surfactant concentration investigated (0.015 wt%) had no measurable interfacial elasticity (also proving no influence from minor impurities like lauric acid). Pure cellulose nanocrystal dispersion also did not show any interfacial elasticity and did not have any foaming properties.

Since their mutual interactions govern the interfacial properties of surfactant–nanoparticle mixtures, we determined the average size and zeta potential of CNC nanorods in the presence of LAE. As the results collected in the ESI† suggest, the zeta potential did not change significantly in the studied concentration range of surfactant with the experimental error around the value for pure nanoparticles as 44 mV (± 5 mV).

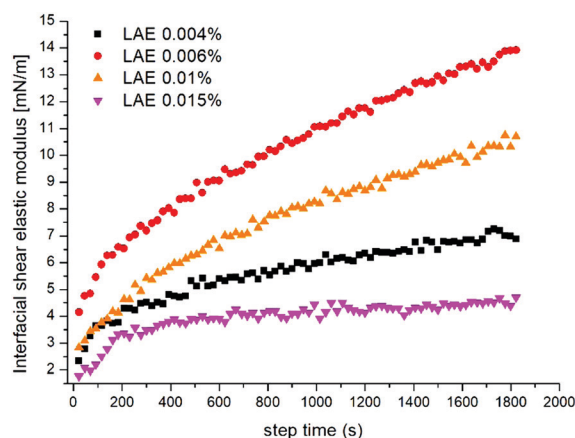


Fig. 10 Time evolution of the interfacial shear elastic modulus of LAE–CNC mixtures at 0.3 wt%. Mixtures under a step strain of 0.5% and 0.05 Hz frequency.

Similar observations were made by Carl *et al.*,⁵¹ who measured the zeta potential of silica nanoparticles in the presence of alkylamines and found that the zeta potential did not significantly change with the cationic surfactant concentration up to flocculation. It was previously reported that zeta potential change at submillimolar LAE concentrations was very limited and particles were attached with their ends exposing most of their negatively charged surfaces to the electric field.²⁹ When compared with dodecyltrimethylammonium bromide–DTAB (M_w 308.34 g mol⁻¹) at the same concentration relative to the surfactant c.m.c. (0.0072 wt%), the zeta potential of CNC increased only to -37 mV. DTAB had much lower adsorption kinetics, which was also influenced by the presence of nanoparticles and had 2 times lower foamability. No detailed experiments were carried out, but DTAB foams did not show enhanced foam stability (results not shown).

The dynamic light scattering (DLS) experiments showed the significant change of diffusion coefficient of CNC mixed with different LAE concentrations. CNC translational diffusion coefficients were in good agreement with the previously reported literature data.⁵² For CNC dispersion without the addition of a surfactant, the average hydrodynamic diameter was 96 nm with the polydispersity index (PDI) of 0.63 (*cf.* Table S2 in the ESI†). For the addition of LAE up to 0.008 wt%, the size did not significantly change and was about 80–90 nm with PDI = 0.56. For the surfactant concentration of 0.015 wt%, some aggregation was observed since the average hydrodynamic diameter increased to 187 nm with much higher PDI (0.85), which was in agreement with earlier conclusions from the surface tension data.

The AFM image presented in the ESI† shows the morphology of the CNC layer deposited on solid PEI-coated silica. A dense, randomly oriented nanoparticle network formed at a CNC concentration of 0.6 wt% could be observed with the electrostatic interactions determining the coverage of the surface. A similar morphology of nanocrystals was observed for the mixture with 0.015 wt% concentration of LAE.

Therefore, a clear correlation exists between the maximum drainage time of the liquid film and foam life-time with the interfacial viscoelastic properties of LAE–CNC mixture at 0.006 wt% surfactant concentration. This maximum can be attributed to the co-adsorption of the surfactant and partly hydrophobized CNC nanoparticles that tend to self-assemble in the interfacial layer. Around this concentration, the surface coverage with nanocrystals reaches a maximum, and they tend to make aggregated structures, which correspond to a maximum of dilatational and shear elastic moduli. Maestro *et al.*⁵³ investigated bubbles with adsorbed CTAB-coated silica nanoparticles. When the surfactant concentration was increased, the dilatational elastic modulus of the air/dispersion interface increased accordingly. It was also shown that the increased elastic modulus could prevent coarsening and slow down foam evolution. Carl *et al.*⁵¹ demonstrated that upon increasing the alkylamine concentration, SiO₂ nanoparticles might form a gel network in the foam that led to increased lifetimes. Kedzior showed that a cationic surfactant and an anionic cellulose nanocrystal mixture stabilized the mini-emulsion polymerisation of PMMA.⁵⁴

Large interfacial shear moduli can be attributed to the electrostatic interaction of particles in the interfacial layer and the effect of excluded volume enhanced by the elongated shape of CNC nanoparticles. Additionally, quadrupolar capillary interactions may induce the self-assembly of particles at the interfaces. In particular, at a curved bubble surface, nanoparticle structures may prolong a thin film lifetime. Considering the cellulose nanocrystal dimensions, with the length of 100 nm and diameter of 5 nm, the magnitude of surface shear moduli may indicate contact line undulations of the order of 10 nm,⁵⁵ which seems to be realistic for twisted CNC crystals assembling side-to-side with their hydrophobic facets at the curved bubble interface. Cylindrical CNC crystals deform the interface and are non-uniformly wetted along their long and short axis. In particular, for a shorter axis, perpendicular to cellulose chains, hydrophobic and hydrophilic domains can be found.⁵⁶

The shape of CNC nanoparticles favors the formation of networks at a much lower surface coverage than silica nanospheres. The possibility of forming CNC microstructures was demonstrated by scanning electron microscopy images of loosely dried CNC dispersions of high concentration (1% w/w), as presented in the ESI.† They show a regular structure of CNC formed upon drying when there is a constant increase of local CNC concentration. It can be seen that individual nanocrystals orient into a highly porous structure with pore diameters from several to about 20 micrometres. The presence of such structures can provide additional stability to dry foams formed with the LAE–CNC mixtures.

Conclusions

Cellulose nanocrystals (CNCs) and cationic surfactant lauroyl ethyl arginate (LAE) synergistically affect coalescence time of liquid films and stability of foam. Coalescence times were at a maximum in the mixture of 0.3 wt% concentration of CNC and 0.006 wt% of LAE. In those conditions, quasi equilibrated fluid films were formed long before coalescence and stayed undeformed until their break-down. The average thickness of these quasi-equilibrated films was below 100 nm; the film symmetric circular border was much thicker than that at its centre and showed stratification with the step size of the order of nanoparticle hydrodynamic diameter that can be the evidence of steric (structural) forces.⁵⁷ For the surfactant concentrations below and above 0.006 wt%, we observed film dimpling and much shorter lifetimes. Besides, the presence of cellulose nanocrystals doubled the initial film thickness as compared to a pure LAE solution at the same optimal concentration.

Cellulose nanocrystals acted as a foam booster in submillimolar LAE concentrations, much below the LAE critical micelle concentration. The presence of cellulose nanoparticles influences LAE adsorption kinetics (rarely equilibrium surface tension values) and enhances foamability and foam stability. Drainage in the LAE–CNC mixtures with a high LAE concentration (0.015 wt%) was continuous and the foam column broke with the half-life time of 30 minutes, probably due to the antifoaming effect of

hydrophobized CNC aggregates. At lower LAE concentrations, a much higher foam half-life was measured and two foam drainage steps could be distinguished. The first step occurred instantly after foam formation and was related to liquid release from the initially thick liquid lamella. The second drainage step was coarsening-related, and bubbles were rearranged and new lamellas were created before coalescence, having different initial liquid contents. In 0.006 wt% LAE mixed with 0.3 wt% CNC, the highest foam stability is attained.

Electrostatic interaction of LAE and CNC facilitates interfacial nanoparticle hydrophobization and affects the equilibrium surface tension for LAE concentrations below c.m.c. The optimal LAE (0.006 wt%) concentration for liquid film and foam stability corresponds to the critical aggregation concentration (c.a.c.) observed in the ionic surfactant–polyelectrolyte mixtures. At this concentration, surface coverage by nanoparticles is at the maximum and the dynamic surface tension is largely affected by the kinetics of their adsorption that is reflected in the maximum of the interfacial dilatational elasticity modulus. The mutual LAE–CNC interactions increase the interfacial shear elastic moduli, due to the synergistic adsorption of surfactant and partially hydrophobized CNC at air/water interfaces and the possible formation of viscoelastic networks at the interface due to CNC aggregation. Similar observations were made before for negatively charged spherical nanoparticles in the presence of a cationic surfactant.^{51,53}

Interfacial shear elastic modulus was found to grow due to further CNC aggregation and rearrangement. Shear deformations are sensitive to cellulose nanocrystal intermolecular interactions. Besides, electrostatic interaction for particles in the interfacial layer and the effect of excluded volume were enhanced by the elongated shape of CNC nanoparticles, and capillary interactions may induce self-assembly of particles at the interfaces which contribute to enhanced shear elasticity of the LAE–CNC mixtures.

Our experiments have demonstrated that single bubble coalescence times are well correlated with foam column stability, in which drainage, coarsening and coalescence are coupled, but these processes can be distinguished in the early stages of foam life, before drying. We demonstrated the correlation of increased kinetic stability of foams formed with LAE–CNC mixtures with viscoelastic properties of interfaces and kinetics of single fluid film drainage. The kinetic stability can be achieved by tuning the electrostatic and hydrophobic interactions of nanoparticles by surfactant adsorption.

Conflicts of interest

There are no conflicts to declare.

Acknowledgements

This work was partially funded by the National Science Centre of Poland (grant number 2016/21/B/ST8/02107) and statutory subsidy for Jerzy Haber Institute of Catalysis and Surface Chemistry PAS. AC has been partly supported by EU Project

POWR.03.02.00-00-I004/16. International academic exchange was funded by European Social Fund (POWR.03.03.00-00-PN13/18). We thank Vineeth Chandran Suja (Stanford University, USA) for technical assistance in conducting the DFI experiments, Giorgio Battilana (CNR-ICMATE, Italy) for SEM microscopy imaging, Robert Hołyst (Institute of Physical Chemistry, Polish Academy of Sciences, Poland) and Szczepan Zapotoczny (Department of Chemistry, Jagiellonian University, Poland) for providing laboratory facilities.

References

- 1 D. Exerova and P. Kruglyakov, *Foam and Foam Films*, Elsevier Science, 1997.
- 2 W. Drenckham and A. Saint-Jalmes, *Adv. Colloid Interface Sci.*, 2015, **222**, 228–259.
- 3 E. Santini, E. Jarek, F. Ravera, L. Liggieri, P. Warszyński and M. Krzan, *Colloids Surf., B*, 2019, **181**, 198–206.
- 4 Z. Briceño-Ahumada, W. Drenckhan and D. Langevin, *Phys. Rev. Lett.*, 2016, **116**, 128302.
- 5 S. T. Tobin, A. J. Meagher, B. Bulfin, M. Möbius and S. Hutzler, *Am. J. Phys.*, 2011, **79**, 819.
- 6 P.-S. Hahn and J. C. Slattery, *AIChE J.*, 1985, **31**(6), 950–956.
- 7 J.-C. Joye and C. A. Miller, *Langmuir*, 1992, **8**, 3083–3092.
- 8 A. Kannan, I. C. Shieh and G. G. Fuller, *J. Colloid Interface Sci.*, 2019, **550**, 128–138.
- 9 J.-D. Chen, P.-S. Hahn and J. C. Slattery, *AIChE J.*, 1988, **34**(1), 140–143.
- 10 A. Nikolov and D. Wasan, *Adv. Colloid Interface Sci.*, 2014, **206**, 207–221.
- 11 M. Gupta, R. Van Hooghten, P. Fischer, D. Zeynel Gunes and J. Vermant, *Rheol. Acta*, 2016, **55**, 537–546.
- 12 K. Malysa and K. Lunkenheimer, *Curr. Opin. Colloid Interface Sci.*, 2008, **13**, 150–162.
- 13 A. Stocco, W. Drenckhan, E. Rio, D. Langevin and B. P. Binks, *Soft Matter*, 2009, **5**, 2215–2222.
- 14 M. B. J. Meinders and T. V. Vliet, *Adv. Colloid Interface Sci.*, 2004, **108**, 119–126.
- 15 S. I. Kam and W. R. Rossen, *J. Colloid Interface Sci.*, 1999, **213**, 329–339.
- 16 Z. P. Du, M. P. Bilbao-Montoya, B. P. Binks, E. Dickinson, R. Ettelaie and B. S. Murray, *Langmuir*, 2003, **19**, 3106–3108.
- 17 B. P. Binks, M. Kirkland and J. A. Rodrigues, *Soft Matter*, 2008, **4**, 2373–2382.
- 18 L. Liggieri, E. Santini, E. Guzmán, A. Maestro and F. Ravera, *Soft Matter*, 2011, **7**, 7699–7709.
- 19 T. N. Hunter, R. J. Pugh, G. V. Franks and G. J. Jameson, *Adv. Colloid Interface Sci.*, 2008, **137**, 57–81.
- 20 T. Horozov, *Curr. Opin. Colloid Interface Sci.*, 2008, **13**, 134–140.
- 21 W. Y. Hamad, *Cellulose Nanocrystals, Properties, Production and Applications*, Wiley, 2017.
- 22 I. A. Sacui, R. C. Nieuwendaal, D. J. Burnett, S. J. Stranick, M. Jorfi, C. Weder, E. J. Foster, R. T. Olsson and J. W. Gilman, *ACS Appl. Mater. Interfaces*, 2014, **6**, 6127–6138.

- 23 T. Abitbol, D. Kam, Y. Levi-Kalisman, D. G. Gray and O. Shoseyov, *Langmuir*, 2018, **34**(13), 3925–3933.
- 24 Y. Ogawa, *Nanoscale*, 2019, **11**, 21767–21774.
- 25 T. Phan-Xuan, A. Thuresson, M. Skepo, A. Labrador, R. Bordes and A. Matic, *Cellulose*, 2016, **23**, 3653–3663.
- 26 P. Bertsch and P. Fischer, *Langmuir*, 2019, **35**, 7937–7943.
- 27 N. T. Cervin, E. Johansson, J.-W. Benjamins and L. Wågberg, *Biomacromolecules*, 2015, **6**(3), 822–831.
- 28 H. A. Wege, S. Kim, V. N. Paunov, Q. Zhong and O. D. Velev, *Langmuir*, 2008, **24**, 9245–9253.
- 29 K. Chi and J. M. Catchmark, *Carbohydr. Polym.*, 2017, **175**, 320–329.
- 30 B. L. Tardy, *et al.*, *Curr. Opin. Colloid Interface Sci.*, 2017, **29**, 57–67.
- 31 L. Bai, W. Xiang, S. Huan and O. J. Rojas, *Biomacromolecules*, 2018, **19**(5), 1674–1685.
- 32 R. Alargova, D. Warhadpande, V. Paunov and O. Velev, *Langmuir*, 2004, **20**, 10371–10374.
- 33 B. Madivala, S. Vandebriel, J. Franssaer and J. Vermant, *Soft Matter*, 2009, **5**, 1717–1727.
- 34 K. D. Danov and P. A. Kralchevsky, *J. Colloid Interface Sci.*, 2005, **287**, 121–134.
- 35 R. Van Hooghten, L. Imperiali, V. Boeck, R. Sharma and J. Vermant, *Soft Matter*, 2013, **9**, 10791–10798.
- 36 G. Nawrocki, P.-A. Cazade, D. Thompson and M. Cieplak, *J. Phys. Chem. C*, 2015, **119**, 24404–24416.
- 37 D. C. Malaspina and J. Faraudo, *Adv. Colloid Interface Sci.*, 2019, **267**, 15–25.
- 38 L. Botto, E. P. Lewandowski, M. Cavallaro Jr. and K. J. Stebe, *Soft Matter*, 2012, **8**, 9957–9971.
- 39 A. Nikolov, K. Kondiparty and D. Wasan, *Langmuir*, 2010, **26**(11), 7665–7670.
- 40 J. M. Frostad, D. Tammara, L. Santollani, S. Bochner de Araujo and G. G. Fuller, *Soft Matter*, 2016, **12**, 9266–9279.
- 41 A. Kannan, I. C. Shieh, D. L. Leiske and G. G. Fuller, *Langmuir*, 2018, **34**(2), 630–638.
- 42 G. Lin, J. M. Frostad and G. G. Fuller, *Phys. Rev. Fluids*, 2018, **3**, 114001.
- 43 E. Hecht, *Optics*, Pearson Education Inc., 2002.
- 44 Y. Zhang and V. Sharma, *Soft Matter*, 2015, **11**, 4408–4417.
- 45 W. Osten, *Optical Inspection of Microsystems*, CRC Press, 2017.
- 46 L. E. Scriven, *Chem. Eng. Sci.*, 1960, **12**, 98–108.
- 47 J. Lucassen and M. van den Tempel, *Chem. Eng. Sci.*, 1972, **27**, 1283–1291.
- 48 S. Vandebriel, A. Franck, G. G. Fuller, P. Moldenaers and J. Vermant, *Rheol. Acta*, 2010, **49**(2), 131–144.
- 49 S. Krishnamurthy, P. Bhattacharya, P. E. Phelan and R. S. Prasher, *Nano Lett.*, 2006, **6**(3), 419–423.
- 50 K. Malysa, K. Lunkenheimer, R. Miller and C. Hartenstein, *Colloids Surf.*, 1981, **3**, 329–338.
- 51 A. Carl, A. Bannuscher and R. von Klitzing, *Langmuir*, 2015, **31**(5), 1615–1622.
- 52 J. H. Sim, S. Dong, K. Röemhild, A. Kaya, D. Sohn, K. Tanaka, M. Roman, T. Heinze and A. R. Esker, *J. Colloid Interface Sci.*, 2015, **440**, 119–125.
- 53 A. Maestro, E. Rio, W. Drenckhan, D. Langevin and A. Salonen, *Soft Matter*, 2014, **10**, 6975–6983.
- 54 S. A. Kedzior, H. S. Marway and E. D. Cranston, *Macromolecules*, 2017, **50**(7), 2645–2655.
- 55 P. A. Kralchevsky and K. Nagayama, *Particles at Fluid Interfaces*, Elsevier Science, 2001.
- 56 T. Rosenau, A. Potthast and J. Hell, *Cellulose Science and Technology Chemistry, Analysis, and Applications*, Wiley, 2019.
- 57 A. D. Nikolov and D. T. Wasan, *Langmuir*, 1992, **8**, 2985–2994.

Viscoelastic interfaces comprising cellulose nanocrystals and lauroyl ethyl arginate for enhanced foam stability

Agnieszka Czakaj^a, Aadithya Kannan^b, Agnieszka Wiśniewska^c, Gabriela Grześ^d, Marcel Krzan^a,

Piotr Warszyński^a, Gerald G. Fuller^b

corresponding author. Email address: ncczakaj@cyf-kr.edu.pl

^a Jerzy Haber Institute of Catalysis and Surface Chemistry PAS, Kraków, Poland

^b Department of Chemical Engineering, Stanford University, Stanford, USA

^c Institute of Physical Chemistry, Polish Academy of Sciences, Warsaw, Poland

^d Department of Chemistry, Jagiellonian University, Kraków, Poland

Supporting information

Bulk viscosity

Shear viscosity measurements were performed by Malvern Kinexus Pro rotational rheometer with cone - plate geometry with diameter 50 mm, angle 1 degree, and 0.3 mm of a gap. The experiments were conducted in controlled shear stress mode with constant temperature 298K. All concentrations were prepared twice, sonicated for a time of 10 min and measured. The range of shear stress was 0.01 to 1.25 Pa. Assuming the proportional relation for shear stress and shear rate for Newtonian fluid, the dynamic viscosity was calculated by extrapolation to zero shear rate. The results are collected in Table S1.

Table S1. Bulk viscosity of the investigated mixtures of CNC nanoparticles (0.3% wt.) with LAE

	Zero shear rate viscosity
CNC 0.3%	0.00136 Pa s
LAE 0.005% - CNC 0.3%	0.00142 Pa s
LAE 0.01% - CNC 0.3%	0.00135 Pa s
LAE 0.015% - CNC 0.3%	0.00165 Pa s

CNC particle size and zeta potential

Size of CNC nanoparticles was measured by dynamic light scattering with Malvern Nano ZS instrument. Each measurement was repeated three times and standard error from 3 measurements is given.

Zeta potential of all LAE – CNC mixtures was measured by laser Doppler velocimetry with Malvern Nano ZS instrument. Each measurement was repeated three times. No viscosity correction was applied. The average error (standard deviation) was 5 mV maximum.

The results of measurements are given in Table S2.

Table S2. The changes of the hydrodynamic diameter and zeta potential of CNC nanoparticles on the addition of LAE.

	Mean diffusion coefficient [$\mu\text{m}^2/\text{s}$]	Hydrodynamic diameter [nm] (polydispersity index)	Zeta potential [mV]
LAE	-	-	70
CNC 0.6% wt.	5.08	96 (0.63)	-44
LAE 0.004% - CNC 0.3% wt.	5.61	88 (0.56)	-44
LAE 0.006% - CNC 0.3% wt.	6.36	77 (0.52)	-50
LAE 0.008% - CNC 0.3% wt.	5.59	88 (0.50)	-
LAE 0.015% - CNC 0.3% wt.	2.65	187 (0.82)	-45

Lauroyl ethyl arginate

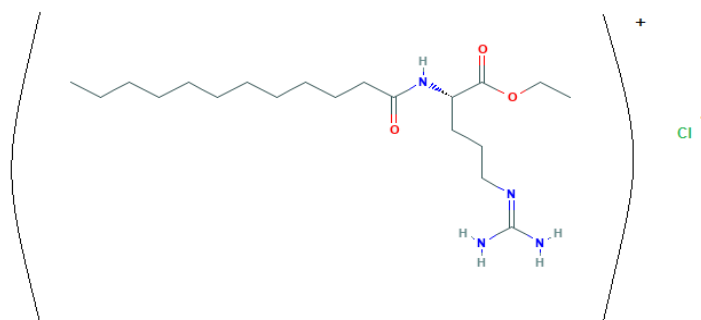


Fig. S1 Lauroyl ethyl arginate molecular structure (pubchem.ncbi.nlm.nih.gov/compound/188214)

Atomic force microscopy imaging

Atomic Force Microscopy (AFM) images were obtained using a Dimension Icon AFM (Bruker, Santa Barbara, CA) working in QNM[®] mode with SCANASYST-AIR tips (nominal spring constant of 0.4 Nm⁻¹). Cellulose nanocrystals were deposited layer-by-layer on a silicon wafer treated with piranha solution and with aqueous polyethyleneimine solution 0.1 g/100 mL (MW 750 000) to form positive anchor layer for negatively charged LAE-CNC species.

Figures S2 and S3 illustrate AFM images of dry film of cellulose nanocrystals deposited from 0.6% wt. Solution and dry film of cellulose nanocrystals deposited from LAE- CNC (0.015% : 0.3% wt.) mixture.

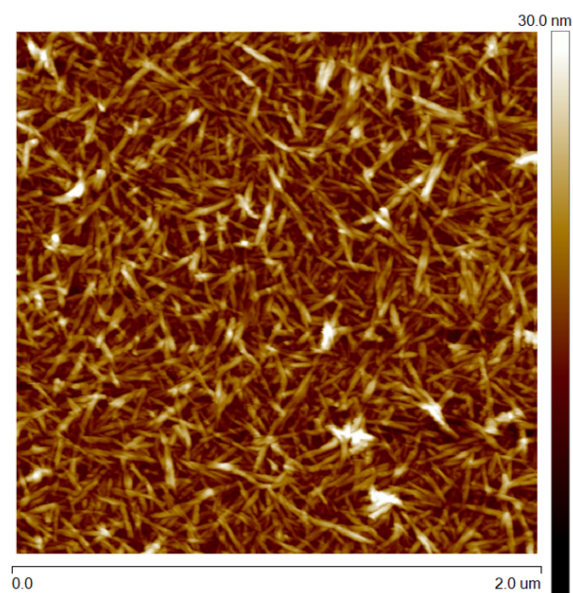


Fig. S2. Dry film of cellulose nanocrystals deposited from 0.6% wt. solution layer-by-layer at polyethyleneimine – coated Si wafer.

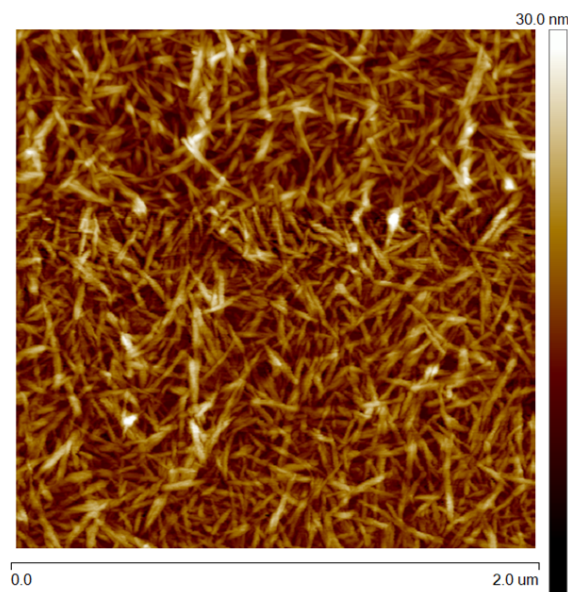


Fig. S3. Dry film of cellulose nanocrystals deposited from LAE - CNC (0.015% : 0.3% wt.) mixture layer-by-layer at polyethyleneimine – coated Si wafer.

Scanning electron microscopy imaging

A drop of cellulose nanocrystals suspension (initial concentration 1 % wt.) was dried directly on the microscopic stage in atmospheric conditions. Samples were imaged without additional modification with Scanning Electron Microscopy (SEM) LEO 1450VP, Electron Microscopy Ltd., Cambridge, U.K.

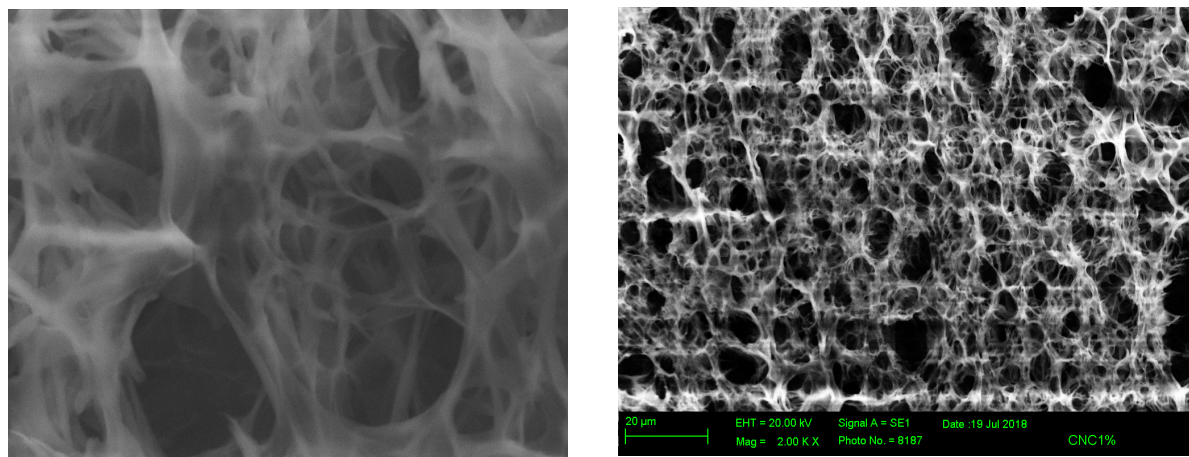


Fig. S4. The images of 3D structure formed with CNC nanoparticles after drying the drop of suspension.

Foaming



Fig. S5. Foams produced by double syringe method from LAE – CNC 0.3% mixtures. Left: 0.004% wt. LAE, Middle: 0.006% wt. LAE, Right 0.015% wt. LAE. Different starting point of foaming should be taken into account.

Table of contents graphics



Fig. S6. Fluid film of the bubble with cellulose nanocrystals assembled at the air/liquid interface (zoom).


 Cite this: *Soft Matter*, 2020, 16, 5094

DOI: 10.1039/d0sm90090g

rsc.li/soft-matter-journal

Correction: Viscoelastic interfaces comprising of cellulose nanocrystals and lauroyl ethyl arginate for enhanced foam stability

 Agnieszka Czakaj,^{*a} Aadithya Kannan,^b Agnieszka Wiśniewska,^c Gabriela Grześ,^d Marcel Krzan,^a Piotr Warszyński^a and Gerald G. Fuller^b

 Correction for 'Viscoelastic interfaces comprising of cellulose nanocrystals and lauroyl ethyl arginate for enhanced foam stability' by Agnieszka Czakaj *et al.*, *Soft Matter*, 2020, **16**, 3981–3990, DOI: 10.1039/C9SM02392E.

The authors would like to correct Fig. 8. Due to the original colours used, not all of the lines on the graph were visible. The corrected version of Fig. 8 is shown below.

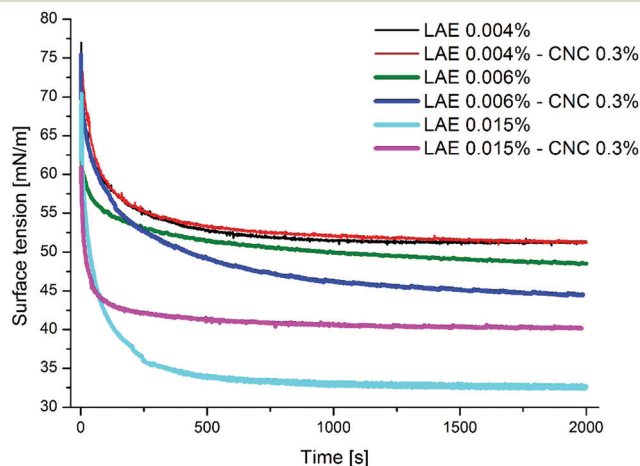


Fig. 8 Time evolution of the dynamic surface tension as a function of LAE concentration without and with the presence of 0.3 wt% CNC.

The Royal Society of Chemistry apologises for these errors and any consequent inconvenience to authors and readers.

^a Jerzy Haber Institute of Catalysis and Surface Chemistry PAS, Krakow, Poland. E-mail: ncczakaj@cyf-kr.edu.pl

^b Department of Chemical Engineering, Stanford University, Stanford, USA

^c Institute of Physical Chemistry, Polish Academy of Sciences, Warsaw, Poland

^d Department of Chemistry, Jagiellonian University, Krakow, Poland



Article

The Effect of Electrolytes and Urea on the Ethyl Lauroyl Arginate and Cellulose Nanocrystals Foam Stability

Agnieszka Czakaj ^{*}, Marcel Krzan  and Piotr Warszyński 

Jerzy Haber Institute of Catalysis and Surface Chemistry, Polish Academy of Sciences, ul. Niezapominajek 8, 30-239 Krakow, Poland; marcel.krzan@ikifp.edu.pl (M.K.); piotr.warszynski@ikifp.edu.pl (P.W.)

* Correspondence: agnieszka.czakaj@ikifp.edu.pl

Abstract: Carboxylated cellulose nanocrystals (cCNC) are highly dispersible particles useful in many industries. In particular, they can be applied to form Pickering emulsions and foams for “green” applications in the cosmetics, pharmaceutical industry or food processing. We demonstrated that carboxylated cellulose nanocrystals enhance foamability and foam stability when mixed with cationic surfactant ethyl lauroyl arginate (LAE), having superior properties over sulfated cellulose nanocrystals (sCNC) concerning surfactant concentration range and foam volume. Mixtures of LAE and cCNC were characterized for their hydrodynamic diameter, zeta potential, surface tension and surface rheological properties. The influence of electrolytes, namely, sodium chloride, guanidine hydrochloride and sodium salicylate, and the addition of concentrated urea to LAE-cCNC mixtures on foamability and foam stability were investigated. Electrolytes in the concentration of 5 mM showed a moderate effect on foam stability. In contrast, spectacular foam collapse was detected after adding concentrated urea. The preliminary rheological data from the pendant drop oscillations revealed low elastic modulus upon urea addition and the loss modulus that increased with the frequency, which suggested a viscous interfacial layer.

Keywords: ethyl lauroyl arginate; surface dilational elasticity; foam; interfacial rheology; cellulose nanocrystals



Citation: Czakaj, A.; Krzan, M.; Warszyński, P. The Effect of Electrolytes and Urea on the Ethyl Lauroyl Arginate and Cellulose Nanocrystals Foam Stability. *Appl. Sci.* **2022**, *12*, 2797. <https://doi.org/10.3390/app12062797>

Academic Editor: Fabrice Goubard

Received: 2 February 2022

Accepted: 4 March 2022

Published: 9 March 2022

Publisher's Note: MDPI stays neutral with regard to jurisdictional claims in published maps and institutional affiliations.



Copyright: © 2022 by the authors. Licensee MDPI, Basel, Switzerland. This article is an open access article distributed under the terms and conditions of the Creative Commons Attribution (CC BY) license (<https://creativecommons.org/licenses/by/4.0/>).

1. Introduction

Cellulose present in plant cell walls is the most abundant polysaccharide and sustainable biopolymer on the Earth. It consists of glucose molecules linked with β -1,4-glycosidic bonds. As a raw material, cellulose has been used in the industry for 150 years [1]. Nanocellulose particles, with at least one dimension in the nanoscale, have been increasingly applied in the newest technologies [2,3]: piezoelectricity and wearable electronics [4], pigments [5], flocculants [6], wound healing materials, drug carriers, implants and tissue engineering [7], coatings, adhesives, antibacterial packaging materials [8], thickeners and rheology modifiers [9], nano-templates, [10] reinforcing agent for composites, foams and aerogels [11], Pickering foams and emulsions [12].

Cellulose nanocrystals released by chemical hydrolysis or oxidation were first produced in 1947. They possess three essential properties: colloidal stability in polar solvents, nano-size and high crystallinity. Since 1990, they have been manufactured in tonne-per-day quantities. They are suitable for commercial applications, including the preparation of foams. In the process of sulfuric acid hydrolysis, glycosidic bonds of cellulose chains are broken, especially in less crystalline regions, and some hydroxy groups on cellulose surfaces are esterified. Released nano-sized crystalline particles, partially esterified, are called sulfated cellulose nanocrystals (sCNC) (containing carbon–oxygen–sulfur bond) [13].

Carboxylated cellulose nanocrystals (cCNC) can be produced in a batch process with dilute hydrogen peroxide oxidation [14]. The cCNC has a relatively low surface charge density compared to sulfated cellulose nanocrystals. They are also less crystalline and have a relatively high surface area.

Cellulose is chiral in many length scales from molecules up to mesophases. Importantly, nanocellulose crystals and fibers are twisted [15], which affects the exposure of their more hydrophobic crystallographic planes at the air/water interface. Depending on their concentration, cellulose nanocrystals may form liquid crystals in water [16]. The liquid crystalline behavior of cellulose nanocrystals (CNC) is solvent-dependent, which can be explained with more efficient hydrogen bonding between CNC at lower dielectric screening. Cellulose nanocrystals form needle-like elongated micro-aggregates with broad size distribution in low dielectric solvents [17].

Ethyl lauroyl arginate is a cationic surfactant manufactured from biodegradable compounds. It hydrolyses to other surface-active substances in water: N α -lauroyl-L-arginine (LAS) or dodecanoic (lauric) acid. In our previous work, we described its interfacial properties [18] and determined critical micelle concentration (CMC) at about 1 mmol/L.

Foaming properties are interesting from many technological perspectives, including flotation and detergency. There are several methods of foam formation characterization, including the double syringe technique [19], which provides foams consisting of tiny bubbles of relatively uniform size [20]. Foaming experiments carried out with the double syringe for a commercial brand of LAE (85% purity) showed that at concentrations below 0.35 mM, its solution did not form foams surviving more than several minutes. On the contrary, when mixed with hydrophilic sulfated cellulose nanocrystals, foams could be stable for up to 4 h [21]. Nanometric sCNC with sulfate hydrophilic groups moderately interact with LAE at low surfactant concentrations, and particle zeta potential and hydrodynamic diameter do not change significantly. The explanation of enhanced foam stability in LAE-sCNC mixtures is far from trivial. A slight increase in dispersion viscosity, high interfacial shear elasticity and flow-induced plugs in the Plateau borders may contribute to the enhanced foam stability. On the other hand, sCNC aggregates in the foam films may have an opposite antifoaming effect.

Upon aggregation, cellulose nanocrystals form rods with a high aspect ratio and rectangular cross-section that can be crucial for explaining foam stability in the mixtures with surfactants. The aspect ratio of nanocellulose can be a key parameter determining the stability of Pickering emulsions [22]. Emulsion stability is also inversely proportional to the surface charge density of cellulose nanocrystals, since less charged CNC are more amphiphilic [23]. Thus, cellulose nanocrystals' surface charge density can affect interfacial properties and foaming properties at the liquid/air interface [24].

The redispersion of sulfated CNC can impact the rheological properties of their dispersions [25]. They adsorb at the liquid/air interface after several hours when the addition of salt screens their charge [26]. CNC forms lyotropic liquid crystals at concentrations above 1% by weight [27]. It was shown that the addition of cellulose nanocrystals enhances the stability of methylcellulose foams after the formation of gels [28]. There were other reports concerning the influence of nanocellulose on foaming properties [29], where size and bulk rheology of nanocellulose played a significant role. However, only a few studies have been related to simple liquid foams without gelled phase, without polymers as additives and with nanocellulose in the form of nanocrystals.

Various additives modify the electrostatic properties of nanoparticles, the interaction of nanoparticles and surfactants and the foaming properties of their mixtures. The addition of monovalent electrolyte decreases electrostatic repulsion between particles and enhances surfactant adsorption at the interface, due to lower electrostatic repulsion between ionic molecules [30]. Sodium salicylate belongs to organic counterions and hydrotropes solubilizing hydrophobic compounds. It can interact with other surfactants or nanoparticles electrostatically and hydrophobically. It enables the transition of surfactant structure in the solution from spherical micelles to worm-like micelles [31]. Research on interfacial layer viscoelasticity in such systems is rarely reported for surfactant–nanoparticle systems. Some works were devoted to protein interfacial layers that demonstrated that sodium salicylate could dramatically reduce interfacial viscoelasticity of the protein films and change the

properties of wheat dough. It was hypothesized that sodium salicylate acts as a hydrogen bond breaker [32,33].

As it is known from the literature, urea increases critical micelle concentration of surfactants [34], increases counterion dissociation [35], displaces the water from the surface of ionic surfactants, helps solvate the hydrophobic micelle cores by localizing at their surfaces, and changes the micelle shape and the number of surfactants associating in the micelle [36]. Recent data show urea orients at the interface within the hydrogen-bonded water network. Its orientation depends on the sign of the charged interface—the net orientation of urea is possible only in the presence of surfactants. Depending on the concentration, urea orients with its C=O group toward a positively charged interface, as shown by characteristic vibrational modes of urea detected by SFG spectroscopy [37].

It was evidenced that urea can improve the solubility and stability of cellulose in alkaline solutions [38]. Urea can compete with water for hydrogen bonding that, together with ionic interactions, contribute the most to the protein tertiary structure. The structure might be entirely destroyed at the urea concentration of 8 mol/L. Guanidine hydrochloride (GuaHCl), is an even stronger protein denaturant than urea. It contains a common cation as a positively charged group of LAE and is well known for its chaotropic properties. In protein solutions, it acts as an unfolding agent [39]. It is also known that urea forms hydrogen bonding with protein backbone amides at high concentrations, while guanidine hydrochloride acts preferentially on hydrophobic residues of the protein [39]. Ethyl lauroyl arginate contains an amide bond between the hydrocarbon chain and guanidinium hydrophilic headgroup; therefore, it can be hypothesized that urea should have a strong effect on LAE interfacial layer. The additional factor that should be taken into account while comparing the urea and GuaHCl effect is the low concentration of GuaHCl that can be used in the experiment to avoid aggregation of surfactant and particles.

In this work, we compared the foaming properties of mixtures of LAE and carboxylated and sulfated CNC. Then, we studied the effect of the addition of electrolytes, a common salt—NaCl, hydrotropic sodium salicylate, and chaotropic guanidine hydrochloride or urea on ethyl lauroyl arginate—carboxylated CNC dispersions bulk and interfacial properties. We attempted to correlate surface tension and dilational viscoelastic properties of dispersions with their foamability and foam stability. Since LAE is a food-grade cationic surfactant with antimicrobial activity against a wide range of food pathogens and spoilage organisms, its foaming properties, enhanced with biopolymeric nanoparticles, can find potential application in cosmetic or pharmaceutical products. Our findings could contribute to the reduction in the amount of surfactant that is necessary to show significant surface activity, emulsification and foaming properties. On the other hand, they can provide information about the selection of components that could be used as defoamers.

2. Materials and Methods

Ethyl lauroyl arginate (LAE), under commercial name Mirenat-P/100 (about 90% LAE surfactant content), was generously provided by Vedeqsa (Barcelona, Spain). Sodium chloride (99%), guanidine hydrochloride (>99% purity), sodium salicylate and urea 8 M Bio Ultra was acquired from Sigma-Aldrich (Poznań, Poland). NaCl was calcinated at 650 °C for eight hours before use. The stock solution was prepared in deionized cold water (4 °C, ~20 MΩ cm) and then diluted to the appropriate concentration. Stock solution and dilutions were used within one day.

Commercially available carboxylated cellulose nanocrystals, DextraCel manufactured by Anomera (Montreal, QC, Canada), used in this work were in the form of sodium salt spray-dried powder with the specification: zeta potential range −40 to −50 mV, diameter 5–10 nm, length 150–200 nm, carboxyl content 0.12–0.20 mmol/g. As has been described by Delepierre et al. [40], cCNC are 150 ± 30 nm in length, 5 ± 2 nm in diameter (approx. round cross-section) with apparent hydrodynamic size 81 ± 1 nm. Their total charge measured by conductometric titration is 141 ± 10 mmol/kg, and surface charge density is 0.16 e/nm². The shear viscosity of 2% solution at 10 s^{−1} is 1.6 mPa s and is purely

Newtonian at $0.1\text{--}10\text{ s}^{-1}$. Zeta potential is $-21 \pm 1\text{ mV}$. Cellulose nanocrystals were dispersed carefully in water by adding small portions of CNC and stirring to achieve a concentration of 0.6% by weight. They were sonicated [Sonic 6D; Polsonic, Warsaw, Poland] after mixing. The cCNC dispersion was added drop by drop to surfactant solution under constant stirring. The concentration of 5 mM was chosen for electrolytes when preparing different mixtures of 0.3% by weight of cCNC from the same stock of particles 0.6 wt.%, dispersed in water to avoid particle aggregation, which may affect foaming properties and interfacial rheology.

2.1. Foaming

Foaming experiments were carried out with the double syringe technique [19–21]—with two single-use medical syringes of 60 mL volume connected by a narrow tube. First, 20 mL of LAE-CNC solution and 40 mL of air were mixed, and the solution passed from one syringe to the other ten times. After that, it stood vertically, and after about 15–30 s, it was possible to read out the foam and liquid levels and determine initial foam volume. Note that here, foam volume was measured only up to 280 min.

2.2. Particle Characterization

The size and zeta potential of cCNC nanoparticles and LAE-cCNC dispersions was measured, respectively, by dynamic light scattering [41] and by laser Doppler velocimetry with Malvern Nano ZS instrument as described earlier [21]. Each measurement was repeated three times. No viscosity correction was applied. The average error (standard deviation) of zeta potential measurement was 5 mV maximum.

2.3. Surface Tension

The surface tension of samples was measured using the pendant drop technique [42] with a Sinterface PAT-1M tensiometer immediately after surfactant solution or dispersion preparation. A drop of solution (11 μL) was created from a 2 mm diameter steel capillary and kept in the thermostated chamber for 2000 s. The camera recorded the drop profile, and the Young–Laplace equation was fitted to calculate the surface tension [43]. Drop oscillations were applied after reaching the surface tension equilibrium by imposing drop volume (area) changes of less than 10% of the volume. Then, Fourier transform of the surface tension variations was calculated and the surface dilational modulus was determined as the complex number [44]:

$$\varepsilon = A_0 \frac{\Delta\sigma_1}{\Delta A_1} = \varepsilon_r + i\varepsilon_i = \varepsilon_d + i\omega\nu_d \quad (1)$$

where $\varepsilon_r, \varepsilon_i$ are the real and imaginary part of the dilational elasticity modulus, ε_d is dilational elasticity, ν_d is the dilational viscosity, ω is the oscillation frequency, A_0 is the average area of the drop, ΔA_1 and $\Delta\sigma_1$ are the principal Fourier components of the area and surface tension variations that correspond to the frequency of drop oscillations.

3. Results and Discussion

3.1. Foaming

Figure 1 illustrates foam half-life (the time after which 50% of the foam breaks) as the function of surfactant concentration for foams generated after 10th cycle of mixing the air and the 20 mL of LAE-CNC dispersion in connected syringes.

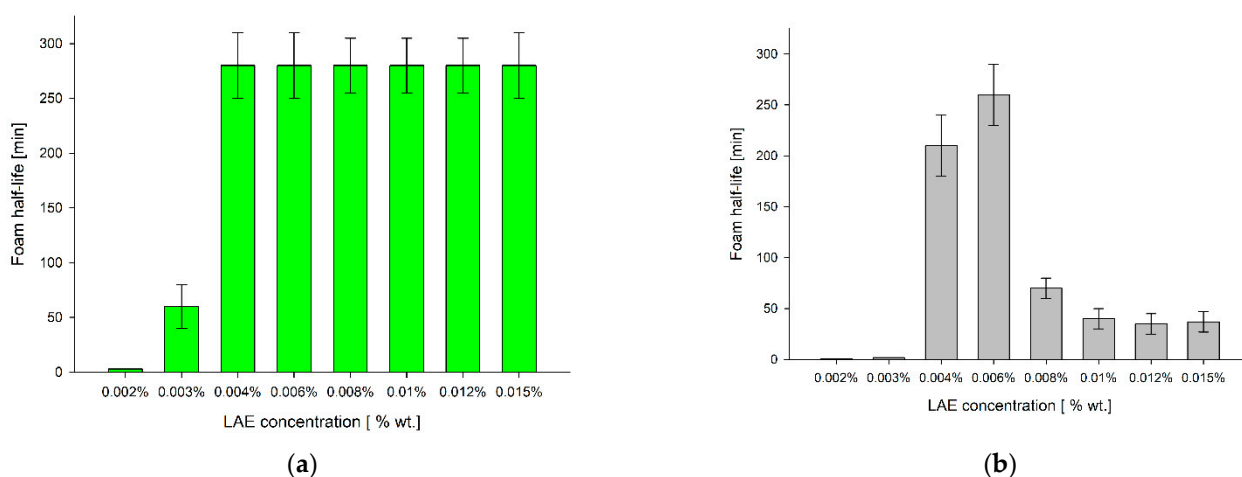


Figure 1. Foam half-life of dispersion of the 0.3 wt.% cellulose nanocrystals with various LAE concentrations; (a) cCNC; (b) sCNC, (see ref. [21]). Maximum observation time 280 min.

Foam and liquid volume could be measured after approximately 30 s and observed for up to 280 min. As shown in Figure 1a, for all concentrations above 0.004%, foam half-life was at least 280 min. In contrast, for sCNC foam half-life was at maximum for 0.006 wt.% of LAE and then decreased for higher surfactant concentrations (Figure 1b) [21]. The aggregation can be the reason for the limited foam stability in the case of sCNC. The results presented in Figure 1 show a threshold value of surfactant concentration (0.003%, 0.07 mM) in the LAE-cCNC mixture, at which foam stability significantly increased. That threshold value was slightly higher for sCNC (0.004 wt.%). Since the zeta potential of nanoparticles in the LAE-cCNC dispersion (−35 mV) was lower than in LAE-sCNC (−40 mV), they can be more amphiphilic, as suggested in [23].

The LAE concentration above the foam stability threshold (0.006 wt.%) was selected to study the effect of various additives on foaming and interfacial properties of the LAE-cCNC suspension. It should be noted that no stable foam can be formed at that surfactant concentration without nanoparticles. The results collected in Table 1 illustrate that at the surfactant concentration corresponding to the LAE-sCNC maximum foam lifetime, cCNC are much more efficient at foaming. The foam volume was almost doubled for carboxylated CNC compared to sulfated ones, while its stability was also prolonged.

Table 1. Initial foam volume and foam half-life in LAE 0.006 wt.%—CNC 0.3 wt.% dispersions with respect to CNC hydrophilic groups.

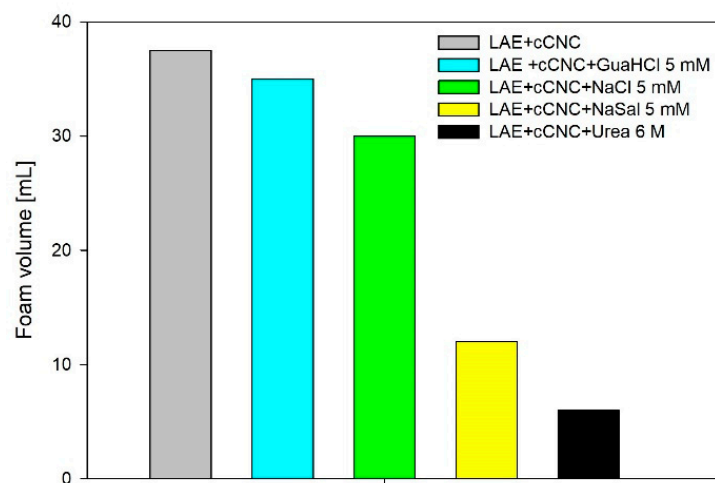
	LAE-sCNC	LAE-cCNC
Foam volume [mL]	19 ± 1	37 ± 1
Foam half-life [min]	260 ± 20	>280

To elucidate the possible reason for the differences in foam stability between two types of CNC for LAE concentration above 0.008 wt.%, we measured the dependence of cCNC hydrodynamic size on the surfactant concentration. The results are listed in Table 2. They show that carboxylated cellulose nanocrystals are resistant to aggregation up to 0.02 wt.% LAE. Moreover, they indicate that cCNC were less aggregated than sCNC. For the surfactant concentration 0.015 wt.% the hydrodynamic size of cCNC was 112 nm (PDI 0.44), significantly smaller and less polydisperse than for sCNC—187 nm (PDI 0.82) [21]. That seems to support the hypothesis that the defoaming effect of large aggregates can cause lower foam stability of sCNC-LAE dispersion.

Table 2. The hydrodynamic diameters of cCNC dispersions with increasing LAE concentrations.

cCNC 0.3 wt.% with	Hydrodynamic Diameter [nm] (Polydispersity Index)
0.008% LAE	87 (0.38)
0.01% LAE	88 (0.30)
0.015% LAE	112 (0.44)
0.02% LAE	206 (0.78)
0.05% LAE	~7000 (1.00)

Figure 2 illustrates the effect of additives—ionic and non-ionic—on the initial foam volume, generated with the double syringe technique. The addition of monovalent electrolytes, sodium chloride or guanidinium hydrochloride at a concentration of 5 mmol/L to LAE-cCNC mixtures did not change foam volume significantly. The difference was seen for 5 mM sodium salicylate, which contains a bulky surface-active anion that can effectively penetrate the interfacial layer formed by cationic LAE and cCNC. The foam volume decreased to about 12 mL, more than three times with respect to LAE-cCNC without additives, or more than two times with respect to one with NaCl. The most significant effect of reducing the initial foam volume was seen for dispersions containing 6 mol/L urea. Right after the foam formation, it filled the whole syringe; however, it collapsed very quickly. The first possible readout of the foam and liquid volume characterizing the foamability, which could be compared with other systems, was made after 30 s.

**Figure 2.** Foam volume of LAE 0.006 wt.% and carboxylated nanocrystals 0.3 wt.% with additional compounds in the dispersion.

Foam half-life for the LAE-cCNC dispersion with added electrolytes (NaCl, NaSal and GuaHCl) was reduced to c.a. 200 min (Figure 3). Note that the foam half-life of the dispersion with 5 mM of NaSal was the same as for other electrolytes, despite lower foamability. That means that the foam drainage rate was independent of the type of salt. As mentioned above, the most significant difference in foam stability was noted in the dispersion containing 6 mol/L urea. The foam half-life was reduced to less than 1 min, coinciding with the fast draining period.

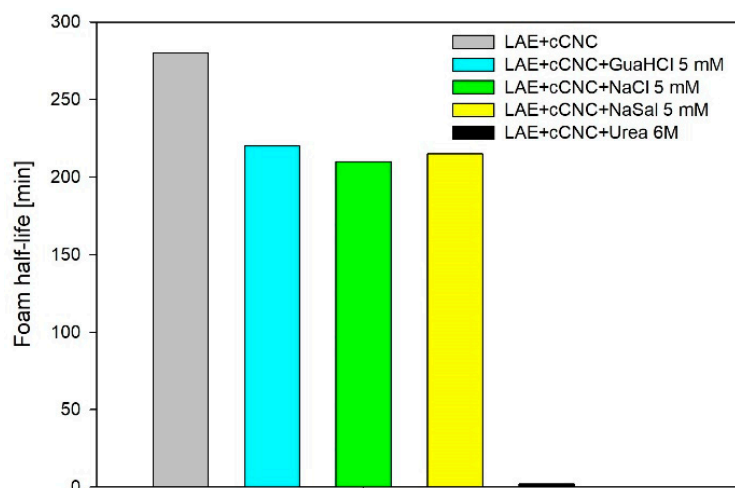


Figure 3. Foam half-life in the dispersion of LAE 0.006 wt.% and cCNC 0.3 wt.% with the addition of NaCl, NaSal, GuaHCl and urea.

3.2. Zeta Potential and Hydrodynamic Diameter

The results of the zeta potential and hydrodynamic diameter measurements of carboxylated CNC are collected in Table 3. Zeta potential measurements indicate that carboxylated nanoparticles are slightly less charged than sulfated [17]. Spray-dried powdered carboxylated CNC were easier to disperse upon sonication; however, the measured hydrodynamic diameter had large polydispersity. Upon adding 5 mM of NaCl or NaSal to LAE 0.006 wt.%—cCNC 0.3 wt.%, dispersion, the zeta potential was only slightly reduced, whereas the addition of the same concentration of GuaHCl decreased the potential by c.a. 10 mV. A similar decrease could be observed at the addition of 6 M of urea. In the case of NaCl and GuaHCl, the decrease in zeta potential was accompanied by a large (almost twice) increase in hydrodynamic diameter, indicating aggregation. No changes were observed when 5 mM NaSal was added to the dispersion, whereas for 6 mol/L urea, the dispersion turbidity almost disappeared, as seen by the naked eye. Nevertheless, the hydrodynamic diameter of 100 nm, with a considerably lower polydispersity, could be measured. The effect of urea was also checked for 0.015 wt.% LAE concentration. Similarly to 0.006 wt.% of LAE, the urea addition increased the dispersion size from 112 nm to 132 nm but reduced polydispersity from 0.44 to 0.35. The plausible explanation of those changes could be that despite the average size (by intensity) of the dispersion grows, the larger cellulose nanocrystals aggregates are destroyed by the addition of urea since it enhances cellulose solubility [38].

Table 3. Zeta potential and hydrodynamic diameter of cCNC dispersions of LAE 0.006% and additional compounds.

LAE 0.006 wt.%—cCNC 0.3 wt.% with:	Zeta Potential [mV]	Hydrodynamic Diameter [nm] (Polydispersity Index)
No additives	-35 ± 5	77 (0.44)
NaCl 5 mmol/L	-30 ± 5	197 (0.53)
Urea 6 mol/L	-26 ± 4	101 (0.28)
Sodium salicylate 5 mmol/L	-31 ± 4	108 (0.43)
Guanidine hydrochloride chloride 5 mmol/L	-26 ± 3	209 (0.52)

3.3. Surface Tension

Figure 4 illustrates surface tension kinetics in LAE-cCNC mixtures at LAE concentration 0.006 wt.% and cCNC 0.3 wt.%, in the presence of added 5 mM NaCl, NaSal, GuaHCl and 6 mol/L urea. In general, the addition of cCNC to the surfactant solution decreased the equilibrium surface tension from 48 mN/m for pure 0.006 wt.% LAE (cf. Figure 5) to 40 mN/m for the dispersion with 0.3 wt.% cCNC. Similar results were obtained previously for sCNC [21]. In the case of sodium chloride and guanidinium chloride addition, compared with “no salt” conditions, some decrease in the surface tension was observed at short adsorption times. That effect is similar to one observed for ionic surfactants resulting from the screening of the electrostatic interactions. On the other hand, at longer adsorption times, a small surface tension increase could be noted, which may be explained by aggregation of nanoparticles and more extensive surfactant binding to those aggregates in the suspension. That can be correlated with some reduction in foam stability.

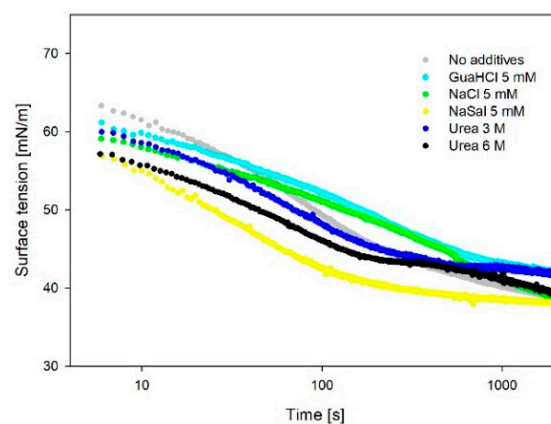


Figure 4. Surface tension of the dispersion of LAE 0.006 wt.% and cCNC 0.3 wt.% with the addition of NaCl, NaSal, GuaHCl and urea.

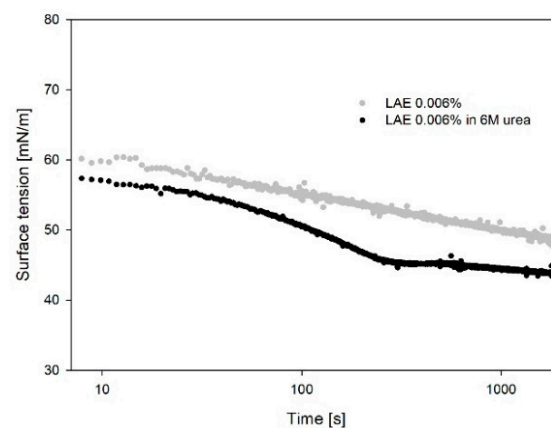


Figure 5. The effect of the addition of urea (6 mol/L) on the surface tension of 0.006 wt.% LAE—Mirenat solution (85% purity).

Sodium salicylate had the strongest effect on the surface tension, due to the surface activity of the salicylate anion that can more effectively neutralize the positive charge of LAE cations at the interface. Characteristic differences in surface tension kinetics could be observed by adding 6 M urea. The surface tension value first seemed to reach a plateau and then decreased. The addition of urea caused a faster decrease in the surface tension compared to the pure LAE-cCNC mixture; however, after the 2000 s of adsorption, similar surface tension values (c.a. 40 mN/m) could be observed. A similar effect of urea was observed for the surfactant solutions without cCNC, as demonstrated in Figure 5.

The frequency dependence of the dilational elasticity modulus measured by the oscillating drop technique was illustrated in Figure 6. For the LAE-cCNC dispersion without additives, the modulus values are similar to 0.006 wt.% LAE solution and c.a. are three times lower than LAE-sCNC at the same concentrations. That can be the effect of higher charge and bigger size of sCNC aggregates or their different arrangement at the interface. On the other hand, the imaginary part of the dilational elasticity for the surfactant solution without CNC was constant in that frequency rate and equal to 3 mN/m. Thus, the addition of 0.3 wt.% cCNC increases the dilational viscosity of an interface.

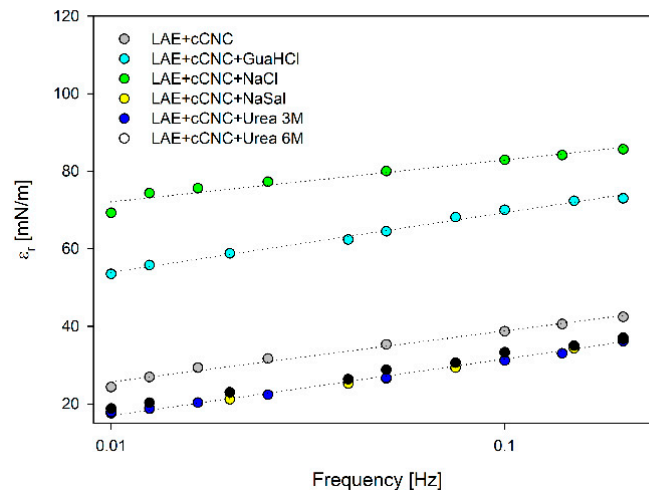


Figure 6. The frequency dependence of the dilational elasticity modulus in LAE-cCNC dispersions with the addition of 5 mmol/L electrolytes (guanidine hydrochloride, sodium chloride, sodium salicylate) and with urea at concentrations as indicated.

The addition of 5 mM NaCl resulted in the highest dilational elasticity. That can be attributed to the decrease in the electrostatic repulsion between charged cellulose nanocrystals that can pack closely at the interface. Data presented in Figure 6 indicate that adding 5 mM of guanidine hydrochloride also increased the elastic modulus (although less than 5 mmol/L NaCl); however, the surface layer became more viscous (c.f. Figure 7). The origin of that effect is unclear, but it demonstrates that both counterions and coions can affect the dilatational moduli at liquid interfaces with ionic surfactants [45]. Specific ion effects relevant for foaming were described in the literature [46]. In our case, both NaCl and GuaHCl show an almost equal effect on foaming properties of LAE-cCNC at the concentration of 5 mmol/L, despite different surface dilational viscoelastic properties. Adding 5 mmol/L NaSal or 6 mol/L urea to the LAE-cCNC dispersion caused a slight decrease in elasticity modulus compared to pure LAE-cCNC. The qualitatively different behavior of the imaginary part of the dilational modulus was observed for those dispersions. Upon addition of GauHCL, NaSal or urea, its values were increased compared to ones for LAE-cCNC, while 5 mM NaCl caused their decrease. Thus, the addition of the simple salt (NaCl) renders the interfacial layer more elastic, presumably due to closer packing of nanocrystals. The presence of hydrotropic NaSal or urea can induce forming of some dissipative structures at the interface; however, that aspect needs further investigation. In those cases, foaming was reduced: for NaSal, a relatively stable form was observed, while no stable foam could be obtained for urea.

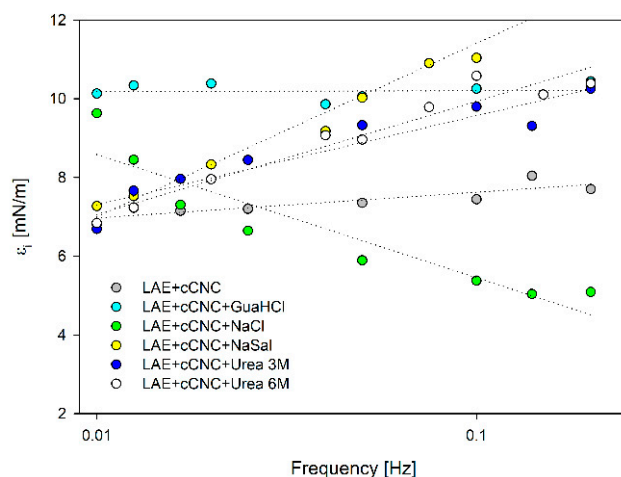


Figure 7. The frequency dependence of the imaginary part of dilational modulus in LAE-cCNC dispersions with 5 mM electrolytes: guanidine hydrochloride, sodium chloride, sodium salicylate and urea at concentrations 3 mol/L or 6 mol/L.

Our findings suggest that urea impact on the interfacial properties of LAE-cCNC dispersion can be of complex origin that is not directly reflected in the equilibrium and dynamic interfacial properties. Urea can disrupt the water structure and become oriented at the interface in the presence of ionic surfactants [37]. Due to enhanced cellulose solubility, urea can also affect the aggregation of nanocrystals and their orientation at interfaces. In particular, the stability of foams in the LAE-cCNC dispersions may be attributed to the lamellar arrangement of nanoparticles, as was demonstrated for the surfactant mesophases [47]. That arrangement may be disrupted by urea (and to a lesser extent by NaSal), which leads to foam destabilization.

4. Conclusions

Foam stability in ethyl lauroyl arginate (LAE) mixtures has a complex origin, including the adsorption of surfactant at the interface, its dynamics at the expanded/contracted interface and the formation of bulk and interfacial aggregates with carboxylated cellulose nanocrystals (cCNC), which change at the time of the foam drainage. Cellulose nanocrystals decorated with oppositely charged surfactants adsorb at the water/air interface, lower the surface tension and modify the surface viscoelastic properties. They reduce drainage and prevent coalescence. Large cellulose nanocrystals aggregates have a significant effect on foam stability, as they accumulate in the Plateau borders and prevent drainage. On the other hand, large aggregates with randomly oriented nanocrystals in the foam films can act as defoamers.

The presence of electrolytes such as sodium chloride and guanidine hydrochloride at a small concentration of 5 mM did not change foamability and foam stability, despite a two-fold increase in the surface dilational elasticity. The hydrodynamic diameter of cellulose nanocrystals also increased twice in size, due to electrostatic screening of CNC repulsion. The surface-active anion of sodium salicylate adsorbs at the interface and effectively screen electrostatic interactions of the LAE hydrophilic group. The foamability of LAE-cCNC mixtures in the presence of 5 mmol/L NaSal was much lower, but the foam stability did not change. Such an effect can be explained by the significant influence of cellulose nanocrystals on overall foam stability.

A dramatic decrease in the quantity of obtained foam volume and lack of its stability were observed for LAE-cCNC mixtures containing 6 mol/L urea. Minor changes of the equilibrium and dynamic surface tension upon the addition of urea cannot explicate that decrease. The plausible explanation can be its orientation at the interface in the presence of ionic surfactants and charged nanocrystals and the disruption of the water structure. Urea can also destroy large lamellar cCNC aggregates that reduce foam drainage. Despite the

chaotropic nature of both guanidine hydrochloride and urea, their effect on ethyl lauroyl arginate—carboxylated CNC dispersions bulk and interfacial properties—are different. The differences in the effect of those denaturants on the bulk and interfacial properties of protein solutions have been described before [48,49]. Our work is the first demonstration of the urea effect on surfactant—nanoparticles interfacial properties and foaming. Future experiments can reveal the complexity of molecular interactions in this system. Importantly, urea affects the interfacial properties of ethyl lauroyl arginate. Further experiments will reveal if it is connected to surfactant hydrolysis, formation of some interfacial structures or other effects. Detailed analysis of different urea concentrations and hydrodynamic size of cellulose nanoparticles can determine the extent of large nano-aggregates solubility. Data presenting the influence of urea on hydrodynamic size are very consistent for the LAE concentration studied. Thin film balance experiments can assess the direct influence of aggregate sizes on film stability. It should be noted that nanoparticle aggregation and their size distribution can affect the thin film stability in a complex way [50]. Investigations of thin film stability are very interesting for the explanation of the influence of some factors controlling foam stability, but other ones such as water drainage or gas permeabilities of liquid films can also be influenced by the aggregation of nanoparticles.

Author Contributions: Conceptualization, A.C. and P.W.; methodology, P.W., A.C. and M.K.; validation, A.C., P.W. and M.K.; formal analysis, P.W.; investigation, A.C.; resources, M.K.; data curation, A.C.; writing—original draft preparation, A.C.; writing—review and editing, P.W. and M.K.; visualization, A.C.; software, M.K.; supervision, P.W.; project administration, M.K.; funding acquisition, M.K. and P.W. All authors have read and agreed to the published version of the manuscript.

Funding: This research was funded by the National Science Centre of Poland (grant number 2016/21/B/ST8/02107) and statutory subsidy for Jerzy Haber Institute of Catalysis and Surface Chemistry PAS. AC has been partly supported by EU Project POWR.03.02.00-00-I004/16.

Institutional Review Board Statement: Not applicable.

Informed Consent Statement: Not applicable.

Data Availability Statement: The data presented in this study are freely available from the authors upon a reasonable request.

Acknowledgments: Figure 1b was reproduced from ref. [21] with permission from The Royal Society of Chemistry.

Conflicts of Interest: The authors declare no conflict of interest. The funders had no role in the design of the study; in the collection, analyses, or interpretation of data; in the writing of the manuscript, or in the decision to publish the results.

References

1. Klemm, D.; Kramer, F.; Moritz, S.; Lindstrom, T.; Ankerfors, M.; Gray, D.; Dorris, A. Nanocelluloses: A new family of nature-based materials. *Angew. Chem. Int. Ed.* **2011**, *50*, 5438–5466.
2. Klemm, D.; Cranston, E.D.; Fischer, D.; Gama, M.; Kedzior, S.A.; Kralisch, D.; Kramer, F.; Kondo, T.; Lindström, T.; Nietzsche, S.; et al. Nanocellulose as a natural source for groundbreaking applications in materials science: Today's state. *Materialstoday* **2018**, *21*, 720–748. [[CrossRef](#)]
3. Kontturi, E.; Laaksonen, P.; Linder, M.B.; Nonappa, Gröschel, A.H.; Orlando, J.; Rojas, O.J.; Ikkala, O. Advanced materials through assembly of nanocelluloses. *Adv. Mater.* **2018**, *30*, 1703779. [[CrossRef](#)] [[PubMed](#)]
4. Wang, J.; Carlos, C.; Zhang, Z.; Li, J.; Long, Y.; Yang, F.; Dong, Y.; Qiu, X. Piezoelectric nanocellulose thin film with large-scale vertical crystal alignment. *ACS Appl. Mater. Interfaces* **2020**, *12*, 26399–26404. [[CrossRef](#)]
5. Droguet, B.E.; Liang, H.-L.; Frka-Petesic, B.; Parker, R.M.; De Volder, M.F.L.; Baumberg, J.J.; Vignolini, S. Large-scale fabrication of structurally coloured cellulose nanocrystal films and effect pigments. *Nat. Mater.* **2021**, *21*, 352–358. [[CrossRef](#)]
6. Koshani, R.; Tavakolian, M.; van de Ven, T.G.M. Cellulose-based dispersants and flocculants. *J. Mater. Chem. B* **2020**, *8*, 10502–10526. [[CrossRef](#)]
7. Shen, X.; Shamshina, J.L.; Berton, P.; Gurau, G.; Rogers, R.D. Hydrogels based on cellulose and chitin: Fabrication, properties, and applications. *Green Chem.* **2016**, *18*, 53–75. [[CrossRef](#)]
8. Chowdhury, R.A.; Nuruddin, Md.; Clarkson, C.; Montes, F.; Howarter, J.; Youngblood, J.P. Cellulose nanocrystal (CNC) coatings with controlled anisotropy as high-performance gas barrier films. *ACS Appl. Mater. Interfaces* **2019**, *11*, 1376–1383. [[CrossRef](#)]

9. Gicquel, E.; Bras, J.; Rey, C.; Putaux, J.-L.; Pignon, F.; Jean, B.; Martin, C. Impact of sonication on the rheological and colloidal properties of highly concentrated cellulose nanocrystal suspensions. *Cellulose* **2019**, *26*, 7619–7634. [[CrossRef](#)]
10. Chakraborty, A.; Nonappa; Mondal, B.; Chaudhari, K.; Rekola, H.; Hynninen, V.; Kostainen, M.A.; Ras, R.H.A.; Pradeep, T.J. Near-infrared chiral plasmonic microwires through precision assembly of gold nanorods on soft biotemplates. *Phys. Chem. C* **2021**, *125*, 3256–3267. [[CrossRef](#)]
11. Lavoine, N.; Bergström, L. Nanocellulose-based foams and aerogels: Processing, properties, and applications. *J. Mater. Chem. A* **2017**, *5*, 16105–16117. [[CrossRef](#)]
12. Lam, S.; Velikov, L.P.; Velez, O.D. Pickering stabilization of foams and emulsions with particles of biological origin. *Curr. Opin. Colloid Interface Sci.* **2014**, *19*, 490–500. [[CrossRef](#)]
13. Vanderfleet, O.M.; Cranston, E.D. Production routes to tailor the performance of cellulose nanocrystals. *Nat. Rev. Mater.* **2021**, *6*, 124–144. [[CrossRef](#)]
14. Andrews, M.P.; Morse, T. Method for Producing Functionalized Nanocrystalline Cellulose and Functionalized Nanocrystalline Cellulose Thereby Produced. U.S. Patent 20,170,260,298 A1, 14 September 2017.
15. Usov, I.; Nyström, G.; Adamcik, J.; Handschin, S.; Schütz, C.; Fall, A.; Bergström, L.; Mezzenga, R. Understanding nanocellulose chirality and structure–properties relationship at the single fibril level. *Nat. Commun.* **2015**, *6*, 7564. [[CrossRef](#)]
16. Surov, O.V.; Voronova, M.I.; Zakharov, A.G. Functional materials based on nanocrystalline cellulose. *Russ. Chem. Rev.* **2017**, *86*, 907–933. [[CrossRef](#)]
17. Kang, K.; Eremin, A. Solvent-dependent morphology and anisotropic microscopic dynamics of cellulose nanocrystals under electric fields. *Phys. Rev. E* **2021**, *103*, 032606. [[CrossRef](#)] [[PubMed](#)]
18. Czakaj, A.; Jarek, E.; Krzan, M.; Warszyński, P. Ethyl lauroyl arginate, an inherently multicomponent surfactant system. *Molecules* **2021**, *26*, 5894. [[CrossRef](#)]
19. Drenckhan, W.; Saint-Jalmes, A. The science of foaming. *Adv. Colloid Interface Sci.* **2015**, *222*, 228–259. [[CrossRef](#)]
20. Briceño-Ahumada, Z.; Drenckhan, W.; Langevin, D. Coalescence in draining foams made of very small bubbles. *Phys. Rev. Lett.* **2016**, *116*, 128302-1-5. [[CrossRef](#)]
21. Czakaj, A.; Kannan, A.; Wiśniewska, A.; Grześ, G.; Krzan, M.; Warszyński, P.; Fuller, G.G. Viscoelastic interfaces comprising of cellulose nanocrystals and lauroyl ethyl arginate for enhanced foam stability. *Soft Matter* **2020**, *16*, 3981–3990. [[CrossRef](#)]
22. Kalashnikova, I.; Bizot, H.; Bertoini, P.; Cathala, B.; Capron, I. Cellulosic nanorods of various aspect ratios for oil in water Pickering emulsions. *Soft Matter* **2013**, *9*, 952–959. [[CrossRef](#)]
23. Kalashnikova, I.; Bizot, H.; Cathala, B.; Capron, I. Modulation of cellulose nanocrystals amphiphilic properties to stabilize oil/water interface. *Biomacromolecules* **2012**, *13*, 267–275. [[CrossRef](#)] [[PubMed](#)]
24. Cervin, N.T.; Johansson, E.; Benjamins, J.-W.; Wågberg, L. Mechanisms behind the stabilizing action of cellulose nanofibrils in wet-stable cellulose foams. *Biomacromolecules* **2015**, *16*, 3, 822–831. [[CrossRef](#)] [[PubMed](#)]
25. Fazilati, M.; Ingelsten, S.; Wojno, S.; Nypelö, T.; Kádár, R. Thixotropy of cellulose nanocrystal suspensions. *J. Rheol.* **2021**, *65*, 1035. [[CrossRef](#)]
26. Bertsch, P.; Diener, M.; Adamcik, J.; Scheuble, N.; Geue, T.; Mezzenga, R.; Fischer, P. Adsorption and interfacial layer structure of unmodified nanocrystalline cellulose at air/water interfaces. *Langmuir* **2018**, *34*, 15195–15202. [[CrossRef](#)]
27. Delepierre, G.; Eyley, S.; Thielemans, W.; Weder, C.; Cranston, E.D.; Zoppe, J.O. Patience is a virtue: Self-assembly and physico-chemical properties of cellulose nanocrystal allomorphs. *Nanoscale* **2020**, *12*, 17480–17493. [[CrossRef](#)]
28. Hu, Z.; Xu, R.; Cranston, E.D.; Pelton, R.H. Stable aqueous foams from cellulose nanocrystals and methyl cellulose. *Biomacromolecules* **2016**, *17*, 4095–4099. [[CrossRef](#)]
29. Xiang, W.; Preisig, N.; Ketola, A.; Tardy, B.L.; Bai, L.; Ketoja, J.A.; Stubenrauch, C.; Rojas, O.J. Surface activity and foaming capacity of aggregates formed between an anionic surfactant and non-cellulosics leached from wood fibers. *Biomacromolecules* **2019**, *20*, 6, 2286–2294. [[CrossRef](#)]
30. Para, G.; Jarek, E.; Warszyński, P.; Adamczyk, Z. Effect of electrolytes on surface tension of ionic surfactant solutions. *Colloids Surf. A Physicochem. Eng. Asp.* **2003**, *222*, 213–222. [[CrossRef](#)]
31. Sharma, V.K.; Srinivasan, H.; Mitra, S.; Garcia-Sakai, V.; Mukhopadhyay, R.J. Effects of hydrotropic salt on the nanoscopic dynamics of DTAB micelles. *Phys. Chem. B* **2017**, *121*, 5562–5572. [[CrossRef](#)]
32. Ogawa, T.; Matsumura, Y. Revealing 3D structure of gluten in wheat dough by optical clearing imaging. *Nat. Commun.* **2021**, *12*, 1708. [[CrossRef](#)] [[PubMed](#)]
33. Tschögl, N.W.; Alexander, A.E. The surface chemistry of wheat gluten II. Measurements of surface viscoelasticity. *J. Colloid Sci.* **1960**, *15*, 168–182. [[CrossRef](#)]
34. Ruiz, C.C. Micelle formation and microenvironmental properties of sodium dodecyl sulfate in aqueous urea solutions. *Colloids Surf. A Physicochem. Eng. Asp.* **1999**, *147*, 349–357. [[CrossRef](#)]
35. Kumari, S.; Sonu, K.; Halder, S.; Aggrawal, R.; Sundar, G.; Saha, S.K. Effect of urea on solvation dynamics and rotational relaxation of coumarin 480 in aqueous micelles of cationic gemini surfactants with different spacer groups. *ACS Omega* **2018**, *3*, 3079–3095. [[CrossRef](#)]
36. Kancharla, S.; Dong, D.; Bedrov, D.; Tsianou, M.; Alexandridis, P. Structure and interactions in perfluorooctanoate micellar solutions revealed by small-angle neutron scattering and molecular dynamics simulations studies: Effect of urea. *Langmuir* **2021**, *37*, 17, 5339–5347. [[CrossRef](#)]

37. Moll, C.J.; Versluis, J.; Bakker, H.B. Direct observation of the orientation of urea molecules at charged interfaces. *J. Phys. Chem. Lett.* **2021**, *12*, 10823–10828. [[CrossRef](#)]
38. Xiong, B.; Zhao, P.; Hu, K.; Zhang, L.; Cheng, G. Dissolution of cellulose in aqueous NaOH/urea solution: Role of urea. *Cellulose* **2014**, *21*, 1183–1192. [[CrossRef](#)]
39. Heyda, J.; Okur, H.I.; Hladilkova, J.; Rembert, K.B.; Hunn, W.; Yang, T.; Dzubiella, J. Guanidinium can both cause and prevent the hydrophobic collapse of biomacromolecules. *J. Am. Chem. Soc.* **2017**, *139*, 863–870. [[CrossRef](#)]
40. Delepierre, G.; Vanderfleet, O.M.; Niinivaara, E.; Zakani, B.; Cranston, E.D. Benchmarking cellulose nanocrystals Part II: New industrially produced materials. *Langmuir* **2021**, *37*, 8393–8409. [[CrossRef](#)]
41. Bhattacharjee, S.J. In relation to the following article “DLS and zeta potential—What they are and what they are not?”. *Control. Release* **2016**, *235*, 337–351. [[CrossRef](#)]
42. Javadi, A.; Mucic, N.; Karbaschi, M.; Won, J.Y.; Fainerman, V.B.; Sharipova, A.; Aksenenko, E.V.; Kovalchuk, V.I.; Kovalchuk, N.M.; Makievski, A.; et al. Interfacial Dynamics Methods. In *Encyclopedia of Colloid and Interface Science*; Tadros, T., Ed.; Springer: Berlin/Heidelberg, Germany, 2013.
43. Loglio, G.; Pandolfini, P.; Miller, R.; Makievski, A.V.; Ravera, F.; Ferrari, M.; Liggieri, L. Drop and bubble shape analysis as tool for dilational rheology studies of interfacial layers. In *Novel Methods to Study Interfacial Layers*; Möbius, D., Miller, R., Eds.; Elsevier: Amsterdam, The Netherlands, 2001; pp. 439–483.
44. Ravera, F.; Ferrari, M.; Santini, E.; Liggieri, L. Influence of surface processes on the dilational visco-elasticity of surfactant solutions. *Adv. Colloid Interface Sci.* **2005**, *117*, 75–100. [[CrossRef](#)] [[PubMed](#)]
45. Firouzi, M.; Kovalchuk, V.I.; Loglio, G.; Miller, R. Salt effects on the dilational viscoelasticity of surfactant adsorption layers. *Curr. Opin. Colloid Interface Sci.* **2022**, *57*, 101538. [[CrossRef](#)]
46. Amani, P.; Karakashev, S.I.; Grozev, N.A.; Simeonova, S.S.; Miller, R.; Rudolph, V.; Firouzi, M. Effect of selected monovalent salts on surfactant stabilized foams. *Adv. Colloid Interface Sci.* **2021**, *295*, 102490. [[CrossRef](#)] [[PubMed](#)]
47. Briceño-Ahumada, Z.; Maldonado, A.; Impéror-Clerc, M.; Langevin, D. On the stability of foams made with surfactant bilayer phases. *Soft Matter* **2016**, *12*, 1459–1467. [[CrossRef](#)]
48. Lim, W.K.; Rösgen, J.; Englander, S.W. Urea, but not guanidinium, destabilizes proteins by forming hydrogen bonds to the peptide group. *Proc. Natl. Acad. Sci. USA* **2009**, *106*, 2595–2600. [[CrossRef](#)]
49. Tikhonov, M.M.; Akentiev, A.V.; Noskov, B.A. Influence of guanidine hydrochloride and urea on the dynamic surface properties of lysozyme solutions. *Mendeleev Commun.* **2015**, *25*, 288–289. [[CrossRef](#)]
50. Rullier, B.; Axelos, M.A.V.; Langevin, D.; Novales, B. β -Lactoglobulin aggregates in foam films: Effect of the concentration and size of the protein aggregate. *J. Colloid Interface Sci.* **2010**, *343*, 330–337. [[CrossRef](#)]

Article

The Influence of the Surface Chemistry of Cellulose Nanocrystals on Ethyl Lauroyl Arginate Foam Stability

Agnieszka Czakaj ^{1,*}, Emmanouil Chatzigiannakis ², Jan Vermant ³, Marcel Krzan ¹ and Piotr Warszyński ^{1,*}

¹ Jerzy Haber Institute of Catalysis and Surface Chemistry, Polish Academy of Sciences, ul. Niezapominajek 8, 30-239 Krakow, Poland

² Polymer Technology Group, Department of Mechanical Engineering, Eindhoven University of Technology, P.O. Box 513, 5600 MB Eindhoven, The Netherlands

³ Department of Materials, ETH Zürich, Vladimir-Prelog-Weg 5, 8093 Zürich, Switzerland

* Correspondence: agnieszka.czakaj@ikifp.edu.pl (A.C.); piotr.warszynski@ikifp.edu.pl (P.W.)

Abstract: Guanidine-based surfactant ethyl lauroyl arginate (LAE) and cellulose nanocrystals (CNCs) form complexes of enhanced surface activity when compared to pure surfactants. The LAE-CNC mixtures show enhanced foaming properties. The dynamic thin-film balance technique (DTFB) was used to study the morphology, drainage and rupture of LAE-CNC thin liquid films under constant driving pressure. A total of three concentrations of surfactant and the corresponding mixtures of LAE with sulfated (sCNC) and carboxylated (cCNC) cellulose nanocrystals were studied. The sCNC and cCNC suspension with LAE formed thin films, with stability increasing with surfactant concentration and with complex rheological properties. In the presence of LAE, the aggregation of CNC was observed. While the sCNC aggregates were preferentially present in the film volume with a small fraction at the surface, the cCNC aggregates, due to their higher hydrophobicity, were preferentially located at film interfaces, forming compact layers. The presence of both types of aggregates decreased the stability of the thin liquid film compared to the one for the LAE solution with the same concentration. The addition of CNC to LAE was critical for foam formation, and foam stability was in qualitative agreement with the thin films' lifetimes. The foam volume increased with the LAE concentration. However, there was an optimum surfactant concentration to achieve stable foam. In particular, the very resistant foam was obtained with cCNC suspensions that formed the interfaces with a complex structure and rheology. On the other hand, at high LAE concentrations, the aggregates of CNC may exhibit antifoaming properties

Keywords: foam stability; dynamic thin-film balance; cellulose nanocrystals; surface chemistry; surface tension; fluid film; surface dynamics; interfacial phenomena



Citation: Czakaj, A.; Chatzigiannakis, E.; Vermant, J.; Krzan, M.; Warszyński, P. The Influence of the Surface Chemistry of Cellulose Nanocrystals on Ethyl Lauroyl Arginate Foam Stability. *Polymers* **2022**, *14*, 5402. <https://doi.org/10.3390/polym14245402>

Academic Editor: José Ignacio Velasco

Received: 1 November 2022

Accepted: 5 December 2022

Published: 9 December 2022

Publisher's Note: MDPI stays neutral with regard to jurisdictional claims in published maps and institutional affiliations.



Copyright: © 2022 by the authors. Licensee MDPI, Basel, Switzerland. This article is an open access article distributed under the terms and conditions of the Creative Commons Attribution (CC BY) license (<https://creativecommons.org/licenses/by/4.0/>).

1. Introduction

Foamability and foam stability are interesting for many technological processes, including flotation, cleaning, cosmetic application and food processing. Immediately after its formation, foam undergoes various simultaneous and inter-related disruptive processes such as coarsening, drainage and coalescence. Foams with prolonged stability can be created from dispersions of surfactant with nanoparticles or even from surface active particles without surfactants [1]. Mixed systems allow us to obtain the desired technological properties with the reduced amount of surfactant, and thus, with lower costs and environmental impact. Foam can be treated as the ensemble of connected bubbles separated by thin liquid films of a continuous liquid phase [2]. Apart from the adsorption and desorption of surface-active species and their effect on surface tension, many other factors such as capillarity, hydrodynamic forces, interfacial rheology and intermolecular interactions play a role in thin liquid film stability. In particular, the film's critical thickness, at which its rupture is observed, increases with the applied pressure drop [3]. Minor differences in the balance of forces can result in thin films' lifetimes spanning over six orders of magnitude [3].

Recent progress in film dynamics has been facilitated by the development of the dynamic thin-film balance (DTFB) technique [4] with improved pressure and temperature control, which originated from the setup of Sheludko [5], and the single bubble with the interferometric technique for precise control of spatially resolved film thickness. In a modified version of the Sheludko cell, which consists of a microfabricated thin-film holder that resembles a bike wheel, the thin-film hole is connected radially to the external annulus by 24 channels. Therefore, larger disjoining pressures can be measured, the drainage is radial and symmetric, and the device is suitable for a small number of samples and reuses [4,6–11].

The generalised Stokes–Laplace–Reynolds equation describes the dynamic pressure balance that characterises the drainage of the thin liquid film [4]. The hydrodynamic pressure $P_H(h, r)$ is given by a local pressure balance:

$$P_c + \frac{2\sigma}{R} = P_H(h, r) + P_\infty - \Pi_d(h, r) + \frac{\sigma}{2r} \frac{\partial}{\partial r} \left(r \frac{\partial h}{\partial r} \right) \quad (1)$$

where P_c is the externally applied pressure across the film, which induces drainage, $2\sigma/R$ is the Laplace pressure due to curvature of the Plateau border (σ is the surface tension and R is the bike wheel hole's radius), and P_∞ is the pressure at the meniscus, $\Pi_d(h, r)$ is the disjoining pressure; the last term describes local Laplace contributions of curvature differences [4].

In general, the equilibrium properties, such as the disjoining pressure, do not suffice to explain the thinning and rupture dynamics, and hydrodynamics need to be studied using the DTFB. It can give complementary information to other experimental surface science techniques such as interfacial rheology. In particular, dynamic thin-film balance enables us to visualise surface flows and assess whether interfaces are stress-carrying (immobile) or stress-free (mobile), and hence provide insight into the effect of Marangoni stresses or surface rheology. Moreover, with the DTFB technique, one can visualise particles structuring in the thin film, the existence of the aggregates, nucleation of lipids and black film formation [4].

Ethyl lauroyl arginate is an arginine-based, biodegradable surfactant with strong surface activity. Combined with cellulose nanocrystals, it allows the formation of stable, environmentally friendly foams. In previous work, some of the present authors used the dynamic fluid interferometry/rising bubble technique. They observed significant immobilisation of the interface in thin films generated from solutions of ethyl lauroyl arginate (LAE) and cellulose nanocrystals (sCNCs) with sulfate hydrophilic groups [12]. A significant immobilisation of the interface in thin films was revealed. The drainage of an initially dimpled thin film of the mixture of surfactant with non-surface-active nanoparticles was significantly slower compared to the pure surfactant solution with the equivalent concentration. Within the narrow concentration range that was studied, film stability was found to depend on the surfactant/nanoparticle ratio. The intermediate surfactant concentration, mixed with CNCs and filtered, exhibited the highest coalescence time. The drainage of non-filtered LAE-CNC solution was even slower and proceeded by a dynamic reorganisation of large cellulose nanocrystal aggregates, which in other cases usually act as antifoam species. The LAE-CNC dispersions had high interfacial shear elasticity. Other researchers found a comparable value of interfacial shear elasticity of the same concentration (0.3% by weight) of CNCs in solutions where electrostatic repulsive interactions were screened by adding salt [13]. The possible effect of bulk viscosity in such concentrations of high-aspect-ratio CNCs cannot be excluded.

The CNCs are highly charged with a predominantly hydrophilic surface; thus, a hydrophobic modification is needed for their attachment to the air/water interface [14]. Undoubtedly, a CNC suspension without the addition of a surfactant does not foam. Thus, the hydrophobic modification of CNCs is standard practice. One such example is the hydrophobic modification of cellulose in the form of nanofibers and nanocrystals (length 300 nm) by adsorption of cationic octylamine, which enhances foam stability [15]. The

improved foam stability was attributed to the increased bulk viscoelastic properties and nanocellulose charge. Positively charged ethyl lauroyl arginate interacts electrostatically with negatively charged cellulose nanocrystals, modifies their surface properties and induces aggregation. With both hydrophobic modification and aggregation at play, it is hard to predict the surface tension of surfactant–nanoparticle mixtures. For example, didecyldimethyl ammonium bromide had lower surface activity in CNC suspensions than pure surfactant [16]. On the contrary, the surface activity of commercial LAE in the mixture with CNCs was prevalently higher than pure surfactant [12,13]. The rate of addition of a surfactant may change the aggregation path of nanoparticles; hence, it has consequences for the hydrodynamic diameter of the dispersion and its turbidity [12,13]. For the CNC suspensions and surfactant concentration $c \ll CMC$, the zeta potential of cellulose nanocrystals does not significantly change. For example, adding LAE at concentrations below 0.01 wt%, neither decreases the negative value of CNCs' zeta potential nor increases their hydrodynamic diameter [12,13].

The solution of ethyl lauroyl arginate usually contains other surface-active substances, impurities from synthesis and hydrolysis products that modify the kinetics and equilibrium surface tension of solutions. As described before [17], fresh LAE solution hydrolyses to $N\alpha$ -lauroyl-L-arginine (LAS) or dodecanoic acid, which may form the heterodimers LAE-dodecanoate anion or LAE-LAS. The surface activity of such mixed solutions is significantly changed, and the complexity of the surfactant's rheological response increases. Thus, in the mixture with cellulose nanocrystals, various surface-active compounds exist with different interactions with cellulose nanocrystals. Additionally, the base-catalysed hydrolysis of LAE induces a decrease in the solution pH that may influence the weakly charged groups at the surface of the cellulose nanoparticles.

In this work, thin-film balance drainage experiments coupled with micro-interferometric imaging were carried out under an applied constant pressure drop. The experiment was designed to simulate pressure changes accompanying bubbles prior to coalescence and compare cellulose nanocrystals' effect with different surface hydrophilic groups with respect to foaming properties. Different particles were chosen because the aggregation ratio varies the rheological response and surface flow to a great extent [18–20]. Our work aims to fill a gap in nanocellulose research concerning the effect of CNCs' surface chemistry on their application potential. Although researchers point out that cCNCs find applicability in many technologies, their interfacial properties have not been studied, specifically for foaming. Moreover, to the best of our knowledge, the thin-film balance technique has not been used so far to study the effect of surfactants and cellulose nanocrystals on thin film behaviour.

Analytical grade ethyl lauroyl arginate and two types of commercially available cellulose nanocrystals were used: sCNCs with sulfate ester groups and cCNCs with carboxyl groups, both having comparable size and surface charge [12,13]. Industrially produced CNCs compare well with CNCs extracted at a bench scale, with all material containing highly crystalline, high-aspect-ratio cellulose nanocrystals [21–25]. Sulfate-based cellulose nanocrystals derived from cellulose by sulfuric acid hydrolysis are widely available. Carboxylic cellulose nanocrystals are manufactured with the technology of H_2O_2 oxidation [21,22]. So far, they have not been well characterised yet for their interfacial properties. Both sulfate ester and carboxylic CNCs are particles with faces of different hydrophilicity, and tuning their exposure to water might be essential for foaming properties [12,13,26]. By combining the TFB technique and interfacial properties measurements, we show how the complex interactions between the surfactant and the CNCs affect the surface pressure, disjoining pressure, surface rheology and adsorption dynamics in mixed LAE-CNC systems.

2. Materials and Methods

Ethyl lauroyl arginate, United States Pharmacopeia analytical standard (declared purity of 99%), was purchased from Merck. The stock solution was prepared in cold deionised water (4 °C, 20 MΩ cm) and then diluted to the appropriate concentration. Stock solution and dilutions were used within one day if not described otherwise. Cellulose nanocrystals with sulfate half ester groups were purchased from Celluforce (diameter 5 nm, length 100 nm, sulfate content 0.25 mmol/g). Cellulose nanocrystals with carboxyl groups were purchased from Anomera (zeta potential range −40 to −50 mV, diameter 5–10 nm, length 150–200 nm, carboxyl content 0.12–0.20 mmol/g). Cellulose nanocrystals were dispersed carefully in water to achieve a concentration of 0.6% by weight and were subsequently sonicated. The CNC solution was added dropwise to the surfactant solution under constant stirring to achieve a final concentration of 0.3 wt% cellulose nanocrystals in all solutions.

2.1. Surface Activity and Dilation Rheology

The surface tension of samples was measured immediately after surfactant solution or dispersion preparation using the pendant drop technique with a Sinterface PAT-1M tensiometer (Sinterface Technologies e.K., Berlin, Germany). A drop of solution (11 μL) was created from a 2 mm diameter capillary and kept in the thermostated chamber for up to 2000 s. The drop profile was monitored and fitted with the Young–Laplace equation to calculate the surface tension until it did not change during the consecutive measurements. Then, the value of the equilibrium surface tension was recorded.

For the dilational rheological measurements, drop-size oscillations were applied after reaching the surface tension equilibrium by imposing drop volume (area) changes of less than 10% of the volume. Fourier transform of the surface tension variations was calculated, and an apparent surface dilational modulus was determined as a complex number.

2.2. Particle Characterisation

The size of CNC nanoparticles was measured by dynamic light scattering with the Malvern Nano ZS instrument (Malvern, Worcestershire, UK). Each measurement was repeated three times. The zeta potential of all LAE-CNC suspensions was measured by laser Doppler velocimetry with the Malvern Nano ZS instrument. Each measurement was repeated three times. No viscosity correction was applied. The average error (standard deviation) was 5 mV maximum.

2.3. Thin-Film Balance

The setup of the TFB, as illustrated in Figure 1, and the experimental procedure were described previously by Chatzigiannakis et al. [4]. It consists of an upright fixed-stage microscope, a pressure control system, an in-house fabricated anodised aluminium pressure chamber, in which the bike wheel microfluidic device was placed. The bike wheel chip was manufactured by photolithography. It consists of a diamond-drilled hole with a diameter of 1 mm and a thickness of 400 μm and 24 channels—the spokes of the bike wheel (width of 45 μm and depth of 20 μm) connected to the hole, all leading to a circular channel of larger dimensions. The chip was glued onto a titanium holder using two-component epoxy. The pressure was controlled by a piezoelectric pressure control system with a resolution of 1 Pa and a maximum pressure of 20 kPa. It was connected to the pressure chamber by rigid PTFE tubing with an inner diameter of 0.1 mm. The film was visualised with a Nikon Eclipse FN1 fixed-stage upright microscope (to minimise vibrations) and a 10x long working distance objective with a mounted Hamamatsu ORCA-Flash4.0 CMOS camera (Hamamatsu Photonics Europe GmbH, Herrsching, Germany). A monochromatic wavelength of 508 nm was used for the reflection. Its digitalised image was converted to thickness according to the Sheludko equation [4,5].

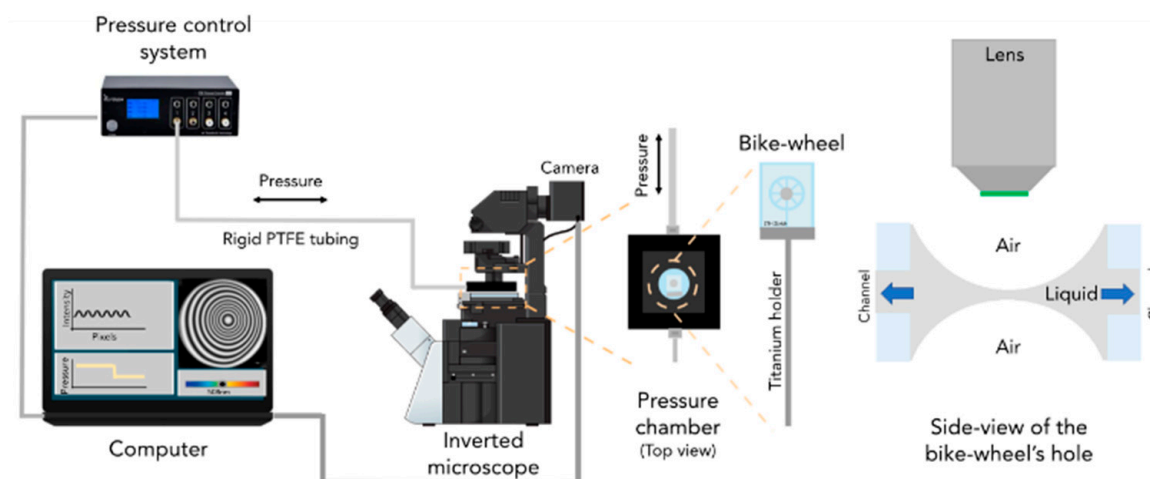


Figure 1. Scheme of the thin-film balance setup used in the film imaging experiments. Reprinted from [4].

The experimental procedure consisted of the following steps. Initially, the thick fluid film (micron-size thickness) was created in the orifice of the thin-film balance. By adjusting the pressure in steps of 1 Pa, the equilibrium pressure P_{eq} was determined and the film was visible when the first interference fringes appeared at the thickness of a few μm . P_{eq} is the sum of all the contributions in the static thick film (cf. Equation (1)). After that, the pressure inside the film was increased with the applied pressure step of 100 Pa. The film started to drain. Buildup of hydrodynamic pressure caused the expansion of the film. A sequence of images was collected by the camera with a maximum 10 ms temporal resolution. The measured coalescence time (film lifetime) corresponded to the time interval between the onset of film expansion and the rupture of the film.

2.4. Foaming

The double-syringe method was applied for foaming experiments. Foams were generated by manually pushing 15 mL LAE-CNC solution and 30 mL of air from one medical-grade syringe to the other syringe connected to the former through a narrow tube [12,13,27–29]. After ten cycles, syringes were left in the vertical position. Initial foam volume was ascribed as the volume after 1 min from the foam formation.

3. Results and Discussion

3.1. Suspension Characterisation

The surface tension of analytical standard LAE and the suspension of nanoparticles with LAE are given in Table 1.

Table 1. The surface tension of analytical standard, pure and nanoparticle-dispersed ethyl lauroyl arginate. Contents of CNCs, 0.3 wt%.

LAE Concentration [mM]	Surface Tension [mN/m]		
	LAE	LAE-cCNC	LAE-sCNC
0.075	60 ± 0.5	55 ± 1	46 ± 1
0.15	51 ± 0.5	38 ± 1	43 ± 1
0.35	32 ± 0.5	33 ± 1	36 ± 1

Depending on LAE concentration, the equilibrium surface tension of the suspension is either lower, similar or higher than the surface tension of the surfactant solutions. At low LAE concentrations, the nanoparticles are partly hydrophobised, and the synergistic effect of LAE and CNC on surface activity was observed. This effect is stronger for the cCNC

suspension. At high LAE concentrations, the surface activity is surfactant-dominated, but some surfactant is consumed by adsorption at nanoparticles. All studied LAE concentrations were much smaller than critical micelle concentration CMC, which for the surfactant analytical standard surfactant was 1.0 mM [12,13,17].

The hydrodynamic diameter and zeta potential of the cellulose nanoparticle suspension, as well as a suspension with LAE surfactant, are given in Table 2.

Table 2. Hydrodynamic diameter and zeta potential of pure cellulose nanocrystals and those in the mixtures with ethyl lauroyl arginate. Contents of CNCs, 0.3 wt%.

	Size [nm] (PDI)	Zeta Potential [mV]	Size [nm] (PDI)	Zeta Potential [mV]
	cCNC		sCNC	
Pure nanocrystals	77 (0.44)	-38 ± 5	96 (0.63)	-44 ± 5
CNC-LAE 0.075 mM	94 (0.40)	-38 ± 5	105 (0.51)	-47 ± 5
CNC-LAE 0.15 mM	75 (0.42)	-33 ± 5	77 (0.52)	-50 ± 5
CNC-LAE 0.35 mM	120 (0.40)	-29.5 ± 5	187 (0.82)	-45 ± 5

The size of cCNCs seems to be systematically smaller and less monodisperse than sCNCs, while their zeta potential is less negative, significantly decreasing with the addition of LAE. That could be the result of decreasing the negative charge of cCNCs by LAE adsorption; however, that effect seems to be absent for the sCNC suspension. On the other hand, it may be due to a partial protonation of surface carboxyl groups as the pH of the suspension decreases due to the hydrolysis of LAE.

The concentration of CNCs (0.3 wt%) was selected to minimise the influence of the bulk viscosity on the interfacial properties of the suspensions and, possibly, on the foam stability. It was shown that, below the concentration of 1%, CNC viscosity is only slightly modified, and suspensions do not show shear-thinning behaviour [26]. The viscosity for the sCNC and LAE-sCNC suspensions in the studied concentration range was determined previously by some of the authors [12,13]. The measured viscosity of 1.3 mPas for sCNC CelluForce, in agreement with the literature [21–26,30], was the same for cellulose nanocrystals and LAE-sCNC (at 0.23 mM LAE). Moreover, the estimated rate of the film thinning was the same for 0.35 mM and 1 mM of LAE and 0.3 wt% of sCNCs. Knowing the rate of the thin-film thinning is directly dependent on viscosity, we concluded that minor viscosity differences were not relevant for LAE-CNC film lifetimes and foam stability. A small viscosity increase to 1.6 mPa s was observed for 0.35 mM LAE and sCNCs, which was attributed to the aggregation confirmed by DLS measurements [12,13]. Therefore, that concentration was chosen as the maximum concentration for further experiments. We assumed that, up to that concentration, a similar viscosity for cCNCs was expected. As was demonstrated by Delepierre et al. [30], the viscosity of 2wt% cCNCs, which was a concentration over three times higher than in our case, was only 1.6 mPa s (10 s^{-1}).

3.2. Thin-Film Balance

The films of the pure LAE surfactant at a concentration of 0.075 M drained fast down to an equilibrium thickness of approximately 15 nm. Drainage occurred in 5–10 s, depending on surfactant concentration, and proceeded symmetrically. The short drainage times are expected for these concentrations in surfactant films [31,32] and are indicative of the relatively small magnitude of Marangoni stresses opposing the bulk outflow of the liquid. Drainage stopped when the equilibrium thickness was reached. This thickness resulted from the repulsive electrostatic interactions counteracting the sum of the applied pressure and the attractive van der Waals forces.

The film with 0.075 mM LAE was already unstable at a 100 Pa pressure change, while those with 0.15 mM LAE and 0.35 mM LAE were stable at this initially applied

pressure. Images of films at the end of drainage after the applied 100 Pa pressure step are presented in Figure 2. Additional pressure ramps for the assessment of the critical pressure for rupture revealed that film with 0.15 mM LAE broke at the applied pressure of 200 Pa, whereas 0.35 mM LAE broke at 1250 Pa. That can be attributed to the increase in the electrostatic disjoining pressure. With increasing LAE concentration, its adsorption at water/air interface [33] and, consequently, the interfacial charge increases. The same phenomenon was observed for the solution of another cationic surfactant, tetradecyl trimethyl ammonium bromide [33].

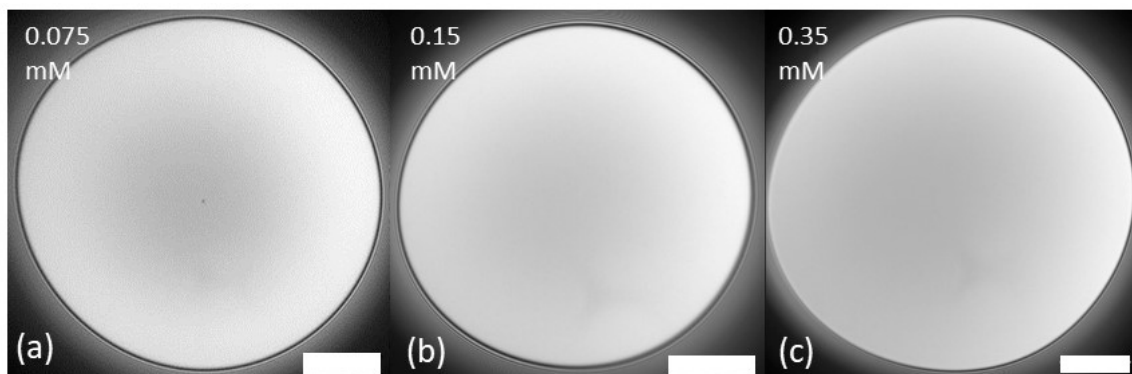


Figure 2. Morphology of LAE surfactant films after the pressure step of 100 Pa at the end of the drainage. (a) LAE 0.075 mM (the film was unstable, the image was taken before the rupture after c.a. 40 s drainage); (b) LAE 0.15 mM; (c) LAE 0.35 mM. Scale bar 100 μm .

In pure surfactant solutions, below critical micelle concentration that form common black films of almost constant thickness morphology, the differences are usually not observed. However, for the lowest concentration, a small black spot in the middle of the film can be seen. The small spot is attributed to limited surfactant spreading at low concentrations [34].

The morphology of mixed LAE-CNC thin films was more complex and, as illustrated in Figures 3 and 4, dependent on the ratio of surfactant/particle concentration. The morphology and drainage of films depended on the type of CNC: sulfated or carboxylated. Drainage is presented as videos in the Supplementary Materials: Video S1: LAE 0.075 mM, Video S2: LAE 0.15 mM, Video S3: LAE 0.35 mM, Video S4: LAE 0.075 mM sCNC, Video S5: LAE 0.15 mM sCNC, Video S6: LAE 0.35 mM SCNC, Video S7: LAE 0.075 mM cCNC, Video S8: LAE 0.15 mM cCNC, Video S9: LAE 0.35 mM cCNC.

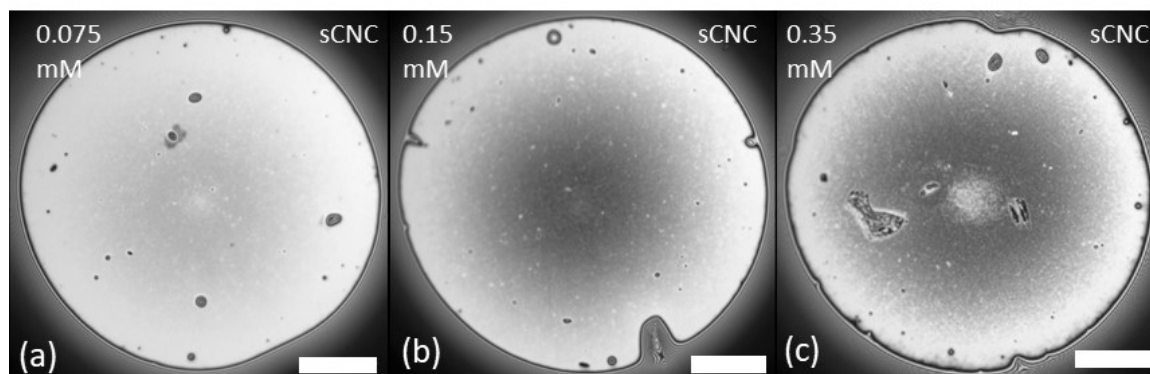


Figure 3. Morphology of LAE-sCNC films at the end of drainage after the pressure step of 100 Pa. (a) CNC-LAE 0.075 mM; (b) CNC-LAE 0.15 mM; (c) CNC-LAE 0.35 mM. Cellulose nanocrystal concentration, 0.3 wt%. Scale bar is 100 μm .

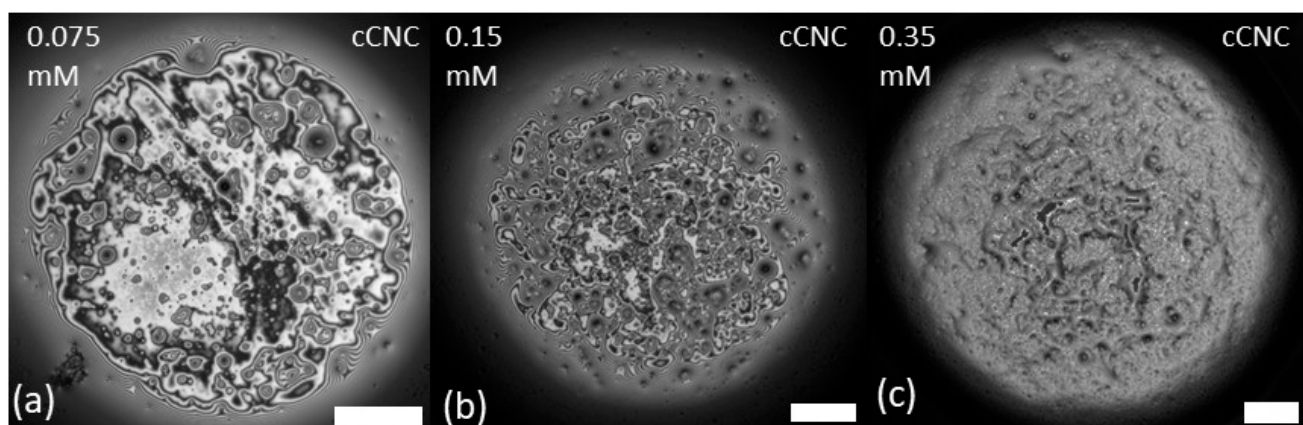


Figure 4. Morphology of LAE-cCNC films after the pressure step of 100 Pa at the end of the drainage. (a) CNC-LAE 0.075 mM; (b) CNC-LAE 0.15 mM; (c) CNC-LAE 0.35 mM. Cellulose nanocrystal concentration, 0.3 wt%. Scale bar is 100 μm .

As illustrated in Figure 3, all LAE-sCNC films at the end of drainage after the pressure step of 100 Pa were stable and relatively uniform, with most nanoparticles in the film volume and some nanoparticle aggregates at the interface. The film with sCNC-LAE 0.35 mM reached a steady state, and after 10 min, an additional 50 Pa pressure jump was applied. That resulted in the film breaking. After reforming the film with a new portion of the suspension, its morphology seemed to be uniform, with a small dimple (cf. Figure 5a). The coalescence time in a thin film for the medium concentration of LAE correlates well with results previously obtained for the moving bubble (DFI method) [12].

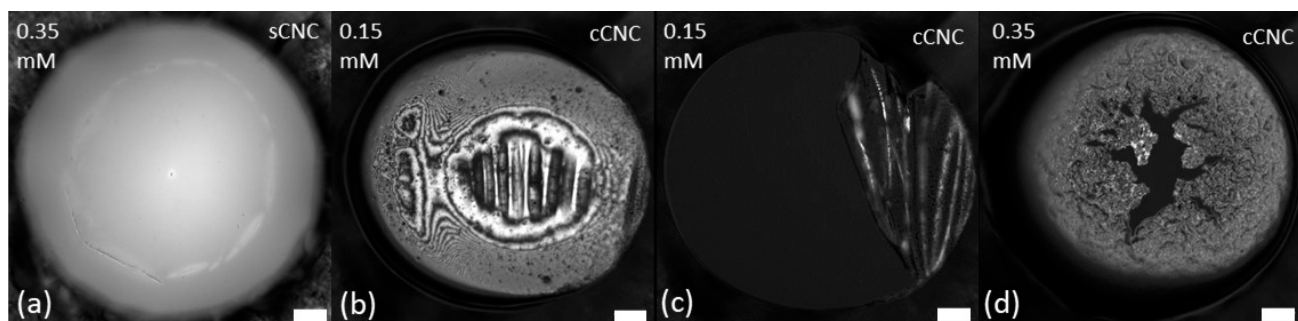


Figure 5. Morphology of LAE-cCNC films after film reforming. Complex interactions of LAE-sCNC (a), cCNC-LAE 0.15 mM while reforming the film after rupture (b,c) and cCNC-LAE 0.35 mM (d). Scale bar 100 μm .

In contrast, as illustrated in Figure 4, the LAE-cCNC films were populated by larger cCNC aggregates for all surfactant concentrations. They seem to have the tendency to occupy the interface and the coverage increased with surfactant concentration. Film drainage occurred at regions where no aggregates were present, and its rupture was preceded by the formation of a Newton black film (regions with a thickness of approximately 10 nm), with the thin regions displacing the adsorbed particles. Such an effect hints that excess surfactant might compete for the surface, destabilising the CNC network.

When the film was reformed after rupturing, we observed the formation of a thick rigid interface formed with LAE-cCNC aggregates. The applied pressure change resulted in the wrinkling of the interfacial layer and, finally, the film's rupture (cf. Figure 5b,c). For cCNC-LAE 0.35 mM, the thin film was much thicker, the structure less uniform, and the rupture proceeded with a surfactant black film displacing the cCNC-rich interface rather than wrinkling and folding (Figure 5d).

The observed differences between the film behaviour of sCNC and cCNC suspensions can originate from the more efficient hydrophobisation of cCNCs by LAE and their flow-induced aggregation during the film formation. Besides the electrostatic interaction, the guanidine group of LAE can form a bidentate hydrogen bond with the carboxyl surface group of cCNCs that contributes to enhanced hydrophobisation.

Film lifetime (coalescence time), which includes both drainage and rupture time, increased systematically with surfactant concentration without and for both particle types, as presented in Figure 6. As discussed above, the effect of higher viscosity can be excluded in the CNC concentration used in our experiments. The effect of the bulk viscosity for polymer solutions on coalescence time was characterised with dynamic thin-film balance, including the same pressure step of 100 Pa, as in this experiment [7]. The drainage time increased linearly with viscosity in agreement with the Stokes–Laplace–Reynolds equation for polymer solutions of polyisobutylene. The difference in coalescence time for solutions with viscosities of 3.5 mPa s and 7.5 mPa s was equal to 40 s. It cannot be expected that viscosity differences not exceeding 0.5 mPa s for LAE-CNC solutions (viscosities between 1.3–1.6 mPa s) can result in coalescence time differences reaching 50 s. The film coalescence time exceeded 600 s for LAE concentrations of 0.15 mM and 0.35 mM. The film lifetime of the suspension of CNC with LAE was, in general, shorter than that of the surfactant solution with the same concentration. That means that the presence of aggregates, either in the film volume (sCNCs) or at its surface (cCNCs), leads to its destabilisation. That can be explained by the antifoam action of large aggregates, which seems to be in agreement with our previous findings for the sCNCs and industrial-grade LAE [12,13]. Alternatively, it can be explained by the decrease in the effective LAE concentration by complexation with CNCs and thus the decrease in the electrostatic disjoining pressure. On the other hand, the sCNC-LAE 0.35 mM film was very stable up to high pressure, which may result from the formation of a rigid, solid-like interface.

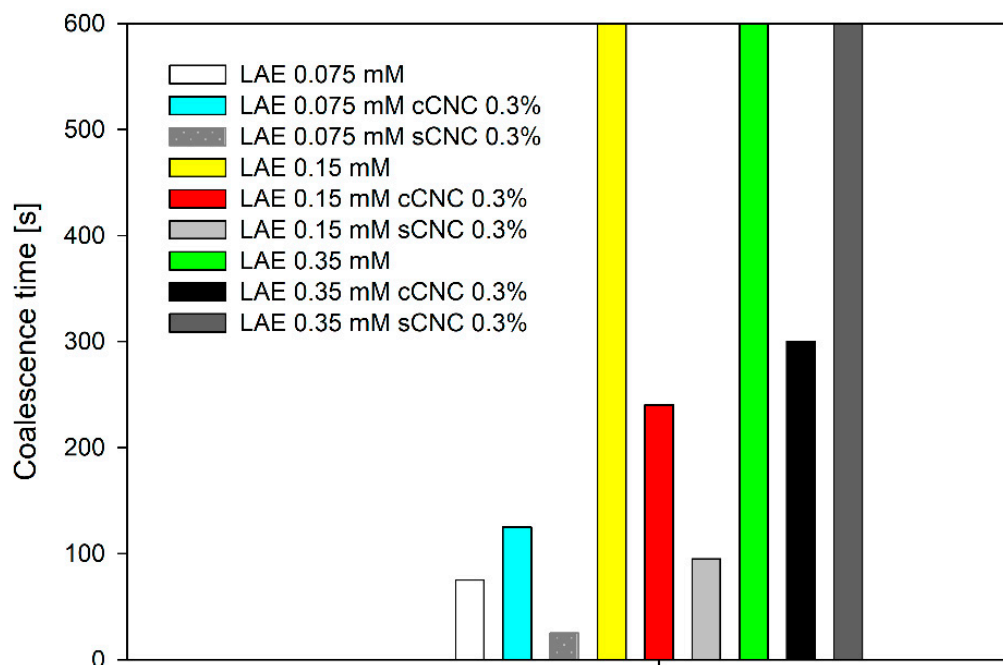


Figure 6. The thin films' lifetime after equilibration and the pressure step of 100 Pa. For pure LAE, 0.15 mM and 0.35 mM LAE and 0.35 mM LAE and sCNC, film lifetime exceeded 600 s.

3.3. Interfacial Rheology

The apparent elastic modulus in the mixture with cCNCs did not differ significantly from the values obtained for pure surfactant [12,13], and the apparent loss modulus was almost invariant to particle addition and concentration, as is illustrated in Figure 7. That

indicates that the transfer of surfactant/nanoparticles is much faster than the drop oscillations. On the contrary, the apparent elastic modulus for sCNCs was almost three times higher than for cCNCs. In contrast, the apparent loss moduli for sCNCs decreased significantly with oscillation frequency, as shown in Figure 8. A high elastic modulus and the apparent decrease in the loss modulus are typically observed for rheological complex interfaces due to shear effects. These results, with high apparent elasticity for all LAE concentrations, seem to contradict the ones obtained with the thin-film balance technique, where LAE-CNC films were unstable for 0.075 mM LAE; however, one needs to consider different geometry and flow patterns that can favour nanoparticle aggregation in the thin fluid film. Furthermore, for rheologically active interfaces with cellulose nanocrystals, the drop shape might show deviations from the Young–Laplace equation [35,36]. Thus, the results of the pendant drop oscillations experiment, suitable for the determination of surfactant transport effects, cannot explain the complexity of the LAE-CNC interface and does not reflect the rheological response at the complex interface.

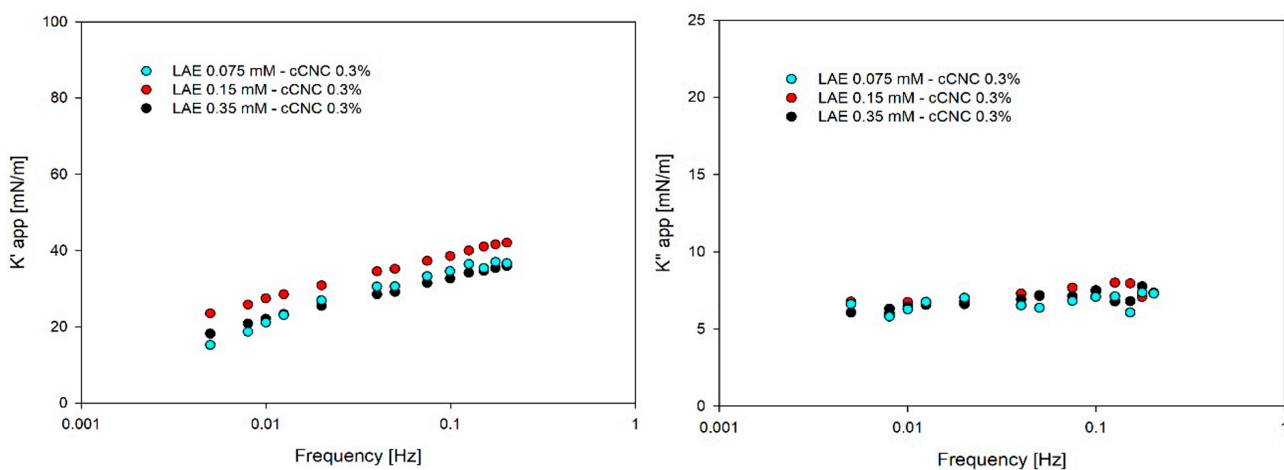


Figure 7. Apparent elastic (K') and loss (K'') moduli for cCNC suspensions with various concentrations of LAE (0.075 mM, 0.15 mM and 0.35 mM).

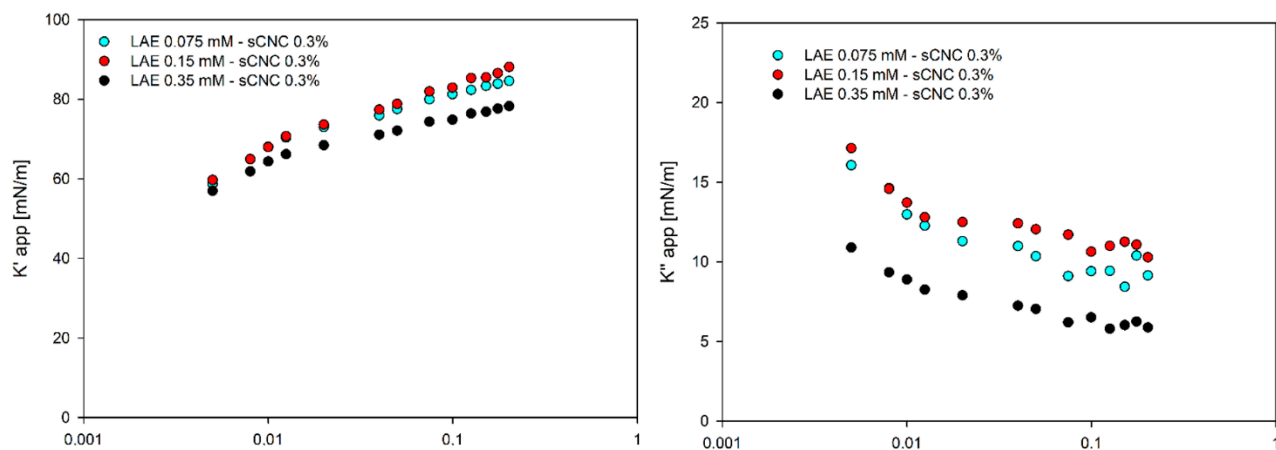


Figure 8. Apparent elastic (K') and loss (K'') moduli for sCNC suspensions with various concentrations of LAE (0.075 mM, 0.15 mM and 0.35 mM).

3.4. Foaming

The results concerning the initial foam volume and foam half-life for suspensions of cellulose nanocrystals with LAE are presented in Figures 9 and 10. For the selected LAE concentrations of 0.075 mM, 0.15 mM and 0.35 mM, it was impossible to produce stable foams with the double-syringe method. Apparently, the concentration of surfactant was too small to stabilise the foam, with a significant coarsening effect destabilising submillimeter bubbles. Mikhailovsakaya et al. [37] showed that the stability of thin films could be correlated directly if we study foam films at the same capillary number and limit coarsening effect. Relatively stable thin film obtained for 0.15 mM and 0.35 mM LAE concentrations in the thin-film balance experiment is only the estimate of the macroscopic system with the evolution of bubble size, non-uniform surface stresses and the time-dependent aggregation of nanoparticles.

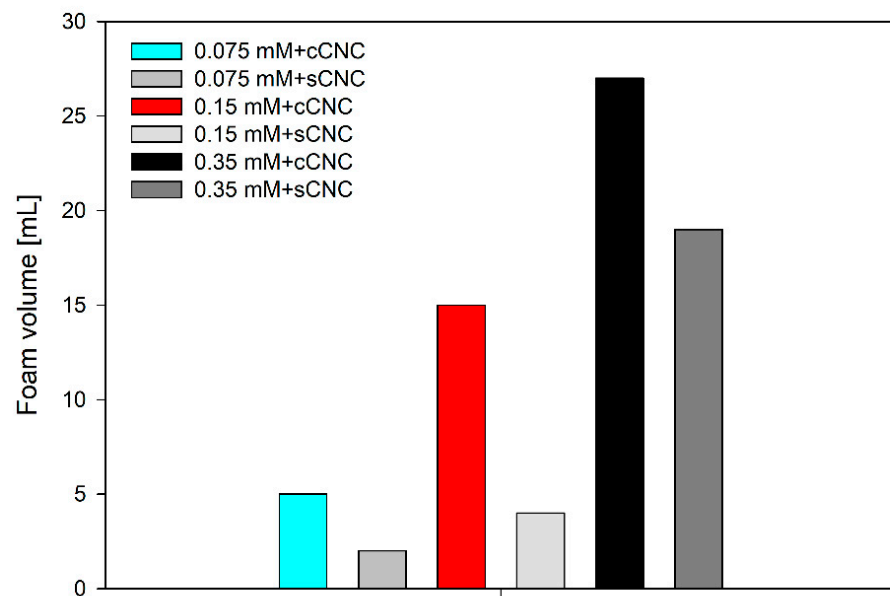


Figure 9. Initial foam volume obtained from 15 mL of LAE-cCNC or sCNC dispersed with double-syringe method. Foam volume was recorded 1 min after the foaming cycle.

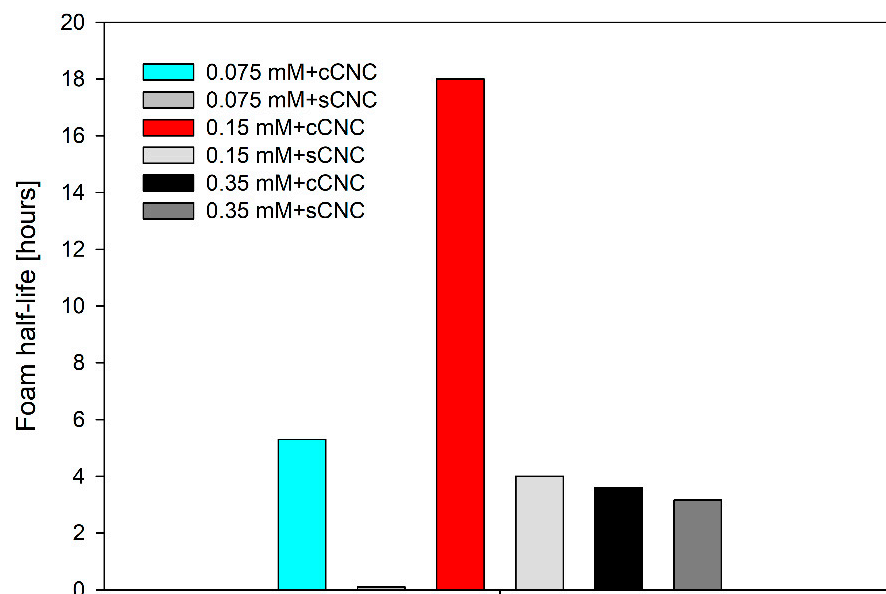


Figure 10. The half-life of foams formed in the CNC-LAE suspensions with the double-syringe method.

In the suspension of cellulose nanocrystals with ethyl lauroyl arginate, the foamability was directly correlated to surfactant concentration. The same trend was observed in the thin films' lifetime; however, the initial foam volume was c.a. two times higher for cCNCs than for sCNCs.

Assuming the same volume of air injected into the solution, foamability differences can be explained by the higher hydrophobicity of cCNCs. In particle-stabilised foams, foamability depends on the number of particles, the size of aggregates and their hydrophobicity [38]. Interestingly, the polydispersity of cCNC solution is lower than sCNCs, but their interfacial aggregation is much higher, as seen from thin-film balance experiments. The half-life of foams formed in the CNC-LAE suspensions with the double-syringe method is illustrated in Figure 10. The optimal concentration of LAE (0.15 mM) seems to exist for both types of cellulose nanocrystals. Moreover, the lifetime of foam generated in the cCNC suspension was much longer than in the sCNC suspension. In particular, the highly resistant foam could be observed for the suspension of cCNCs and 0.15 mM LAE. That can be explained by the formation of a compact layer of LAE-cCNC aggregates that prevents bubble coarsening and coalescence. Contrary to the thin films' measurements, where the film lifetime was increased with LAE concentration, the highest foam stability was observed for 0.15 mM LAE for both types of cellulose nanocrystals. This may result from the antifoaming action of larger aggregates that induce premature film rupture [39].

4. Conclusions

The suspensions of cellulose nanocrystals (CNCs) with ethyl lauroyl arginate (LAE) have superior foaming properties compared to the counterparts with only individual components, due to the synergistic action at the liquid film interfaces. It is, however, known that the interfacial properties of the suspensions depend on the type of chemical functionality at the surface of cellulose nanocrystals. In present work, the interfacial behaviour of carboxylated cellulose nanocrystals (cCNCs) have been compared with sulfated cellulose nanocrystals (sCNCs) in the presence of LAE. The carboxylated ones (cCNCs) seemed more prone to hydrophobisation with LAE at a concentration much below critical micelle concentration CMC, presumably due to the formation of a bidentate hydrogen bond between the carboxyl groups of cCNCs and guanidine groups of LAE [40]. The drainage experiments in the thin-film balance could exemplify differences between sCNC and cCNC dispersions in the thin films, as it allows direct visualisation of the tendency for particle aggregation and the presence or absence of interfacial flow. The sCNC and cCNC suspensions with LAE formed thin films, with stability increasing with surfactant concentration and with complex rheological properties. While the sCNC aggregates were preferentially present in the film volume with a small fraction at the surface, the cCNC aggregates, due to higher hydrophobicity, were preferentially located at film interfaces, forming compact layers. They also had the tendency to undergo flow-induced aggregation. The presence of both types of aggregates decreased thin liquid film stability compared to the one for the LAE solution with the same concentration.

The LAE solution at concentrations well below CNCs did not foam, and the presence of CNCs in the suspension was critical for its formation. The results of foamability and foam stability are in qualitative agreement with the ones from the thin-film balance experiments. The foam volume increased with the LAE concentration. However, there was an optimum surfactant concentration to achieve a stable foam. In particular, the very resistant foam could be obtained with cCNCs that formed, as the thin-film balance experiments demonstrated, the interfaces with a complex structure and rheology. On the other hand, at high LAE concentrations, the aggregates of CNCs might show antifoaming properties.

Our results indicate that combining the CNC suspension characterisation, thin-film balance analysis and foaming measurements allows the optimisation of LAE-CNC formulations and the determination of the effects affecting foam stability in the complex surfactant/nanoparticle systems.

Supplementary Materials: The following supporting information can be downloaded at: <https://www.mdpi.com/article/10.3390/polym14245402/s1>, Video S1: LAE 0.075 mM, Video S2: LAE 0.15 mM, Video S3: LAE 0.35 mM, Video S4: LAE 0.075 mM sCNC, Video S5: LAE 0.15 mM sCNC, Video S6: LAE 0.35 mM sCNC, Video S7: LAE 0.075 mM cCNC, Video S8: LAE 0.15 mM cCNC, Video S9: LAE 0.35 mM cCNC.

Author Contributions: Conceptualisation, A.C., E.C., J.V., P.W., M.K.; methodology, E.C., A.C.; software, E.C.; validation, J.V., P.W. and M.K.; formal analysis, J.V., P.W., M.K.; investigation, E.C., A.C.; resources, J.V., P.W., M.K.; data curation, E.C., A.C.; writing—original draft preparation, A.C.; writing—review and editing, E.C., M.K., P.W., J.V.; visualisation, E.C., A.C.; supervision, J.V., M.K., P.W.; project administration, J.V., M.K., P.W.; funding acquisition, A.C., J.V., M.K., P.W. All authors have read and agreed to the published version of the manuscript.

Funding: This project received funding from the European Union’s Horizon 2020 research and innovation programme under grant agreement No 731019 (EUSMI). This research was also funded by the National Science Centre of Poland (grants number 2016/21/B/ST8/02107 and 2022/45/B/ST8/02058) and a statutory subsidy for the Jerzy Haber Institute of Catalysis and Surface Chemistry PAS. A.C. has been partly supported by EU Project POWR.03.02.00-00-I004/16.

Institutional Review Board Statement: Not applicable.

Data Availability Statement: The data presented in this study are openly available from the authors upon reasonable request.

Acknowledgments: Figure 1 was reproduced from ref. [4] with permission from The Royal Society of Chemistry.

Conflicts of Interest: The authors declare no conflict of interest. The funders had no role in the design of the study; in the collection, analyses, or interpretation of data; in the writing of the manuscript, or in the decision to publish the results.

References

1. Binks, B.P.; Campbell, S.; Mashinchi, S.; Piatko, M.P. Dispersion behavior and aqueous foams in mixtures of a vesicle-forming surfactant and edible nanoparticles. *Langmuir* **2015**, *31*, 2967–2978. [\[CrossRef\]](#)
2. Stocco, A.; Rio, E.; Binks, B.P.; Langevin, D. Aqueous foams stabilised solely by particles. *Soft Matter* **2011**, *7*, 1260–1267. [\[CrossRef\]](#)
3. Stubenrauch, C.; von Klitzing, R. Disjoining pressure in thin liquid foam and emulsion films—New concepts and perspectives. *J. Phys. Condens. Matter* **2003**, *15*, 1197–1232. [\[CrossRef\]](#)
4. Chatziannakis, E.; Veenstra, P.; Bosch, D.; Vermant, J. Mimicking coalescence using a pressure-controlled dynamic thin balance. *Soft Matter* **2020**, *16*, 9410–9422. [\[CrossRef\]](#)
5. Sheludko, A. Thin liquid films. *Adv. Colloid Interface Sci.* **1967**, *1*, 391–464. [\[CrossRef\]](#)
6. Chatziannakis, E.; Jaensson, N.; Vermant, J. Thin liquid films: Where hydrodynamics, capillarity, surface stresses and intermolecular forces meet. *Curr. Opin. Colloid Interface Sci.* **2021**, *53*, 101441. [\[CrossRef\]](#)
7. Chatziannakis, E.; Vermant, J. Dynamic stabilisation during the drainage of thin film polymer solutions. *Soft Matter* **2021**, *17*, 4790–4803. [\[CrossRef\]](#)
8. Bergeron, V. Disjoining pressures and film stability of alkyltrimethylammonium bromide foam films. *Langmuir* **1997**, *13*, 3474–3482. [\[CrossRef\]](#)
9. Bergeron, V.; Radke, C.J. Disjoining pressure and stratification in asymmetric thin-liquid films. *Colloid Polym. Sci.* **1995**, *273*, 165–174. [\[CrossRef\]](#)
10. Cascao-Pereira, L.G.; Johansson, C.; Blanch, H.W.; Radke, C.J. A bike-wheel microcell for measurement of thin-film forces. *Colloids Surf. A Physicochem. Eng. Asp.* **2001**, *186*, 103–111. [\[CrossRef\]](#)
11. Kannan, A.; Shieh, I.C.; Leiske, D.L.; Fuller, G.G. Monoclonal antibody interfaces: Dilatation mechanics and bubble coalescence. *Langmuir* **2018**, *34*, 630–638. [\[CrossRef\]](#) [\[PubMed\]](#)
12. Czakaj, A.; Kannan, A.; Wiśniewska, A.; Grześ, G.; Krzan, M.; Warszyński, P.; Fuller, G.G. Viscoelastic interfaces comprising of cellulose nanocrystals and lauroyl ethyl arginate for enhanced foam stability. *Soft Matter* **2020**, *16*, 3981–3990. [\[CrossRef\]](#) [\[PubMed\]](#)
13. Czakaj, A.; Krzan, M.; Warszyński, P. The effect of electrolytes and urea on the ethyl lauroyl arginate and cellulose nanocrystals foam stability. *Appl. Sci.* **2022**, *12*, 2797. [\[CrossRef\]](#)
14. Bertsch, P.; Fischer, P. Adsorption and interfacial structure of nanocelluloses at fluid interfaces. *Adv. Colloid Interface Sci.* **2020**, *276*, 102089. [\[CrossRef\]](#) [\[PubMed\]](#)
15. Cervin, N.T.; Johansson, E.; Benjamins, J.-W.; Wågberg, L. Mechanisms behind the stabilising action of cellulose nano-fibrils in wet-stable cellulose foams. *Biomacromolecules* **2015**, *16*, 822–831. [\[CrossRef\]](#) [\[PubMed\]](#)

16. Hu, Z.; Ballinger, S.; Pelton, R.; Cranston, E.D. Surfactant-enhanced cellulose nanocrystal Pickering emulsions. *J. Colloid Interface Sci.* **2015**, *439*, 139–148. [[CrossRef](#)] [[PubMed](#)]
17. Czakaj, A.; Jarek, E.; Krzan, M.; Warszyński, P. Ethyl lauroyl arginate, an inherently multicomponent surfactant system. *Molecules* **2021**, *26*, 5894. [[CrossRef](#)]
18. Bai, L.; Xiang, W.; Huan, S.; Rojas, O.J. Formulation and stabilisation of concentrated edible oil-in-water emulsions based on electrostatic complexes of a food-grade cationic surfactant (ethyl lauroylarginate) and cellulose nanocrystals. *Biomacromolecules* **2018**, *19*, 1674–1685. [[CrossRef](#)]
19. Holthoff, H.; Egelhaaf, S.U.; Borkovec, B.; Schurtenberger, P.; Sticher, H. Coagulation rate measurements of colloidal particles by simultaneous static and dynamic light scattering. *Langmuir* **1996**, *12*, 5541–5549. [[CrossRef](#)]
20. Rullier, B.; Axelos, M.A.V.; Langevin, D.; Novales, B. β -Lactoglobulin aggregates in foam films: Effect of the concentration and size of the protein aggregates. *J. Colloid Interface Sci.* **2010**, *343*, 330–337. [[CrossRef](#)]
21. Lam, E.; Hemraz, U.D. Preparation and surface functionalization of carboxylated cellulose nanocrystals. *Nanomaterials* **2021**, *11*, 1641. [[CrossRef](#)] [[PubMed](#)]
22. Teixeira, L.T.; Ferreira Braz, W.; Correia de Siqueira, R.N.; Omar Ginoble Pandoli, O.G.; Gerales, M.C. Sulfated and carboxylated nanocellulose for Co^{+2} adsorption. *J. Mater. Res. Technol.* **2021**, *15*, 434–447. [[CrossRef](#)]
23. Reid, M.S.; Vilalobos, M.; Cranston, E.D. Benchmarking cellulose nanocrystals: From the laboratory to industrial production. *Langmuir* **2017**, *33*, 1583–1598. [[CrossRef](#)] [[PubMed](#)]
24. Andrews, M.P.; Morse, T. Method for Producing Functionalised Nanocrystalline Cellulose and Functionalized Nanocrystalline Cellulose Thereby Produced. U.S. Patent 20,170,260,298, 2017. (Application Granted 28 August 2008).
25. Made in Quebec: The Sky Is the Limit for Nanocrystals. Available online: <https://www.mcgill.ca/innovation/article/made-quebec/made-quebec-sky-limit-nanocrystals> (accessed on 18 September 2022).
26. Capron, I.; Rojas, O.J.; Bordes, R. Behaviour of nanocelluloses at interfaces. *Curr. Opin. Colloid Interface Sci.* **2017**, *29*, 83–95. [[CrossRef](#)]
27. Gaillard, T.; Roché, M.; Honorez, C.; Jumeau, M.; Balan, A.; Jedrzejczyk, C.W.; Drenckhan, W. Controlled foam generation using cyclic diphasic flows through a constriction. *Int. J. Multiph. Flow* **2017**, *96*, 173–187. [[CrossRef](#)]
28. Drenckham, W.; Saint-Jalmes, A. The science of foaming. *Adv. Colloid Interface Sci.* **2015**, *222*, 228–259. [[CrossRef](#)]
29. Calabrese, V.; Haward, S.J.; Shen, A.Q. Effects of shearing and extensional flows on the alignment of colloidal rods. *Macromolecules* **2021**, *54*, 4176–4185. [[CrossRef](#)]
30. Delepierre, G.; Vanderfleet, O.M.; Niinivaara, E.; Zakani, B.; Cranston, E. Benchmarking cellulose nanocrystals Part II: New industrially produced materials. *Langmuir* **2021**, *37*, 8393–8409. [[CrossRef](#)]
31. Traykov, T.T.; Manev, E.D.; Ivanov, I.B. Hydrodynamics of thin liquid films. Experimental investigation of the effect of surfactants on the drainage of emulsion films. *Int. J. Multiph. Flow* **1977**, *3*, 485–494. [[CrossRef](#)]
32. Bhamla, M.S.; Chai, C.; Alvarez-Valenzuela, M.A.; Tajuelo, J.; Fuller, G.G. Interfacial mechanisms for stability of surfactant-laden films. *PLoS ONE* **2017**, *12*, e0175753. [[CrossRef](#)]
33. Schulze-Schlarman, J.; Buchavzov, N.; Stubenrauch, C. A disjoining pressure study of foam films stabilised by tetradecyl trimethyl ammonium bromide C_{14}TAB . *Soft Matter* **2006**, *2*, 584–594. [[CrossRef](#)] [[PubMed](#)]
34. Tchoukov, P.; Mileva, E.; Exerowa, D. Drainage time peculiarities of foam films from amphiphilic solutions. *Colloids Surf. A Physicochem. Eng. Asp.* **2004**, *238*, 19–25. [[CrossRef](#)]
35. Yeung, A.; Zhang, L. Shear effects in interfacial rheology and their implications on oscillating pendant drop experiments. *Langmuir* **2006**, *22*, 693–701. [[CrossRef](#)]
36. Nagel, M.; Tervoort, T.A.; Vermant, J. From drop-shape analysis to stress-fitting elastometry. *Adv. Colloid Interface Sci.* **2017**, *247*, 33–51. [[CrossRef](#)] [[PubMed](#)]
37. Alexandrov, N.A.; Marinova, K.G.; Gurkov, T.D.; Danov, K.D.; Kralchevsky, P.A.; Stoyanov, S.D.; Blijdenstein, T.B.; Arnau-dov, L.N.; Pelan, E.G.; Lips, A. Interfacial layers from the protein HFBII hydrophobin: Dynamic surface tension, dilatation-al elasticity and relaxation times. *J. Colloid Interface Sci.* **2012**, *376*, 296–306. [[CrossRef](#)] [[PubMed](#)]
38. Mikhailovskaya, A.; Chatzigiannakis, E.; Renggli, D.; Vermant, J.; Monteux, C. From individual liquid films to macroscopic foam dynamics: A comparison between polymers and a nonionic surfactant. *Langmuir* **2022**, *38*, 10768–10780. [[CrossRef](#)] [[PubMed](#)]
39. Garrett, P.R. Defoaming: Antifoams and mechanical methods. *Curr. Opin. Colloid Interface Sci.* **2015**, *20*, 81–91. [[CrossRef](#)]
40. Zafar, A.; Melendez, R.; Geib, S.J.; Hamilton, A.D. Hydrogen bond controlled aggregation of guanidinium-carboxylate derivatives in the solid state. *Tetrahedron* **2002**, *58*, 683–690.

SCIENTIFIC ACHIEVEMENTS

PUBLICATIONS

2022

The influence of the Surface Chemistry of Cellulose Nanocrystals on Ethyl Lauroyl Arginate Foam Stability. Agnieszka Czakaj, Emmanouil Chatzigiannakis, Jan Vermant, Marcel Krzan, Piotr Warszyński. *Polymers* 2022,14(24),5402.

The effect of electrolytes and urea on the ethyl lauroyl arginate and cellulose nanocrystals foam stability. Agnieszka Czakaj, Marcel Krzan, Piotr Warszyński, *Applied Sciences* 2022,12(6),2797.

Surface Properties of Saponin-Chitosan Mixtures. Marcel Krzan, Natalia García Rey, Ewelina Jarek, Agnieszka Czakaj, Eva Santini, Francesca Ravera, Libero Liggieri, Piotr Warszyński, Björn Braunschweig. *Molecules* 2022,27,7505.

2021

Ethyl lauroyl arginate, an inherently multicomponent surfactant system. Agnieszka Czakaj, Ewelina Jarek, Marcel Krzan, Piotr Warszyński *Molecules* 2021,26(19),5894.

2020

Viscoelastic interfaces comprising of cellulose nanocrystals and lauroyl ethyl arginate for enhanced foam stability. Agnieszka Czakaj, Aadithya Kannan, Agnieszka Wiśniewska, Gabriela Grześ, Marcel Krzan, Piotr Warszyński, Gerald G. Fuller. *Soft Matter* 2020,16,3981-3990.

Correction: Viscoelastic interfaces comprising of cellulose nanocrystals and lauroyl ethyl arginate for enhanced foam stability. Agnieszka Czakaj, Aadithya Kannan, Agnieszka Wiśniewska, Gabriela Grześ, Marcel Krzan, Piotr Warszyński, Gerald G. Fuller. *Soft Matter* 2020,16,5094-5094.

CONFERENCES

Synergistic foaming properties of lauroyl ethyl arginate and cellulose nanocrystals, EUFOAM 2020 online, [Agnieszka Czakaj](#), Piotr Warszyński, Marcel Krzan.

[M. Krzan](#), E. Jarek, A. Czakaj, E. Santini, F. Ravera, L. Ligierri, P. Warszyński, B. Braunschweig, EUFOAM 2020 online.

[Agnieszka Czakaj](#), Marcel Krzan, Piotr Warszyński, Linear viscoelastic properties of cellulose nanocrystals – lauroyl ethyl arginate, Annual European Rheology Conference 2019, Portoroz (Slovenia) 8-11.04.2019.

[Agnieszka Czakaj](#), Małgorzata Kabat, Ewelina Jarek, Marcel Krzan, Piotr Warszyński, Foaming and emulsifying properties of cellulose nanofibers – lauroyl ethyl arginate. 61th Meeting of Polish Chemical Society, Kraków, 17-21.09.2018.

Ewelina Jarek, Eva Santini, Agnieszka Czakaj, Małgorzata Kabat, Francesca Ravera, Libero Liggieri, Piotr Warszyński, Marcel Krzan, Surface properties of Saponin and Chitosan solutions in relation to their foamability, 61 PTChem, Kraków, 17-21.09.2018.

POSTERS

Agnieszka Czakaj, Aadithya Kannan, Gerald G. Fuller, Marcel Krzan, Piotr Warszyński, Dynamic fluid film interferometry for coalescence study in lauroyl ethyl – arginate – cellulose nanocrystals mixtures, European Colloid and Interface Society (ECIS) 2019, 8-13.09.2019, Leuven (Belgium).

PROJECTS

European Union's Horizon 2020 Research and Innovation Programme under grant agreement No 731019 "Interfacial properties of lauroyl ethyl arginate and cellulose nanocrystals" (European Union Soft Matter Infrastructure), Research carried out in ETH Zürich; **Project leader**.

Solaris National Synchrotron Radiation Centre in Kraków (Poland), successful proposal (proposal number) 201040 for 2 days of experiments with Cryo-EM facilities; **Project leader**.

National Science Centre of Poland, grant number 2016/21/B/ST8/02107, project leader dr Marcel Krzan, *Opracowanie nowoczesnej technologii wytwarzania stabilnych biologicznych filmów powierzchniowych o właściwościach drobnoustrojów i leczniczych*; **Project participant**.

INTERNSHIPS

2019, research internship (1 month), Stanford University, Department of Chemical Engineering, Stanford (USA)

2018, research internship (1 week), Institute of Physical Chemistry Polish Academy of Sciences, Warszawa (Poland)

2018, research internship (1 week), National Research Council – CNR, Institute of Condensed Matter Chemistry and Technologies for Energy, Genova (Italy)